Improving Energy Efficiency and Motion Control in Load-Carrying Applications using Self-Contained Cylinders

Daniel Hagen

UiA University of Agder

Daniel Hagen

Improving Energy Efficiency and Motion Control in Load-Carrying Applications using Self-Contained Cylinders

Doctoral Dissertation for the Degree *Philosophiae Doctor (PhD)* at
the Faculty of Engineering and Science, Specialisation in Mechatronics

University of Agder
Faculty of Engineering and Science
2020

Acknowledgments

<div align="center">

Daniel Hagen

Grimstad, Norway

March 2020

</div>

Abstract

Because of an increasing focus on environmental impact, including CO_2 emissions and fluid spill pollution, inefficient hydraulic systems are being replaced by more environmentally friendly alternatives in several industries. For instance, in some offshore applications that have multiple diesel generators continuously running to produce electricity, all hydraulic rotating actuators supplied from a central hydraulic power unit have been replaced with AC induction motors containing a variable frequency drive and gearbox. However, hydraulic linear actuators are still needed in most load-carrying applications mainly because of their high reliability associated with external impact shocks. Moreover, their force capacity is higher than that of their linear electro-mechanical counterparts. Valve-controlled linear actuators (cylinders) supplied from a centralized hydraulic power unit are standard in offshore load-carrying applications. In addition to the advantages mentioned above of hydraulic linear actuators, they have, nevertheless, a number of important drawbacks, which include: 1) a high level of energy consumption due to significant power losses caused by flow throttling in both the pipelines and valves, 2) reduced motion performance due to the influence of load-holding valves, 3) high CO_2 emissions and fuel costs related to the diesel generator that supplies electricity to the hydraulic power unit, 4) significant potential for hydraulic fluid leakage because of many leakage points, 5) demanding efforts with respect to installation and maintenance, as well as 6) costly piping due to the centralized hydraulic power supply.

The work presented in this dissertation and the appended papers are devoted to replacing inefficient hydraulic linear actuation systems traditionally used in offshore load-carrying applications with more environmentally friendly solutions. Two alternative technologies are identified, namely electro-mechanical and electro-hydraulic self-contained cylinders. The feasibility of replacing conventional valve-controlled cylinders with self-contained cylinder concepts is investigated in two relevant case studies.

First, it was discovered that the permissible average transmitted power of an off-the-shelf **electro-mechanical** actuator is lower than the average power required by the operational sequence of the present offshore case-study. Consequently, it is not possible to both avoid overheating the actuator and guarantee that productivity will not be limited by

doing so. Further, an off-the-shelf self-contained **electro-hydraulic** cylinder is not iden-
tified for the present requirements, including passive-load holding capability, high-energy
efficiency, electric regenerative capabilities, increased motion performance potential, high-
power density, reduced fluid spill potential, capability of delivering up to 1.7 m of travel
length above 100 kN of force as well as more than 0.15 m/s velocity in four-quadrant
operations. Hence, a new type of self-contained architecture, previously non-existent in
the literature or commercially available off-the-shelf, is designed and implemented on a
single-boom crane.

Secondly, the proposed self-contained electro-hydraulic cylinder is both numerically
and experimentally compared with the conventional valve-controlled cylinder used for
benchmarking in terms of motion performance, energy efficiency, and compactness. The
novel electro-hydraulic drive system is experimentally proven to be a valid alternative
to conventional valve-controlled systems for applications where passive load-holding is
required in terms of both dynamic response and energy consumption. Several benefits
are numerically analyzed and experimentally validated, such as faster rise time, shorter
settling time, less overshoot, significantly improved position tracking, and reduction of
pressure oscillations. The self-contained solution enables significant energy savings due
to its throttle-less and power-on-demand nature. Because of the regenerative capability,
a considerable amount of the consumed energy may be recovered. More specifically, this
means that a larger amount of the energy taken from the electrical grid can be used
effectively if the recovered energy is reused, an option that is not possible in state-of-the-
art valve-controlled systems where passive load-holding valves are employed.

Next, a design analysis carried out on the single-boom crane shows that the self-
contained electro-hydraulic cylinder provides several benefits more than provided by the
off-the-shelf electro-mechanical cylinder. It is more compact in terms of space occupation
of the application's structure, has a lower weight, requires less installed electrical power,
and is expected to have a lower cost. A self-sufficient and completely sealed hydraulic
actuation system also reduces the risk of fluid spill pollution in typical offshore applications
where a centralized hydraulic power unit supplies multiple valve-controlled actuators.
Moreover, the improved energy efficiency reduces the diesel generators' CO_2 emissions
and fuel costs, helping fluid power to become a cleaner technology, thereby reducing the
offshore industry's overall environmental impact.

Lastly, an additional survey is carried out to identify and review the commercially
available and published literature on design methods that could have the potential to
automate the design of actuation systems. This dissertation presents the challenges and
requirements identified concerning a proposed framework that must be solved in order to
realize a viable computerized tool for automating the design of actuation systems.

Publications

Eight scientific articles are appended to this dissertation and will be referred to by their character. The following listed papers have been published or accepted for publication in peer-reviewed conference proceedings and journals and are printed in their original state:

Paper A D. Hagen, W. Pawlus, M. K. Ebbesen, and T. O. Andersen. Feasibility Study of Electromechanical Cylinder Drivetrain for Offshore Mechatronic Systems. In *Journal of Modeling, Identification and Control*, 38(2):59-77, 2017.

Paper B D. Hagen, D. Padovani, and M. K. Ebbesen. Study of a Self-Contained Electro-Hydraulic Cylinder Drive. In *2018 Global Fluid Power Society PhD Symposium (GFPS)*, Samara, Russia, 18-20 July 2018.

Paper C D. Padovani, S. Ketelsen, D. Hagen, and L. Schmidt. A Self-Contained Electro-Hydraulic Cylinder with Passive Load-Holding Capability. In *Energies*, 12(2):292, 2019.

Paper D D. Hagen, D. Padovani, and M. Choux. Enabling Energy Savings in Offshore Mechatronic Systems by using Self-Contained Cylinders. In *Journal of Modeling, Identification and Control*, 40(2):89-108, 2019.

Paper E D. Hagen, D. Padovani, and M. Choux. Design and Implementation of Pressure Feedback for Load-Carrying Applications with Position Control. In *Sixteenth Scandinavian International Conference on Fluid Power, SICFP19*, Tampere, Finland, 22-24 May 2019.

Paper F D. Hagen, D. Padovani, and M. Choux. A Comparison Study of a Novel Self-Contained Electro-Hydraulic Cylinder versus a Conventional Valve-Controlled Actuator – Part 1: Motion Control. In *Actuators*, 8(4):79, 2019.

Paper G D. Hagen, D. Padovani, and M. Choux. A Comparison Study of a Novel Self-Contained Electro-Hydraulic Cylinder versus a Conventional Valve-Controlled Actuator – Part 2: Energy Efficiency. In *Actuators*, 8(4):78, 2019.

Paper H D. Hagen, D. Padovani, and M. Choux. Guidelines to Choose Between Self-Contained Electro-Hydraulic and Electro-Mechanical Cylinders. Accepted for presentation at the *15th IEEE Conference on Industrial Electronics and Applications (ICIEA)*, Kristiansand, Norway, 9-13 November 2020.

Contents

Nomenclature

Abbreviations

AC   alternating current

ACC accumulator

ATEX explosive atmosphere

AV   auxiliary valves

BR   braking resistor

CAD computer-aided design

C   cylinder

CO   cooler

CV   check valve

DC   direct current

ED   electric drive

EHC electro-hydraulic cylinder

EMC electro-mechanical cylinder

EMS energy storage management system

EV   electro-valve

F   filter

FOC field-oriented control

GA   guide arm

Gm   gain margin

HD   heavy-duty

HMI human-machine interface

HPU hydraulic power unit

LGA lower guide arm

LHV load-holding valve

MA   main arm

GUI graphical user interface

OPT optimization

PI   proportional-integral

PLC programmable logic controller

PMSM permanent magnet synchronous motor

POCV pilot-operated check valve

P   hydraulic pump/motor unit

PRM pipe racking machine

PWM pulse width modulation

RV   pressure-relief valve

SBC single-boom crane

SD   servo-drive

SIM simulation

UGA upper guide arm

VCC   valve-controlled cylinder

V   valve

Symbols

a constant value used in the tanh function

A_d discharge area

α,β two-phase representation perpendicular axes

A_p piston area

A_r piston rod-side area

A_s poppet seat area

A_x pilot stage area

β_{oil} bulk modulus of hydraulic fluid

B_v viscous friction coefficient

C_d discharge coefficient

C hydraulic capacitance

ζ_m damping ratio

Δp pressure differential

D_P hydraulic units' displacement

dq fixed phasor representation

E^s back electromotive force

e_{x_c} linear position error

F_C Coulomb friction force

F_f linear friction force

F_L equivalent load force

f_S static friction coefficient

F_{S0} springs' pre-load force

f_v viscous friction coefficient

G gravitational load force

h_c maximum cylinder stroke

i_0 continuous current at standstill

$i_{a,b,c}$ three-phase current

i_{cont} continuous current

i_d flux-producing current component

i_g gearing ratio

i_q torque-producing current component

I^s_s space vector current

j imaginary unit

J_{tot} total inertia of the rotor and the mechanical load

κ_{air} adiabatic air constant

k_f high-pass filter gain

k_I integral gain

k_P proportional gain

k_q flow gain

k_S spring stiffness

K space vector scaling constant

k_V valve flow gain

l screw drive lead

λ scaling factor

L_s stators inductance

M equivalent mass

μ_{vol}	constant volumetric efficiency	τ_{fS}	friction forces' time constant
$\omega_{n,m}$	natural frequency	τ_L	external load torque
n_p	number of pole pairs	τ_S	torque losses
ω_c	phase crossover frequency	θ_m	mechanical rotor position
ω_m	mechanical rotor speed	θ_r	electrical angular position
ω_r	electrical angular velocity	$u_{a,b,c}$	voltage input signal
$p_{acc,0}$	pre-charge pressure in the accumulator	u_d	flux-producing voltage component
		u_{ED}	electric-drive on/off signal
p_{atm}	atmospheric pressure	u_{EV}	electro-valve on/off signal
p_{cr}	cracking pressure	u_{FC}	feedback controller signal
p	hydraulic pressure		
p_L	effective load pressure	u_{FF}	feedforward signal
ψ_R	constant flux modulus	u_{PF}	pressure feedback signal
Ψ_R^s	rotor flux linkage	u_q	torque-producing voltage component
p_x	pilot pressure	V	hydraulic volume
Q	hydraulic flow	$V_{a,b,c}$	three-phase supply voltage
$Q_{P,e}$	effective flow rate of the hydraulic unit	$v_{a,b,c}$	three-phase voltage
		V_{acc}	effective accumulator gas volume
Q_S	flow losses	ε_{air}	volumetric air content
ρ	density of the hydraulic fluid	V_{DC}	direct current supply voltage
R_s	stators resistance	$\dot{V}$	displacement flow
s	complex variable in s-plane	V_s^s	space vector voltage
τ_0	continuous torque at standstill	x_c	linear position
τ_{cont}	continuous torque	$\dot{x}_c$	linear velocity
τ_m	mechanical rotor torque	$\ddot{x}_c$	linear acceleration
τ_{em}	electro-magnetic torque	x_{POCV}	poppet lift
τ_f	time constant of the high-pass filter	x_V	relative valve opening

xiv

Chapter 1

Introduction

This chapter introduces the research presented in this dissertation. The conventional hydraulics used on an offshore oil drilling rig to actuate the equipment involved in the oil well construction process is first reviewed, and its main drawbacks are highlighted. As a consequence of the petroleum industry's concerns about current actuation systems in use, the motivation behind the main research question, i.e. mitigating negative environmental impacts and improving motion control of load-carrying applications, is then put forward. Finally, the investigated research objectives and dissertation outline are presented.

Background

The background of this research is related to the drawbacks of centralized hydraulic power distribution of hydraulically actuated applications. A relevant scenario involving the hydraulic actuators used on an offshore oil drilling rig to actuate multiple applications included in the oil well construction process is considered; see [1] for more information about these applications. A real life example where multiple diesel generators are continually run in order to supply electricity to an offshore installation is illustrated in Fig. 1.1. A significant amount of this electric power is used to generate hydraulic power through one or more hydraulic power units (HPUs) consisting of variable-displacement hydraulic pumps driven by AC induction motors at a constant speed. Both the size and number of HPUs depend on the different types of applications that are typically installed on a drilling rig and the total flow requirement of the actuators involved. Further, hydraulic power is distributed to the hydraulic actuators through hydraulic piping. In total, three pipelines (i.e., the constant supply pressure of typically 207 bar, the return pressure, and the drain) are distributed between the HPU and the hydraulic interface of each hydraulically actuated application.

For each hydraulic actuator (cylinder or motor), an individual electrical actuated spool
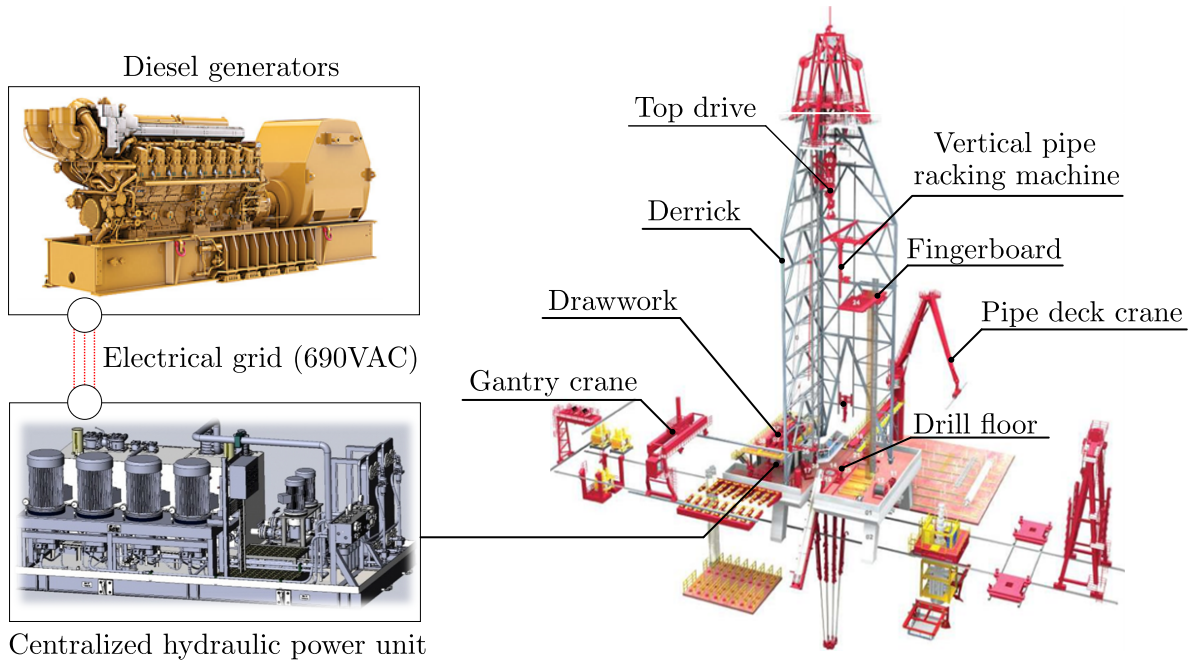
Figure 1.1: Conventional centralized hydraulic power supply distributed to multiple applications on an offshore oil drilling rig.

valve (i.e., the control element) typically controls the mechanical output (i.e., linear/rotary position and speed or force/torque). Depending on the functionality of the actuator to perform the desired operation, various types of control valves (e.g., on/off valves, directional valves, proportional directional control valves, pressure control valves) are used. Further, the control valve is actuated by the commands provided by the operator through the human-machine interface (HMI) and the control systems' inputs/outputs, e.g., manual mode (open-loop) or auto mode (closed-loop) with motion feedback. Additionally, because of safety regulations (e.g., ISO 17096 and DNVGL-ST-0378), passive load-holding devices are required in all load-carrying applications.

Conventional valve-controlled hydraulic actuation systems are characterized by high levels of reliability and power capability, excellent force density, a great amount of overload protection (e.g., shock absorption), adequate fluid management (i.e., filtration and cooling), and proper safety features. However, the following essential drawbacks are also present:

- high **energy consumption** related to the constant hydraulic pressure supply and throttling in the pipelines, control valves, and load-holding devices;

- reduced **motion performance** due to the influence of the passive load-holding functionality;

- high CO_2 **emissions** and **fuel costs** related to the diesel generators;

- significant potential for **leakage** of hydraulic fluid because of several leakage points;

2

- high **cost**, increased **weight**, extra **space occupation**, difficult **maintenance**, and challenging **installation** related to the hydraulic pipelines and the control valves located on the different applications.

Motivation and Problem Statement

Due to the essential drawbacks mentioned earlier and the world's increasing focus on reducing the environmental impact of the oil and gas industry, electrification of oil well construction processes is an ongoing trend [2]. Replacing hydraulics with electrical actuation can increase both efficiency and motion control, eliminating the risk of fluid spills. However, hydraulic linear actuators (cylinders) are still needed in many load-carrying applications because they do not cause any critical issues related to reliability, and their force density is higher than that of their linear electro-mechanical counterparts [3]. Moreover, since the linear electro-mechanical actuator cannot absorb external shocks in standby mode, there is a high risk of failure (e.g., jamming) that could cause the ongoing operation to stop. Reliability and productivity are indeed the most important performance criteria in offshore applications because of their remote location and the high cost of down time [1]. A relevant example of this scenario is the vertical pipe racking machine (Fig. 1.2) implemented on state-of-the-art offshore drilling rigs [4]. The pipe racking machine is a column-type multipurpose pipe handling machine that combines the functionality of different traditional types of pipe handling equipment in one machine (see Chapter 3 for a more detailed description). This machine performs the following tasks:

- moving stands (typically three or four sections of connected drill-pipe) between the desired fingerboard slot and the well-center where a machine (e.g., an iron roughneck) located on the drill floor connects or disconnects the drill-pipes that make up the drill string;

- building stands for storage inside the fingerboard while drilling;

- handling of a single drill-pipe, drill-collar, or casing from a horizontal to vertical position and vice versa;

- lifting operation on the drill floor, i.e., the main arm can be used as a crane.

This offshore application was previously actuated by means of conventional hydraulics alone. However, during the last decade, all hydraulic motors used for controlling the different rotational motions have been replaced by AC induction motors, all of which have a variable frequency drive and gearbox (AC drivetrains). Hence, among the main actuators involved in the operational motion cycle (i.e., the tripping sequence explained
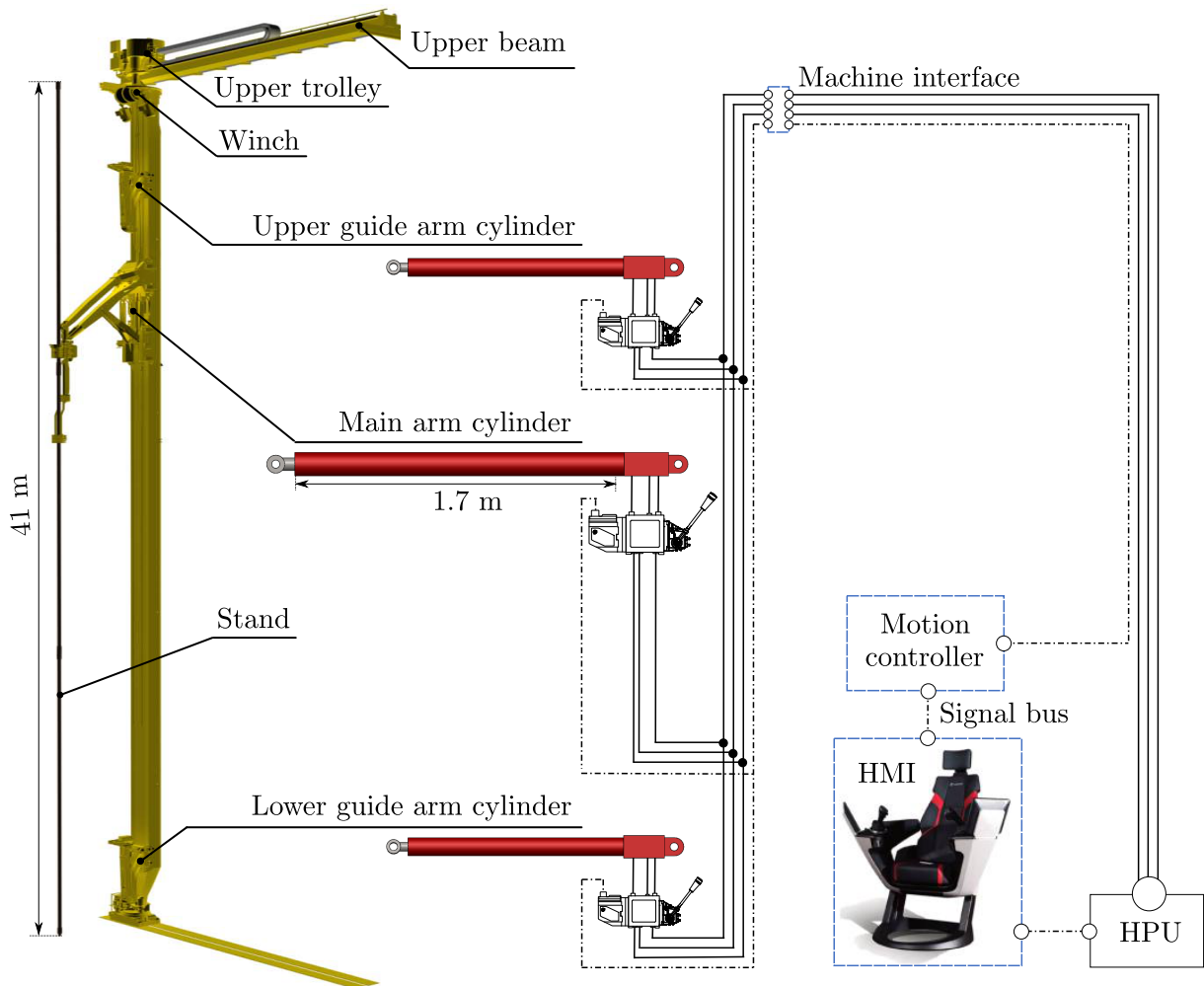
Figure 1.2: Vertical pipe racking machine – hydraulic power supply and control signal distributed to the reach arm's valve-controlled cylinders.

in Chapter 3), only the linear actuators used for controlling the synchronized horizontal motion of the three reach arms (i.e., the lower guide arm, the main arm, and the upper guide arm) are still hydraulically actuated through a constant pressure supplied from the centralized HPU. These valve-controlled cylinders (Fig. 1.2) include a pressure compensated proportional directional control valve typically used in mobile applications in combination with a passive load-holding device, i.e., one or two counterbalance valves [5]. Additional hydraulic actuators used for auxiliary functions (e.g., opening and closing of guides, stabbing, clamping, motor brakes, etc.) have not been considered at this stage of the research since their flow demand is insignificant compared to that of the reach arms cylinders, and their performance does not affect the motion accuracy relevant for the considered operational sequence.

In addition to the motivation for reducing CO_2 emissions and fuel costs by lowering the electric power consumption of the HPUs, there is a possibility to supply offshore drilling rigs with "greener" electricity from land via submarine cables. Significant cost

savings can be achieved by limiting offshore installations' power demands and, hence, the dimension of expensive submarine cables can be reduced. Further, the use of electric batteries in explosive atmospheres (ATEX) [6] on offshore oil drilling rigs has recently been approved [7], thereby creating an opportunity for possible emergency operation of the electric prime movers and storage of regenerated electric energy.

When considering the apparent disadvantages of existing hydraulic actuation systems and the current increasing focus on electrification to reduce the environmental footprint of the oil well construction process, this research puts forth the following research question:

> **Is there a suitable alternative to centralized hydraulic-powered valve-controlled linear actuators that is environmentally friendly yet does not compromise the motion performance of load-carrying applications?**

The new actuation system must satisfy the following requirements:

- passive-load holding capability (safety features);

- high energy efficiency and electric regenerative capabilities (energy-saving potential);

- increased motion performance potential (productivity);

- high power density (compactness);

- reduced fluid spill potential (environmentally friendly);

- capable of delivering up to 1.7 m of travel length above 100 kN of force and more than 0.15 m/s velocity in four-quadrant operations.

Research Objectives

This research project aims to identify more environmentally friendly linear actuators and investigate the consequences and limitations associated with replacing the conventional hydraulic linear actuation systems subjected to the requirements mentioned above by achieving the following objectives:

1. identify and review state-of-the-art linear actuators that may be suitable for the considered requirements;

2. identify a relevant offshore load-carrying application and investigate the operational sequence in terms of energy-saving potential;

3. investigate if the more environmentally friendly and commercially available linear actuator concepts are a feasible alternative to the conventional hydraulic linear actuation system in the present case study;

4. if an off-the-shelf alternative is not feasible to the present case study, identify a new concept that could have the potential to be a viable alternative;

5. analyze the new actuation system experimentally on a relevant load-carrying application and compare its motion performance and energy efficiency with the conventional hydraulic linear actuator;

6. evaluate the main consequences and limitations associated with replacing the conventional hydraulics with the more environmentally friendly alternatives.

Additionally, investigate if there exist design tools that have the potential to automate the investigation of the above steps.

Outline

The remainder of this dissertation is divided into three main chapters. Chapter 2 describes the functionality and mathematical representation of the considered state-of-the-art alternative linear actuators in such a way that the reader will not need to study several of the appended papers in order to grasp these actuators' technical aspects. Chapter 3 presents the research methodologies and main results identified in this investigation. Finally, Chapter 4 concludes the dissertation by presenting the research contributions and identifying possible areas for further work.

The previously listed papers are included at the conclusion of this dissertation, and the reader is encouraged to read the appended papers in order to learn more details about the experiments which have been conducted throughout the project.

Chapter 2

State-of-the-Art

First, this chapter presents a survey of state-of-the-art linear actuators that can have the potential to replace conventional valve-controlled cylinders commonly used in load-carrying applications. Next, the functionality and mathematical representation of the identified alternative actuation systems are described.

The effort involved with replacing conventional valve-controlled cylinders with linear electro-mechanical actuators (cylinders) has been a popular research topic and engineering task for several decades (especially in aerospace systems), as attempts have on the one hand been made to reduce system weight, installation complexity and maintenance effort [8–12]. However, on the other hand, predicting an actuator's life cycle is challenging, and due to the fact that an electro-mechanical actuator cannot absorb shocks in standby mode, there is a high risk of failure (e.g., jamming that could have dangerous consequences). Therefore, electro-mechanical cylinders (EMCs) are still not accepted in commercial airplanes as primary actuators for flight control. As a result, linear electro-hydrostatic actuators (cylinders) have been introduced. This electro-hydraulic technology, as explained by [13], first introduced in aerospace systems, demonstrated that the disadvantages of traditional hydraulics can be significantly reduced. Indeed, these compact and self-contained electro-hydraulic cylinders (EHCs) are now used in the aerospace industry, e.g., for flaps control in commercial airplanes [14] and primary flight control surfaces in the Lockheed Martin F-35 fighter aircraft [15].

In other industries, hydraulics have been successfully replaced by electro-mechanical actuators in numerous applications, especially in rotary motion applications (e.g., use of AC drivetrains in offshore oil drilling equipment [2]), increasing both motion control (accuracy), energy efficiency, and eliminating fluid spills. However, hydraulic cylinders are still needed in most load-carrying applications because they do not cause any critical issues related to reliability, and their force density is higher than that of their linear electro-mechanical cylinder. Thus, in the case of linear actuators, hydraulics have been replaced

mainly in low power applications (i.e., below 5 kW), where disadvantages such as increased wear, difficult overload protection, and forces capability are accepted [16]. Consequently, in order for hydraulic component manufacturers to stay competitive, the idea of combining the advantages of electric drives and hydraulics has been further explored in many fields of application in recent years, resulting in the development of compact and self-contained EHCs [16–19].

Both the EMC (Fig. 2.1a) and EHC (Fig. 2.1b) are defined as compact and self-contained cylinders that are characterized by their electrical input, power-on-demand nature related to the variable frequency drive, sealed enclosure, and linear mechanical output.

(a)

(b)
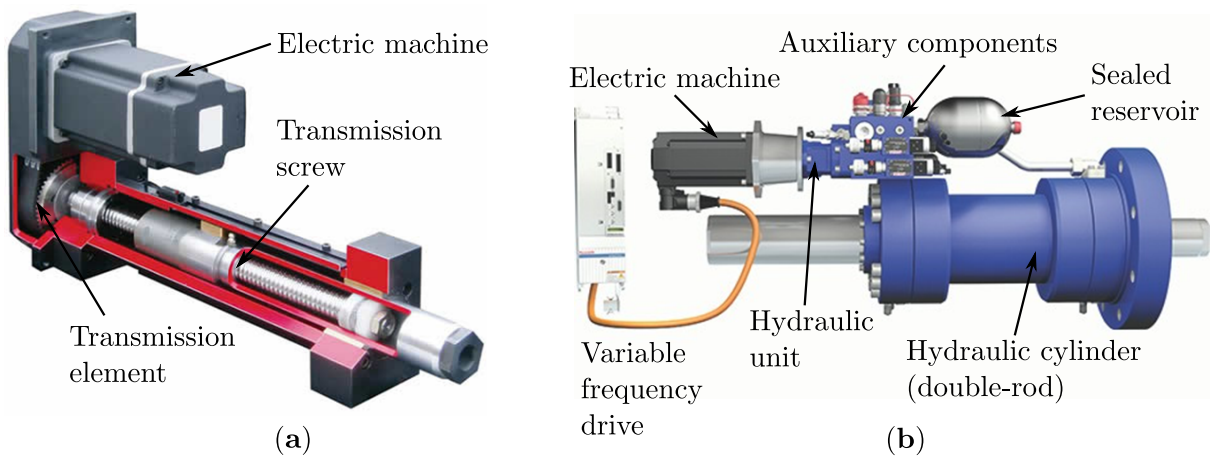
Figure 2.1: Self-contained cylinders: (a) electro-mechanical [20]; (b) electro-hydraulic [21].

A common feature of both actuation systems is that they consist of a variable-speed electric prime mover (i.e., an electric machine controlled by a variable frequency drive) and a linear transmission system that converts the rotational mechanical output of the electric machine into linear mechanical output. The two self-contained cylinders differ in their transmission technology. The EMC consists of a mechanical transmission element (e.g., a gear belt) and transmission screw (e.g., a ball-screw), while the EHC consists of a hydraulic (hydrostatic) transmission system, including a hydraulic pump/motor unit, sealed reservoir, auxiliary valves, and hydraulic cylinder.

The following sections aim to describe the functionality and mathematical representation of the two identified self-contained cylinder concepts that are investigated in Chapter 3. First, the considered type of electric drive used as the prime mover is described. Next, the two linear transmission technologies are separately discussed in terms of availability, functionality, control demand, and numerical modeling approach.

2.1 Electric Prime Mover

The electric prime mover (Fig. 2.2) consists of two main components, namely the electric machine and variable frequency drive. Both components of the electric drive considered in this research are off-the-shelf. The electric machine, a surface mounted (non-salient) permanent magnet synchronous motor (PMSM), is usually the preferred choice for compact and self-contained systems due to its significant power density and energy efficiency compared to, e.g., standard industrial AC induction motors. The variable frequency drive consists of three main components.
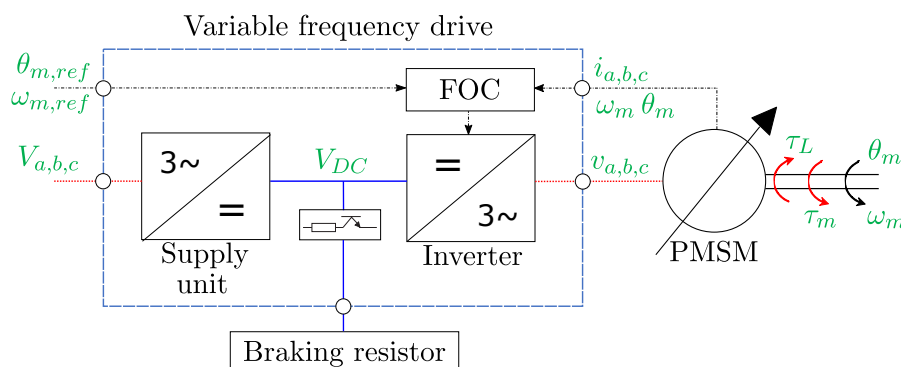
Figure 2.2: Simplified schematic of the commercial electric drive concept addressed in this research as the self-contained cylinder's prime mover.

First, the supply unit converts the three-phase input voltage ($V_{a,b,c}$) from the electrical grid to a DC voltage supply (V_{DC}). Next, the considered field-oriented control (FOC) module controls the voltage ($v_{a,b,c}$) through the pulse width modulation (PWM) inverter. In addition to the space vector modulation algorithm, the control module includes a cascaded current ($i_{a,b,c}$), speed (ω_m), and position (θ_m) feedback control architecture. An external braking resistor (BR) is connected to the DC bus to dissipate the regenerated power into heat (dynamic braking) when the electric machine operates as a generator. However, there exist solutions where the regenerated power can be used profitably, such as happens with power-sharing via a common DC bus between multiple electric prime movers, returning regenerated power to the electrical grid, or ensuring energy storage on an electro-chemical storage device [22].

The modeling and control approach of the electric prime mover studied in this research is based on the work of [23] according to the dynamic equivalent circuit in Fig. 2.3a and the control structure in Fig. 2.3b.
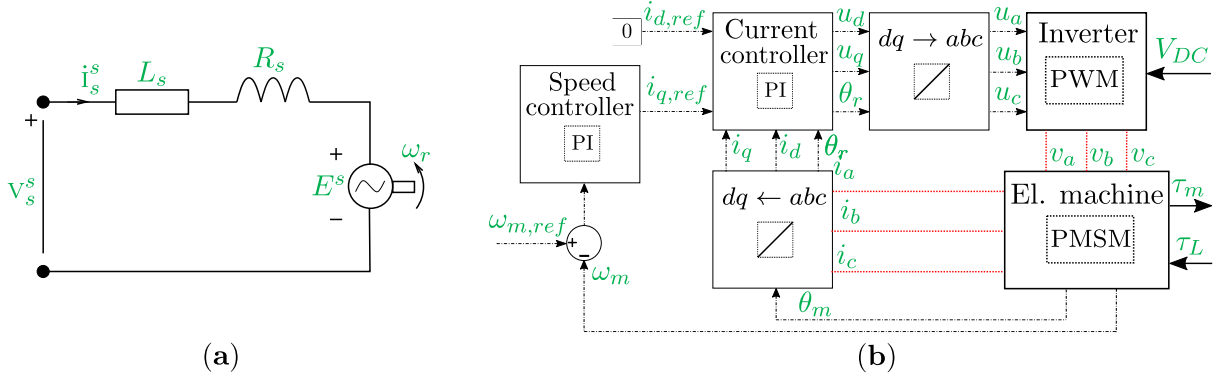
Figure 2.3: The considered numerical model of the electric prime mover: (**a**) dynamic equivalent circuit representing the permanent magnet synchronous motor; (**b**) block diagram of the variable speed controller (the outer loop position feedback controller is omitted in the figure for simplicity).

The electro-magnetic dynamics of the PMSM is represented in stator coordinates by

$$L_s \cdot \frac{d\mathrm{i}_s^s}{dt} = \mathrm{v}_s^s - R_s \cdot \mathrm{i}_s^s - \underbrace{j \cdot \omega_r \cdot \Psi_R^s}_{E^s}, \tag{2.1}$$

including the stator inductance (L_s), resistance (R_s), and the space vectors for current (i_s^s), voltage (v_s^s), and the back electromotive force (E^s). The E^s is given by the electrical angular velocity (ω_r) and the rotor flux linkage space vector (Ψ_R^s), which is produced by the permanent magnets. The stator voltage is defined by transforming the electrical machines' three-phase input voltage ($v_{a,b,c}$) into a two-phase representation ($v_{\alpha,\beta}$) using the well-known Clarke transformation:

$$\mathrm{v}_s^s = \begin{bmatrix} v_\alpha \\ v_\beta \end{bmatrix} = K \begin{bmatrix} \frac{2}{3} & -\frac{1}{3} & -\frac{1}{3} \\ 0 & \frac{1}{\sqrt{3}} & -\frac{1}{\sqrt{3}} \end{bmatrix} \begin{bmatrix} v_a \\ v_b \\ v_c \end{bmatrix}, \tag{2.2}$$

where $K = 1/\sqrt{2}$ is the space vector scaling constant for RMS-values. Furthermore, the two-phase stator current is transformed into a three-phase current using the reverse Clarke transformation:

$$\begin{bmatrix} i_a \\ i_b \\ i_c \end{bmatrix} = \frac{1}{K} \begin{bmatrix} 1 & 0 \\ \frac{1}{2} & \frac{\sqrt{3}}{2} \\ -\frac{1}{2} & -\frac{\sqrt{3}}{2} \end{bmatrix} \underbrace{\begin{bmatrix} i_\alpha \\ i_\beta \end{bmatrix}}_{\mathrm{i}_s^s}. \tag{2.3}$$

Then, with perfect field orientation (i.e., with exact knowledge of the flux angle obtained by measuring the angular position of the rotor) the electro-magnetic torque production is derived by

$$\tau_{em} = \frac{3 \cdot n_p}{2 \cdot K^2} \cdot \psi_R \cdot i_q, \tag{2.4}$$

where n_p is the number of pole pairs, ψ_R the constant flux modulus, and i_q the torque-producing current component. Since the flux is created from inside the rotor, then the flux-producing current component (i_d) can be controlled to zero (Fig. 2.3b) when below the rated speed and to a negative value in the field weakening range (i.e., above-rated speed). However, the second case will reduce the torque capability, which is maximum when $i_d = 0$. In this case, the mechanical dynamics is described by

$$J_{tot} \cdot \frac{d\omega_m}{dt} = \tau_{em} - B_v \cdot \omega_m - \tau_L, \tag{2.5}$$

where J_{tot} is the total inertia of the rotor and mechanical load, $\omega_m = \omega_r/n_p$ is the mechanical rotor speed, B_v is the viscous friction coefficient, and τ_L is the external load torque. Finally, the mechanical rotor torque transferred to the linear transmission system is derived by

$$\tau_m = \tau_{em} - B_v \cdot \omega_m. \tag{2.6}$$

The switching of the space vector PWM inverted is not included in the numerical investigation because it is not necessary for sufficiently simulating motion control and analysis of the losses in the electric machine. Moreover, the losses due to the harmonics created by the PWM are minor compared to the overall losses in state-of-the-art electric drives and can be included by an efficiency constant. Hence, the electric machines' three-phase input voltage ($v_{a,b,c}$) is directly connected to the voltage control signal ($u_{a,b,c}$) from the current controller that is transformed through the reverse Clark-Park transformation, as shown in Fig. 2.3b. Conversely, the Clark-Park transformation, when considering the current, first transforms the three-phase representation to a two-phase representation using Clark's transformation (2.2) before transforming the $\alpha\beta$ representation to a fixed phasor, dq, representation with the Park transformation:

$$\begin{bmatrix} i_d \\ i_q \end{bmatrix} = \begin{bmatrix} \cos(\theta_r) & \sin(\theta_r) \\ -\sin(\theta_r) & \cos(\theta_r) \end{bmatrix} \begin{bmatrix} i_\alpha \\ i_\beta \end{bmatrix}, \tag{2.7}$$

where $\theta_r = \theta_m \cdot n_p$ is the angle of the rotating reference frame (i.e., the electrical angular position). For a more detailed description of the space vector modulation algorithm and cascaded proportional-integral (PI) controllers, see, for instance, [23, 24].

2.2 Electro-Mechanical Drive System

When investigating commercially available types of EMCs, the heavy-duty version from Rexroth [25] was identified in [3] (Paper A) to be one of the most suitable off-the-shelf electro-mechanical linear actuators for the considered requirements. The drive system is

available in different configurations (Fig. 2.4), with or without a gearbox, using either a
ball-screw assembly (Fig. 2.5a) or planetary roller-screw assembly (Fig. 2.5b). Depending
on the configuration and external load, the drive system is capable of handling up to 290
kN axial force, velocities up to 1 m/s, and up to 1.7 m of travel.

(a)   (b)

Figure 2.4: Different motor mounting configurations [25]: (a) via timing (gear) belt side
drive; (b) directly via coupling.

(a)   (b)
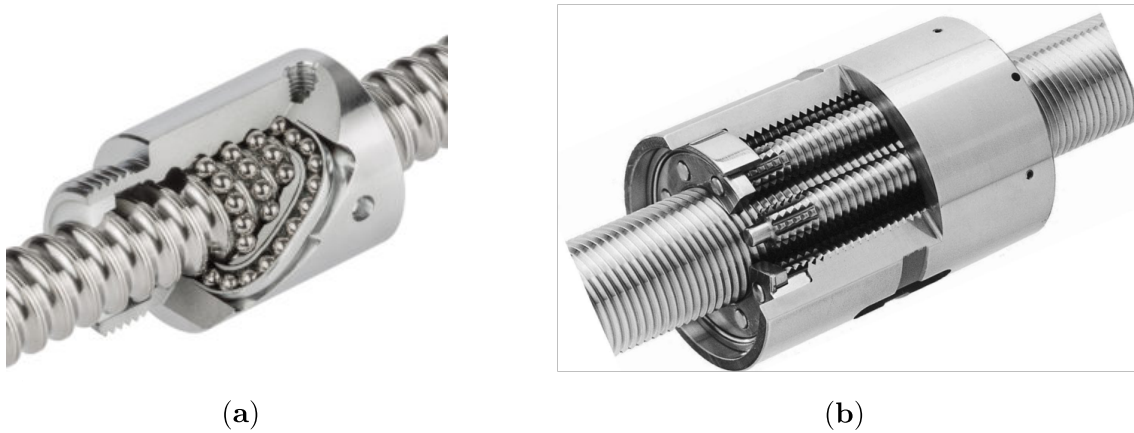
Figure 2.5: Different screw assemblies: (a) ball-screw [26]; (b) planetary roller-screw [27].

In this research project, a simple approach has been considered to describe the me-
chanical transmission output variables since the transmission system of the EMC is sig-
nificantly stiff, and the backlash of state-of-the-art screw assemblies is negligible. First,
the electric machines' load torque is derived by

$$\tau_L = (F_L + F_{f,emc}) \cdot \frac{l}{2\pi \cdot i_g}, \tag{2.8}$$

where F_L is the equivalent load force acting on the cylinder, $F_{f,emc}$ the mechanical friction
force, i_g the gearing ratio, and l the lead of the screw transmission. The mechanical friction

can be modeled in different ways, e.g., the combined mechanical fiction can be included either as an efficiency constant (often provided by the manufacturer) or by using the Stribeck friction model as described later in (2.26). Next, the rotary output variables of the electric prime mover are converted to linear variables, such as the force:

$$F_c = \frac{2\pi \cdot i_g}{l} \cdot \tau_m - F_{f,emc}, \tag{2.9}$$

the position:

$$x_c = \frac{l}{2\pi \cdot i_g} \cdot \theta_m, \tag{2.10}$$

and the velocity:

$$\dot{x}_c = \frac{l}{2\pi \cdot i_g} \cdot \omega_m. \tag{2.11}$$

To control the linear motion of the EMC, the integrated controller containing motion and current feedback of the electric drive (Fig. 2.2) is sufficient, and only by using the inverse of (2.10) and (2.11) will the desired linear motion profile be converted to the control input (Fig. 2.6) of the electric prime mover.
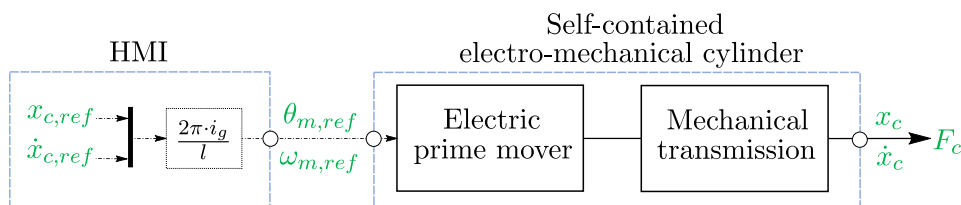
Figure 2.6: The self-contained electro-mechanical cylinder's control structure.

2.3 Electro-Hydraulic Drive System

Today, a considerable number of self-contained electro-hydraulic linear actuators are commercially available whether they are off-the-shelf or customized for a specific application, e.g., Rexroth SHA [21], Servi Hybrid Drive [28], Parker Compact EHA [29], and Voith SelCon [30]. However, when considering the requirements relevant to this research, a suitable off-the-shelf and general-purpose EHC that is compact and self-contained has not been identified based on commercially available information. Typically, the commercial actuators that are often designed for low-power applications (below 5 kW), lack passive-load holding capability, are not entirely sealed systems, are not capable of operating in four-quadrant, and are not capable of regenerating electric power. Hence, a comprehensive literature survey has been carried out to identify state-of-the-art EHC concepts that have the potential to satisfy the requirements presented earlier in Chapter 1 and replace conventional valve-controlled cylinders in load-carrying applications.

2.3.1 Classification and Review

Based on the considered requirements, a literature survey focusing on identifying relevant
EHC concepts that have the potential to be self-contained was first presented in [31]
(Paper B) and further updated in [32] (Paper C). In addition, only concepts having a
single-rod (differential) cylinder arranged in a closed-circuit configuration with a sealed
reservoir are regarded as being relevant concepts. The following three EHC configurations
are identified in the technical literature:

1. **Variable-displacement hydraulic unit and fixed-speed prime mover:** The
   cylinders' motion is controlled by varying the hydraulic unit's displacement. This
   approach is prevalent among multi-actuator machines (e.g., excavators [33]) since a
   unique charge pump supplies the displacement adjustment system of each hydraulic
   unit. The prime mover can be either an electric motor or a combustion engine.

2. **Fixed-displacement hydraulic unit and variable-speed electric prime mover:**
   The electric prime mover controls both the speed and rotational direction of the
   fixed-displacement hydraulic units' shaft, controlling the motion of the hydraulic
   cylinder [34–37]. The electric machine can be either a PMSM [35] or an AC induc-
   tion (asynchronous) motor [38].

3. **Variable-displacement hydraulic unit and variable-speed electric prime
   mover:** Both the electric prime mover and variable-displacement hydraulic unit
   actively control both the cylinders' motion and force and are prevalent amongst
   process applications [39].

The concept of using a variable-speed electric prime mover and a fixed-displacement
hydraulic unit (configuration 2) has been chosen for this study because it offers high com-
pactness, low system complexity, and simple control. Moreover, a variable-displacement
hydraulic unit would require additional components to control the displacement, increas-
ing the overall size and control demands. However, in terms of scalability and reliability,
the configurations that have a constant-speed variable-displacement hydraulic unit could
be a better choice for high power applications if compactness and energy efficiency are
not essential [40]. Furthermore, if the cost aspect is not critical and the application does
require a high level of drive stiffness, high control flexibility, or high energy efficiency, the
combination of variable-speed and variable-displacement components would be beneficial.
Further on, [40] proposes a classification (Fig. 2.7) of the chosen EHC configuration along
with a comparison between the different classes (Tab. 2.1).
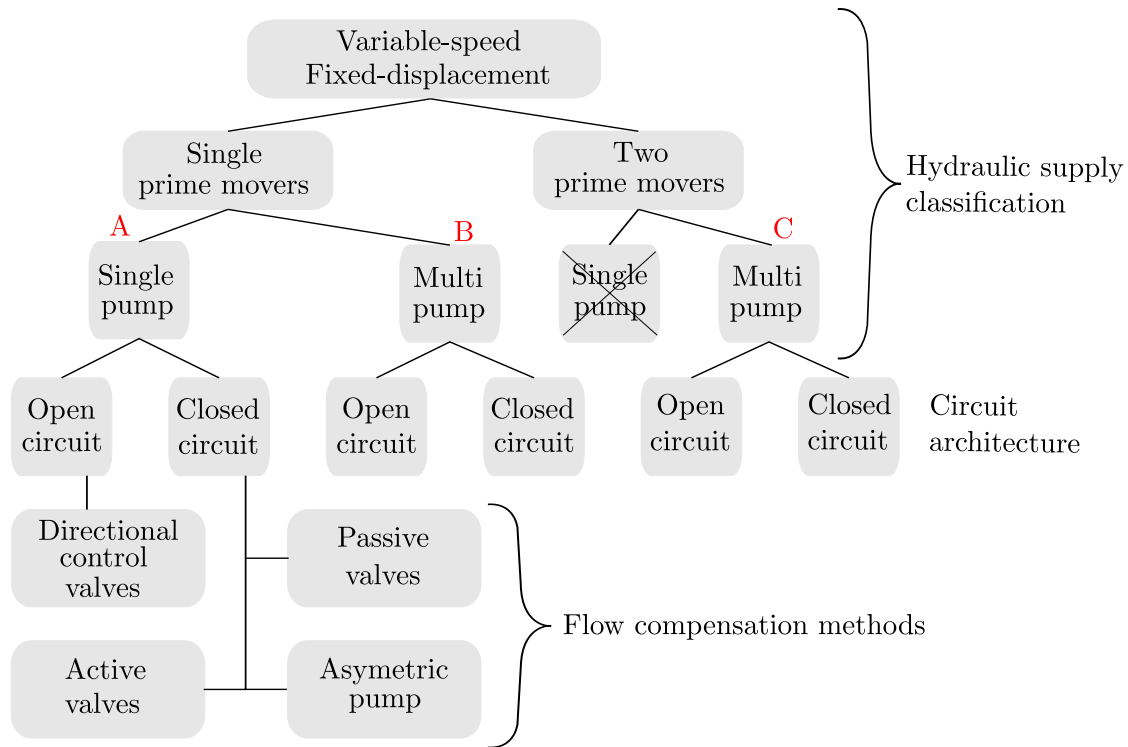
Figure 2.7: Classification of electro-hydraulic cylinders with a variable-speed electric prime mover and a fixed-displacement hydraulic unit [40].

Table 2.1: Comparison of the characteristics of three of the classes studied in [40]. Four different grades are used, ranging from $(--)$ to $(++)$, with $(--)$ being the worst.

Characteristics	Class A	Class B	Class C
Ability to control drive stiffness	$-$	$-$	$++$
Ability to handle highly dynamic/switching loads	$--$	$+$	$++$
Drive compactness and flexibility	$++$	$++$	$+$
Hydraulic circuit simplicity	$+$	$++$	$++$
Control simplicity	$+$	$+$	$-$
Degree of scalability	$-$	$-$	$+$

From Fig. 2.7, class A, which includes a single electric prime mover and a single hydraulic pump/motor unit (P) arranged in a closed circuit (Fig. 2.8), is expected to be the cheapest alternative for doing preliminary experimental testing. Nonetheless, as highlighted in Tab. 2.1, this setup does not represent the most promising concept concerning controllability and scalability. Hence, in high power applications (i.e., torque above 180 Nm demanded by the electric prime mover), if a redundant capability is more important than cost and compactness, or if the drive stiffness or the ability to handle highly dy-
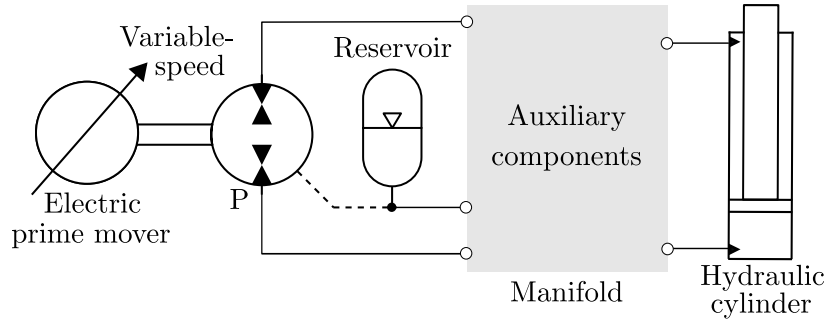
Figure 2.8: The self-contained electro-hydraulic cylinder architecture addressed in this research (simplified schematic) [31] © 2018 IEEE.

namic/switching loads is essential (e.g., in servo applications), class C would be a more suitable alternative. However, according to test results presented in the literature, class A represents a well-proven, self-contained architecture that can operate in all four quadrants and recover electric energy using off-the-shelf components. Furthermore, concerning the considered power range between 5 and 25 kW and the motion control requirements of typical offshore load-carrying applications, the self-contained architecture representing class A, as shown in Fig. 2.8 has been chosen as a starting point for this research on replacing inefficient valve-controlled cylinders.

As explained in the following, in addition to valves for passive flow compensation and load-holding, auxiliary components such as pressure-relief valves to prevent over-pressurization, anti-cavitation valves, a filter as well as a cooler (if necessary) are included in the EHC architecture. A single-rod cylinder is in many applications preferred because of its superior force density that allows a more compact layout. As a consequence, in closed-circuit configurations, methods for balancing the differential flow dictated by the unequal areas are essential to implement. As shown in Fig. 2.7, three main flow compensation methods are addressed in the literature using either active valves [41], passive valves [37, 42], or an asymmetric hydraulic unit [43–46]. Additionally, concepts using multiple fixed-displacement units [16, 35, 47–52] or two single-rod cylinders in parallel [53] are reported in the literature. Some problems related to instability and uncontrolled pressure oscillations are addressed involving the passive valves (e.g., shuttle valves [37] and pilot-operated check valves [54]), under highly dynamic/switching loads [34]. The passive method presented by [42] is further investigated since it represents a very simple approach where two pilot-operated check valves are installed between the pump and reservoir (e.g., an accumulator); this is similar to the commercial announced concept of Rexroth [21, 55]. The pilot-operated check valves are arranged in such a manner that each opening pilot line of the pilot-operated check valves senses the pressure of the opposite side in the closed circuit (Fig. 2.9).
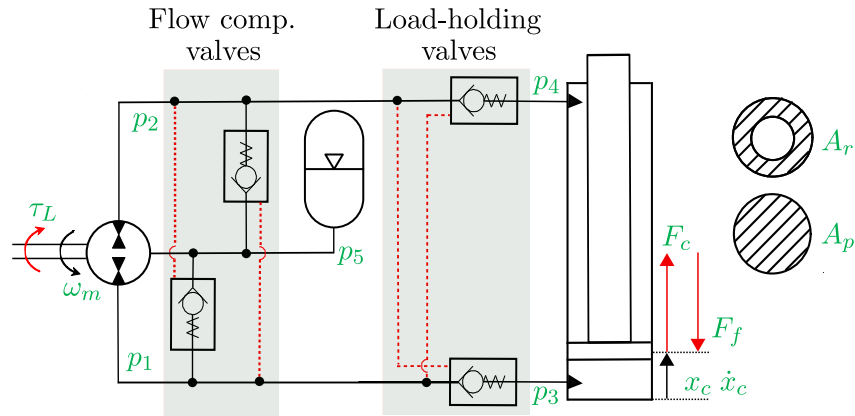
Figure 2.9: The identified state-of-the-art closed-circuit hydraulic transmission system with implemented passive flow compensation and load-holding valves (simplified schematic).

A more detailed review of the flow compensation methods is described in Papers B and C. Further, only a limited amount of research addresses the passive load-holding capability of EHCs. This feature serves the purpose of maintaining a given cylinder position without supplying any power to the system. An initial solution involves a commercialized system [29,56], where pilot-operated check valves are installed between the hydraulic unit and cylinder. It is here as well that the hydraulic connections are arranged in such a manner that each opening pilot line of the pilot-operated check valves senses the pressure of the opposite side (Fig. 2.9). A similar approach is also presented in the EHC concept announced by Rexroth [21,55]. However, this self-contained architecture is only capable of two-quadrant operations. Alternatively, passive load-holding devices grounded on counterbalance valves were studied in [36,57,58] for low-power EHCs.

The conclusion from this state-of-the-art survey is that the architecture proposed by [36,57] is the only EHC concept identified that may be considered as a compact and self-contained actuation system that can operate in four-quadrants with passive load-holding capability. However, since counterbalance valves are used as load holding valves, the actuator cannot regenerate energy since the pump needs to build up pressure in order to enable flow through the counterbalance valve. Hence, the concept of using pilot-operated check valves is considered for the self-contained EHC base line concept (Fig. 2.9) that is further investigated in Chapter 3.

2.3.2 Control Strategy

A traditional closed-loop position feedback control strategy, similar to what is used to control the position of state-of-the-art valve-controlled cylinders (Fig. 1.2), can also be used for EHCs having a variable-speed electric prime mover and a fixed displacement hy-

draulic unit [48]. In traditional offshore motion control applications a velocity feedforward and a deadband compensation element are also included [59]. However, in EHC concepts, the issue of deadband in the control valve (i.e., overlap in the valves' spool) is eliminated since a control valve is not used for motion control. Further, in the case of automatic operations, the HMI, based on commands from the operator, generates motion reference signals (i.e., the desired linear velocity ($\dot{x}_{c,ref}$) and linear position ($x_{c,ref}$)) to the linear motion controller (Fig. 2.10). During manual operation, the operators' joystick signal is provided directly to the velocity feedforward, and the feedback controller is disabled, i.e., operator in the loop control. The linear motion controller consists of the combination of two blocks, namely the velocity feedforward element and the position feedback controller.
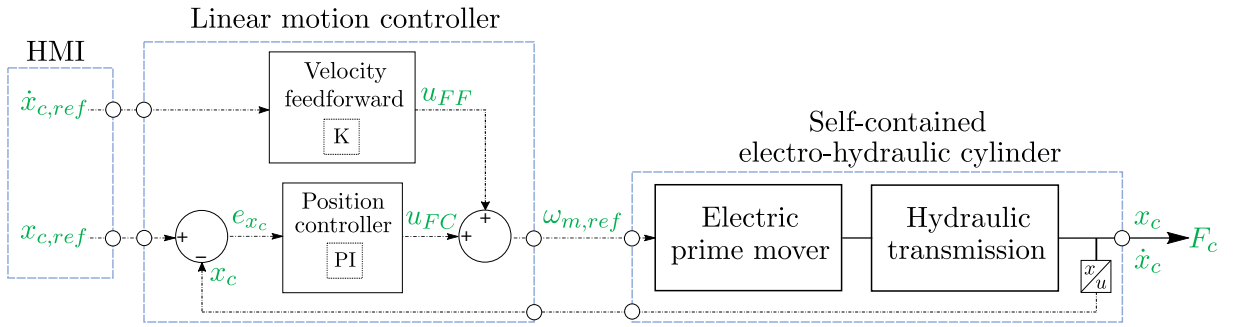
Figure 2.10: The self-contained electro-hydraulic cylinder's control structure.

The summation of the feedforward signal (u_{FF}) and the position feedback control signal (u_{FC}) represents the desired control input to the electric prime mover by

$$\omega_{m,ref} = u_{FF} + u_{FC}. \tag{2.12}$$

The feed forward signal is derived, depending on the operation condition, by

$$u_{FF} = \begin{cases} \frac{A_p}{D_P \cdot \mu_{vol}} \cdot \dot{x}_{c,ref}, & \text{if } \dot{x}_c \geq 0 \text{ and } \Delta p_P \geq 0 \text{ (i.e., I quadrant)} \\[2ex] \frac{A_r \cdot \mu_{vol}}{D_P} \cdot \dot{x}_{c,ref}, & \text{if } \dot{x}_c \geq 0 \text{ and } \Delta p_P < 0 \text{ (i.e., II quadrant)} \\[2ex] \frac{A_r}{D_P \cdot \mu_{vol}} \cdot \dot{x}_{c,ref}, & \text{if } \dot{x}_c < 0 \text{ and } \Delta p_P < 0 \text{ (i.e., II quadrant)} \\[2ex] \frac{A_p \cdot \mu_{vol}}{D_P} \cdot \dot{x}_{c,ref}, & \text{if } \dot{x}_c < 0 \text{ and } \Delta p_P \geq 0 \text{ (i.e., IV quadrant)} \end{cases}, \tag{2.13}$$

where A_p is the piston area, A_r piston rod-side area, D_P the hydraulic units' displacement, and μ_{vol} the constant volumetric efficiency, e.g., $\mu_{vol} = 0.95$. Finally, the control signal from the position feedback controller is given by

$$u_{FC} = e_{x_c} \cdot \left(k_P + k_I \cdot \frac{1}{s} \right), \tag{2.14}$$

where $e_{x_c} = x_{c,ref} - x_c$ is the measured position error, k_P the proportional gain, and k_I the integral gain.

2.3.3 System Modeling

Assuming that the dynamic response of the electric prime mover is significantly faster than the hydraulics, the prime movers' dynamics can be represented by

$$G_m(s) = \frac{\omega_m(s)}{\omega_{m,ref}(s)} = \frac{\omega_{n,m}^2}{s^2 + 2 \cdot \omega_{n,m} \cdot \zeta_m \cdot s + \omega_{n,m}^2}, \tag{2.15}$$

where $\omega_{n,m}$ is the natural frequency and ζ_m is the damping ratio of the second-order transfer function.

The hydraulics is modeled using a well-established approach that has been successfully tested in the past, e.g. by [41]. The well-known pressure build-up equation is applied several times to evaluate the systemic pressure (e.g., p_{1-5} labeled in Fig. 2.9) by

$$\dot{p}_i = \frac{\beta_{oil,i}}{V_i} \cdot \left(\sum Q_i - \dot{V}_i \right), \tag{2.16}$$

where $\beta_{oil,i}$ is the effective bulk modulus of hydraulic fluid, V_i is the volume of the fluid, $\sum Q_i$ is the net-flow entering or leaving the ith hydraulic volume, and $\dot{V}_i$ is the displacement flow (i.e., the time derivative of the expansion). The effective bulk modulus of the ith hydraulic capacitance is modeled by

$$\beta_{oil,i} = \frac{1}{\frac{1}{\beta_{oil,0}} + \varepsilon_{air,i} \cdot \left(\frac{1}{(p_i + p_{atm}) \cdot \kappa_{air}} - \frac{1}{\beta_{oil,0}} \right)}, \tag{2.17}$$

where $\beta_{oil,0}$ is the bulk modulus of the hydraulic fluid and $\varepsilon_{air,i}$ the effective volumetric air content derived by

$$\varepsilon_{air,i} = \frac{1}{\frac{1-\varepsilon_{air,0}}{\varepsilon_{air,0}} \cdot \left(\frac{p_{atm}}{p_i} \right)^{\frac{1}{\kappa_{air}}} + 1}, \tag{2.18}$$

where $\varepsilon_{air,0}$ is the volumetric air content of the hydraulic fluid at atmospheric pressure (p_{atm}), and κ_{air} is the adiabatic air constant. The volumes of the transmission lines are assumed to be constant whereas the equations related to the actuator require the piston areas, piston position, and maximum cylinder stroke (h_c). The capacitance (C_i) used in the pressure build-up equation associated with the hydro-pneumatic accumulator (Fig. 2.9) is represented by

$$C_5 = \frac{V_{5,0}}{\beta_{oil,5}} + \frac{V_{acc}}{\kappa_{air}} \cdot \frac{p_{acc,0}^{\frac{1}{\kappa_{air}}}}{p_5^{\frac{\kappa_{air}+1}{\kappa_{air}}}}, \tag{2.19}$$

where V_{acc} is the effective accumulator gas volume, and $p_{acc,0}$ is the the pre-charge pressure in the accumulator.

Concerning flow rates, the contributions ascribed to the different components are clarified in the sequel. The flow rates through the pilot-operated check valves are computed using the orifice equation:

$$Q_i = C_{d,i} \cdot A_{d,i} \cdot x_{V,i} \cdot \sqrt{\frac{2}{\rho} \cdot |\Delta p_{V,i}|} \cdot \text{sign}(\Delta p_{V,i}), \qquad (2.20)$$

where $\Delta p_{V,i}$ is the pressure differential across the i$^{\text{th}}$ valve, $C_{d,i}$ the discharge coefficient, $A_{d,i}$ the discharge area, ρ the density of the hydraulic fluid, and $x_{V,i}$ the relative valve opening. Regarding the pilot-operated check valves, when they are not closed, two operating modes characterize their function (i.e., the "normal flow" condition takes place when the pilot stage is detached from the poppet and the valve is subjected to "reverse flow" if both the pilot stage and poppet are in contact). The poppet lift results from the force equilibrium that is expressed differently depending on the flow condition:

$$x_{POCV,i} = \begin{cases} \frac{(p_{i,in} - p_{i,out}) \cdot A_{s,i} - F_{S0,i}}{k_{S,i}}, & \text{normal flow} \\ \frac{(p_{x,i} - p_{i,in}) \cdot A_{x,i} + (p_{i,in} - p_{i,out}) \cdot A_{s,i} - F_{S0,i}}{k_{S,i}}, & \text{reverse flow} \end{cases}, \qquad (2.21)$$

where $p_{i,in}$ is the inlet pressure, $p_{i,out}$ the outlet pressure, $A_{s,i}$ the area of the poppet seat, $A_{x,i}$ the area's pilot stage, $p_{x,i}$ is the pilot pressure, $k_{S,i}$ the spring stiffness, and $F_{S0,i}$ the springs' pre-load force. The poppet dynamics is simulated via a first-order transfer function. Next, the flow rate of both the check valves and the pressure-relief valves is computed by

$$Q_i = \begin{cases} 0, & \text{if } p_{i,in} < p_{i,out} + p_{i,cr} \\ k_{V,i} \cdot (p_{i,in} - p_{i,out} - p_{i,cr}), & \text{if } p_{i,in} \geq p_{i,out} + p_{i,cr} \end{cases}, \qquad (2.22)$$

where $k_{V,i}$ is the valve flow gain, and $p_{i,cr}$ the cracking pressure.

The effective magnitudes of the hydraulic unit are evaluated by means of flow losses ($Q_S \geq 0$) and torque losses ($\tau_S \geq 0$) derived from steady-state experimental data [60] of a reference axial-piston unit with displacement equal to $D_{P,ref}$. Equal losses are assumed for all quadrants and are scaled to the desired displacement (D_P) by using the scaling laws that refer to the quantities of the reference unit:

$$\lambda = \sqrt[3]{\frac{D_P}{D_{P,ref}}} \rightarrow \begin{cases} Q_S &= \lambda^2 \cdot Q_{S,ref} \\ \tau_S &= \lambda^3 \cdot \tau_{S,ref} \end{cases}, \qquad (2.23)$$

where λ is the scaling factor, Q_S the flow losses, and τ_S the torque losses. Next, the effective flow rate of the hydraulic unit is given by

$$Q_{P,e} = D_P \cdot \omega_m - Q_S \cdot \text{sign}(\Delta p_P), \qquad (2.24)$$

where $\Delta p_P = p_1 - p_2$ is the pressure drop across the hydraulic unit. The flow rate direction is dictated by the rotational direction of the prime mover, and the sign convention accounts for the direction of the leakage flow that is forced to go from the high-pressure port to low-pressure port. The flow losses are completely attributed to internal leakages, and the pressure losses in the transmission lines, cooler, and filter are neglected mainly due to the drive's compact configuration.

The mechanical output force of the actuator is determined by

$$F_c = p_3 \cdot A_p - p_4 \cdot A_r - F_{f,ehc}, \tag{2.25}$$

where p_3 is the piston chamber pressure, p_4 the rod chamber pressure, and $F_{f,ehc}$ is the cylinders' friction force described by the Stribeck friction model:

$$F_{f,ehc} = f_v \cdot \dot{x}_c + \tanh(\dot{x}_c \cdot a) \cdot \left(F_C + f_S \cdot e^{-\frac{\dot{x}_c \cdot \tanh(\dot{x}_c \cdot a)}{\tau_{fS}}} \right), \tag{2.26}$$

where $\dot{x}_c$ is the velocity of the actuator, a is the constant value used in the tanh function, while the different coefficients account for the viscous friction (f_v), the Coulomb friction (F_C), the static friction (f_S) and the friction forces' time constant (τ_{fS}). Finally, the effective shaft load torque is determined by

$$\tau_L = \frac{D_P \cdot \Delta p_P}{2\pi} + \tau_S \cdot \text{sign}(\omega_m), \tag{2.27}$$

where the sign of Δp_P determines the torque direction, and the sign convention accounts for the direction of the torque losses.

Chapter Summary

This chapter presented the survey carried out in this research to identify more environmentally friendly alternatives that may serve as suitable replacements for conventional valve-controlled cylinders typically used in offshore load-carrying applications. Since the technical literature indicates some critical issues related to the mechanical transmission of electro-mechanical cylinders, an additional self-contained electro-hydraulic cylinder based on state-of-the-art configurations has been identified. Furthermore, the technical background in terms of numerical modeling and motion control of the two alternative actuator technologies, namely the electro-mechanical and electro-hydraulic self-contained cylinders, is presented. The next chapter explains the methodologies used and main results obtained from the study carried out with regard to applying the two identified self-contained cylinder concepts to two load-carrying application case studies.

Chapter 3

Research Methodology and Results

Two alternative linear actuator concepts, namely electro-mechanical and electro-hydraulic self-contained cylinders, were identified in Chapter 2. This chapter presents the methodologies used and main results obtained during this study with regard to replacing conventional valve-controlled cylinders (VCCs) in load-carrying applications with more environmentally friendly alternatives. First, two case studies involving two separate load-carrying applications and their operational sequences are presented. Secondly, the self-contained EMC and EHC are designed in accordance with these case studies. Since a suitable off-the-shelf EHC was not identified in the state-of-the-art review, a new EHC architecture is proposed and investigated in this research. Subsequently, the feasibility of the two self-contained cylinders is examined in the two case studies. Further, the proposed EHC is experimentally compared with the VCC benchmark system regarding motion performance and energy efficiency when driving a single-boom crane. Additionally, a more compact design of the EHC is studied for future implementation on the single-boom crane and compared with the EMC regarding design impact when replacing the original hydraulic cylinder. An overview of advantages and disadvantages when substituting a traditional VCC with either a self-contained EMC or EHC is then presented. Lastly, an additional survey is carried out in order to investigate if any computerized design tool exists that can automate the process of designing, analyzing, and comparing different types of actuation solutions for the purpose of finding the best actuation system for a given application.

3.1   Case Studies

The two considered load-carrying applications and their operational sequences are presented as follows.

3.1.1   The Pipe Racking Machine

The vertical pipe racking machine (PRM), as introduced in Chapter 1 and illustrated in Fig. 3.1, represents a relevant energy-saving scenario for testing the identified self-contained cylinders in comparison with conventional VCCs. The column is connected through rack and pinion systems to the upper beam (Fig. 1.2) and lower rail. The lower rail is mounted directly on the drill floor, whereas the upper beam is connected to the derrick (Fig. 1.1). The column includes an upper guide arm (UGA) and lower guide arm (LGA) that are designed to guide the top and bottom of the stand – while it is in motion – with the help of guide heads. The reach arm located in the middle is the main arm (MA); it is accountable for holding the stand in a secure grip with its gripper head. All reach arms are equipped with a conventional VCC, which allows for the extension and retraction (i.e., horizontal motion) necessary to position a stand either in the desired fingerboard slot or at the well-center. The PRM is designed to handle sections of drill-pipes, drill-collars, or casings up to 41 m long. It is also designed to handle up to 14 metric tonnes of payload. However, during a typically repetitive operation, as explained below, the payload is only around 1.5 metric tonnes. Two (redundant) AC drivetrains are located on both the upper trolley (Fig. 1.2) and lower trolley, controlling the horizontal movement of the column along the tracks. The winch located on top of the column (Fig. 1.2) is used to hoist and lower the main arm (i.e., the stand) using redundant AC drivetrains. Then, the redundant AC drivetrains located between the bottom of the column and lower trolley make it possible for the column to slew (rotate) on its vertical axis.

This operational sequence, as presented in Fig. 3.1b, is the professed tripping in/out cycle. It takes place when the drill-string is assembled or disassembled during a well-construction process. During this sequence, the PRM continually moves between the well-center and the fingerboard where the stands are stored. The leading specification rating of these machines is the tripping speed (i.e., how many stands can be moved between the well-center and fingerboard, or vice versa, per hour). In this study, the PRM and its operational sequence are used as a simulation case study when investigating the feasibility of replacing the remaining VCCs involved in motion control with self-contained cylinders. This case study was first introduced in [3] (Paper A) when the motion control of the main arm was considered for an off-the-shelf EMC. The mechanical system (Fig. 3.1a) is modeled using the multibody system library in MATLAB-Simulink. The model is based on the approach presented in Paper A, where a planar multibody system of the main arm was mathematically represented and simulated. Further, in Paper D, the two guide arms, column, lower trolley, and lower rail were also included in the numerical model to investigate the whole operational sequence. The motion profile of all actuators and the kinematics of the three reach arms are explained in detail in Paper D.

(a)

0-1: The MA gripper and GAs guide close around the stand, the winch lifts the MA (the stand) for 1 m and the arms retract from the well-center position to the inner reach position;

1-2: the PRM starts to trolley and rotates 180°;

2-3: the PRM continues to trolley until reaching the set-point (a 9 m traveling is performed);

3-4: the three arms extend until the set-point of 4 m is reached, the stand is lowered for 2 m to the floor, and the main arm gripper and guide arms guide open while the machine returns back to well-center in reverse steps.

(b)

Figure 3.1: The vertical pipe racking machine: (**a**) CAD assembly; (**b**) operation sequence steps of the reach (R), the winch (W), the trolley (T), and the slew (S) motion, when moving a stand from the well-center to the desired fingerboard slot (simplified top-view).

3.1.2 The Single-Boom Crane

The single-boom crane shown in Fig. 3.2a is chosen as a second case study since it represents a relevant mechanism to several load-carrying applications (e.g., the main boom of knuckle boom cranes) and combines different operating conditions, including motion against both resistant external loads and overrunning external loads, i.e., the I quadrant and IV quadrants, respectively, as shown in Fig. 3.6. It also offers the opportunity of testing the essential passive load-holding capability. Furthermore, the crane application is available at the University of Agder for experimental testing, including a state-of-the-art VCC with passive load-holding capability, and hydraulic power supplied by a centralized HPU. The test setup was built explicitly for having a flexible structure in the crane boom,

25

Figure 3.2: The single-boom crane: (**a**) CAD assembly illustrating the implementation of the original hydraulic cylinder; (**b**) simplified schematic of the equivalent load model applied to the hydraulic cylinder illustrating the high-pressure piston-side (p_3) and the low-pressure rod-side (p_4) ports.

which induces pressure oscillations in the hydraulic cylinder that represent a challenging (worst-case) scenario involving motion control of load-carrying applications, which are typically subjected to a harsh offshore environment. The case study is investig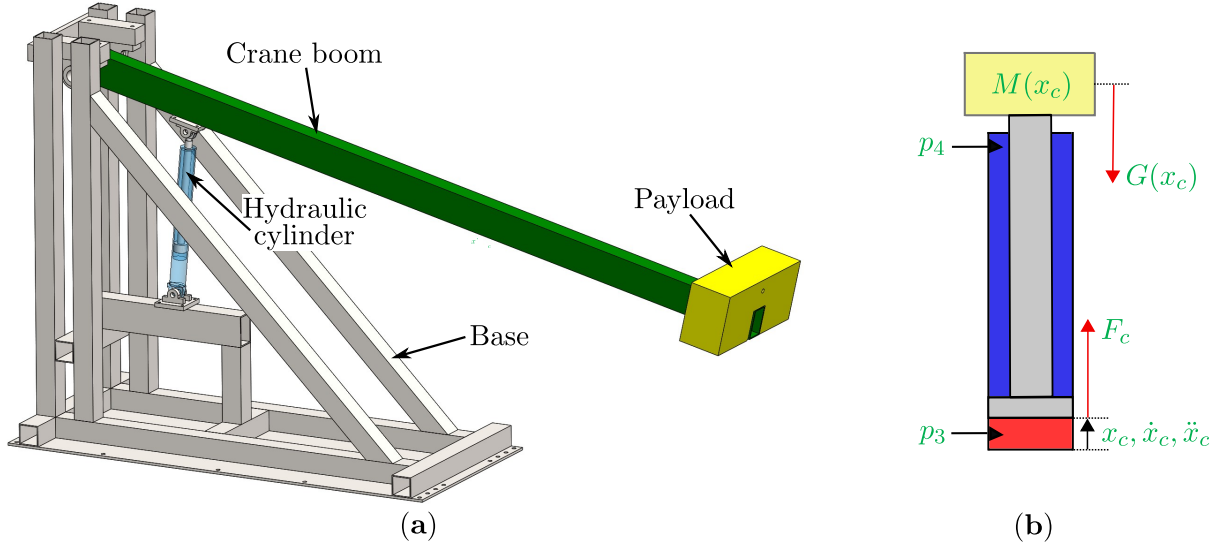ated when lifting and lowering the crane boom (i.e., the linear actuator is extended and retracted) at different velocities. The single-boom crane case study was first introduced in [32] (Paper C) and further used in Paper E,F,G, and H.

Two numerical models representing the mechanical system of the single-boom crane are derived for system simulations when interfacing with the investigated linear actuation systems. A rigid equivalent nonlinear load model (Fig. 3.2b) was derived in Paper C based on Lagrangian mechanics to extract the actuator dynamics:

$$M(x_c) \cdot \ddot{x}_c = F_c - G(x_c), \tag{3.1}$$

where F_c is the mechanical force delivered by the linear actuator, $\ddot{x}_c$ is the linear acceleration, and M and G are, respectively, the equivalent mass and gravitational load as a function of the actuators' effective stroke, i.e., the linear position (x_c). Next, a flexible multibody model was derived in [5] (Paper E) based on the finite segment method [61] to investigate the use of pressure feedback to reduce the pressure oscillation. This approach, as further described by [62,63], serves the purpose of representing the relevant flexibility of the crane-boom. The numerical model is represented using the multibody system library in MATLAB-Simulink.

3.2 Design Analysis

Based on available information from manufacturers' catalogs, the off-the-shelf heavy-duty EMC from Rexroth [25] is considered to be a potential alternative to the conventional VCC. However, as discovered in Paper A, and reported in the technical literature, there are some critical issues related to the mechanical transmission system. Hence, an additional EHC based on state-of-the-art self-contained configurations is further investigated.

3.2.1 Sizing Principles

The principles used when sizing the electric prime mover as well as the drive system of the two self-contained cylinder technologies are presented as follows.

Electric Prime Mover

The electric drive that serves as the prime mover in the self-contained cylinders includes the variable-frequency drive that is connected to the electrical three-phase grid controlling the rotational motion of the electric machine. As explained in [64] © 2020 IEEE (Paper H), the components of the electric prime mover are chosen based on the following steps:

1. determine the requirements such as the maximum and continuous speed, torque, current, and power requirements of the considered work cycle;

2. select the supply unit and PMSM combination;

3. identify the desired control performance and required interface (i.e., communication standards, input/outputs, and safety features);

4. define the control function (e.g., open-loop or closed-loop controller architecture);

5. select any necessary accessories (e.g., mains filters and chokes, brake resistors/units, capacity modules, cables, and software).

The variable-frequency drive is sized for the continuous output current i_{cont} so that:

$$i_{cont} \geq \frac{\tau_{cont}}{\tau_0} \cdot i_0, \tag{3.2}$$

where τ_{cont} is the required continuous torque, and τ_0 and i_0 are the PMSMs' continuous torque and current at standstill, respectively. The continuous operating characteristic S1 (60K), according to EN 60034-1, is used when sizing the electric drive.

Electro-Mechanical Cylinder

According to common industrial practice, the EMC is designed based on the following steps [64] © 2020 IEEE:

1. select the type of screw assembly and its dimensions (i.e., diameter and lead) based on the required stroke length, average power and dynamic load requirements of the considered work cycle, and desired service life;

2. select the electric prime mover and gearbox combination based on the desired control performance, maximum and continuous speed, torque, and current requirements.

These aspects are addressed in detail in Paper H.

Electro-Hydraulic Cylinder

The EHC is designed based on the following steps [64] © 2020 IEEE:

1. size the cylinders' stroke capability according to the requirements of the application and size the piston and rod diameter based on the maximum load force and buckling criteria;

2. size the hydraulic unit based on the displacement and speed required to deliver the demanded flow dictated by the actuators' desired motion cycle;

3. size the electric prime mover in terms of maximum and continuous speed, torque, and current requirements;

4. size the hydro-pneumatic accumulator based on the exchange volume and desired maximum and minimum pressure in the reservoir;

5. size the load-holding valves so that the pressure drop is kept minimal in order to maintain an efficient throttle-less system (i.e., increased throttling may result in the need for an oil cooler) and select a proper pilot ratio and cracking pressure to ensure intended functionality;

6. size the flow balancing valves and the oil filter so that the reservoir pressure is kept below the pressure limits of the hydraulic components in order to ensure proper functionality;

7. size the pressure-relief valves based on the maximum allowed pressure of the hydraulic components and on the force limitations of the cylinder in order to satisfy the buckling criteria.

Details about the procedure mentioned above are outlined in Paper H.

3.2.2   Design of the Electro-Mechanical Cylinder

First, in Paper A an EMC is dimensioned and numerically investigated with a focus on feasibility when replacing the VCC of the PRMs' main arm. Due to the required stroke (travel length) of 1.7 m, which is the upper limit of the considered EMC, only the largest planetary roller-screw assembly was available (EMC-HD 180). According to the sizing principles, only the screw assembly having a diameter of 75 mm and a lead of 10 mm in combination with a directly mounted MSK-101E PMSM, and a gearbox found in the manufacturers' catalogue [25] having a 5:1 gear ratio was considered suitable.

Secondly, the single-boom crane case study that requires a shorter stroke (0.5 m) was considered in Paper H to investigate if an off-the-shelf EMC configuration is feasible for continuous operations, such as heave compensation systems or the studied tripping sequence of the PRMs' reach arms. Three suitable motor and gear combinations were identified from the manufacturers' catalog [25] using a ball-screw assembly having a diameter of 63 mm and a lead of 20 mm (EMC-HD 125). A larger screw assembly is expected to have a significantly longer service life. However, the initial length of the larger screw assembly (EMC-HD 150) is too long to fit inside the base of the crane (Fig. 3.3). Furthermore, only the timing belt side drive was considered since the direct mounting adds additional length. The EMC configuration, including the smallest (i.e., cheapest) electric prime mover configuration, has been chosen with the intention of being implemented on the single-boom crane in the future, as illustrated in Fig. 3.3.
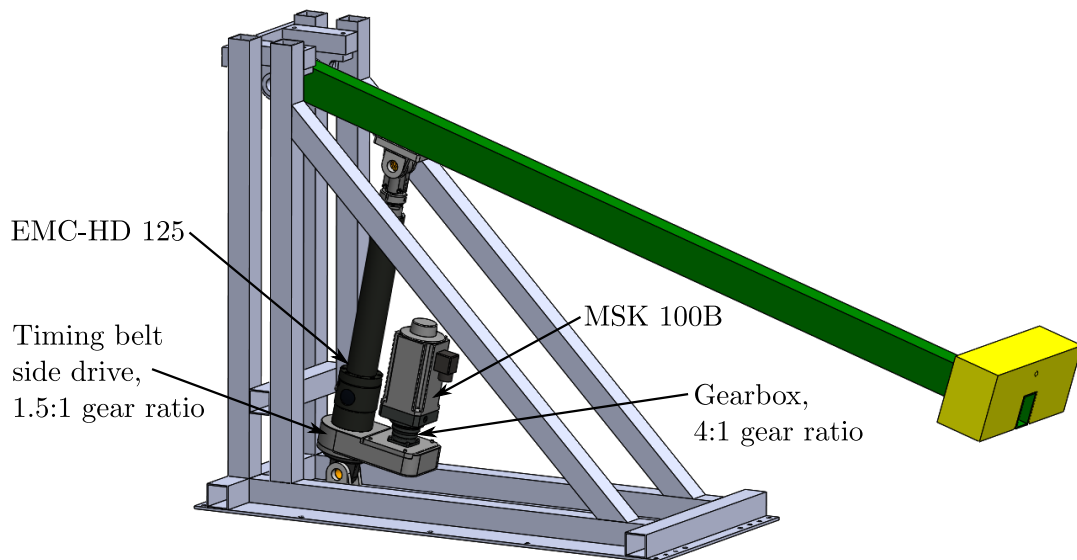

Figure 3.3: CAD assembly illustrating the implementation of the Rexroth heavy-duty electro-mechanical cylinder [25].

3.2.3 Design of the Electro-Hydraulic Cylinder

The identified self-contained EHC baseline concept, as presented in Fig. 2.9, is further investigated in this study. A high-fidelity mathematical representation of a preliminary EHC concept is first presented in Paper B in combination with a numerical investigation intended to evaluate the motion performance with passive-load holding in four-quadrant operations in view of future implementation. Further, in Paper C, the components of the investigated architecture (Fig. 3.5) are sized and selected from manufacturers' catalogs according to the requirements of the single-boom crane case study and dimensions of the original hydraulic cylinder. Lastly, in Paper D, the EHC components (model parameters) were scaled to the three reach arms' cylinders of the PRM case study.

Passive Load-Holding

The passive load-holding functionality identified in the state-of-the-art survey that is based on commercial EHCs using the pilot pressure from the opposite pump port (Fig. 2.9) is further investigated. This method, as demonstrated in Paper C, tends to be unstable since the check valves are unintentionally opened and closed during operation when the system must operate in all four quadrants. Hence, a considerable effort is carried out to identify a suitable method for controlling the pilot-operated check valves used for load-holding purposes.

A concept using two on/off electro-valves (Fig. 3.4a) was first proposed in Paper B based on inspiration from the concept of [65]. When the on/off valves are de-energized, the load-holding valves' pilot pressure is equal to the reservoir pressure. When they are energized, the pilot pressure is equivalent to the highest system pressure. Inspired by [66,67], the concept is then modified and presented in Paper C using a 3/2 electro-valve (EV) to control the pilot pressures (Fig. 3.4b).

Two different load-holding strategies are considered. Passive load holding takes place when motion is not desired, and the desired position is within the wanted error limit. The load-holding valves then close by deactivating the electro-valve signal u_{EV} according to the following logic:

$$u_{EV} = \begin{cases} 1, & |\dot{x}_{c,ref}| > 0 \text{ and } u_{ED} > 0 \\ 0, & |\dot{x}_{c,ref}| = 0 \text{ and } |e_{x_c}| < 0.5 \text{ mm} \end{cases}. \tag{3.3}$$

Next, in order not to consume electric energy in load-holding phases, the signal u_{ED} enabling torque on the electric machine is switched off when motion is not desired and the load-holding valves are closed. Conversely, active load holding is performed by controlling the desired piston position using the electric prime mover while the load-holding valves are kept open.
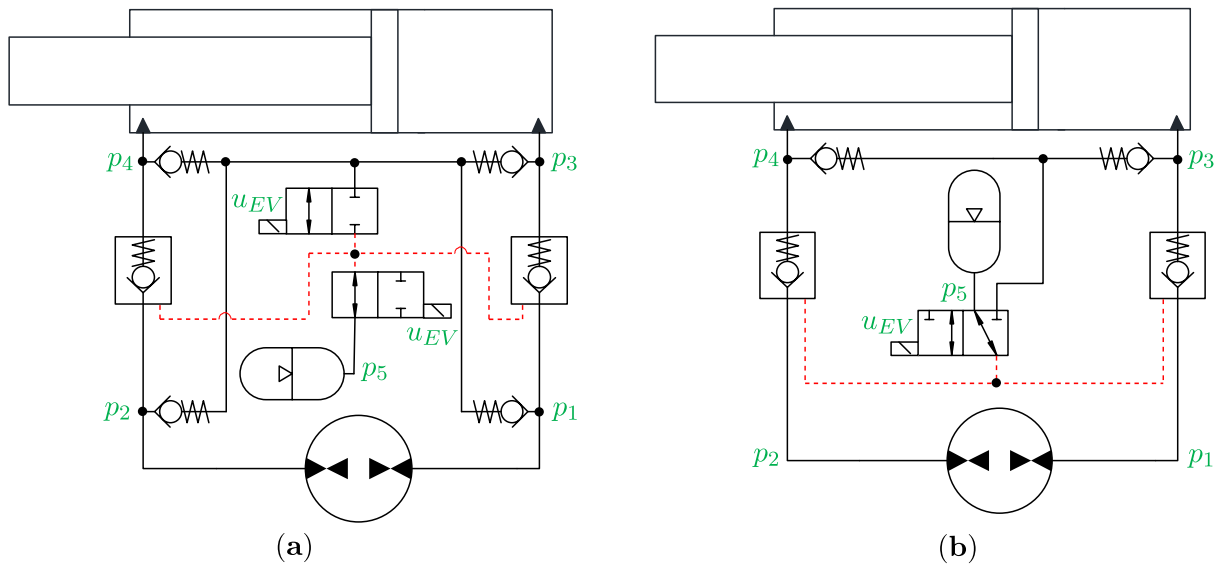
Figure 3.4: Simplified schematic of the studied passive load-holding circuits when $u_{EV} = 0$: (**a**) two on/off electro-valves; (**b**) 3/2 electro-valve.

Investigated Architecture

The EHC architecture proposed in this research (Fig. 3.5) can operate in four quadrants, includes passive load-holding devices, and can regenerate electric power.
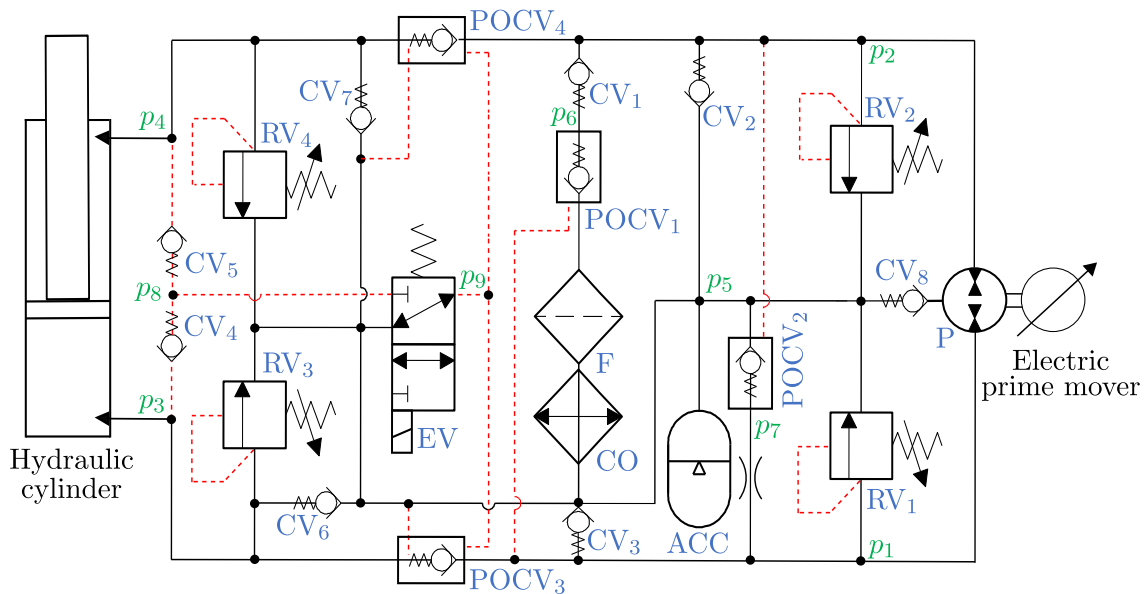
Figure 3.5: The novel self-contained electro-hydraulic cylinder addressed in this research.

The auxiliary components are implemented in a manifold, and the bladder-type accumulator (ACC) represents the sealed reservoir. The differential flow dictated by the cylinders' unequal areas is balanced by both the two pilot-operated check valves $POCV_1$ and $POCV_2$ as well as the check valves CV_1 and CV_2. Furthermore, CV_2 and CV_3 are installed to prevent cavitation in the hydraulic unit. The pilot-operated check valves

$POCV_3$ and $POCV_4$ are used as passive load-holding devices by isolating the cylinder
when the 3/2 electro-valve is not actuated. Motion is enabled when the electro-valve is
energized, resulting in transference of the highest cylinder pressure, selected through the
CV_4 and CV_5, into the opening pilot line of the load-holding valves. The check valves CV_6
and CV_7 are installed between the actuator sides and the accumulator to avoid cavitation
in the cylinder chambers. The pressure-relief valves (RV_1–RV_4) implemented on both
pump ports and on both cylinder ports, are installed to prevent over-pressurization. Fi-
nally, an oil cooler (CO) and a low-pressure filter (F) complete the hydraulics. Figure 3.6
takes advantage of a simplified system representation to outline the operating condition
in each quadrant.
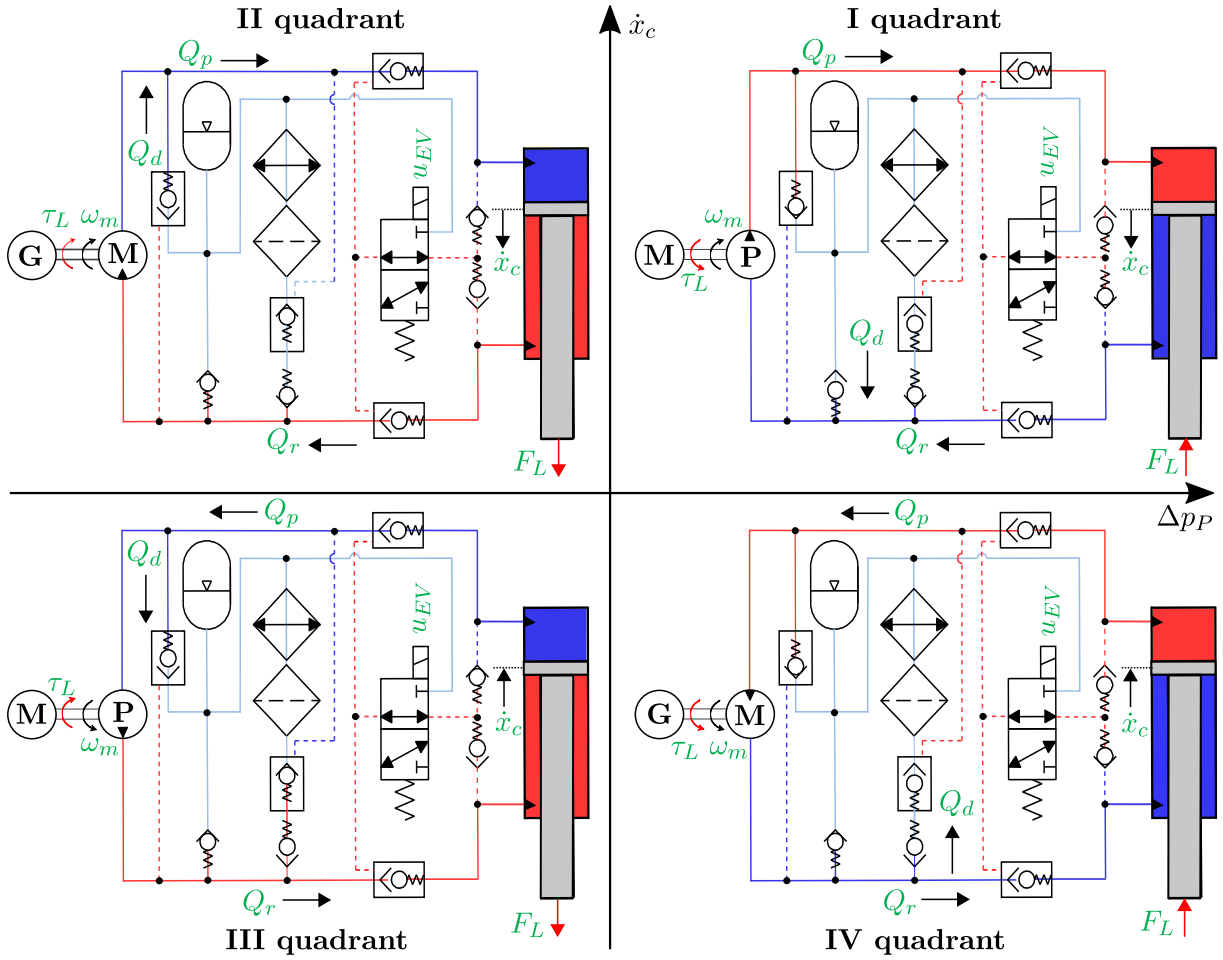
Figure 3.6: Simplified illustration of the self-contained electro-hydraulic cylinder func-
tioning in four quadrants when $u_{EV} = 1$. **P** denotes that the hydraulic unit is operating
as a pump, **M** – the hydraulic unit and the electric machine is operating as a motor, and
G – the electric machine is operating as a generator.

Flow directions and pressure levels are highlighted: the red color indicates the high-
pressure side, the blue color indicates the low-pressure side, Q_p is the cylinder flow on
the piston-side, Q_r is the cylinder flow on the rod-side, and $Q_d = Q_p - Q_r$ represents the

differential flow. For any given speed of the electric prime mover, the actuator velocity is higher in the left half-plane because the flow through the hydraulic unit is going to (or is coming from) the actuators' rod-side chamber, which has a smaller piston area than the piston-side. Furthermore, it should be noted that this systemic architecture fits particularly well with applications characterized by frequent overrunning loads acting on the actuator (e.g., cranes). The differential flow is forced to go through both the filter and oil cooler when the EHC is operating in the IV quadrant (i.e., when lowering the crane boom), thereby ensuring proper fluid conditioning.

3.3   Feasibility Studies

The feasibility of replacing conventional VCCs with either of the two considered self-contained cylinder concepts is investigated through simulations in both case studies. Additionally, the proposed EHC concept is implemented and examined when connected to the original hydraulic cylinder of the single-boom crane.

3.3.1   Application of the Electro-Mechanical Cylinder

Based on a literature survey and numerical investigation of replacing the VCC of the PRMs' main arm, Paper A discusses advantages and disadvantages related to the reliability, safety, and durability of EMCs with respect to the design criteria of offshore drilling applications. Based on this investigation, it has been determined that the considered off-the-shelf EMC [3]:

- provides good energy-efficiency, simple installation (plug and play), low maintenance, high stiffness (accuracy), and reduced space occupation on the offshore installation in comparison to the centralized hydraulic power supply and piping;

- has low durability at high load force due to wear and tear on the transmission screw, and little overload protection against shock loads;

- is nevertheless an appealing alternative to VCCs since it allows for the elimination of local hydraulic circuits and removal of the fluid spill risk;

- has the potential to reduce maintenance costs due to the absence of weak parts such as seals and hoses, which are subjected to the harsh environment of the oil drilling process;

- requires electric power only when it is needed, compared to centralized powered VCCs where a continuous load on the HPU must be ensured regardless of whether or not the hydraulic power is used for actuation;

- has high static load capabilities; however, the permissible transmitted power will limit productivity considerably.

Also, an off-the-shelf EMC with long stroke (travel) and high load capabilities certified for ATEX, which is necessary for most oil drilling equipment, was not identified. However, there exist PMSMs that are ATEX certified, and the mechanical transmission system has the potential to become certified for this requirement.

It is also worth noting that for the commercially available configurations considered in this research, only the largest planetary roller-screw assembly is possible for the PRMs' main arm cylinder because of the required stroke of 1.7 m. The planetary roller-screw has higher friction losses compared with the ball-screw. Consequently, based on the manufacturers' recommendations [25], avoidance of overheating in the transmission screw cannot be guaranteed without reducing the average speed of the investigated motion cycle. Alternatively, customization, such as adding external cooling or applying a transmission screw with a larger dimension, has the potential to increase the permissible power.

Finally, as explained earlier, an off-the-shelf EMC was successfully designed for continuous operation on the single-boom crane case study based on common industrial practice. However, experimental verification of the proposed design is necessary and is considered as further work.

3.3.2   Application of the Electro-Hydraulic Cylinder

First, in Paper C, the proposed EHC concept (Fig 3.5) was implemented and tested when driving the single-boom crane (Fig. 3.7), and a high-fidelity model representing the proposed EHC was experimentally validated. Furthermore, pressure feedback was implemented on the control algorithm and empirically tuned, resulting in considerably increased position tracking performance. Next, in Paper D, the EHC components (model parameters) were scaled to the three reach arms' cylinders of the PRM case study, and the energy-saving potential was numerically analyzed in comparison to the simulated valve-controlled system supplied from a central hydraulic power unit.

Experimental Testing

The experimental testbed depicted in Fig. 3.7 was built and commissioned to drive the single-boom crane with the proposed EHC concept. Details about the self-contained system are described earlier in Section 3.2.3, while the components used to implement and analyze this solution are presented in Paper C and G. Communication between the embedded programmable logic controller (PLC) where the linear motion control algorithm is implemented and the servo-drive (SD) (i.e., the variable frequency drive and control
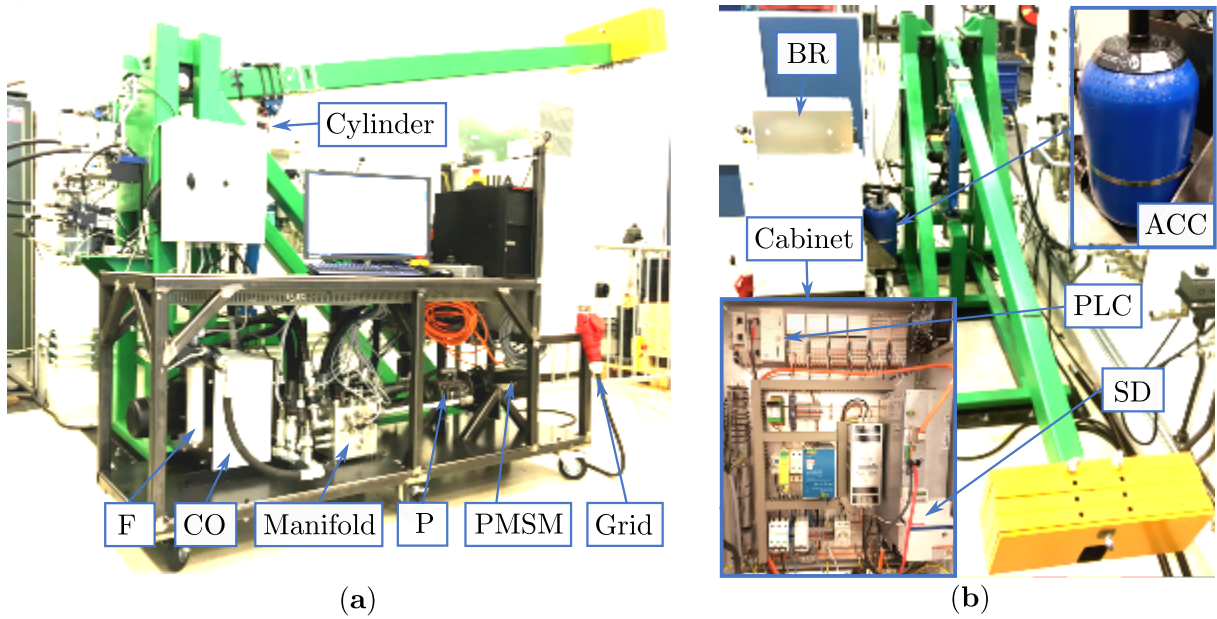
Figure 3.7: The proposed self-contained electro-hydraulic system implemented on the single-boom crane: (**a**) overview of the portable testbed interfacing with the electrical grid and hydraulic cylinder; (**b**) detailed view of the single-boom crane, the accumulator, the braking resistor, and the cabinet dedicated to the PLC and the servo-drive.

module) is processed through a Sercos signal bus interface with 250 μs sample rate. Besides the measured electric power, all data is processed through a real-time interface (i.e., UDP send/read with a 1 ms sample rate) between the PLC and a desktop computer using the Simulink real-time library. The test data from the measured electric power was first obtained at a 50 ms sample rate using a power analyzer and then further processed in the MATLAB-Simulink environment. Lastly, mineral oil ISO VG 46 was used as hydraulic fluid.

The initial open-loop testing (i.e., only the velocity feedforward part of the motion controller shown in Fig. 2.10 is activated) confirms that the combination of the highly flexible structure of the crane boom and the low damping nature of the self-contained hydraulic system result in induced pressure oscillations, as shown in Fig. 3.8.

Moreover, when the EHC is controlled in a closed-loop according to the standard motion control strategy (Fig. 2.10), the PI-controller gains must be selected at a significantly low level in order to avoid increasing oscillations in the crane boom during motion, resulting in poor position tracking performance. Consequently, a pressure-feedback approach was implemented on the control structure to add artificial damping that allows for significantly higher PI-controller gains and cancellation of pressure fluctuations in the hydraulic system. The improved motion controller and active damping feature are explained later in this chapter along with the motion performance and energy efficiency results.
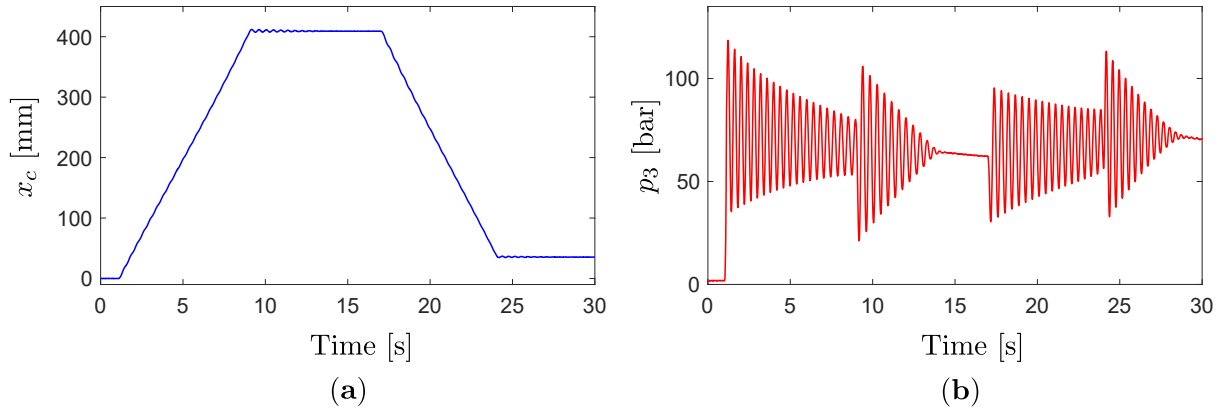
Figure 3.8: Induced oscillations [32]: (**a**) piston position; (**b**) piston-side pressure.

In addition, a minor adverse effect on the motion performance caused by the passive load-holding functionality has been identified. As pointed out in Paper F, there is a reduced pressure spike in the piston-side chamber when the load-holding is commanded, causing a minor position drop of 1.7 mm in closed-loop motion control. Furthermore, the position drop increases even more (depending on the piston position) when the crane is controlled in open-loop. This issue has been further investigated, and the load-holding control was improved using a pressure control strategy that eliminates the position drop. However, this improvement has not been included in this dissertation and is considered as further work since the results will be published in a forthcoming paper.

During continuous testing when lifting and lowering the crane-boom, it was discovered that heat generation in the hydraulic system is minimal. Moreover, when the oil cooler is bypassed, there was no sign of temperature increase in the hydraulic fluid that was measured in several places in the hydraulic circuit. Since the investigated testbed was not built to be utterly compact at this stage of the research, investigating the thermal effect is considered to be further work. See, for instance, [68–70], concerning studies on the thermal aspects of self-contained EHCs.

Energy Saving Potential

A new layout (Fig. 3.9) for the motion control of the PRM was proposed in Paper D to benefit from the regenerative capability of EHC. The main idea is to replace the original flow requiring VCCs with EHCs to remove the requirement for an external hydraulic supply. It is assumed that the remaining hydraulic actuated auxiliary functions of the PRM can be powered from a minor internal HPU. Hence, only electric power is distributed to the PRM. To fully exploit available new technologies in electric drives and the connectivity trend in the ongoing fourth industrial revolution (Industry 4.0), a common DC bus distribution is proposed in combination with a decentralized servo-drive for each of the
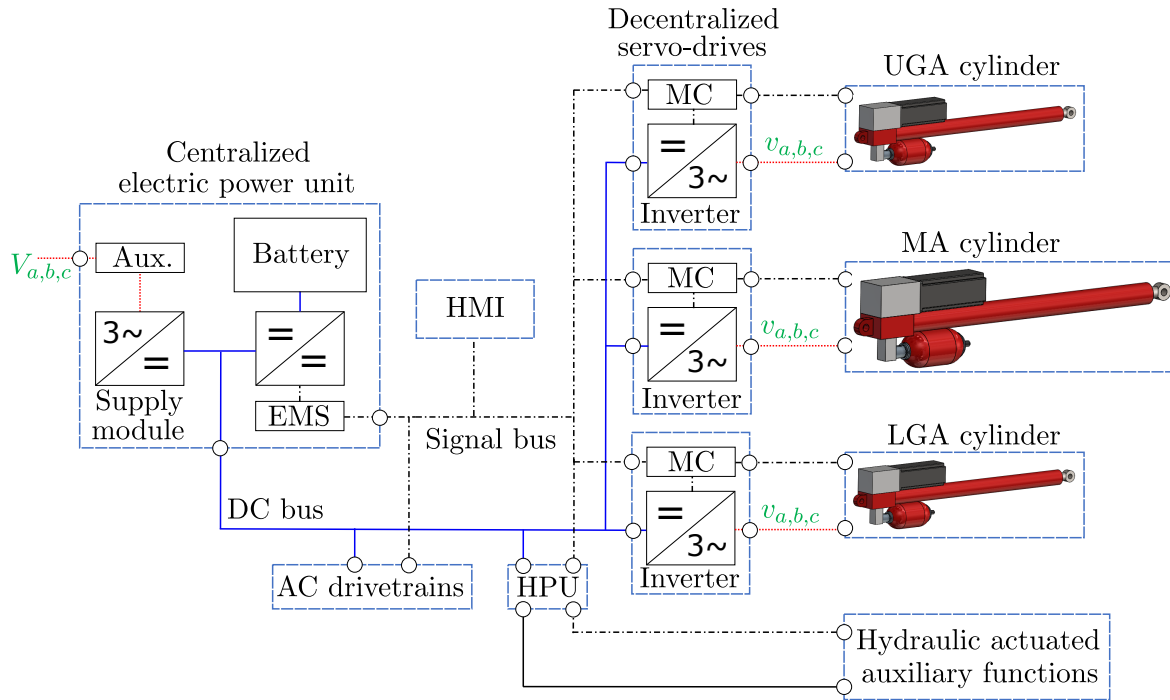
Figure 3.9: Proposed electric power distribution layout when using self-contained electro-hydraulic cylinders in combination with existing AC drivetrains and an internal HPU.

actuators. The servo-drive placed near the electric machine consists of the inverter and motion control module (MC). The considered motion controller combines the standard control structure of the electric prime mover explained in Section 2.1, with a control architecture and additional feedback signals that ensure the cylinder position and active damping. The DC bus is powered from a centralized electric power unit, including the auxiliary components such as the mains filter and choke, the supply module that converts the AC voltage from the electrical grid to a DC bus voltage, and the electro-chemical storage unit (i.e., the battery). The battery is connected to the DC bus through a DC/DC converter and controlled by the energy storage management system (EMS). The battery can be used for energy storage when the electric prime movers are regenerating power, i.e., when the main arm is extending, the guide arms are retracting, the winch is lowering, and the drivetrains of the travel or slew motion are braking. The battery can be used either for emergency operations in case of power shutdown or to reduce the use of diesel generators to supply electricity to the offshore installation [7]. Lastly, the HMI includes the control system, emergency stop modules for safety functionalities, and the motion trajectory generators of the individual actuator. The control system (e.g., a PLC) communicates with the decentralized servo-drives and energy storage management system using a standard bus communication protocol, e.g., Profibus, Modbus, Sercos, etc.

When considering the total energy of the mechanical system, assuming 100% efficient energy recovery, there is a potential for the PRM case study to regenerate 27.5% of

the consumed energy during the operational sequence. However, due to the losses in the electric prime movers (13%), the hydraulic units (32%), and the combined friction losses in the hydraulic cylinder end mechanical system (15%), a significant portion of the potential regenerative energy is dissipated. When considering the three reach arms, only 6% of the total energy can potentially be recovered. However, if a hydraulic unit with better efficiency is used (e.g., a constant efficiency of 90%), the potential regenerated energy could be increased up to 45%. Compared to the original VCCs, the energy-saving potential of using EHCs is 83% without affecting the systems' performance. Furthermore, applying a more efficient hydraulic unit to the EHCs results in an energy-saving potential of 91% (88% when considering a more efficient pump for the centralized HPU).

3.4   Comparative Analysis

Experimental comparison has been carried out in this research to identify if the proposed self-contained EHC is a suitable alternative to state-of-the-art VCCs. Additionally, Paper H, investigates the design impact when replacing the conventional hydraulic cylinder with either of the two self-contained cylinder technologies. The work has been carried out on the single-boom crane case study with a focus on both the motion performance (Paper F) and energy efficiency (Paper G) of the complete actuation systems. A common control strategy and a model-based design approach have been used in order to make an impartial comparison between the self-contained EHC and benchmark system.

3.4.1   The Benchmark System

The VCC, when taken into account as the benchmark system (Fig. 3.10), consists of a centralized hydraulic power unit providing a constant supply pressure (p_S) and fixed return pressure (p_R) as well as the drain (p_D) to the valve-controlled system. The components of the HPU are the AC induction motor (IM) driving the variable-displacement axial piston pump (P) at a constant speed. The pressure level of the supply pressure is controlled by the absolute pressure limiter, while a pressure-relief valve (RV) is installed for safety.

The linear motion controller explained in the following sends a control signal u_V to the pressure-compensated, proportional directional control valve (PDCV) controlling the motion of the hydraulic cylinder. The state-of-the-art flow control valve contains two essential elements, namely the main spool with integrated closed-loop position control and the pressure compensator (PC). The pressure compensator ensures a constant pressure drop across the metering edge, which in turn provides a load-independent flow and deadband, simplifying the complexity of the feedback controller to achieve satisfactory motion performance. Furthermore, the pressure compensator reduces any disturbance from other
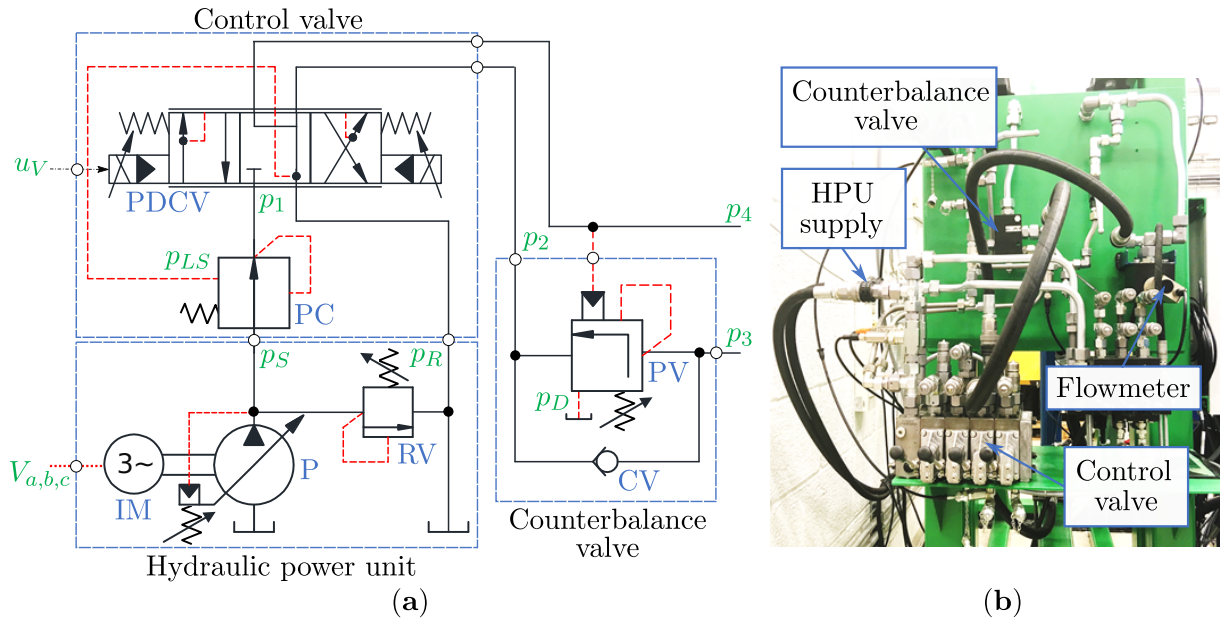
Figure 3.10: The centralized powered valve-controlled system implemented on the single-boom crane: (**a**) simplified schematic of the hydraulic system; (**b**) detailed view of the hydraulic test setup interfacing with the hydraulic power unit and cylinder.

VCCs connected to the same hydraulic power supply. The considered load-holding valve, a vented counterbalance valve with a pilot ratio 3:1, consists of a by-pass check valve (CV) and a pilot-operated poppet valve (PV) for controlling an overrunning load (i.e., when lowering the crane boom). Lastly, the VCC test setup has instruments with sensors for measuring the pressures labeled in Fig. 3.10a, as well as the rod-side flow rate and linear position. Figure 3.10b depicts a portion of the valve-controlled test setup. Details about the components used to implement and analyze this solution are presented in Paper G.

3.4.2 Improved Motion Control

Pressure feedback was successfully implemented in the control structure (Fig. 3.11) and tested on the EHC in Paper C, in order to actively damp out the induced oscillations.

The same approach is also investigated in Paper E and tested on the benchmark system, resulting in significant improvements. Further, in Paper F, a model-based design approach using validated linear models is performed to select proper parameters for the linear motion controller and high-pass filtered pressure feedback of both the EHC and benchmark system.

Pressure Feedback

Pressure feedback adds artificial damping to the hydraulic system. When analyzing the linearized system model presented in Paper F, it is demonstrated that pressure feed-
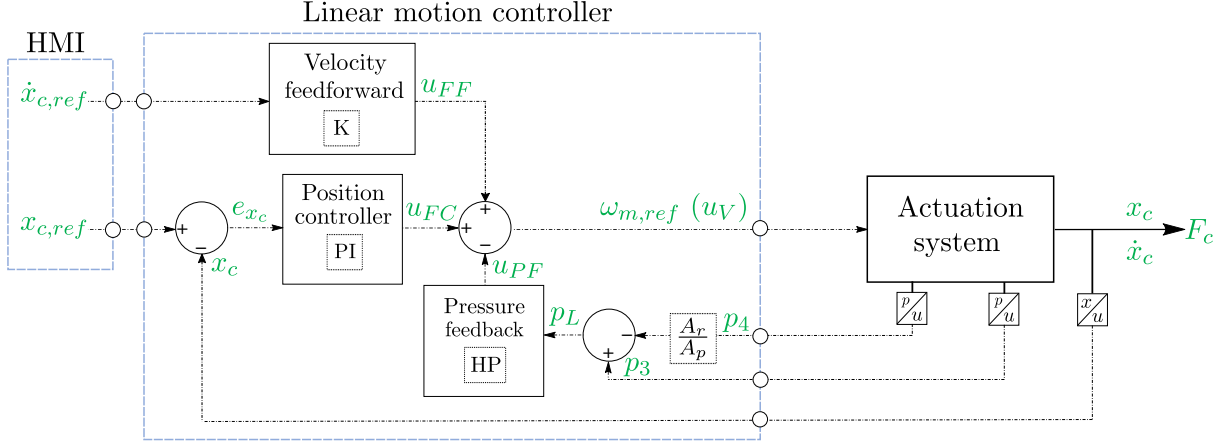
Figure 3.11: The improved control structure, including high-pass filtered pressure feedback.

back can increase the system's damping and gain margin. Hence, significantly higher PI-controller gains can be used while still ensuring a stable system, resulting in better position tracking performance and faster response. The pressure feedback can be applied using either a direct, gradient, low-pass filtered, or high-pass filtered approach [49]. The method using high-pass filtered pressure feedback [71, 72] is preferred because the other approaches are challenging to implement experimentally due to the fact that the measured pressure level in the steady-state will yield a signal that commands the actuator to move. Hence, the steady-state pressure must continuously be updated and subtracted from the measured pressure levels to avoid this critical problem; this is challenging because of the high nonlinearities of the hydraulic system, external loads that change during the operating cycle, and the noise of the pressure feedback signal. The algorithm of the proposed high-pass filtered pressure feedback is implemented in the control structure (Fig. 3.11) by

$$u_{PF} = k_q^{-1} \cdot \frac{k_f \cdot s}{\tau_f \cdot s + 1} \cdot p_L, \tag{3.4}$$

where k_q^{-1} is the inverse of the identified flow gain, k_f is the gain and τ_f is the time constant of the high-pass filter, and $p_L = p_3 - A_r/A_p \cdot p_4$ is the actuators' effective load pressure.

A linear control design analysis is carried out in Paper F for the EHC with pressure feedback and demonstrates that the original damping ratio of 0.052 was increased to one desired value (i.e., 0.5), resulting in a 14.5% higher gain margin. According to [73], the damping ratio of the hydraulic system should be between 0.5 and 0.7. The improved motion performance of the EHC is presented later in this section.

Additionally, the benchmark system benefits from implementing pressure feedback. The combination of a counterbalance valve and pressure compensated control valve tends to introduce oscillatory behavior or even instability. This behavior undermines both

performance and operational safety, especially when the external load is overrunning. Applying pressure feedback to valve-controlled systems has been a popular research topic for many years, as the intent is to stabilize the system when lowering the crane boom (i.e., only rod-side pressure is used for pressure feedback). However, in Paper E, an approach that stabilizes the system during both piston extension and retraction with closed-loop position control was successfully implemented on the single-boom crane. Because the studied control valve has a significantly slower response (bandwidth) than, e.g., servo-valves, the implementation of the valve dynamics inverse was proposed in order to successfully stabilize the system when the piston-side pressure was also included as pressure feedback. The experimental results show a significant reduction of the VCC's oscillatory behavior, as shown in Fig. 3.12, when operated with a closed-loop position control during a complete work cycle.
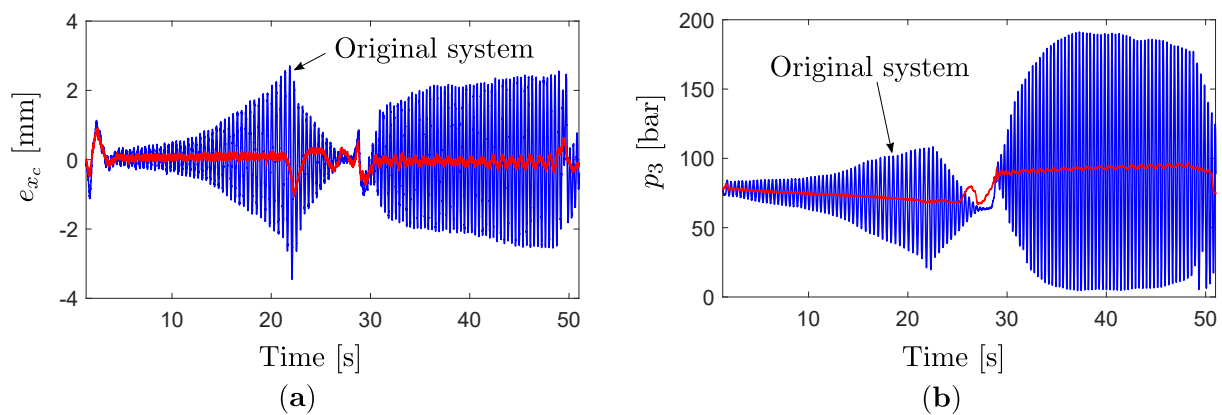
Figure 3.12: Effect of implementing pressure feedback on the benchmark system [31]: (**a**) piston position error; (**b**) piston-side pressure.

The maximum position error when lifting the crane-boom has been reduced from 3.5 mm to 1 mm, and the average position error during lowering has been approximately 0.2 mm. In comparison to the system without pressure feedback, this is a reduction of almost 90%.

As an alternative to pressure feedback, the actuator's acceleration and velocity can be estimated or measured and used as active damping. However, to identify the best practice, this solution is being considered for future work for comparison with pressure feedback. This method has already been implemented in a commercial variable-speed and position controller for the Sytronix electro-hydraulic drive system by Rexroth [74].

Model-Based Design

A model-based design approach has been carried out in Paper F to derive the control parameters for both the EHC and conventional VCC using experimentally validated models.

When designing the control parameters, the pressure feedback's parameters (i.e., the filter gain and time constant of the high-pass filter) are first chosen so that the desired damping ratio of the system is obtained before designing the linear motion controller for the original system. A complete description of the process used to derive these parameters is presented in Paper F. Further on, the proportional and integral gains of the position feedback controller algorithm (2.14) are obtained based on the gain margin (Gm), and the phase crossover frequency (ω_c) identified from a frequency response analysis (i.e., using Bode plots according to the procedure proposed in [75]) by

$$k_P = 10^{\frac{Gm(\omega_c)}{20}}, \tag{3.5}$$

and

$$k_I = 0.1 \cdot \omega_c \cdot k_P. \tag{3.6}$$

Next, based on the reference velocity of the piston ($\dot{x}_{c,ref}$), the piston area, and the flow gain, the velocity feedforward element is derived by

$$u_{FF} = \frac{A_p}{k_q} \cdot \dot{x}_{c,ref}. \tag{3.7}$$

The identified control parameters for both the EHC and benchmark system are presented in Paper F.

3.4.3 Motion Performance

Three closed-loop tests are carried out in Paper F to analyze the motion performance of the EHC compared to the benchmark system. First, a step response test (Fig.3.13) is performed with a maximum payload (i.e., mass equal to 304 kg) to test the closed-loop response time.

Then, a work cycle test (Fig. 3.14) with maximum payload and various velocity setpoints is carried out to assess the tracking error. Lastly, the single-boom crane is also actuated both with a half payload and without any payload to explore the actuation system's robustness in dealing with load variations (see plots in Paper F). The empirical results demonstrate that the necessary passive load-holding function of the EHC can safely maintain the cylinder position when motion is not desired. The control algorithm also seems to be robust in spite of load variation. Furthermore, the EHC outperforms the benchmark system when driving the single-boom crane on all fronts.

As shown in Fig.3.13a, the EHC achieves 61% less overshoot, 10 ms faster rising time, and 75% faster settling time. The active pressure feedback in the EHC reduces the pressure oscillations (Fig.3.13b) more effectively than the VCC since the electric prime
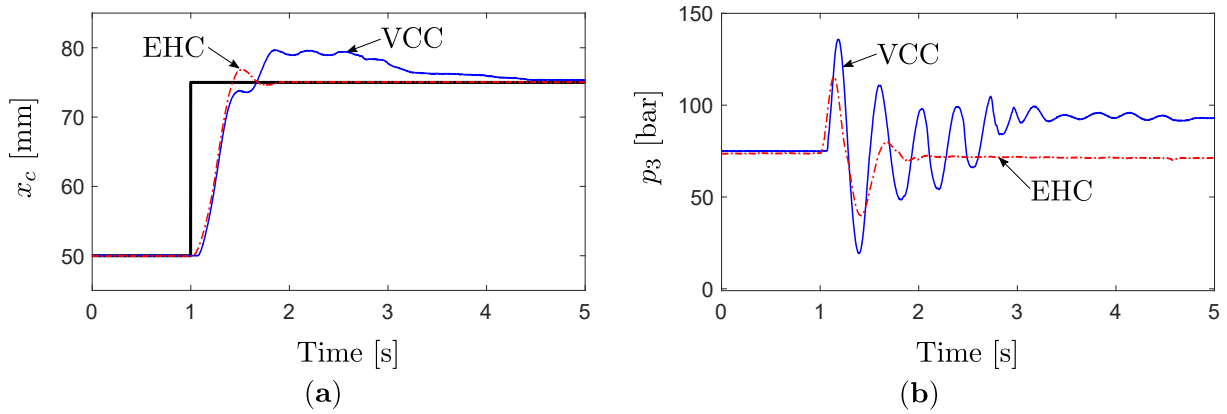
Figure 3.13: Closed-loop position step response [76]: (**a**) commanded and measured piston positions; (**b**) piston-side pressures.
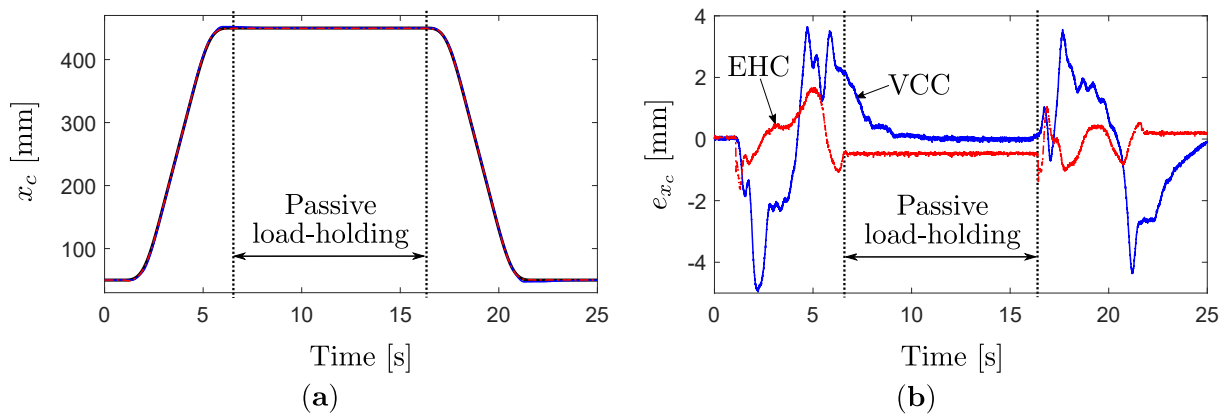
Figure 3.14: Closed-loop position tracking [76]: (**a**) commanded and measured piston positions; (**b**) tracking error.

mover has about 95% higher bandwidth than the control valve. Further, as shown in Fig. 3.14, the EHC has up to 66% less tracking error than the benchmark system for the considered motion cycle.

3.4.4 Energy Efficiency

It is experimentally shown, in Paper G, that the EHC enables 62% energy savings in a representative work cycle (Fig. 3.15) due to its throttle-less and power-on-demand nature. Moreover, up to 77% of the energy taken from the electrical grid can be used effectively if the recovered energy is reused (as shown in Fig. 3.15b after 18 s). This option is not possible in the state-of-the-art valve-controlled systems. More specifically, the following aspects have emerged from the study [77]:

- the power demand (Fig. 3.15) of the electric prime mover during steady-state operations is reduced to 4.8 kW versus 7.6 kW in the valve-controlled system (37% less) throughout the examined work cycle;
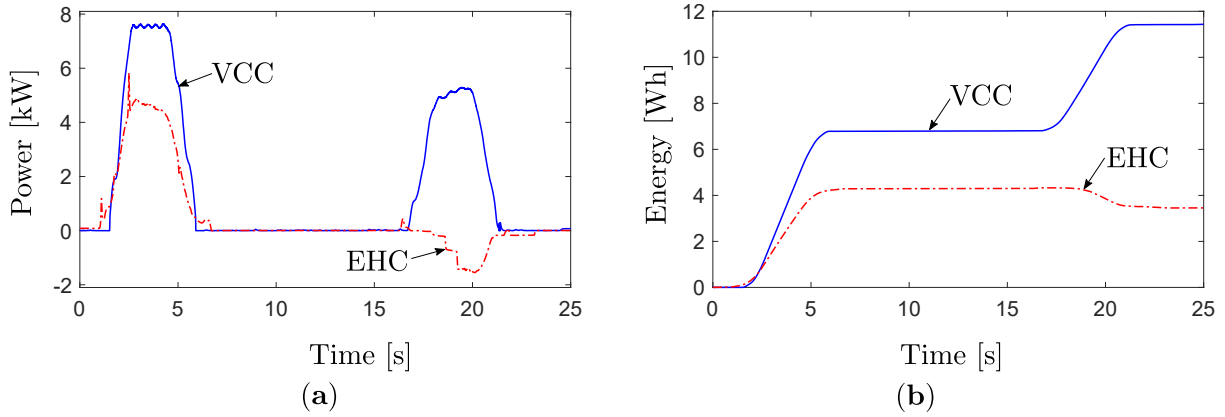
Figure 3.15: Consumption during a complete working cycle [77]: (**a**) power; (**b**) energy.

- using passive load-holding results in an energy savings of 18.4% in comparison to active load-holding;

- the systems' overall efficiency of the EHC, being approximately 57% during actuation, turns out to be highly satisfying compared to the 22% efficiency level of the VCC with a constant-pressure supply;

- the EHC recovers a significant amount of energy (i.e., 20% of the consumed energy) during the proposed work cycle. Hence, when assuming a realistic 94% regeneration efficiency to return the recovered energy to the electrical grid, then 77% of the total input energy can be used effectively. In contrast, this efficient operation is not feasible in the VCC where, rather than being recovered, the available energy is dissipated in the hydraulic system when the load acting on the cylinder is overrunning;

- an alternative scenario based on a load-sensing pump concept is also considered for the VCC; while its energy consumption decreases from 11.44 Wh to 9.20 Wh (Fig. 3.16b), it remains inefficient with respect to the EHC with a total energy consumption of 4.34 Wh (Fig. 3.16a).

The power levels and efficiencies of the different sub-systems of the EHC (i.e., the electric drive (ED), hydraulic unit (P), auxiliary valves (AV), and the hydraulic cylinder (C)) and benchmark system (i.e., the HPU, control valve (V), load-holding valve (LHV), and hydraulic cylinder) are separately evaluated while lifting and lowering the single-boom crane (SBC).

Figure 3.16: The energy distribution during a complete work cycle [77]: (**a**) EHC; (**b**) VCC when simulating a load-sensing pump and the HPU losses.
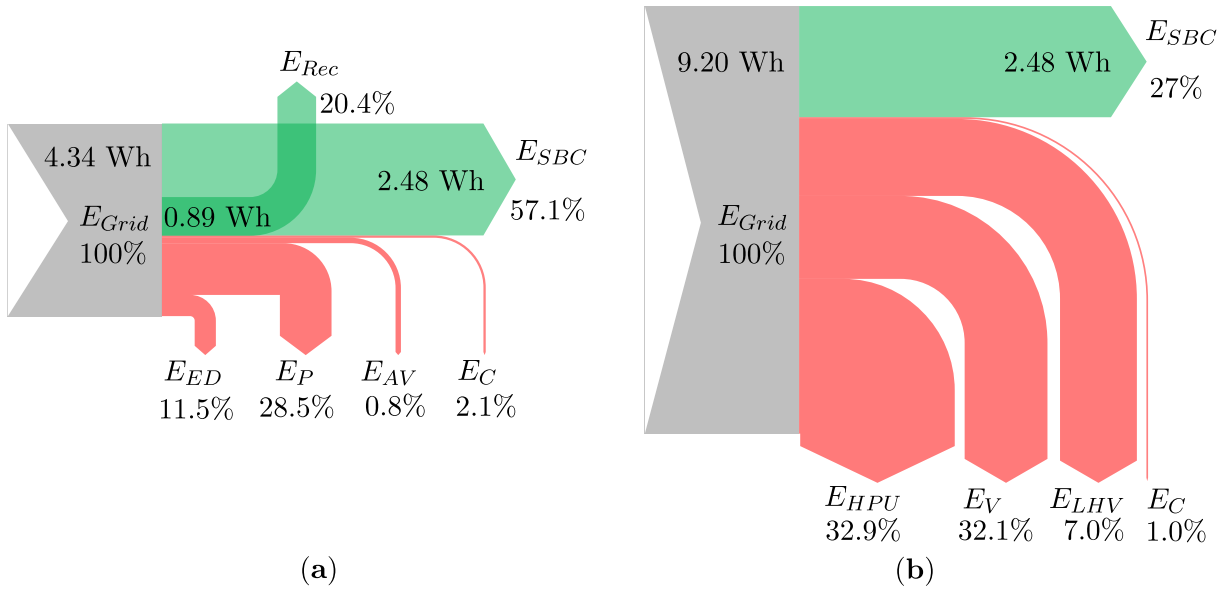
3.4.5 Design Impact

The two self-contained linear actuator technologies are further investigated in Paper H with a focus on their design impact (Fig. 3.17b) when replacing the original hydraulic actuator on the single-boom crane.

The EHC shows several benefits over the EMC, such as 20% higher continuous power capability, 47% less installed electric power, 79% longer expected service life, 33% higher maximum force capability, 25% less overall mass, and 40% less installation length. The EHC is also more robust when handling impact forces and is expected to have about a 50% lower initial cost. For work cycles requiring an average continuous transmitted power above 2 kW, there are no available configurations of the considered EMC [25] due to the limitations on the permissible continuous power being transmitted by the screw assembly. For the electro-hydraulic solution, the PMSM's rated torque is the limiting factor. For higher torque requirements (i.e., above 180 Nm as pointed out in [78]), there are AC induction machines available that can be used. Further, the EMC is expected to show better motion performance due to its higher drive stiffness, requires less control effort, has higher energy efficiency, and allows for lower system complexity, all of which results in a more straightforward design approach.

Regarding the PRM case study, different configurations of the off-the-shelf EMC were considered for implementation on the main arm (Paper A), as illustrated in Fig. 3.17a in comparison to the original hydraulic cylinder.

As a side note with regard to future implementation, the electro-hydraulic power unit of the compact and EHC design does not necessarily need to be mounted directly on the
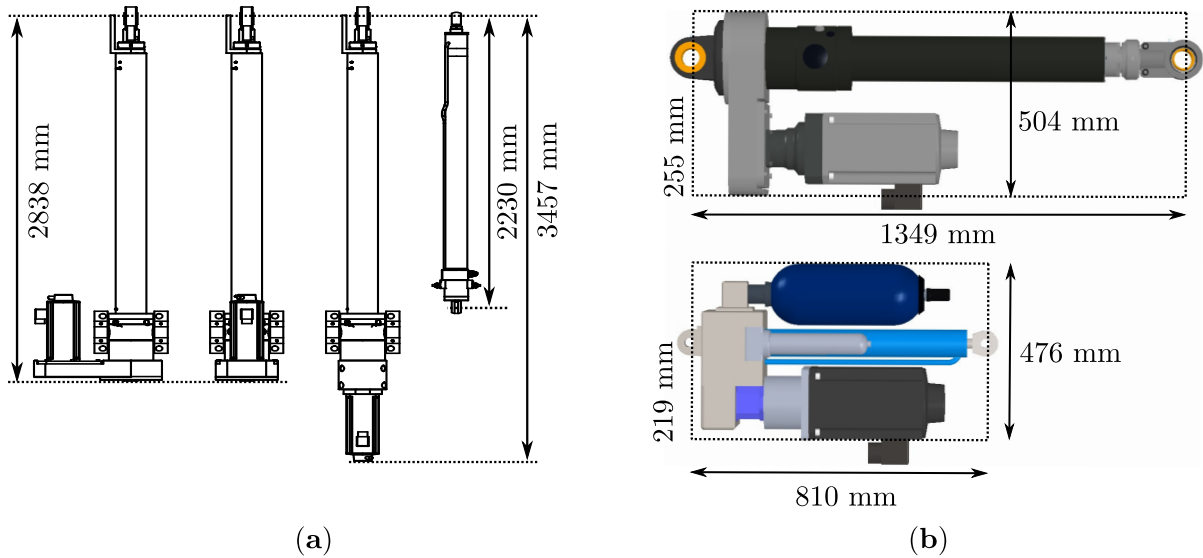
Figure 3.17: Installation size comparison: (**a**) different motor mounting configuration of the dimensioned electro-mechanical cylinder for the main arm cylinder of the pipe racking machine [3]; (**b**) the dimensioned electro-mechanical and electro-hydraulic self-contained cylinders for the single-boom crane [64] © 2020 IEEE.

hydraulic cylinder, as shown in Fig. 3.17b. For example, the original hydraulic cylinder of the single-boom crane could have been used, and the electro-hydraulic system can be installed in the structure of the application and connected to the hydraulic cylinder by means of hydraulic lines. However, if hydraulic hoses need to be used, then the load-holding valves must be attached directly to the hydraulic cylinder as required by safety regulations. In addition, as pointed out, by [78], the choice of hydraulic circuit architecture and components (e.g., either PMSM or AC induction machines) significantly affect the weight and required amount of installed power. When combined with the weight of the hydraulic cylinder itself, [78] discovered that for the knuckle boom crane case study, the EHCs are between 37% to 50% heavier than the hydraulic cylinder itself, which is used in the conventional valve-controlled systems. Hence, both the design configuration and component selection should be optimized for each specific application and its work cycle to maximize the benefits of self-contained cylinders. Furthermore, the mechanical mechanisms should be designed so that the self-contained cylinders can utilize the maximum advantages of electric regeneration and compactness.

3.4.6 Characteristics

To evaluate the consequences and limitations associated with choosing any of the two self-contained alternatives as a replacement for conventional hydraulic cylinders, Tab. 3.1, presents an overview of the positive and negative outcomes (without considering the

occupied space, cost, and energy losses of the centralized hydraulic power unit and the piping). This overview is intended to be a general guideline for choosing between the electro-mechanical and electro-hydraulic drive solution when replacing traditional VCCs; thus, additional general knowledge from the technical literature is included.

When designing an actuation system for a specific application, the information available from the component catalogs and details obtained from the manufacturers are usually sufficient. This is because the application manufacturers want to use existing, well-known and well-proven actuation system components, suppliers, support facilities, etc. [79]. In this manner, the designer can use both knowledge built up over a long period of time (e.g., human resources and experiences) and non-assignable properties like trusting the reliability of the components' manufacturers. However, selecting the optimal actuation system and eliminating sub-optimal solutions early in the design phase can have a significant impact on the project's capacity, total cost, and performance of the application [80]. The offshore case study (Fig. 3.1) investigated in this research is an excellent example of a complex application that would have benefited from having a computerized design tool when replacing the centralized powered valve-controlled cylinders with a more environmentally friendly alternative. Consequently, the next section presents an additional study carried out in this research on identifying a design tool that can automatically perform the design, feasibility, and comparative analysis when considering using different solutions and component manufacturers to select the best suitable actuation system.

Table 3.1: Comparison of the investigated self-contained cylinders' characteristics with respect to the benchmark system [64]. Five different grades are used ranging from $(--)$ to $(++)$, with $(--)$ being the worst, and 0 representing a similar performance to that of the benchmark system. Results that are based on general knowledge from the technical literature are denoted by *, while results that are related to ongoing research are denoted by ?.

Category:	Criterion:	EMC	EHC
Design	Compactness	$--$	$-$
	Force per mass	$--$	$-$
	Power density	$--$	$-$
	Design complexity	$+$	$-$
	Enclosure protection	0	0
	Control effort*	$+$	0
	Scalabillity*	$--$	$-$
	Cost	$--$	$-$
Operation	Impact absorption*	$--$	0
	Reliability*	$--$	0?
	Energy efficiency	$++$	$++$
	Thermal absorption	$--$	$-$?
	Accuracy*	$++$	$+$
	Drive stiffness*	$++$	$-$
	Max force	$-$	0
	Max velocity	$++$	$+$
	Max acceleration	$++$	$-$
	Max continuous output power	$--$	$-$
Safety	Passive load-holding	-?	0
	Fail-safe*	$-$	0
	Overload protection*	$-$	$+$
Application	Installed power	$+$	$++$
	Fluid spill risk*	$++$	$+$
	Maintenance effort*	$++$	$+$?
	Durability*	$--$	0?
	Commissioning effort	$++$	$+$

3.5   Towards Automated Design

The actuation system, along with control systems and the mechanical structure design, ranges among the top key players to improving an application's motion performances and energy efficiency. The optimal design of actuation systems consists of finding the best combination (according to the desired objective(s)) of components that can deliver necessary and sufficient mechanical power (through desired speed and force/torque) to each mechanical degree of freedom, enabling the application to perform one or more characteristic work cycles.

To stay competitive, application and actuation system manufacturers continuously have to improve their design procedures in order to obtain the best possible trade-off between engineering costs and performance. Designing the best suitable actuation system for a given application requires a well defined and comprehensive set of specifications which, depending on the application, may consist of a great variety of hardly comparable requirements and constraints, such as motion performance, energy consumption, cost, weight, size, etc. Moreover, technical, industrial, and environmental standards must also be satisfied. Finally, these specifications must be compared to the performance characteristics of all components to determine whether the actuation system can perform the required task or not.

Designing the best suitable actuation system is a process of comparing various actuation systems based on sets of components from different principal modes of energy transfer that are available from a broad range of manufacturers. When considering the different actuator technologies and suitable combinations of components that are available on the market, the design task becomes a complex and iterative process that is difficult for a design engineer to handle without applying sophisticated computerized design tools. Most often, the search for a suitable design relies mostly on the intuition and experience of the designer. Therefore, the obtained design often consists of a limited variety of actuation system components, unwarranted complexity, or high costs [81]. Actuation systems are often designed in an overly conservative manner to work under high load levels, whereas in reality, maximum load conditions acting upon them comprise only an insignificant part of the overall loads they experience [82].

There are various levels of design ranging from requirement analysis and topologies down to detail design. There is a clear danger that system engineering activities are performed only at the top level of design. Thus, to make any impact on the application development process, the designer must consider all levels of their design so that a holistic (mechatronic) view will be maintained through all stages of it. This can be achieved if common system modeling is used where the interaction with other sub-systems, such as the actuation system and mechanical system, and the whole application can be optimized

using top-level requirements [83]. Furthermore, considering the control system, mechanical design, and actuation system as one mechatronic system design [84] allows for global optimization since the one can affect the two others. On the contrary, using a sequential approach may lead to sub-optimal solutions. This is because in a mechatronic design process (Fig. 3.18), structural and dimensional synthesis is addressed as an integrated design task that includes the determination of both the topology and dimensions of the application's mechanical and actuation systems as well as its control parameters.
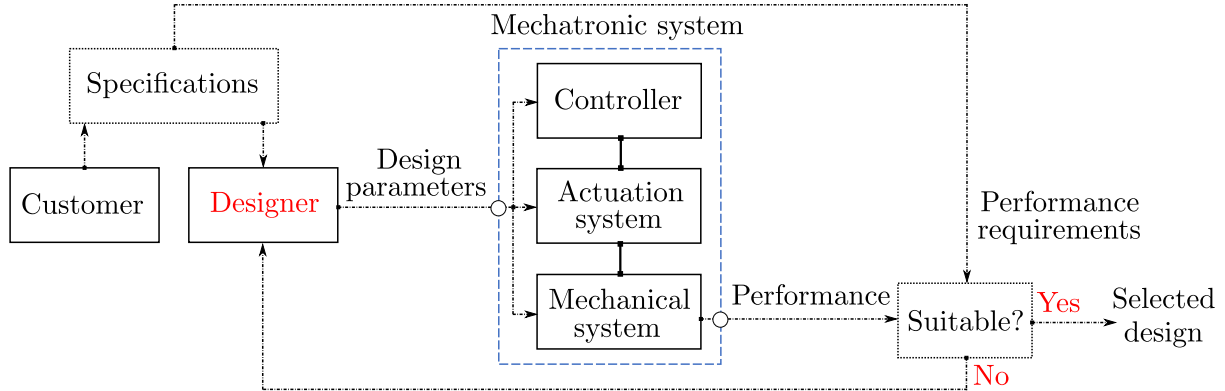

Figure 3.18: Mechatronic design process as an iterative feedback process.

This may be done in two distinctly different methods, i.e., in serial or parallel [85]. In serial synthesis, the topologies are generated beforehand, and then the actual sizing is carried out, whereas in parallel synthesis, the topology and the dimensions are varied simultaneously. In both methods, the controller is tuned simultaneously during the dimensioning of the application.

The lack of well established, systematic engineering methods needed to form the basic set-off in the analysis and design of complete actuation systems is apparent [86]. Therefore, this survey focuses on identifying the main obstacles that prevent the development and widespread use of a computerized design tool for various types of actuation systems and applications.

3.5.1 Literature Review

According to [87], previous research into actuator selection has focused on application-specific domains [88], selection of individual actuation technologies [89], different computing platforms [90], or database development [91]. In the study presented by [87], only two general design tools for selection of actuators were found: 1) the web-based actuator selection tool presented by [90] and 2) the actuator classification and selection tool presented by [91].

Therefore, a comprehensive literature study is carried out in this section to identify

commercially available design tools and relevant published methods with respect to selecting the best suitable actuation systems. The literature review aims at determining what functionalities and elements are missing for a computerized design tool to be able to automatically select the best configuration of an actuation system for the given requirements of a specific application and its operational sequence. A literature matrix is presented in Tab. 3.2 concerning the following four functionalities that are considered necessary to include in an automated actuation system design tool software application:

1. a database that allows the designer to add different actuators and customize data;

2. a graphical user interface (GUI) that allows the designer to formulate relevant requirements and automatically compares different actuators to select the best actuation systems;

3. a GUI that allows the designer to formulate design inputs and automatically generate mathematical models at a level that corresponds to commercial modeling and simulation software;

4. a GUI that allows the designer to automatically formulate the design optimization problem at a level that corresponds to a commercial optimization software application.

The proposed literature review is categorized by the type of platform that either the design tool or method is implemented on, i.e., selection procedures and strategies described in the literature, software applications installed on a desktop computer, design tools or guidelines located on a website, or simulation-based (SIM-based) optimization (OPT) approaches using commercialized or open-source modeling, simulation, and optimization software.

The conclusion from the literature review is that no tool, either commercial or research-based, can currently provide cross technology, cross topology, and cross catalogs optimal selection. However, the significant increase in digitalization of manufacturers' product data in combination with the increase in computational power, improvement in numerical methods and development of artificial intelligence tools, all imply that the development of a viable automatic design tool is possible.

Table 3.2: Literature review of design tools for actuation systems. The character denotes
the affiliation of the developer and users (if applicable): actuator (component) manufac-
turers (A), component dealers (B), application manufacturers (C), interest organizations
(D), academia (E), independent research centers (F), industry (G). Methods that are
based on only one actuator technology are denoted by *, while functionalities that are
not identified are denoted by ?.

				Functionalities:				
No:	Category:	Dev.:	User:	1	2	3	4	Reference:
1	Literature-based	E	E	No	No	No	No	[88]
2		E	E	No	No	No	No	[87]
3		E	E	No	No	No	No	[92]
4		E	E	No	No	No	No	[93]
5		E	E	No	No	No	No	[94]
6*	Computer-based	E	A	No	No	**Yes**	**Yes**	[95]
7*		E	n/a	No	**Yes**	No	No	[96, 97]
8*		E	E C	No	**Yes**	No	No	[80, 81]
9*?		E	?	?	**Yes**	?	**Yes**	[79, 98–100]
10*		A	B C	No	**Yes**	No	No	[101]
11		A	B C	No	No	No	No	[102]
12*		A	B C	No	**Yes**	No	No	[103]
13*		D	B C G	No	**Yes**	No	No	[104]
14*		D	B C G	No	**Yes**	No	No	[105]
15		E F	A C E F	**Yes**	**Yes**	No	No	[91, 106–111]
16*	& Web-based	A	B C	No	**Yes**	No	No	[112]
17*	& Web-based	E F	A C E F	?	No	Yes	Yes	[113–115]
18	Web-based	A	n/a	No	**Yes**	No	No	[90]
19*		A	B C	No	**Yes**	No	No	[116]
20*		A	B C	No	**Yes**	No	No	[117]
21*	SIM-based OPT	A	E	No	No	No	No	[118]
22*		E	E	No	No	No	No	[119]
23*		E	E	No	No	No	No	[120]
24*		A	E	No	No	No	No	[121]
25*		E	E	No	No	No	No	[122]
26*		E	E	No	No	No	No	[123]
		Continued on next page						

Table 3.2 – continued from previous page

No:	Category:	Dev.:	User:	Functionalities:				Reference:
				1	2	3	4	
27*	SIM-based OPT	E	E	No	No	No	No	[124]
28*		E	E	No	No	No	No	[83]
29*		E	E	No	No	No	No	[125]
30*		E	E	No	No	No	No	[126, 127]
31*		E	E	No	No	No	No	[128]
32*		E	E	No	No	No	No	[129]
33		E	E	No	No	No	No	[85]
34*		E	E	No	No	No	No	[130, 131]
35*		E	E	No	No	No	No	[132]
36*		E	E	No	No	No	No	[86]
37*		E	E	No	No	No	No	[133]
38*		E	E	No	No	No	No	[134]
39*		E	E	No	No	No	No	[135]
40*		E	E	No	No	No	No	[136–140]
41*		E	E	No	No	No	No	[141]
42*		E	E	No	No	No	No	[82]
43*		E	E	No	No	No	No	[142]
44*		E	E	No	No	No	No	[143]
45		E	E	No	No	No	No	[144]

3.5.2 Research Question

The main functionality of an "automated actuation system design tool" is to automatically perform the design of the optimal actuation system in accordance with the given specifications. Selecting the best combination of components must be done via an exploration of various actuator technologies and components from a broad range of manufacturers. Most of the requested design tool functionalities have been reported in the literature to a certain degree. However, a design tool that includes all of the desired features simultaneously was not identified in the literature study; therefore, the following research question is explored:

> **What would it require to create a computerized tool for the automatic design of actuation systems that can compare different actuator technologies and components from different manufacturers? What are the obstacles of doing so, and what challenges must be overcome in order to realize an automated actuation system design tool?**

The main obstacle preventing an automated design tool from being created is related to software development and access to component data. Various types of software developers aim their products at different types of users (designers) with different functionality requirements. Depending on the type of application, some manufacturers can deliver complete off-the-shelf or customized actuation systems. For instance, two types of manufacturers are involved in designing the actuation system for a specific application, i.e., the actuation system (component) manufacturers and the application manufacturer.

In addition to the manufacturers, academia, interest organizations, and independent research centers also develop design tools for actuation systems. Each of the developers introduces different limitations of a general-purpose design tool software for actuation systems. Software developed by actuation system (component) manufacturers is biased since they usually only consider components and topologies from their portfolio. Hence, making comparisons with other manufacturers is complicated; in addition, it might be unfair. Since the actuation system (component) manufacturers rely on the details of the given specifications provided by the application manufacturers, and vice versa, there is a tendency towards oversimplifying load and motion situations (work cycles) as well as other characteristics used in the design process. Further, the reluctance to share vital information such as cost, availability, and performance data is a problem. The latter affects the knowledge of other design tool developers when establishing detailed databases and simulation models with verified performance characteristics. When considering academia and interest organizations, there is an apparent lack of resources to maintain and expand the database. Examples of this are the design tool software presented by [90, 96], where promising software was not further developed. Other reasons why this software fails to become commercially available could merely be the lack of motivation and research focus on developing such design tools. However, research centers, including the Linz Center of Mechatronics Gmbh, seems to have developed a viable tool (SyMSpace) for designing specific actuator components, i.e., electrical machines [114, 115]. For instance, this novel computerized and cloud-based design tool, which is based on further developments of simulation-based optimization tools MagOpt [113], could have the potential to include the optimal design of additional components or even entire topologies. However, this would require having access to the necessary data.

3.5.3   Identified Challenges

Based on the identification completed in this survey, a successful automated actuation system design tool should include all the functionalities and elements depicted in Fig. 3.19.
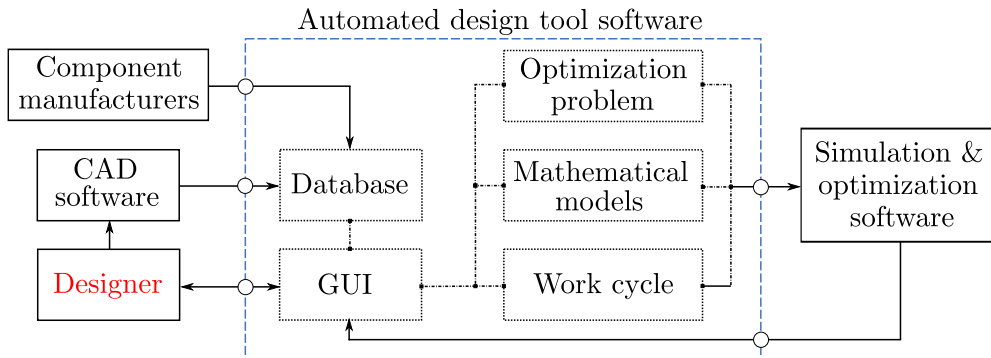

Figure 3.19: Automated actuation system design framework.

Some essential challenges that are identified in the literature survey are discussed in the following.

Graphical User Interface

Having the level of expertise needed to identify possible actuation technologies, select topologies, set up simulation models, as well as test and evaluate control strategies for an application, is not typical for an individual design engineer. Therefore, the essential purpose of the GUI is to aid the designer in defining or selecting predefined suitable topologies based on given specifications, formulate the optimization problem (i.e., objective functions, constraints, and design variables), and generate the numerical simulation model and work cycle. In order for the design tool to be used by non-experts, the GUI must generalize the expert knowledge held by various application designers and actuation system (component) manufacturers. Additionally, non-technical parameters are essential and must be implemented [79]. Further, the GUI must provide information that is as precise as possible to enable clear and effective design decisions. Furthermore, it should not require too highly detailed inputs so that it can be used earlier in the design phases, for instance when design details may not have been finalized [96]. Finally, the GUI must ensure not only that all suitable combinations are evaluated and the best combination selected, but also that all relevant combinations should be scored and highlighted, e.g., through a Pareto front.

Database

The primary limitation of commercially available design tools is that they only include one actuation technology, e.g., electric motors [104] or electro-mechanical cylinders [117].

However, there are some design tools that can select a combination of electric-drives and hydraulic pumps, e.g., SytronixSize from Rexroth [102]. Nonetheless, only components from that specific supplier (e.g., Rexroth) are available. Other tools most often contain a self-constructed database consisting of different components, topologies, and actuation technologies defined by the software developer. Consequently, comparing various actuation technology and brands is not possible. According to the literature review, the only computer-based tool discovered that allows the user to add information manually to the database is the Cambridge Engineering Selector [110]. This software is also referred to as the material selector, and is based on the methods described in [106]. The database of this software can be utilized to include several types of actuators and is used to compare different actuator technologies, see, for instance, [91, 107–109]. Today, this software is commercially available as the Granta Selector by Ansys Granta [111].

The database needs to contain all necessary information about the topologies and components. For example, new control systems and the increase of computational power in embedded systems enable significant extensions of existing actuation systems [79]. Thus, the database must be continuously (automatically) updated and maintained. Doing so [145] presents an exciting concept that can potentially overcome some of these challenges. Further, the concept demonstrates how a knowledge-based (rule-based) selection of principle solutions could be integrated into the planning process and overall engineering work flow. The approach uses standardized plant description models and semantic concepts when selecting actuators and instrumentation devices for industrial process plants.

Characteristics gathered from the research literature and commercially available product data do not necessarily portray the actual maximum performance of any given actuation technology. Some possible reasons for this are presented in [87]. Furthermore, as pointed out by [96], the database must be built up and improved to reflect more properties of applications, components, and the actuation system as a whole. To accomplish this, [96] proposes investigating the use of the Cambridge Engineering Selector [110] due to its features that allow the creation and editing of reference data.

Simulation and Optimization Software

According to [119], it is essential to take the topological properties of the actuation system into consideration in order to develop efficient modeling techniques. Furthermore, only well understood and well-described sub-systems with a high degree of behavioral predictability should be used as building blocks [124]. Consequently, the design tool must determine not only the design variables but also the topology to be applied using either the serial or parallel technique.

The trade-offs between performance, quality, and cost are essential for making design decisions. These trade-offs can be investigated using simulation models. However, the generation of compromises can be both time-consuming and cumbersome, although, through the help of optimization algorithms, the process may be automated [132]. Furthermore, design problems usually consist of a combination of deciding continuous parameters in addition to a discrete selection of components from the database. Hence, there is a need for optimization algorithms that can handle variables of both a discrete and continuous nature. Furthermore, the optimization algorithms must be able to handle multi-criteria/objective nonlinear problems [81]. As pointed out by [92], the comparison of actuators should be expanded to include system-level characterizations of performance. Similarly, the selection of components and design of the control algorithm should be carried out jointly with full awareness of the interactions between the different aspects of the overall design. However, simulation in different physical domains often requires solving nonlinear partial differential equations, and typically, it takes anywhere from minutes up to several hours and days to solve these problems. As pointed out by [113], the computation time bottleneck can be removed by solving the partial differential equations in parallel on a computer cluster.

3.5.4 Required Developments

The essential purpose of a design tool is to aid the designer in selecting the best suitable actuation system by integrating the expert knowledge of application designers and actuation system (component) manufacturers into the selection of the best suitable configuration of actuation system components. In order to be considered fully automated, the design tool must automatically select the optimal combination for the desired application specifications (performance requirements) through a model-based analysis of the different defined topologies (e.g., electro-mechanical cylinder or electro-hydraulic cylinder) and all suitable off-the-shelf components (e.g., linear actuator dimensions, electric and hydraulic motors, gearboxes, variable frequency drives, valves, etc.).

The result of this survey is the following seven key challenges that must be met to realize a viable automated design tool software application for actuation systems:

- both the motion cycle and load cycle (work cycle) must be specified in the GUI, or the database must interface with CAD software to get information from a CAD model of the application to generate a multibody system model used to analyze the load cycle;

- the database must be continuously (automatically) updated and contain all the necessary information (e.g., component data (parameters) and topology templates)

for generating mathematical models for simulations;

- the software must eliminate topologies and components from the database that are
not suitable for the specified work cycle and requirements;

- application specifications must consider non-technical parameters based on the experience of experts and ISO standards;

- the software must generate and interface mathematical models and associated parameters with the simulation software, and automatically program the optimization problem based on the designer's input specifications;

- the simulation and optimization process must be time-efficient (e.g., parallel computation on a cluster) and able to solve multi-objective nonlinear optimization problems and handle variables of both a discrete and continuous nature;

- automated and visual comparison of various topologies and components from different actuator technologies and brands must be possible.

Chapter Summary

Two alternative linear actuation systems to conventional centralized powered valve-controlled cylinders have been investigated in this chapter in two relevant load-carrying application case studies, both in terms of numerical studies and experimental testing. When recalling the positive outcomes obtained about motion control, energy efficiency, and design impact, it is clear that the studied self-contained electro-hydraulic cylinder represents a valid alternative to conventional hydraulic systems where position tracking, reduced oscillations, and energy consumption are essential. Further, the electro-hydraulic solution is preferred over the electro-mechanical counterpart when there exists a risk for high-impact forces, when the required output power is continuously above 2 kW, or when minimal installation space, weight, and costs are key design objectives. Introducing a self-sufficient and completely sealed actuation system will also significantly reduce the risk of fluid spill pollution, helping fluid power to become a cleaner technology. Lastly, a survey carried out to identify and review design tools and design approaches that could have the potential to automate the design of actuation systems is presented. The identified obstacles from the reviewed literature are defined as a research question, and the identified challenges that prevent the development and widespread use of an automated design tool are presented and discussed as they concern a proposed design tool framework.

Chapter 4

Conclusions

The work presented in this research project has been devoted to replacing inefficient hydraulic linear actuation systems traditionally used in offshore load-carrying applications with more environmentally friendly solutions. The following steps, as shown in Fig. 4.1, were carried out during this project to achieve these objectives.
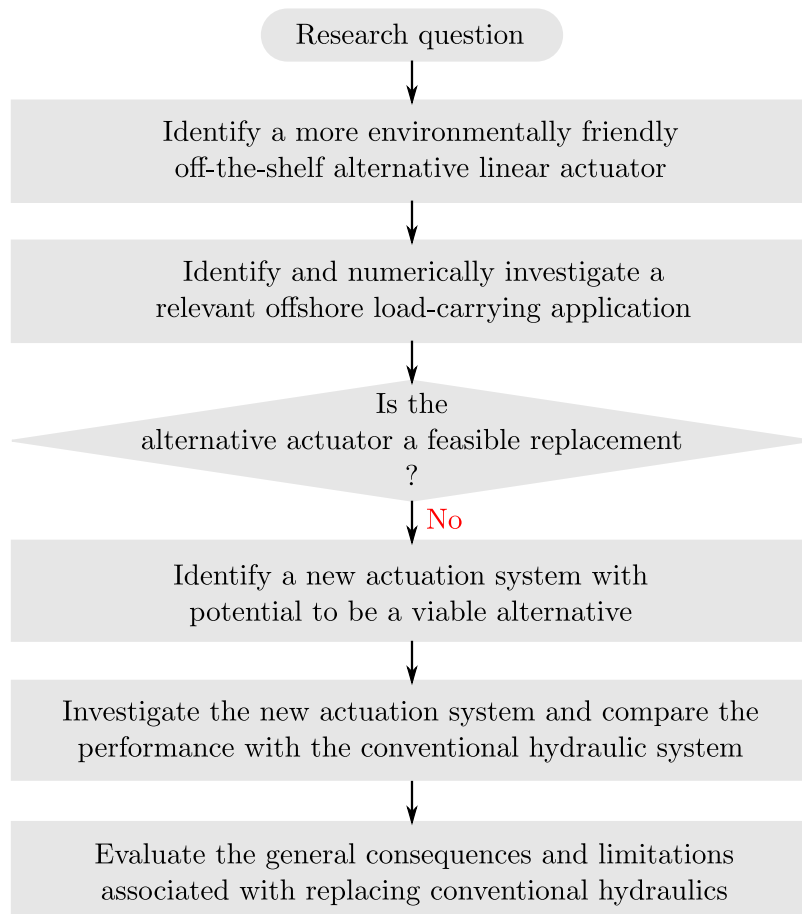

Figure 4.1: Research steps.

Two alternative technologies were identified, namely electro-mechanical and electro-

hydraulic self-contained cylinders. Their feasibility to replace conventional valve-controlled cylinders was numerically investigated in two relevant case studies, and the positive and negative outcomes assessed. First, a survey on replacing the conventional hydraulic actuation system of an offshore pipe racking machine case study was performed. The numerical study showed that the identified off-the-shelf electro-mechanical cylinder was not suitable for the studied motion cycle measured from an offshore oil rig in operation. The permissible average transmitted power of the considered electro-mechanical actuator was lower than the average power required by the operational sequence. Hence, avoiding having the actuator overheat cannot be guaranteed without limiting productivity. In addition, a literature survey identified advantages and disadvantages associated with the reliability, safety, and durability of offshore drilling applications' design criteria, where productivity and safety features are essential. As identified in the technical literature, there are a certain number of critical issues related to the reliability and durability of the electro-mechanical linear actuators, especially in aerospace applications, where failure in the actuation system can have serious consequences. Therefore, an alternative electro-hydraulic linear actuator technology was identified and reviewed. It was discovered that a standardized self-contained electro-hydraulic cylinder concept, including passive load-holding and capability of four-quadrant operations, has not been defined in the identified technical literature. Furthermore, a suitable general-purpose, self-contained electro-hydraulic linear actuator was not found to be commercially available for power levels between 5 and 25 kW. Consequently, the main effort made during this research project was dedicated to defining the electro-hydraulic solution and its passive load-holding capability in four-quadrant operations.

Since an off-the-shelf, self-contained electro-hydraulic cylinder was not available for the considered requirements (i.e., safety features, energy-saving potential, productivity, compactness, environmental-friendly processes, capability of delivering up to 1.7 m of travel length above 100 kN of force, and more than 0.15 m/s velocity in four-quadrant operations), a concept based on state-of-the-art solutions was designed and implemented on a single-boom crane. The proposed electro-hydraulic solution combines the advantages of both electric drives (i.e., power-on-demand, state-of-the-art connectivity, and electrical-regenerative capability) and hydraulics (i.e., reliability, impact absorption, outstanding force density, and fail-safe functionality) in a self-contained and compact unit. The preliminary experimental testing of the proposed self-contained electro-hydraulic system detected a number of issues related to the combination of the low damping in the closed-circuit hydraulic system and the flexible structure of the crane-boom, resulting in significantly reduced motion performance. Consequently, the linear motion controller that was implemented on the self-contained electro-hydraulic cylinder and the conventional

valve-controlled system was improved by including pressure feedback for active damping. Furthermore, a model-based design approach utilizing validated linearized models was used to design proper control parameters for the proposed control systems.

The new actuation system was then experimentally compared with the conventional valve-controlled cylinder used for benchmarking in terms of motion performance and energy efficiency when driving the single-boom crane. The proposed drive system was empirically proven to be a valid alternative to conventional hydraulics for applications where passive load-holding is required both in terms of dynamic response and energy consumption. Several benefits were demonstrated, for example faster rising time, shorter settling time, less overshoot, significantly better position tracking (66%), and reduction of pressure oscillations in a realistic operational sequence. The self-contained solution enables 62% energy savings due to its throttle-less and power-on-demand nature. Moreover, due to regenerative capability, more than 20% of the consumed energy may be recovered; this means that up to 77% of the energy taken from the electrical grid can be used effectively if the recovered energy is reused, an option that is not possible in state-of-the-art hydraulic architecture. Further, a numerical case study focusing on replacing the remaining valve-controlled cylinders of an offshore pipe racking machine supplied from a centralized hydraulic power unit demonstrates that the self-contained electro-hydraulic solution proposes an energy-saving potential of 83%. Moreover, this novel actuation system demonstrated the potential to improve motion performance when controlling the horizontal reach motion, allowing for increased productivity.

During the design analysis carried out on the single-boom crane, where both the electro-mechanical and electro-hydraulic actuation systems were suitable for the studied work cycle, it has been shown that the self-contained electro-hydraulic cylinder provides several benefits over its electro-mechanical counterpart: it is more compact in terms of the space it occupies in the application's structure, weighs less, requires less installed electric power, and is expected to have a lower cost. Moreover, a novel self-sufficient and completely sealed hydraulic actuation system will also reduce the risk of fluid spill pollution in typical offshore applications where a centralized hydraulic power unit supplies multiple valve-controlled actuators. Additionally, the improved energy efficiency will reduce the diesel generators' CO_2 emissions and fuel costs, helping fluid power to become a cleaner technology, thereby reducing the environmental impact of the oil and gas industry.

Lastly, a survey of design tools used for automated design of the actuation system was presented in this dissertation. A thorough search of the relevant literature yielded no commercial design tools that automate the design of the complete actuation system; subsequently, the focus of this survey was to investigate why this is so. A systematic literature review was carried out concerning commercial tools and literature that presents

methods and guidelines for the design and selection of actuators and associated components. Various attempts which approach simulation-based optimization methods that automatically select the best suitable combination of actuation system components were identified. However, no design tools include the comparison of different actuation technologies and components from different manufacturers during the optimization process. Neither are design tools available that include a graphical user interface that can automatically generate the optimization problem, mathematical models, work cycle, as well as perform simulation-based optimization of a complete topology based on the input from the designer. Based on the significant amount of existing software-based design, selection tools, and published developed procedures, the conclusion has been made that it is possible to develop a commercial tool for the automated design of actuation systems that facilitates simulation-based optimization. However, the proposed seven key requirements must be met, the most important appearing to be the involvement of a design tool developer independent of actuation system (component) manufacturers, application manufacturers, interested organizations, and academia. For instance, the most promising design tool identified in this survey (i.e., SyMSpace) is developed at a research center in cooperation with academia, industry (i.e., application manufacturers), and component manufacturers.

4.1 Contributions

Over the course of this research project, six objectives were met when investigating if there is a suitable and more environmentally-friendly alternative to centralized powered valve-controlled linear actuators that does not compromise the productivity of load-carrying applications. The work presented in this dissertation has been published in eight peer-reviewed articles. The dissertation authors' contributions to the research with respect to the objectives are given below.

1. An off-the-shelf electro-mechanical cylinder considered suitable with regard to the requirements was identified and investigated in **Paper A**.

2. An offshore pipe racking machine and its operational sequences (i.e., the tripping sequence) with the potential for saving energy were identified and numerically investigated in **Paper A**.

3. A numerical study was carried out in **Paper A** to study feasibility in terms of motion performance when replacing the conventional hydraulic linear actuation system of the offshore pipe racking machines' main reach arm with the off-the-shelf electro-mechanical cylinder concept.

4. The off-the-shelf electro-mechanical cylinder concept was in **Paper A** proven to be unsuitable for the operational sequence of the investigated offshore case study. Consequently, an alternative linear actuator technology based on an electro-hydraulic configuration was identified and reviewed in **Paper B**, and a novel self-contained electro-hydraulic cylinder solution based on state-of-the-art concepts was proposed and numerically studied. Further, in **Paper C**, the new actuation system (i.e., an architecture not found in the literature) was implemented and tested when driving a single-boom crane. Next, in **Paper D**, the energy-saving potential of the proposed actuation system was numerically studied in the offshore pipe racking machine case study. The remaining valve-controlled cylinders of the three reach arms were replaced with the new self-contained electro-hydraulic concept using a common DC bus for electric power distribution to the electric prime movers located on the application.

5. A common control strategy based on a velocity feedforward, PI feedback controller, and high-pass filtered pressure feedback was used in the comparitive analysis. The proposed motion controller was first implemented and tested on the electro-hydraulic cylinder in **Paper C** and then on the benchmark system in **Paper E**. The pressure feedback method presented in **Paper E** makes use of both actuator pressures to achieve improved stabilization in both piston extension and retraction. However, adding the piston-side pressure to the pressure feedback presents instability due to the low bandwidth of the proportional directional control valve. To solve this, **Paper E** proposes a solution to account for the valve dynamics by implementing the inverse model of the valve dynamics in the pressure feedback algorithm. Next, in **Paper F**, a model-based design approach was performed to select proper control parameters for both actuation systems in order to make a fair comparison. Next, the motion performance (**Paper F**) and energy efficiency (**Paper G**) of the proposed self-contained electro-hydraulic cylinder were experimentally compared with the conventional valve-controlled cylinder driving a single-boom crane.

6. A selection guideline was presented in **Paper H** identifying the general positive and negative outcomes associated with replacing the conventional hydraulic cylinder with either the electro-mechanical or electro-hydraulic drive solution designed explicitly for the work cycle of the single-boom crane.

In addition, during this research project, a considerable amount of work was carried out to identify and review commercially available computer-based design tools and design approaches that could have the potential to automate the design process of entire actuation systems. An unpublished investigation and a design tool framework, including challenges that must be solved to realize an automated actuation system design tool, is

therefore presented in this dissertation for the purpose of producing further developments and publications.

4.2 Further Work

In this research project, the investigated electro-mechanical cylinder has only been numerically studied. Hence, further experimental investigations should be considered in order to gain more in-depth knowledge about using this linear actuator technology in load-carrying applications, e.g., on the single-boom crane, as illustrated in Fig. 3.3. This is especially relevant in terms of reliability, durability, and passive-load holding, which is achieved using the electric machine's internal electro-mechanical brake. Moreover, a numerical model for simulating its thermal behavior should be developed and experimentally validated to investigate the permissible power of the mechanical transmission. This type of numerical tool would be useful when designing an electro-mechanical cylinder for a given work cycle.

One minor adverse effect on the motion performance caused by the passive load-holding functionality has been identified during the testing phase of the proposed self-contained electro-hydraulic cylinder driving the single-boom crane. As pointed out in Paper F, there is a reduced pressure spike in the piston-side chamber when load-holding is commanded, causing a minor position drop. This issue was investigated in this research project, and the load-holding control was improved using a pressure control strategy that eliminates the position drop. However, this improvement is not included in this dissertation. The proposed passive load-holding control strategy and results will be published in a forthcoming paper along with a numerical study and comparison of alternative circuits for controlling the actuation of the load-holding pilot-operated check valves.

The proposed self-contained electro-hydraulic cylinder has been designed and numerically tested in four-quadrant operations. However, as regards the studied experimental testbed using the single-boom crane, it is only possible to test the actuation system operating in two quadrants (i.e., when lifting and lowering the crane boom). Hence, it has been considered to implement and test the mobile, self-contained electro-hydraulic testbed (Fig. 3.7a) on a different hydraulically actuated application where the direction of the external load changes during operation, e.g., on a knuckle boom.

The developed testbed has not been built entirely compact in order that it will be flexible in terms of testing different components. Consequently, during testing, no increased temperature has been measured in the hydraulic system during operation. This is also the case when the oil cooler is bypassed and the single-boom crane is operated continuously. Hence, a more compact configuration of the proposed system is being considered

for future implementation (Fig. 3.17b) for the purpose of testing the thermal behavior of the proposed actuation system.

Energy storage and energy regeneration have not been experimentally investigated in this research project. Indeed, only the electric power and amount of energy dissipated in the external braking resistor has been measured and considered when analyzing the potential energy to be recovered. Hence, the inclusion of additional components that enable energy storage based on battery usage is being considered for future implementation in order to evaluate energy efficiency levels when the regenerated energy is reused. In addition, the proposed layout using multiple self-contained cylinders connected to a common DC bus should be experimentally tested to evaluate energy efficiency levels.

Further, the following potential research topics and developments that will benefit the self-contained electro-hydraulic cylinder have been identified:

- a more compact actuation system could be realized by reducing the size of the accumulator used as volume compensator for the flow imbalance emerging from the asymmetric single-rod cylinder. If a hydraulic unit capable of handling higher cage (drain) pressure (i.e., above 2 bar absolute) was available for four-quadrant operations, a smaller accumulator could be selected. For instance, a conceptual study is presented by [146] aiming to improve the compactness by including a bootstrap reservoir instead of a bladder type hydro-pneumatic accumulator;

- a combined electro-hydraulic unit including both the electric machine and hydraulic unit optimized for desired operating conditions will improve energy efficiency, motion performance, and compactness;

- decentralized and compact servo-drives certified for the explosive environment of oil drilling applications are needed to realize a fully compact layout of the proposed common DC bus distribution on the pipe racking machine (Fig. 3.9).

Finally, as presented in Section 3.5, an additional study has been carried out in this research project to investigate the possibility of performing automated design analysis to identify the best suitable (optimal) actuation system for the given design requirements and work cycle of a specific application. This is especially relevant for self-contained cylinders that have a fixed architecture, as they would then have the potential to realize an automated design using a computer-based design tool for sizing and optimal component selection to maximize energy efficiency, motion performance, and compactness. However, the work presented in this dissertation is considered to be a preliminary study, and further development of the proposed design tool frameworks and proofs-of-concept is required.

Bibliography

[1] M. K. Bak. *Model Based Design of Electro-Hydraulic Motion Control Systems for Offshore Pipe Handling Equipment*. PhD thesis, University of Agder, 2014.

[2] W. Pawlus, M. Choux, and M. R. Hansen. Hydraulic vs. electric: A review of actuation systems in offshore drilling equipment. *Journal of Modeling, Identification and Control*, 37(1):1–17, 2016.

[3] D. Hagen, W. Pawlus, M. K. Ebbesen, and T. O. Andersen. Feasibility Study of Electromechanical Cylinder Drivetrain for Offshore Mechatronic Systems. *Journal of Modeling, Identification and Control*, 38(2):59–77, 2017.

[4] D. Hagen, D. Padovani, and M. Choux. Enabling Energy Savings in Offshore Mechatronic Systems by using Self-Contained Cylinders. *Journal of Modeling, Identification and Control*, 40(2):89–108, 2019.

[5] D. Hagen, D. Padovani, and M. Choux. Design and Implementation of Pressure Feedback for Load-Carrying Applications with Position Control. In *Sixteenth Scandinavian International Conference on Fluid Power*, Tampere, Finland, 2019.

[6] EUR-Lex. ATEX Directive 2014/34/EU. `https://bit.ly/2TPVszm`, Accessed: 2020-03-15.

[7] DNV GL. Northern Drilling's West Mira first rig to receive DNV GL Battery (Power) Class Notation. `https://bit.ly/33iXBXz`, Accessed: 2020-03-15.

[8] C. Helsley. Power by Wire for Aircraft - The All-Electric Airplane. *SAE Transactions*, 86(4):3464–3478, 1977.

[9] W. Swingle and J. Edge. The Electric Orbiter. In *Aerospace Congress and Exposition*, SAE International in United States, 1982.

[10] A. Garcia, J. Cusido, J. A. Rosero, J. A. Ortega, and L. Romeral. Reliable electro-mechanical actuators in aircraft. *IEEE Aerospace and Electronic Systems Magazine*, 23(8):19–25, 2008.

[11] A. Boglietti, A. Cavagnino, A. Tenconi, and S. Vaschetto. The safety critical electric machines and drives in the more electric aircraft: A survey. In *2019 35th Annual Conference of IEEE Industrial Electronics*, pages 2587–2594, Porto, Portugal, 2009.

[12] F. Jian, J.-C. Maré, and F. Yongling. Modelling and simulation of flight control electromechanical actuators with special focus on model architecting, multidisciplinary effects and power flows. *Chinese Journal of Aeronautics*, 30(1):47–65, 2017.

[13] S. Frischemeier. Electrohydrostatic actuators for aircraft primary flight control-types, modelling and evaluation. In *5th Scandinavian International Conference on Fluid Power, SICFP '97*, Linköping, Sweden, 1997.

[14] D. Van Den Bossche. The A380 flight control electrohydrostatic actuators, achievements and lessons learnt. In *25th International Congress of the Aeronautical Sciences*, pages 1–8, Hamburg, Germany, 2006.

[15] Parker. Innovations in Flight Control Systems and Subsystems Brochure. `https://prker.co/2xA80Cg`, Accessed: 2020-03-15.

[16] S. Michel and J. Weber. Energy-efficient electrohydraulic compact drives for low power applications. In *ASME/BATH 2012 Symposium on Fluid Power and Motion Control*, pages 93–107, Bath, UK, 2012.

[17] C. Boes and A. Helbig. Electro hydrostatic actuators for industrial applications. In *9th International Fluid Power Conference*, pages 134–142, Vol. 9. Aachen, Germany, 2014.

[18] A. Helbig. Electrohydrostatic Actuation: An Energy-Efficient Option for Machine Builders. In *Hydraulics & Pneumatics*, Setembro, 2015.

[19] A. Helbig and C. Boes. Electric Hydrostatic Actuation-modular building blocks for industrial applications. In *10th International Fluid Power Conference*, pages 93–102, Dresden, Germany, 2016.

[20] Jena Tec Precision. Ballscrew Linear Actuators: Catalogue. `https://bit.ly/2IKLfxZ`, Accessed: 2020-03-15.

[21] Rexroth. Servo-Hydraulic Actuator – SHA: Presentation DC/ESS21. `https://bit.ly/2wUCP4m`, Accessed: 2020-03-15.

[22] M. Ristic and M. Wahler. Electrification of Hydraulics Opens New Ways for Intelligent Energy-Optimized Systems. In *11th International Fluid Power Conference*, pages 219–231, Aachen, Germany, 2018.

Bibliography

[23] L. Harnefors. *Control of Variable-Speed Drives*. Mälardalen University, 2003.

[24] N. Mohan. *Advanced Electric Drives: Analysis, Control, and Modeling Using MAT-LAB / Simulink*. John Wiley & Sons, Inc., 2014.

[25] Rexroth. *Electromechanical Cylinder EMC – HD: Catalog R999000326*. Bosch Rexroth AG, 2019.

[26] Maurizio Palmieri. Vite e madrevite tecniche a disposizioneVite e madrevite: le diverse soluzioni tecniche a disposizione. `https://bit.ly/33j9zjS`, Accessed: 2020-03-15.

[27] Parker. *Extreme Force Electromechanical Cylinder – Series XFC: Catalog HY08-0890-4/NA*. Parker Hannifin Corporation, 2013.

[28] Servi Group. Servi Hybrid Drive – a complete system in a single unit! `https://bit.ly/38LfwY0`, Accessed: 2020-03-15.

[29] Parker. *Compact EHA – Electro-Hydraulic Actuators for high power density applications: Catalog HY22-3101E 7/13*. Parker Hannifin Corp., 2013.

[30] Voith. SelCon electrohydraulic linear actuator. `https://bit.ly/2We7B2P`, Accessed: 2020-03-15.

[31] D. Hagen, D. Padovani, and M. K. Ebbesen. Study of a Self-Contained Electro-Hydraulic Cylinder Drive. In *2018 Global Fluid Power Society PhD Symposium (GFPS)*, Samara, Russia, 2018.

[32] D. Padovani, S. Ketelsen, D. Hagen, and L. Schmidt. A Self-Contained Electro-Hydraulic Cylinder with Passive Load-Holding Capability. *Energies*, 12(2), 2019.

[33] J. Zimmerman, E. Busquets, and M. Ivantysynova. 40% Fuel Savings by Displacement Control Leads to Lower Working Temperatures – A Simulation Study and Measurements. In *52nd National Conference on Fluid Power*, Las Vegas, NV, USA, 2011.

[34] S. Michel and J. Weber. Electrohydraulic Compact-drives for Low Power Applications considering Energy-efficiency and High Inertial Loads. In *7th FPNI PhD Symposium on Fluid Power*, pages 27–30, Reggio Emilia, Italy, 2012.

[35] T. Minav, P. Sainio, and M. Pietola. Direct Driven Hydraulic Drive Without Conventional Oil Tank. In *ASME/BATH 2014 Symposium on Fluid Power and Motion Control*, Bath, UK, 2014.

[36] G. Altare and A. Vacca. A design solution for efficient and compact electro-hydraulic actuators. *Procedia Engineering*, 106:8–16, 2015.

[37] H. Çalışkan, T. Balkan, and B. Platin. A Complete Analysis for Pump Controlled Single Rod Actuators. In *10th International Fluid Power Conference*, pages 119–132, Dresden, Germany, 2016.

[38] S. H. Cho and R. Burton. Position control of high performance hydrostatic actuation system using a simple adaptive control (SAC) method. *Mechatronics*, 21(1):109–115, 2011.

[39] J. Willkomm, M. Wahler, and J. Weber. Potentials of Speed and Displacement Variable Pumps in Hy- draulic Applications. In *10th International Fluid Power Conference*, pages 379–391, Dresden, Germany, 2016.

[40] S. Ketelsen, D. Padovani, T. O. Andersen, M. K. Ebbesen, and L. Schmidt. Classification and Review of Pump-Controlled Differential Cylinder Drives. *Energies*, 12(7), 2019.

[41] R. Rahmfeld. *Development and Control of Energy Saving Hydraulic Servo Drives for Mobile Systems*. PhD thesis, TU Hamburg-Harburg, 2002.

[42] R. Rahmfeld and M. Ivantysynova. Energy saving hydraulic actuators for mobile machines. In *1st Bratislavian Fluid Power Symposium*, Casta-Pila, Slovakia, 1998.

[43] R. L. Kenyon, D. Scanderbeg, M. E. Nolan, and W. D. Wilkerson. Electro-hydraulic actuator, Patent EP0395420 A2, 1990.

[44] L. Quan. Current State, Problems and the Innovative Solution of Electro-hydraulic Technology of Pump Controlled Cylinder. *Chinese Journal of Mechanical Engineering*, 44(11):87–92, 2008.

[45] D. Zhang, W. Li, Y. Lin, and J. Bao. An overview of hydraulic systems in wave energy application in China. *Renewable and Sustainable Energy Reviews*, 16(7):4522–4526, 2012.

[46] J. Huang, L. Quan, and X. Zhang. Development of a dual-acting axial piston pump for displacement-controlled system. *Institution of Mechanical Engineers, Part B: Journal of Engineering Manufacture*, 228(4):606–616, 2014.

[47] K. G. Cleasby and A. R. Plummer. A novel high efficiency electrohydrostatic flight simulator motion system. In *ASME/BATH 2008 Symposium on Fluid Power and Motion Control*, pages 437–449, Bath, UK, 2008.

Bibliography

[48] B. Brahmer. CLDP - Hybrid Drive using Servo Pump in Closed Loop. In *8th International Fluid Power Conference*, pages 93–102, Dresden, Germany, 2012.

[49] H. C. Pedersen, L. Schmidt, T. O. Andersen, and M. H. Brask. Investigation of New Servo Drive Concept Utilizing Two Fixed Displacement Units. *JFPS International Journal of Fluid Power System*, 8(1):1–9, 2014.

[50] L. Schmidt, D. B. Roemer, H. C. Pedersen, and T. O. Andersen. Speed-Variable Switched Differential Pump System for Direct Operation of Hydraulic Cylinders. In *ASME/BATH 2015 Symposium on Fluid Power and Motion Control*, Chicago, Illinois, USA, 2015.

[51] L. Schmidt, M. Groenkjaer, H. C. Pedersen, and T. O. Andersen. Position Control of an Over-Actuated Direct Hydraulic Cylinder Drive. *Control Engineering Practice*, 64:1–14, 2017.

[52] S. Ketelsen, L. Schmidt, V. H. Donkov, and T. O. Andersen. Energy saving potential in knuckle boom cranes using a novel pump controlled cylinder drive. *Journal of Modeling, Identification and Control*, 39(2), 2018.

[53] T. Wiens and D. Bitner. An efficient, high performance and low-cost energy recovering hydrostatic linear actuator concept. In *ASME/BATH 2016 Symposium on Fluid Power and Motion Control*, pages 1–10, Bath, UK, 2016.

[54] C. Williamson and M. Ivantysynova. Stability and motion control of inertial loads with displacement controlled hydraulic actuators. In *6th FPNI - PhD Symposium*, pages 15–19, Vol. 2. West Lafayette, IN, USA, 2010.

[55] Rexroth. Electrification and digitalization: The fitness program for hydraulics. `https://bit.ly/2IOvAO1`, Accessed: 2020-03-15.

[56] T. Sweeney, P. T. Kubinski, and D. J. Anderson. Electro-hydraulic actuator mounting, Patent US 8161742 B2, 2008.

[57] G. Altare, A. Vacca, and C. Richter. A novel pump design for an efficient and compact electro-hydraulic actuator. In *2014 IEEE Aerospace Conference*, pages 1–12, Big Sky, MT, USA, 2014.

[58] E. Jalayeri, A. Imam, Z. Tomas, and N. Sepehri. A throttle-less single-rod hydraulic cylinder positioning system: Design and experimental evaluation. *Advances in Mechanical Engineering*, 7(5):1–14, 2015.

[59] M. K. Bak and M. R. Hansen. Analysis of offshore knuckle boom Crane-Part Two: Motion control. *Journal of Modeling, Identification and Control*, 34(4):175–181, 2013.

[60] C. Williamson and M. Ivantysynova. The effect of pump efficiency on displacement-controlled actuator systems. In *Tenth Scandinavian International Conference on Fluid Power*, pages 301–326, Tampere, Finland, 2007.

[61] R. L. Huston and Y. Wang. Flexibility Effects in Multibody Systems. In *Computer-Aided Analysis of Rigid and Flexible Mechanical Systems*, pages 351–376. Springer, 1994.

[62] M. K. Bak and M. R. Hansen. Analysis of offshore knuckle boom Crane-Part One: Modeling and parameter identication. *Journal of Modeling, Identification and Control*, 34(4):157–174, 2013.

[63] J. K. Sørensen, M. R. Hansen, and M. K. Ebbesen. Numerical and Experimental Study of a Novel Concept for Hydraulically Controlled Negative Loads. *Journal of Modeling, Identification and Control*, 37(4):195–211, 2016.

[64] D. Hagen, D. Padovani, and M. Choux. Guidelines to Select Between Self-Contained Electro-Hydraulic and Electro-Mechanical Cylinders. In *15th IEEE Conference on Industrial Electronics and Applications (ICIEA)*, accepted for presentation, Kristiansand, Norway, 9-13 November, 2020.

[65] T. I. Hwang. Hydraulic circuit with load holding valves operated by external pilot pressure , Patent EP 2071195 A2, 2009.

[66] B. Xu, X. Ouyang, and H. Yang. Energy-saving system applying pressure accumulators for VVVF controlled hydraulic elevators. In *ASME 2003 International Mechanical Engineering Congress and Exposition*, pages 117–122, Washington, DC, USA, 2003.

[67] H. Yang, W. Sun, and B. Xu. New investigation in energy regeneration of hydraulic elevators. *IEEE/ASME Transactions on Mechatronics*, 12(5):519–526, 2007.

[68] T. Minav, L. Papini, and M. Pietola. A Thermal Analysis of Direct Driven Hydraulics. In *10th International Fluid Power Conference*, pages 235–248, Dresden, Germany, 2016.

[69] N. Karlén, T. Minav, and M. Pietola. Investigation of Thermal Effects in Direct Driven Hydraulic System for Off-Road Machinery. In *9th FPNI Ph.D. Symposium on Fluid Power*, Florianópolis, SC, Brazil, 2016.

[70] S. Michel and J. Weber. Prediction of the thermo-energetic behaviour of an electrohydraulic compact drive. In *10th International Fluid Power Conference*, pages 219–234, Dresden, Germany, 2016.

[71] P. Krus and J.-O. Palmberg. Damping of mobile systems in machines with high inertia loads. *JFPS International Symposium on Fluid Power*, 1989(1):63–70, 1989.

[72] H. C. Pedersen, T. O. Andersen, and M.R. Hansen. Guidelines for Properly Adjusting Pressure Feedback in Systems With Over-Centre Valves. In *BATH/ASME 2016 Symposium on Fluid Power and Motion Control*, Bath, UK, 2016.

[73] J. Mohieddine and A. Kroll. *Hydraulic Servo-systems: Modelling, Identification and Control*. Springer-Verlag London, 2003.

[74] Rexroth. *Rexroth Sytronix SvP 7020 PFC Variable-Speed Positioning of Hydraulic Axes: Catalog R911379550*. Bosch Rexroth AG, 2017.

[75] C. L. Phillips and R. D. Harbor. *Feedback Control Systems*. Prentice-Hall International Editions, 1991.

[76] D. Hagen, D. Padovani, and M. Choux. A Comparison Study of a Novel Self-Contained Electro-Hydraulic Cylinder versus a Conventional Valve-Controlled Actuator—Part 1: Motion Control. *Actuators*, 8(4):79, 2019.

[77] D. Hagen, D. Padovani, and M. Choux. A Comparison Study of a Novel Self-Contained Electro-Hydraulic Cylinder versus a Conventional Valve-Controlled Actuator—Part 2: Energy Efficiency. *Actuators*, 8(4):78, 2019.

[78] S. Ketelsen, T. O. Andersen, M. K. Ebbesen, and L. Schmidt. Mass Estimation of Self-Contained Linear Electro-Hydraulic Actuators and Evaluation of the Influence on Payload Capacity of a Knuckle Boom Crane. In *ASME/BATH 2019 Symposium on Fluid Power and Motion Control*, Longboat Key, Florida, USA, 2019.

[79] T. Erbe, T. Stroehla, R. Theska, and C. Weber. Decision-aid for actuator selection. In *DESIGN 2010, the 11th International Design Conference*, Dubrovnik, Croatia, 2010.

[80] V. Vodovozov, Z. Raud, and M. Egorov. A toolbox to design and study electric drives. In *14th International Power Electronics and Motion Control Conference EPE-PEMC 2010*, pages 142–148, Ohrid, Macedonia, 2010.

[81] V. Vodovozov and J. Laugis. Motor drive design using structured query language. *Estonian Journal of Engineering*, 14(4):334–344, 2008.

[82] W. Pawlus, G. Hovland, M. Choux, D. Frick, and M. Morari. Drivetrain design optimization for electrically actuated systems via mixed integer programing. In *IECON 2015 - 41st Annual Conference of the IEEE Industrial Electronics Society*, pages 001465–001470, Yokohama, Japan, 2015.

[83] P. Krus. Simulation based optimisation for system design. In *14th International Conference on Engineering Design*, pages 459–460, Stockholm, Sweden, 2003.

[84] R. H. Bishop. *The Mechatronics Handbook*. CRC Press, 2002.

[85] T. O. Andersen, H. C. Pedersen, and M. R. Hansen. Mechatronic system design based on an optimisation approach. In *Mechatronics Day 2007-International Workshop on Mechatronics*, pages 1–9, Copenhagen, Denmark, 2007.

[86] H. C. Pedersen, M. R. Hansen, T. O. Andersen, and M. M. Bech. Presenting a Multi-Level Superstructure Optimization Approach for Mechatronic System Design. In *ASME 2010 10th Biennial Conference on Engineering Systems Design and Analysis*, Istanbul, Turkey, 2010.

[87] A. D. Poole and J. D. Booker. Design methodology and case studies in actuator selection. *Mechanism and Machine Theory*, 46(5):647–661, 2011.

[88] J. F. Cuttino, D. D. Newman, J. K. Gershenson, and D. E. Schinstock. A structured method for the classification and selection of actuators for space deployment mechanisms. *Journal of Engineering Design*, 11(1):31–53, mar 2000.

[89] W. Huang. On the selection of shape memory alloys for actuators. *Materials and Design*, 23(1):11–19, 2002.

[90] J. D. Madden and L. Filipozzi. Web-based actuator selection tool. In *SPIE 5759, Smart Structures and Materials 2005: Electroactive Polymer Actuators and Devices (EAPAD)*, pages 9–15, San Diego, California, United States, 2005.

[91] M. Zupan, M. F. Ashby, and N. A. Fleck. Actuator classification and selection—the development of a database. *Advanced Engineering Materials*, 4(12):933–940, 2002.

[92] K. Srinivasan. Toward Broader Education in Control System Design for Mechanical Engineers: Actuation System Selection and Controller Co-design. In *Advances in Mechanisms, Robotics and Design Education and Research*, pages 329–347. Springer, 2013.

[93] V. Ivanov, M. Ruderman, J. Schiffer, and M. Horn. Interdisciplinary design methodology for systems of mechatronic systems focus on highly dynamic environmental

applications. In *IECON 2017 - 43rd Annual Conference of the IEEE Industrial Electronics Society*, pages 4062–4067, Beijing, China, 2017.

[94] P. Livotov, D. Casner, R. Houssin, and J. Renaud. Problem Definition and Identification of Contradictions in the Interdisciplinary Areas of Mechatronic Engineering. In *Advances and Impacts of the Theory of Inventive Problem Solving*, pages 231–242. Springer, 2018.

[95] M. R. Hansen and T. O. Andersen. Automatic Design of Proportional Valve Spools. In *1st International Conference on Computational Methods in Fluid Power Technology, Methods for Solving Practical Problems in Design and Control*, Melbourne, Australia, 2003.

[96] C. C. Egbuna. *An Electric Actuator Selection Aid for Low Cost Automation*. Msc thesis, University of Stellenbosch, 2008.

[97] C. C. Egbuna and A. H. Basson. Electric Actuator Selection Design Aid for Low Cost Automation. In *ICED 09, the 17th International Conference on Engineering Design, Vol. 6, Design Methods and Tools (pt. 2)*, pages 43–54, Palo Alto, CA, USA, 2009.

[98] T. Erbe, J. Król, T. Ströhla, and R. Theska. Selection of Precision Actuators by Novel Function-Structure-Correspondences. In *23rd annual meeting of the American Society for Precision Engineering and the 12th ICPE*, Portland, OR, USA, 2008.

[99] T. Erbe, C. Weber, and K. Paetzold. Actuation Principle Selection–An Example for Trade-Off Assessment by CPM-Approach. In *18th International Conference on Engineering Design (ICED 11), Impacting Society through Engineering Design, Vol. 4: Product and Systems Design*, Lyngby/Copenhagen, Denmark, 2011.

[100] T. Erbe. *Beitrag zur systematischen Aktor- und Aktorprinzipauswahl im Entwicklungsprozess*. PhD thesis, Technischen Universität Ilmenau, 2013.

[101] Parker. EL-Sizing Tool. `https://prker.co/2vrHbj8`, Accessed: 2020-03-15.

[102] Rexroth. Tools and configurators – SytronixSize. `https://bit.ly/3cZNtXX`, Accessed: 2020-03-15.

[103] Rexroth. Rexroth IndraSize – Turbo for Drive Sizing. `https://bit.ly/2TPKKJi`, Accessed: 2020-03-15.

[104] U.S. Department of Energy. The MotorMaster+ Software Tool. `https://bit.ly/2QeV3o8`, Accessed: 2020-03-15.

[105] Natural Resources Canada. CanMOST – Canadian Motor Selection Tool. `https://bit.ly/2U8Vr8x`, Accessed: 2020-03-15.

[106] J. E. Huber, N. A. Fleck, and M. F. Ashby. The selection of mechanical actuators based on performance indices. *Royal Society of London. Series A: Mathematical, physical and engineering sciences*, 453(1965):2185–2205, 1997.

[107] D. J. Bell, T. J. Lu, N. A. Fleck, and S. M. Spearing. MEMS actuators and sensors: observations on their performance and selection for purpose. *Journal of Micromechanics and Microengineering*, 15(7):S153–S164, 2005.

[108] G. Granosik and J. Borenstein. Pneumatic actuators for serpentine robot. In *Climbing and Walking Robots*, pages 719–726. Springer, 2006.

[109] J. Webster. Actuator Requirements and Roadmaps. In *More Intelligent Gas Turbine Engines (Des turbomoteurs plus intelligents)*, pages 136–153. RTO/NATO, 2009.

[110] University of Cambridge. Cambridge Engineering Selector. `https://bit.ly/2Qxk1zh`, Accessed: 2020-03-15.

[111] Ansys Granta. GRANTA Selector. `https://bit.ly/3aYzDU8`, Accessed: 2020-03-15.

[112] SIEMENS. TIA Selection Tool – quick, easy, smart configuration. `https://sie.ag/2QiCPC6`, Accessed: 2020-03-15.

[113] S. Silber, G. Bramerdorfer, A. Dorninger, A. Fohler, J. Gerstmayr, W. Koppelstätter, D. Reischl, G. Weidenholzer, and S. Weitzhofer. Coupled optimization in MagOpt. *Proceedings of the Institution of Mechanical Engineers, Part I: Journal of Systems and Control Engineering*, 230(4):291–299, 2016.

[114] J. Schröck, M. Schrögenhumer, S. Weitzhofer, J. Passenbrunner, and M. Nader. An Integrated Mechatronic Modelling, Simulation, and Optimization Approach for the Customized Design of Active Vibration Damping Solutions. In *2018 Joint Conference-Acoustics*, pages 284–289, Ustka, Poland, 2018.

[115] Linz Center of Mechatronics. SyMSpace: The system model space. `https://bit.ly/2U7PRDx`, Accessed: 2020-03-15.

[116] SKF. Actuator Select. `https://bit.ly/2U5jV2J`, Accessed: 2020-03-15.

[117] Tolomatic. Tolomatic Electric Actuator Sizing Application. `https://bit.ly/2TQOCcN`, Accessed: 2020-03-15.

Bibliography

[118] P. Krus, A. Jansson, and J.-O. Palmberg. Optimization for Component Selection Hydraulic Systems. In *Fourth Bath International Fluid Power Workshop*, Bath, UK, 1991.

[119] A. Jansson. *Fluid Power System Design - A Simulation Approach*. PhD thesis, Linköping University, 1994.

[120] M. R. Hansen and T. O. Andersen. A design procedure for actuator control systems using optimization methods. In *7th Scandinavian International Conference on Fluid Power*, pages 1–20, Linköping, Sweden, 2001.

[121] J. Andersson and P. Krus. Multiobjective Optimization of Mixed Variable Design Problems. In *International Conference on Evolutionary Multi-Criterion Optimization*, pages 624–638. Springer, 2001.

[122] N. Krimbacher, M. Gartenauer, R. Scheidl, M. Garstenauer, and R. Scheidl. Optimization of hydraulic systems by means of numerical simulation. In *2nd International Workshop on Computer Software for Design*, Vol. 7683. Ostrava-Malenovice, Czech Republic, 2001.

[123] A. Bowling and O. Khatib. Actuator Selection for Desired Dynamic Performance. In *IEEE/RSJ International Conference on Intelligent Robots and Systems*, pages 1966–1973, Vol. 2. Lausanne, Switzerland,, 2002.

[124] M. R. Hansen, T. O. Andersen, and H. C. Pederesen. An approach to automated system design of hydraulic systems. In *Power Transmission and Motion Control Workshop*, pages 335–347, Bath, UK, 2003.

[125] E. Papadopoulos and I. Davliakos. A Systematic Methodology for Optimal Component Selection of Electrohydraulic Servosystems. *International Journal of Fluid Power*, 5(3):15–24, 2004.

[126] M. R. Hansen, T. O. Andersen, and H. C. Pederesen. System topology optimization. In *1st International Conference on Computational Methods in Fluid Power Technology, Methods for Solving Practical Problems in Design and Control*, Melbourne, Australia, 2003.

[127] M. R. Hansen and T. O. Andersen. System topology optimization*. *Australian Journal of Mechanical Engineering*, 2(2):133–141, 2005.

[128] F. Roos, H. Johansson, and J. Wikander. Optimal selection of motor and gearhead in mechatronic applications. *Mechatronics*, 16(1):63–72, 2006.

[129] H. C. Pedersen. *Automated hydraulic system design and power management in mobile applications.* PhD thesis, Aalborg University, 2007.

[130] M. R. Hansen and T. O. Andersen. Design Optimization of Hydraulically Actuated Lifting Table Using Mapping Techniques. In *Ninth Scandinavian International Conference on Fluid Power, SICFP'05*, Linköping, Sweden, 2005.

[131] M. R. Hansen, T. O. Andersen, and O. Ø. Mouritsen. A Method for Linked Discrete Design Variables Applied to Lifting Tables. In *12th AIAA/ISSMO Multidisciplinary Analysis and Optimization Conference*, pages 1–8, Victoria, British Columbia, Canada, 2008.

[132] M. Pettersson. *Design Optimization in Industrial Robotics Methods and Algorithms for Drive Train Design.* PhD thesis, Linköping University, 2008.

[133] L. Zhou, S. Bai, and M. R. Hansen. Design optimization on the drive train of a light-weight robotic arm. *Mechatronics*, 21(3):560–569, 2011.

[134] S. Rezazadeh and J. W. Hurst. On the optimal selection of motors and transmissions for electromechanical and robotic systems. In *2014 IEEE/RSJ International Conference on Intelligent Robots and Systems*, pages 4605–4611, Chicago, IL, USA, 2014.

[135] F. Tian and M. Voskuijl. Mechatronic design and optimization using knowledge-based engineering applied to an inherently unstable and unmanned aerial vehicle. *IEEE/ASME Transactions on Mechatronics*, 21(1):542–554, 2015.

[136] G. Cusimano. A procedure for a suitable selection of laws of motion and electric drive systems under inertial loads. *Mechanism and Machine Theory*, 38(6):519–533, 2003.

[137] G. Cusimano. Generalization of a method for the selection of drive systems and transmissions under dynamic loads. *Mechanism and Machine Theory*, 40(5):530–558, 2005.

[138] G. Cusimano. Optimization of the choice of the system electric drive-device—transmission for mechatronic applications. *Mechanism and Machine Theory*, 42(1):48–65, 2007.

[139] G. Cusimano. Choice of electrical motor and transmission in mechatronic applications: The torque peak. *Mechanism and Machine Theory*, 46(9):1207–1235, 2011.

Bibliography

[140] G. Cusimano. Choice of motor and transmission in mechatronic applications: Non-rectangular dynamic range of the drive system. *Mechanism and Machine Theory*, 85:35–52, 2015.

[141] I. A. H. Aly. *Holistic Design: Optimizing Mechatronic Systems Using Multi Objective Optimization*. Msc thesis, American University of Sharjah, 2015.

[142] Ø. Magnussen. *Multirotor Design Optimization: The Mechatronic Approach*. PhD thesis, University of Agder, 2015.

[143] G. Han, F. Xie, and X.-J. Liu. Optimal Selection of Servo Motor and Reduction Ratio for High-Speed Parallel Robots. In *8th International Conference, ICIRA 2015*, pages 109–120, Portsmouth, UK, 2015.

[144] C. Tamm and S. Perfetto. Design and optimization of mechatronic systems using a holistic and parametric simulation approach. *IFAC-PapersOnLine*, 52(15):271–276, 2019.

[145] M. Riedel, E. Arroyo, and A. Fay. Knowledge-based selection of principle solutions for sensors and actuators based on standardized plant description and semantic concepts. In *2015 IEEE 20th Conference on Emerging Technologies & Factory Automation (ETFA)*, Luxembourg, Luxembourg, 2015.

[146] S. Ketelsen, G. Kolks, T. O. Andersen, L. Schmidt, and J. Weber. Bootstrap Reservoir Concepts for Electro-Hydraulic Compact Cylinder Drives. In *12th International Fluid Power Conference (IFK)*, accepted for presentation, Dresden, Germany, 12-14 October, 2020.

————————————————

Paper A

Feasibility Study of Electromechanical Cylinder Drivetrain for Offshore Mechatronic Systems

Daniel Hagen, Witold Pawlus, Morten K. Ebbesen, and Torben O. Andersen

Feasibility Study of Electromechanical Cylinder Drivetrain for Offshore Mechatronic Systems

D. Hagen [1] W. Pawlus [1] M.K. Ebbesen [1] T.O. Andersen [2]

[1] *Department of Engineering Sciences, University of Agder, N-4898 Grimstad, Norway.*
E-mail: daniel.hagen,witold.pawlus,morten.k.ebbesen@uia.no

[2] *Department of Energy Technology, Aalborg University, 9220 Aalborg East, Denmark.*
E-mail: toa@et.aau.dk

Abstract

Currently, there is an increasing focus on the environmental impact and energy consumption of the oil and gas industry. In offshore drilling equipment, electric motors tend to replace traditionally used hydraulic motors, especially in rotational motion control applications. However, force densities available from linear hydraulic actuators are still typically higher than those of electric actuators. Therefore, usually the remaining source of hydraulic power is thereby the hydraulic cylinder. This paper presents a feasibility study on the implementation of an electromechanical cylinder drivetrain on an offshore vertical pipe handling machine. The scope of this paper is to investigate the feasibility of a commercial off-the-shelf drivetrain. With a focus on the motion performance, numerical modeling and simulation are used when sizing and selecting the components of the considered electromechanical cylinder drivetrain. The simulation results are analyzed and discussed together with a literature study regarding advantages and disadvantages of the proposed solution considering the design criteria of offshore drilling equipment. It is concluded that the selected drivetrain can only satisfy the static motion requirements since the required transmitted power is higher than the recommended permissible power of the transmission screw. Consequently, based on the recommendation of the manufacturer, avoidance of overheating cannot be guaranteed for the drivetrain combinations considered for the case study presented in this paper. Hence, to avoid overheating, the average speed of the motion cycle must be decreased. Alternatively, external cooling or temperature monitoring and control system that prevents overheating could be implemented.

Keywords: Mechatronic systems, offshore drilling, hydraulic actuation systems, electromechanical cylinder, modeling and simulation, multibody systems, motion control.

1 Introduction

Since the 1960's, drilling for oil and gas production (well construction) has been carried out in harsh offshore environments like the North Sea. More recently, the drilling process has moved towards operation in ultra deep-water (water depths beyond 1500m) and Arctic areas. Clearly, this has required a significant development of the offshore drilling equipment, especially regarding monitoring and control systems and more

advanced heave compensating technology. Hence, developments in automation and safety of machine operation have contributed to increased usage of multidisciplinary technologies. Therefore, design, production and operation of a typical offshore drilling machine requires synthesis of knowledge from various disciplines, such as mechanical engineering, electrical engineering, control theory, hydraulic actuation systems and many more, in short – mechatronics. This is why an increasing number of offshore drilling systems is considered to

be mechatronic systems and hence, they are referred in this paper to as offshore mechatronic systems (OMS).

The hydraulic actuation systems (drives) used in OMS consist of several hydraulic circuits supplied by a hydraulic power unit (HPU). Hydraulic drives are well known for their high reliability, robust safety features, high power transmission, high load capabilities and good overload protection. In Bak (2014) methods for modeling, parameter identification, design and optimization of an offshore pipe deck (knuckle boom) crane are presented, focusing on accommodating the needs of the system designer. Figure 1 illustrates a typical offshore drilling rig layout.
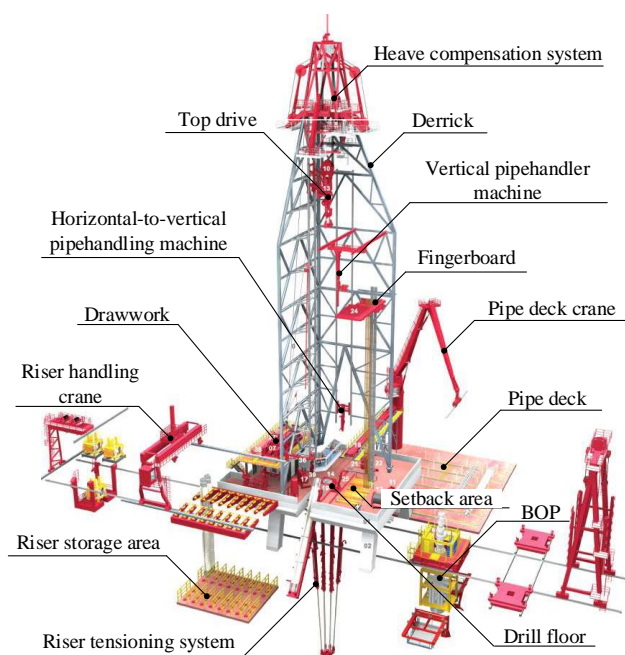
Figure 1: Typical drilling rig layout. Image courtesy of Bak (2014).

Due to an increasing focus on the environmental footprint and energy consumption, offshore oil and gas industry is experiencing a shift in drive systems as highly efficient electric drives tend to replace less efficient hydraulic drives. A review of drive systems encountered in offshore drilling applications is presented by Pawlus et al. (2016a), specifically focusing on giving a comparison of hydraulic and electric rotary drivetrains along with detailed explanations of their advantages and drawbacks.

Currently, the shift from the traditionally used hydraulic motors to electric motors is observed in an increasing number of applications, e.g. top-drive, drawwork, and pipe handling machines. However, the possibility of using both electrical motors and hydraulic cylinders on multi-functional machinery proves

to combine some excellent characteristics from the two branches of actuation technology. To fully benefit from such a hybrid drive solution, there is a need for linear drives capable of operating free of a central HPU, i.e. self-contained with power supplied via electrical wiring.

In other industries, hydraulic cylinders are successfully replaced by self-contained electromechanical cylinder (EMC) drivetrains which increase energy-efficiency and motion accuracy in some applications. The modular self-contained design offers advantages such as plug and play installation and low maintenance. In many industries, disadvantages like increased wear, inadequate overload protection, and decreased load capabilities are accepted. There is, however, insufficient research conducted that compares the electrohydraulic cylinder with valve control (EHC) against the EMC drivetrain for the design criteria which characterize OMS.

A literature survey on this topic shows that there is little available scientific research comparing EMC drivetrains and EHC systems for the harsh environment and load spectra of OMS. Furthermore, the closest research topics found in literature come from the aircraft and aerospace industries. Since the late 1970's, several research and development projects, with such topics as e.g. *More Electric Aircraft* and *Power-by-Wire-Technology*, consider future technology for aircraft flight control systems, aiming to reduce the overall system weight, as well as installation and maintenance effort, according to Frischemeier (1997). Thus, research on replacing traditional EHC systems with EMCs in aircraft flight control and aerospace systems is well documented in literature.

Comparative analysis of different types of mechanical screw transmissions (ball-screw and roller screw) and their design regarding reliability (fail safe modes) is presented by Bodden et al. (2007) and Garcia et al. (2008). To diagnose the condition of an EMC drivetrain, Balaban et al. (2009) demonstrate diagnostic algorithms for aerospace systems. In Narasimhan et al. (2010), an approach that combines the analytical model-based and feature-driven diagnosis approaches for the detection and isolation of single faults is presented.

In addition, a significant number of web articles that compare EMC drivetrains with EHC systems regarding pros and cons can be found on the Internet – a few representative topics are *Hydraulic vs. Electromechanical Actuators* and *Choosing Between Electromechanical and Fluid Power Linear Actuators in Industrial Systems Design.*

More comprehensive literature discussing the screw transmission itself is also of relevance to this study. A dynamic load test using large load, high bandwidth,

60

hydraulic actuation to generate load profiles under force control is demonstrated in Schinstock and Haskew (1996). In Lemor (1996), the efficiency of a screw transmission and the means to improve it and maintain it for the life of the component are discussed and different modes of failure and their most common order of appearance, cases of failures and analysis of those failures are presented. The capabilities and limitations of a roller screw with emphasis on slip tendency is presented in Hojjat and Mahdi Agheli (2009).

Through the above brief survey it is indicated that design and operation of EMC drivetrains for offshore drilling applications are relatively new and yet undiscovered research directions. Therefore, this paper presents a feasibility study of the implementation of an EMC drivetrain in a case study of an offshore vertical pipe handling machine. The scope of this paper is to size and select a commercial off-the-shelf EMC drivetrain from a manufacturer catalog and model the selected drive components based on the information available in a data sheet. State-of-the-art hydraulic actuation systems for offshore drilling applications together with the design criteria and challenges of offshore equipment systems are introduced in Section 2. A modeling and simulation case study is presented in Section 3. Section 4 describes the main components of an EMC drivetrain, sizing principles, and how the EMC drivetrain is modeled. The simulation results are presented in Section 5. Firstly, the system loads and motion cycle of the case study are analyzed to dimension the EMC drivetrain components. Secondly, the component combinations when considering both technical and economic factors based on the sizing principles are selected, and the prescribed motion cycle is simulated. Finally, in Section 6, the simulation results are analyzed, and the motion performance is discussed together with a literature study regarding reliability, safety, and durability of an EMC drivetrain, especially focusing on the design criteria of offshore drilling equipment. The last section contains the conclusion.

2 Actuation of Offshore Mechatronic Systems

Modern offshore drilling equipment systems are considered fully mechatronic systems, and state-of-the-art offshore drilling rigs are often referred to as cyber drilling rigs. OMS include a broad range of highly specialized machines that are used to perform different operations. Beside subsea and pressure control equipment – e.g the BOP (blowout preventer) – the remaining equipment is referred to as topside equipment. A typical drilling rig layout is illustrated in Figure 1. The scope of this paper is to investigate the motion performance of an EMC drivetrain in order to verify if commercial off-the-shelf drives are viable alternative to traditional hydraulic linear drives in OMS.

2.1 Hydraulic Actuation Systems

Normally, the hydraulic actuation system used in OMS consists of several hydraulic circuits supplied by a hydraulic power unit (HPU) with constant supply and return pressures. Together with the control system, the circuits of the actuation system make up a number of motion control sub-systems, each controlling one degree of freedom (DOF). Figure 2 illustrates a simplified schematics of a typical EHC motion control sub-system often used in OMS. It consists of a hydraulic cylinder with integrated position sensor, counterbalance valve and a directional control valve as the main components of the EHC system. The linear motion is controlled with the directional control valve which controls the flow into either of the two cylinder chambers. When the EHC is exposed to negative loads, i.e. piston velocity and load have the same direction, the outlet pressure of the cylinder also needs to be controlled. This is usually handled by the counterbalance valve, which provides a relief valve functionality on the outlet side of the cylinder assisted by the pressure on the inlet side. Depending on the application, negative loads can occur in both directions of motion. In these cases, a counterbalance valve is required on both the piston side and the rod side of the cylinder. Counterbalance valves exist in different variations, e.g. externally vented, non-vented and relief compensated, depending on the various applications they are used for (Bak, 2014). The counterbalance valve serves multiple purposes such as (Sørensen, 2016):

- leak tight load holding

- load holding in case of hose failure

- overload protection

- shock absorption

- cavitation prevention at load lowering

- no drop before lift.

In a hydraulic system where the HPU powers more than one hydraulic actuator, most often a pressure compensated directional control valve with electrohydraulic actuation is used. Such a valve gives a load independent flow control which reduces the requirements for the control system. Also, closed loop spool position control is often used in applications where high position and velocity accuracy are necessary.

61

A typical EHC motion control strategy relies on position feedback from an individual DOF and typically consists of the following elements:

- human-machine interface (HMI)

- set point generator (SPG)

- feedforward controller (FFC)

- feedback controller (FBC).

Apart from the cranes, most of the equipment shown in Figure 1 is operated from operator stations (drilling chairs) located in the drilling control room with a direct view of the equipment located on the drill floor. Besides monitors, push buttons and switches, the operator stations contain two joysticks which the operator uses to generate command signals for the control system. Joystick signals are fed to the SPG where they may be treated in different ways depending on the selected control mode. In open loop control mode, the joystick signal u_{JS} is fed directly to the directional control valve as a feedforward signal (Bak and Hansen, 2013) - see Figure 2.
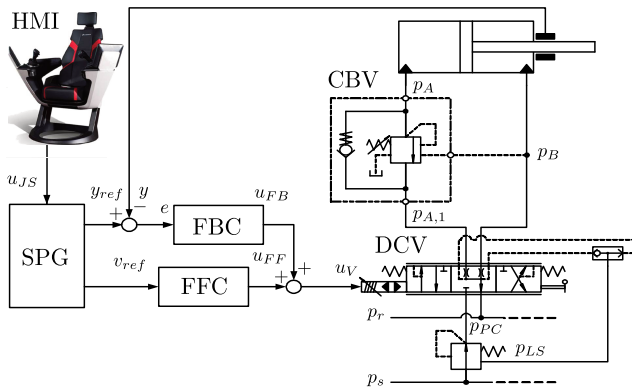
Figure 2: EHC motion control sub-system. Image courtesy of Bak and Hansen (2013).

In closed loop control mode, joystick signals are transformed into velocity and position references for the EHC motions. The latter is used for path control of the tool point, e.g. on a crane where often several DOFs are controlled in a coordinated manner. The FFC is a scaling of the velocity reference v_{ref}, and the FBC is usually a PI controller which compensates for disturbances and accumulated position errors $e = y_{ref} - y$. The control system usually also contains an element that compensates for the deadband of the directional control valve. The system architecture, as shown in Figure 2, is a popular structure because of its simple and, consequently, robust design. Furthermore, the controllers are relatively easy to tune because of the load-independent flow control (Bak, 2014).

2.2 Electrification of Powertrains of OMS

Due to an increasing focus on the environmental impact and reducing the energy consumption, alternating current (AC) motor drives tend to replace hydraulic motors, resulting in advantages such as increased accuracy and energy efficiency, reduced maintenance, and elimination of fluid spills, according to Pawlus et al. (2016a).

However, because of the traditional prevalence of hydraulic drives over electric actuators in translational motion control applications (mainly related to higher force densities available from the former solution), the remaining hydraulic drives on majority of offshore drilling equipment are thereby the hydraulic cylinders (Pawlus et al., 2016a). On the other hand, rotational motion control applications are being gradually dominated by electric motor drives, as illustrated by numerous examples from marine, and oil and gas industries. Obviously, the latter solution is not free of drawbacks. Some of the most typical problems associated with AC motor drives (apart from lower force/torque density) are: the need to use fail-safe brakes (to hold the load when the electrical power is lost), hazardous operation at high load and low speeds (due to reduced cooling capacity and risk of stall conditions), as well as the demand to invest in additional components that would decrease the harmonics or provide for extra cooling (Pawlus, 2016).

More specifically, the shipping sector has developed an interest in using variable speed AC drives for ship propulsion applications (Sakuraba et al., 1992). Similarly, all-electric vessels and dynamic positioning (DP) systems are the concepts that contribute to an increased popularity of electric motors due to the lowered energy consumption, smooth and silent operation, as well as improved controllability properties that they offer compared to traditional hydraulic systems (Yadav et al., 2014). Also, the percentage share of electric actuation systems in oil and gas production units constantly increases, according to Rahimi et al. (2011) and Gallant and Andrews (2006).

Recently, the company Robotic Drilling Systems AS successfully tested their robotic pipe handler. This machine is all-electric and offers features such as handling of pipes from horizontal to vertical position and spinning capability (Austigard, 2016). Furthermore, the machine is self-contained (with integrated hardware control) and offers advantages of being easy to install and automatic exchange of grippers, e.g. for large casing sizes. In addition, a fully electric roughneck and a drill floor robot is in their portfolio. Common for these three machines is that they have entirely abandoned the use of linear drives for motion.

Due to self-contained systems being increasingly

more available, the current benefit of a central HPU will become less attractive in the future. For the offshore industry to follow this trend and still integrate translational motion control in the OMS, there is a need to look at alternative linear drive solutions to the existing hydraulic systems. This is also motivated by the fact that an increasing number of attempts is reported in various industries to replace hydraulic linear drives with all-electric substitutes, as mentioned by Isermann et al. (2002) or Holm et al. (2013). In particular, permanent magnet linear actuators are promising due to the higher force levels they offer, especially when they are combined with additional solutions to increase the provided force even further, such as a double gas spring described by Ummaneni et al. (2007).

2.3 Design Criteria and Challenges

OMS are characterized by a high price, high level of system complexity and low production numbers, according to Bak (2014). Furthermore, in the offshore industry, there are very limited opportunities to build prototypes for verification of the design. Consequently, this requires a significant level of skill and experience to develop and design such systems. Also, due to market competition from conventional low-cost solutions, the focus on manufacturing and development costs is constantly increasing. Hence, the system designers continuously have to improve their design procedures regarding sizing and selection of technical solutions, components, and materials to obtain the best possible trade-off between a wide range of design criteria in an efficient way. Due to the remote location of the drilling platform and high cost of production downtime, reliability and productivity become the most critical performance requirements.

Apart from such obvious design criteria for OMS as displacement, speed and power requirements dictated by the considered application, there are also other challenges exclusively associated with the electrical actuation systems of OMS, according to Pawlus (2016). One of them is to apply harmonics mitigation measures in electric motor drives to prevent voltage notches and overvoltage ringing that can damage the installation and cause threat to personnel offshore (Hoevenaars et al., 2013). In addition, vibration and fatigue damage pose a serious danger to rotating components (e.g. bearings) of any drivetrain. Therefore, the techniques which help to monitor the condition of these elements are becoming increasingly popular, not only in offshore drilling industry (Kandukuri et al., 2016). According to Pawlus et al. (2016b), a solution to lower the associated fatigue and vibration damage is to use smoother motion profiles which are tailor-made for a given application (Pawlus et al., 2016b).

Likewise, selection of the appropriate electric motor type, i.e. induction or permanent magnet, is also considered to be a challenge (Couper et al., 2012). In general, simplicity, robust construction, and relative ease of certification for safe operation in explosive atmospheres (European Commission, 2014) make induction motors exceptionally popular on offshore drilling rigs. However, according to Neleman (2009), the number of Ex certified permanent magnet synchronous motors (PMSMs) is increasing. The use of synchronous machines is mainly motivated by their higher efficiencies and higher torque densities as compared to induction motors, which opens a possibility to reduce the size of the gearbox or even apply a direct drive solution.

Similarly, optimal design of electric powertrains and reduction of unnecessary conservatism when sizing the components is a topic which has proven to generate significant cost- and time-savings in the product development process (Pawlus et al., 2015). When applying the optimal design techniques, not only the dimensioning process itself is improved but also the operating point of the resulting drivetrain can be moved closer to the constraints allowing to utilize the power available from the energy source more efficiently. A complementary approach to designing tailor-made actuation systems is presented in Pawlus et al. (2016c) and is based on thermal modeling of electric actuation systems to avoid using rules of thumb concerning the allowable overloads of EMC drivetrains.

Finally, factors such as safety and environment, cost, maintenance, operation in sensitive regions, potential of automation, and applicability to subsea infrastructure should all affect selection of the most suitable components of actuation systems of OMS – refer to Pawlus et al. (2016a) and the references therein for a more detailed discussion on the above topics.

2.4 Summary

Although the hydraulic actuation systems have established a good track record in the offshore drilling industry (especially when translational motion control is considered), there is observed a growing number of examples where electric motor drives become a tough competitor to this traditional solution. Although there are many case studies in the literature devoted to the superiority of variable speed AC motor drives over hydraulic powertrains in rotational motion control, the research related to the feasibility studies of linear electric actuators in offshore drilling applications is still limited. Hence, this paper presents an analysis of practicability of the implementation of an EMC drivetrain in an offshore pipe handling machine.

63

3 Considered System – Vertical Pipe Handling Machine

The SmartRacker (SR) of Cameron Drilling Systems is used in this paper as a case study for analyzing the feasibility of implementing an EMC drivetrain. The SR is a column type multipurpose pipe (drill-pipe, drill-collar and casing) handling machine that combines the functionality of several traditional pipe handling machines in one machine.
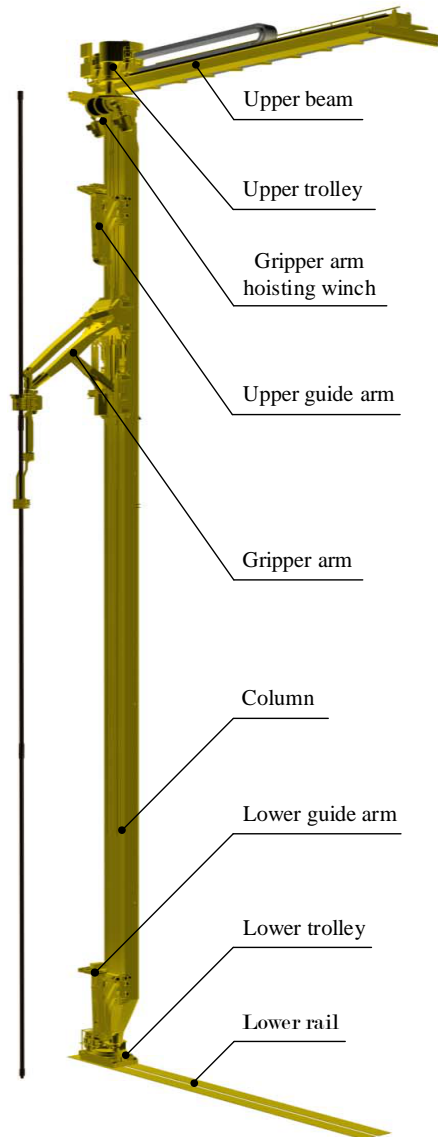

Figure 3: Illustration of the SmartRacker - courtesy of Cameron Sense AS.

The SR can perform the following tasks:

- move stands (two or more joints of pipe connected) between well center and fingerboard

- building of stands for storage inside the fingerboard while drilling

- handling of a single pipe from horizontal to vertical position and vice versa

- lifting operation on drill floor, i.e. the gripper arm can be used as a crane.

As illustrated in Figure 3, the column is supported at the upper beam and lower rail by a track and a rack and pinion system. The lower rail is mounted directly on the drill floor, whereas the upper beam is connected to the structure of the derrick, as shown in Figure 1. In both ends of the column there are located AC motor actuated trolleys that allow for horizontal movement of the machine along the tracks.

The column includes upper and lower guide arms – they are designed to guide the stand, i.e. guide the top and bottom of the pipe being in motion. The arm located in the middle is the gripper arm, responsible for holding the pipe in a secure grip. The AC motor actuated winch located on top of the column is used to hoist or lower the gripper arm. All arms are equipped with an EHC which allows for the extension and retraction in order to position a stand in the finger board or well center. The AC slew motors located on the lower trolley make it possible for the whole machine to rotate about its vertical axis. A comprehensive study on the hoisting winch similar to the gripper arm hoisting winch of the SR is presented in the work done by Pawlus (2016).

In this work, the gripper arm, presented in Figure 4, of the vertical pipe handling machine (Figure 3) is used as a modeling and simulation case study. It is chosen due to the potential to replace the hydraulic linear drive by a more accurate, efficient and environmentally friendly solution.

3.1 Kinematic Structure

The gripper arm is modeled as a planar multibody system using governing equations based on (Nikravesh, 1988) and (Nikravesh, 2008). In total, the model consists of 10 rigid bodies, including the hydraulic lifting cylinder and the pipe (load) connected to the gripper head, as illustrated in Figures 4 and 5. Body 7 includes both the gripper head and the rod of the hydraulic soft stabbing cylinder. The 10 bodies are interconnected by 13 kinematic joints as described in Table 1.

The three body coordinates (x_b, y_b, ϕ_b) are the coordinates of the local reference plane attached to the mass center of the bodies, while the origin of the global reference plane is defined on the drill floor - see Figure 5.
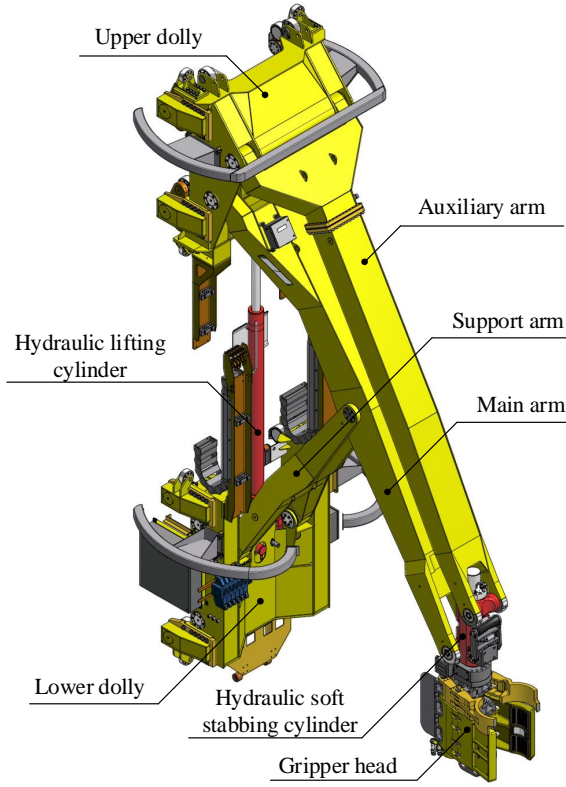
64

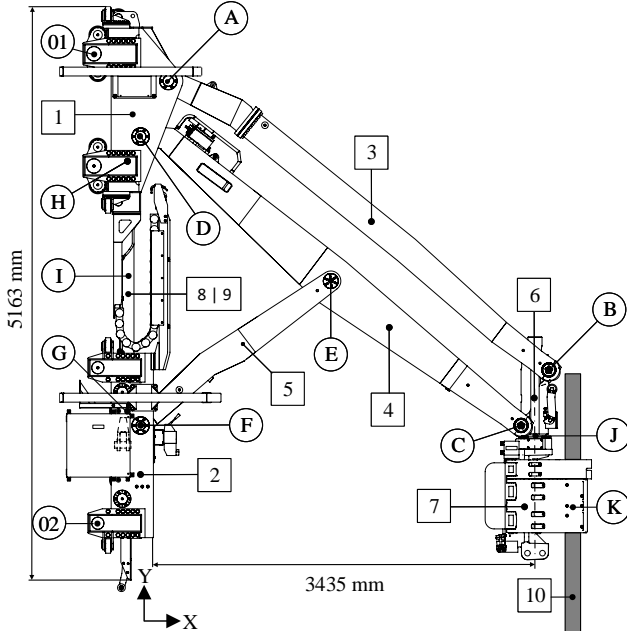Figure 4: SmartRacker® gripper arm - courtesy of Cameron Sense AS.

Figure 5: Gripper arm in fully extended position - courtesy of Cameron Sense AS.

Table 1: Kinematic constraints

Constraint	Description
01	Translational joint, column - body 1
02	Fixed constraint, column - body 2
A	Revolute joint, body 1 - 3
B	Revolute joint, body 3 - 6
C	Revolute joint, body 6 - 4
D	Revolute joint, body 4 - 1
E	Revolute joint, body 4 - 5
F	Revolute joint, body 5 - 2
G	Revolute joint, body 2 - 8
H	Revolute joint, body 1 - 9
I	Translational joint, body 8 - 9
J	Fixed constraint, body 6 - 7
K	Fixed constraint, body 7 - 10

3.2 Inverse Dynamics

To investigate the force that has to be delivered by the lifting cylinder, and the reaction force arising, the following inverse dynamic analysis is performed. A motion cycle logged from an offshore oil rig in operation is assumed to be an input function to the longitudinal driver constraint representing the hydraulic lifting cylinder.

The equations of motion for a planar system consisting of b bodies containing $m = 3b$ coordinates interconnected by kinematic joints can be written as:

$$\mathbf{M}\ddot{\mathbf{q}} = \mathbf{g}^{ext} + \mathbf{g}^c \qquad (1)$$

where $\mathbf{M}$ is the 30×30 mass/inertia matrix:

$$\mathbf{M} = \begin{bmatrix} m_1 & 0 & 0 & 0 & 0 & 0 & 0 \\ 0 & m_1 & 0 & 0 & 0 & 0 & 0 \\ 0 & 0 & J_1 & 0 & 0 & 0 & 0 \\ 0 & 0 & 0 & \ddots & 0 & 0 & 0 \\ 0 & 0 & 0 & 0 & m_{10} & 0 & 0 \\ 0 & 0 & 0 & 0 & 0 & m_{10} & 0 \\ 0 & 0 & 0 & 0 & 0 & 0 & J_{10} \end{bmatrix} \qquad (2)$$

and $\ddot{\mathbf{q}}$ is the 30×1 vector containing the acceleration of the m coordinates. The external forces $\mathbf{g}^{ext}$ are the 30×1 vector containing the gravity forces acting on the bodies, and $\mathbf{g}^c$ is the 30×1 vector containing the reaction forces in the constraints. The b bodies in the system must satisfy the equations of motion, but at the same time they must also satisfy a set of $m = 3 \cdot 10 = 30$ independent constraint equations:

$$\mathbf{\Phi}^{30 \times 1}(\mathbf{q}, t) = \begin{bmatrix} \mathbf{\Phi}^{29 \times 1}(\mathbf{q}) \\ \mathbf{\Phi}^d(\mathbf{q}) - f(t) \end{bmatrix} = \mathbf{0}. \qquad (3)$$

65

The position constraint in the form of Equation 3 is a 30×1 vector containing the kinematic constraints $\mathbf{\Phi}(\mathbf{q})$, as described in Table 1, and the one-DOF longitudinal driver constraint $\mathbf{\Phi^d}(\mathbf{q}, t)$ that produce a displacement between body 8 and 9. The motion cycle obtained from the rig is mimicked by the longitudinal driver function represented by $f(t)$. For position analysis, the constraint vector in Equation 3 is solved numerically using the Newton-Raphson method.

The velocity and acceleration constraints are defined in the following equations:

$$\dot{\mathbf{\Phi}}^{30 \times 1}(\mathbf{q}, t) = \begin{bmatrix} \mathbf{D}\dot{\mathbf{q}} \\ \mathbf{\Phi}^d \dot{\mathbf{q}} - \dot{f}(t) \end{bmatrix} = \mathbf{0} \qquad (4)$$

$$\ddot{\mathbf{\Phi}}^{30 \times 1}(\mathbf{q}, t) = \begin{bmatrix} \mathbf{D}\ddot{\mathbf{q}} + \dot{\mathbf{D}}\dot{\mathbf{q}} \\ \mathbf{\Phi}^d \ddot{\mathbf{q}} + \dot{\mathbf{D}}^d \dot{\mathbf{q}} - \ddot{f}(t) \end{bmatrix} = \mathbf{0} \qquad (5)$$

where $\mathbf{D}$ and $\mathbf{D}^d$ make up the 30×30 Jacobian matrix $\mathbf{\Phi_q}$. The terms $\dot{\mathbf{D}}\dot{\mathbf{q}}$ and $\dot{\mathbf{D}}^d \dot{\mathbf{q}}$ are referred to as the right hand side of the kinematic acceleration equations, and are represented as:

$$\boldsymbol{\gamma} = -\dot{\mathbf{D}}\dot{\mathbf{q}} \qquad (6)$$

$$\boldsymbol{\gamma}^d = -\dot{\mathbf{D}}^d \dot{\mathbf{q}}. \qquad (7)$$

From Equations 4 and 5, the velocity and acceleration can be found by solving the following expressions:

$$\dot{\mathbf{q}} = \mathbf{\Phi_q}^{-1} \begin{bmatrix} \mathbf{0} \\ \dot{f}(t) \end{bmatrix} \qquad (8)$$

$$\ddot{\mathbf{q}} = \mathbf{\Phi_q}^{-1} \begin{bmatrix} \boldsymbol{\gamma} \\ \boldsymbol{\gamma}^d + \ddot{f}(t) \end{bmatrix}. \qquad (9)$$

The sum of reaction forces in the constraints can be expressed by the following equation:

$$\mathbf{g}^c = \mathbf{\Phi_q^T} \boldsymbol{\lambda} \qquad (10)$$

where $\mathbf{\Phi_q^T}$ is the transpose of the Jacobian matrix and it is nonsingular as the constraint equations are linearly independent, and $\boldsymbol{\lambda}$ is a vector containing Lagrange multipliers that are the coefficients in the linear combination. Finally, Equations 1 and 10 are rearranged in order to solve for $\boldsymbol{\lambda}$:

$$\boldsymbol{\lambda} = (\mathbf{\Phi_q^T})^{-1}(\mathbf{M}\ddot{\mathbf{q}} - \mathbf{g}^{ext}). \qquad (11)$$

3.3 Forward Dynamics

Unlike the inverse dynamic analysis where the prescribed motion of the driving coordinates determines the motion of the system, in forward dynamic analysis it is the applied forces and moments that are used to determine the motion (Nikravesh, 2008). Consequently, the longitudinal driver constraint is removed, resulting in a 29×30 Jacobian matrix $\mathbf{\Phi_q}$.

The system of constrained bodies can be solved by the following expression:

$$\begin{bmatrix} \ddot{\mathbf{q}} \\ \boldsymbol{\lambda} \end{bmatrix} = \begin{bmatrix} \mathbf{M} & -\mathbf{\Phi_q^T} \\ \mathbf{\Phi_q} & \mathbf{0} \end{bmatrix}^{-1} \begin{bmatrix} \mathbf{g}^{ext} \\ \boldsymbol{\gamma} \end{bmatrix}. \qquad (12)$$

To introduce displacement in the lifting cylinder, the output of the EMC drivetrain, presented in Section 4.3, is connected as an external force F_{EMC} to bodies 8 and 9, as expressed in the following equation:

$$\mathbf{g}^{ext} = \begin{bmatrix} F_{1,x} \\ F_{1,y} \\ M_{1,\phi} \\ \vdots \\ F_{8,x} \\ F_{8,y} \\ M_{8,\phi} \\ F_{9,x} \\ F_{9,y} \\ M_{9,\phi} \\ F_{10,x} \\ F_{10,y} \\ M_{10,\phi} \end{bmatrix} = \begin{bmatrix} 0 \\ -m_1 g \\ 0 \\ \vdots \\ 0 \\ -m_8 g - F_{EMC} \\ 0 \\ 0 \\ -m_9 g + F_{EMC} \\ 0 \\ 0 \\ -m_{10} g \\ 0 \end{bmatrix}. \qquad (13)$$

In the forward dynamic analysis, the equations of motion expressed in Equation 12 are second-order differential equations and they are solved numerically.

4 Electromechanical Cylinder Drivetrain

The EMC drivetrain is a modular linear drive powered by a drive unit, including a servo motor and converter. A transmission system, including a transmission screw and transmission elements e.g. gearbox (optional), timing-belt side drive or flange and coupling converts the rotary motion to translation - see Figure 15. The main components of an EMC drivetrain are illustrated in Figure 6.

To better describe the properties of an EMC drivetrain, the heavy-duty (EMC-HD) version produced by Bosch Rexroth (2015) is chosen as an exemplary drive. Due to its specific characteristics, the EMC-HD

66

offers advantages in terms of accuracy, dynamics and controllability, and is developed for use in heavy load applications. An overview of its key technical data is presented below according to Bosch Rexroth (2015):

- basic dynamic load rating: 50 to 470 kN

- axial force: up to 290 kN (tension/compression)

- maximum traversing speed: 1 $\frac{m}{s}$
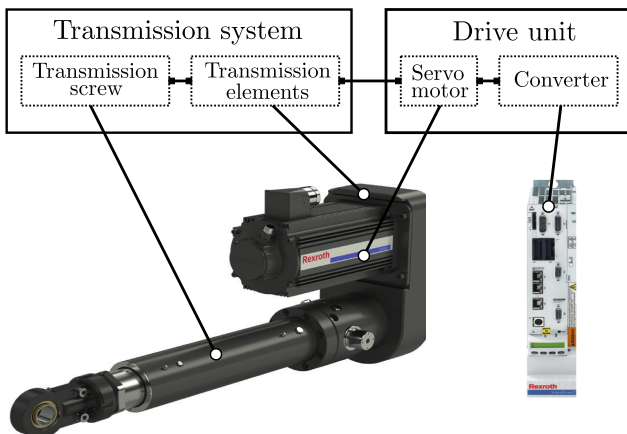
- stroke: up to 1 700 mm

- protection class: IP65.

Figure 6: Bosch Rexroth EMC-HD drivetrain with motor attachment via timing belt side drive. Image courtesy of Bosch Rexroth (2015).

The design is completely modular with an integrated planetary roller screw (PRS) or recirculation ball screw transmission. According to Bosch Rexroth (2015), the EMC-HD is designed for cost-efficient work, even under tough conditions and is suited for bending, lifting, pressing and transporting applications.

Hence, the EMC-HD from Bosch Rexroth (2015) is considered as one of the commercial off-the-shelf EMC drivetrain which closely matches the power (static and dynamic force) and motion performance (displacement length and speed) demand of the case study.

4.1 Transmission Screw

A transmission screw is a widely used mechanism to convert the rotational motion into the translational one. To increase the accuracy of the transmission screw, it is preferred to omit the sliding between the screw shaft and nut. Therefore, transmission screws with rolling elements such as ball screw and roller screw are introduced (Hojjat and Mahdi Agheli, 2009).

In comparison to the hydraulic cylinder, the precision of ball screw and roller screw is high because the

phenomenon of stick-slip is eliminated due to the absence of sliding. One of the areas where friction in hydraulic cylinders represents a constant challenge is in OMS, according to Ottestad et al. (2012). Also, in comparison to the traditional lead screw, the backlash phenomenon can be eliminated by preloading the nut, which lowers the axial deflection and increases the stiffness, according to Hojjat and Mahdi Agheli (2009). Due to the increased diameter and the number of contact surfaces, the roller screw, according to Schinstock and Haskew (1996), is well suited for applications where the loads are large and have a significant shock load content compared to the ball screw.

The roller screw exists in three different designs: planetary, differential planetary and recirculating roller screw. All three designs include the following three elements, as shown in Figure 7: a threaded screw shaft, a threaded or grooved nut and a set of threaded or grooved rollers which engage with both the shaft and the nut (Lemor, 1996).
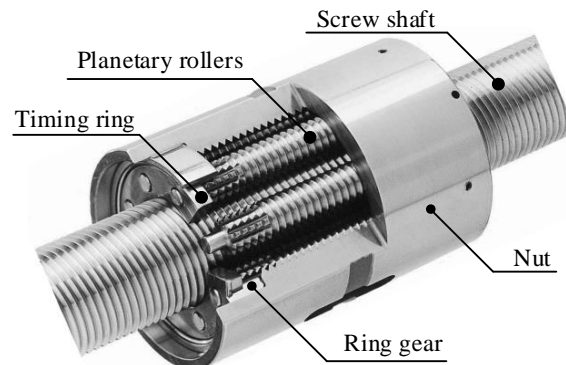

Figure 7: Planetary roller screw (PRS) main components. Image courtesy of Parker (2013).

In most EMC drivetrains, the PRS design is used, according to Lemor (1996). The reason for this is an inherent capacity of PRS to withstand very high accelerations and speeds and its ability to handle heavy loads for a long time. This capability places the PRS between large ball screws and hydraulic cylinders. According to Lemor (1996), PRS compares favorably over ball screws and hydraulic cylinders because its resistance to adverse environment is higher than that of ball screws and the EMC drivetrains is not prone to fluid spills.

4.2 Sizing Principles

To make sure that the EMC drivetrain can deliver sufficient performance when considering both technical and economical factors, the selection of the EMC drivetrain components has to be made early in the design phase

67

of the complete machine. Also, when sizing the EMC drivetrain, it is important to define the system requirements regarding load, speed, and acceleration of the complete motion cycle. According to Bosch Rexroth (2015), the key parameters that have decisive influence on the final solution are:

1. Load: process forces, masses, duty cycle, service life requirements.

2. Dynamics: acceleration, linear speed, cycle time.

3. Geometry: work space, installation space, stroke length, interference elements.

4. Environmental and installation conditions: mounting orientation, degrees of freedom, temperature, humidity, contamination, vibration and shocks.

According to Bosch Rexroth (2015), the type of screw transmission, lead, gear reductions and drive unit can be selected such that the requirements are met precisely and efficiently by stating the acceleration and linear speeds as accurately as possible. A reliable EMC drivetrain solution can be found when the loads are known as accurately as possible. The average load F_m over the entire cycle can be determined when knowing all occurring forces in the application over the entire stroke length.

The average load forms the basis for the nominal life calculation of the EMC drivetrain. When the EMC drivetrain configuration is selected, the dynamic load capacity C can be found in the catalog (Bosch Rexroth, 2015) and the nominal life in number of revolutions and hours can be calculated from the following equations:

$$L_{10} = \left(\frac{C}{F_m}\right)^3 10^6 \ [revolutions] \tag{14}$$

$$L_{10h} = \frac{L_{10}}{n_m} \ [hours] \tag{15}$$

$$n_m = \frac{v_m}{P_{PRS}} \ [rpm] \tag{16}$$

where v_m is the average linear speed and P_{PRS} is the lead (linear movement due to screw) of the PRS.

Considering the power losses, a permissible mechanical drive power is stated in the catalog (Bosch Rexroth, 2015) for each transmission system combination at an ambient temperature of $25°C$ and even distribution of the load over the stroke length. To avoid overheating of the transmission system, the required power of the application P_{app}, should not exceed the permissible transmitted power.

When pre-selecting the servo motor, the following three conditions can be used, according to Bosch Rexroth (2015):

1. The rated speed of the motor must be the same as or higher than the speed required for transmission system (but not exceeding the maximum permissible value):

$$\omega_{m,max} \geq \omega_{ts} \tag{17}$$

where

$$\omega_{ts} = \frac{v_{ref} 2\pi i_{gear}}{P_{PRS}}. \tag{18}$$

2. To achieve high level of control performance, the ratio of mass moments of inertia of the transmission system J_{ts} and the servo motor should for handling applications satisfy:

$$J_r = \frac{J_{ts}}{J_m + J_{br}} \leq 6.0 \tag{19}$$

where J_m and J_{br} are the mass moments of inertia of the servo motor and the motor brake.

3. The ratio of static load moment T_{stat} to the continuous torque of the servo motor T_0 must be less than or equal to the empirical value of 0.6:

$$T_r = \frac{T_{stat}}{T_0} \leq 0.6 \tag{20}$$

where

$$T_{stat} = T_{f,emc} + T_{mg} + T_{eq} \tag{21}$$

and T_{mg} is the vertical weight moment of the load, T_{eq} is the equivalent dynamic torque, as expressed in the following equations:

$$T_{mg} = \frac{F_{mg}P_{PRS}}{2\pi i_{gear}\eta} \tag{22}$$

$$T_{eq} = \frac{F_m P_{PRS}}{2\pi i_{gear}\eta}. \tag{23}$$

where F_{mg} is the load of the moving masses and η is the mechanical efficiency of the EMC drivetrain.

4.3 Modeling of EMC Drivetrain

In the model of the EMC drivetrain, as illustrated in Figure 8, a converter powers and controls the servo motor. The servo motor is connected to the transmission system, including the PRS and a gearbox - see Figure 9. The bodies and masses of the transmission system are included in the multibody system, as described in Section 3.
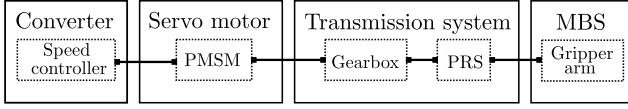
Figure 8: EMC drivetrain model connected to the mechanical system.

4.3.1 Servo Motor

According to the catalog (Bosch Rexroth, 2015), the motor that actuates the EMC-HD is a PMSM. In this paper, the PMSM is modeled in the rotating dq-frame, according to Pillay and Krishnan (1989). The stator input voltages to the model u_{sd} and u_{sq} are obtained in the dq-frame from the three-phase stator voltages u_{sa}, u_{sb}, u_{sc} (and vice versa) through the Park transformation $\mathbf{P}$ (and inverse transformation $\mathbf{P}^{-1}$), defined as (Pillay and Krishnan, 1989):

$$\begin{bmatrix} u_{sd} \\ u_{sq} \\ u_0 \end{bmatrix} = \mathbf{P} \begin{bmatrix} u_{sa} \\ u_{sb} \\ u_{sc} \end{bmatrix} \tag{24}$$

where

$$\mathbf{P} = \frac{2}{3} \begin{bmatrix} \cos(-\theta_e) & \cos(-\theta_e + \frac{2\pi}{3}) & \cos(-\theta_e - \frac{2\pi}{3}) \\ \sin(-\theta_e) & \sin(-\theta_e + \frac{2\pi}{3}) & \sin(-\theta_e - \frac{2\pi}{3}) \\ \frac{1}{2} & \frac{1}{2} & \frac{1}{2} \end{bmatrix} \tag{25}$$

and the transformation angle θ_e is the electric position representing the angle of the rotating reference frame.

The dq-frame is linked to the rotor and is defined as:

$$\theta_e = P_p \theta_r \tag{26}$$

where P_p is the number of pole pairs. It is related to the rotor speed ω_m, as:

$$\omega_e = \frac{d\theta_e}{dt} = P_p \frac{d\theta_r}{dt} = P_p \omega_m. \tag{27}$$

The considered PMSM is modeled using the following state-space equations (Pillay and Krishnan, 1989):

$$\underbrace{\begin{bmatrix} \dot{i}_{sd} \\ \dot{i}_{sq} \\ \dot{\omega}_m \end{bmatrix}}_{\dot{x}} = \mathbf{A} \underbrace{\begin{bmatrix} i_{sd} \\ i_{sq} \\ \omega_m \end{bmatrix}}_{x} + \mathbf{B} \underbrace{\begin{bmatrix} u_{sd} \\ u_{sq} \\ T_L \end{bmatrix}}_{u} \tag{28}$$

$$\underbrace{\begin{bmatrix} i_{sd} \\ i_{sq} \\ \omega_m \end{bmatrix}}_{y} = \mathbf{C} \underbrace{\begin{bmatrix} i_{sd} \\ i_{sq} \\ \omega_m \end{bmatrix}}_{x} \tag{29}$$

where:

$$\mathbf{A} = \begin{bmatrix} -\frac{R}{L} & P_p \omega_m & 0 \\ -P_p \omega_m & -\frac{R}{L} & 0 \\ 0 & \frac{3}{2} \frac{P_p \Psi}{J_{tot}} & -\frac{B_{fm}}{J_{tot}} \end{bmatrix} \tag{30}$$

$$\mathbf{B} = \begin{bmatrix} \frac{1}{L} & 0 & 0 \\ 0 & \frac{1}{L} & 0 \\ 0 & 0 & \frac{1}{J_{tot}} \end{bmatrix} \tag{31}$$

$$\mathbf{C} = \begin{bmatrix} 1 & 0 & 0 \\ 0 & 1 & 0 \\ 0 & 0 & 1 \end{bmatrix}. \tag{32}$$

It is clear that the PMSM model is nonlinear as it contains product terms such as speed ω_m and stator currents i_{sd} and i_{sq} (Pillay and Krishnan, 1989).

Values of stator resistance R, stator inductance L and the torque constant k_t are obtained from the catalog (Bosch Rexroth, 2006). The flux linkage Ψ is then obtained from the following equation (Pillay and Krishnan, 1989):

$$\Psi = \frac{2}{3} \frac{k_t}{P_p}. \tag{33}$$

The combined mass moment of inertia J_{tot} and the combined friction moment $T_{f,emc}$ of the PMSM and the transmission system (PRS and gearbox) reduced with reference to the motor shaft are obtained from the EMC-HD catalog (Bosch Rexroth, 2015). The friction torque is assumed to be the linear viscous friction:

$$T_{fm} = B_{fm} \omega_m \tag{34}$$

where

$$B_{fm} = \frac{T_{f,emc}}{\omega_{m,max}}. \tag{35}$$

The electromagnetic torque is:

$$T_e = \frac{3}{2} P_p \Psi i_{sq} \tag{36}$$

and the equation of motion of the rotor shaft then becomes:

$$T_e = T_L + \underbrace{B_{fm} \omega_m}_{T_{fm}} + \underbrace{J_{tot} \dot{\omega}_m}_{T_a} \tag{37}$$

where T_L is the effective torque on the transmission system and T_a is the acceleration torque - see Figure 9.

69

4.3.2 Transmission System

The transmission system is driven by the electromagnetic torque. Based on Equation 37, the effective torque exerted on the servo motor is determined as:

$$T_L = T_e - T_{fm} - T_a. \tag{38}$$

The transmission screw (PRS) transfers the rotational power into the translational form through:

$$k_{emc} = \frac{2\pi}{P_{PRS}} \tag{39}$$

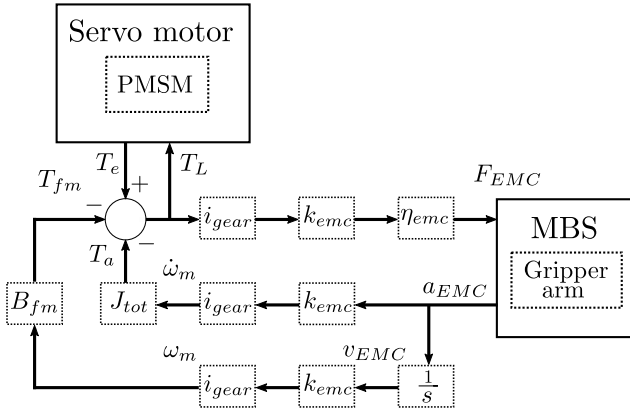where k_{emc} is the drive ratio and P_{PRS} is the lead of the PRS.

Figure 9: Transmission model sub-system.

Considering the direction dependent efficiency η, which represents the efficiency of the EMC drivetrain, the torque balance at the PRS can be derived as (Fu et al., 2015):

$$F_{EMC} = m_9 g + F_{9,y} \tag{40}$$

where m_9 is the moving mass of the transmission system (PRS nut and cylinder rod), g is the gravity, $F_{9,y}$ is the external forces connected to the cylinder rod and F_{EMC} is the PRS input force connected to the gripper arm multibody system, as expressed in Equation 13, which can be written as:

$$F_{EMC} = T_L i_{gear} k_{emc} \eta \tag{41}$$

where i_{gear} is the gearbox ratio.

4.4 Motion Control

The synchronous frame-based field-oriented control is considered to be one of the most popular methods for controlling PMSMs (Wang et al., 2016). As shown in Equation 36, the electromagnetic torque of PMSM can be adjusted by exclusively controlling the current i_{sq}. Therefore, the reference value of $i_{sd,ref}$ is normally set to 0 A. Then, the reference stator currents $i_{sq,ref}$ and $i_{sd,ref}$ are converted to the three-phase currents and compared with the measured actual motor currents i_{sa}, i_{sb}, and i_{sc} in the inverter/pulse width modulation (PWM) section of the torque control circuit. The torque control can be extended to the speed control by adding an external control loop. The considered speed control strategy of the PMSM is illustrated in Figure 10. In the current work, a simple PI controller is used to adjust the motor speed to a desired value.
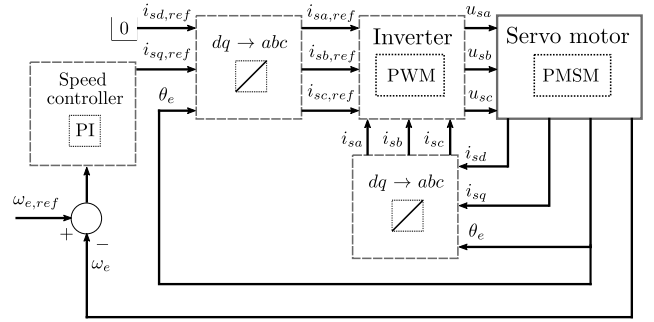
Figure 10: Field-oriented control of PMSM.

5 Simulation Results

In this paper, the vertical pipe handling machine gripper arm, see Figure 3, is used as a modeling and simulation case study. The gripper arm, including the hydraulic lifting cylinder and load (pipe), is numerically modeled and simulated. The kinematic response (position and velocity) of the model is compared against the hydraulically actuated gripper arm motion (extension and retraction of the lifting cylinder) of a full-scale vertical pipe handling machine logged during its operation on an offshore oil rig. In addition, the dynamic behavior of the model is investigated as well to determine the force/torque levels that have to be provided by the designed EMC drivetrain.

5.1 Inverse Dynamic Analysis

To determine the force that has to be delivered by the EMC drivetrain, the inverse dynamic analysis of the gripper arm is performed. The prescribed motion of the driving coordinates determines the motion of the system. This prescribed motion, i.e. position, velocity and acceleration profiles, is implemented in the longitudinal driver constraint function to represent the

70

motion cycle of the hydraulic lifting cylinder, as described in Section 3.

The velocity input v_{ref} shown in Figure 11 represents the controller input signal used in the real-world machine.
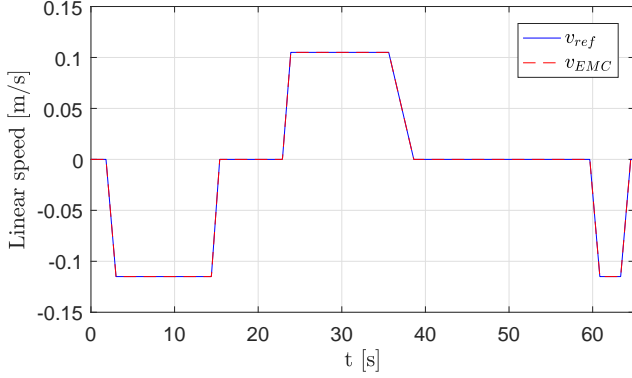

Figure 11: EMC drivetrain speed.

To verify the kinematics of the multibody system model, the horizontal reach position (x-direction) of the gripper head (body 7) and the displacement of the longitudinal driver are compared against the logged position of the gripper head reference point and cylinder displacement - see Figure 12 and 13.
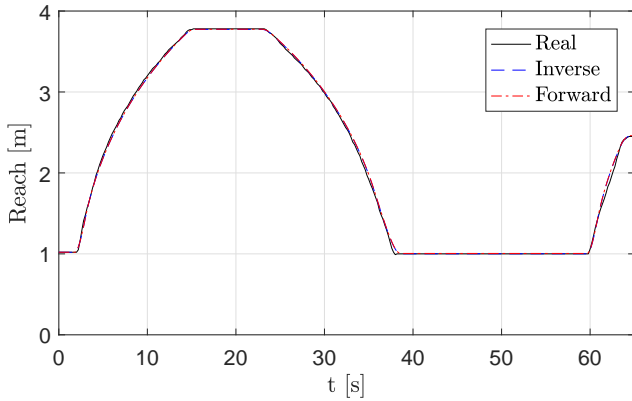
Figure 12: Gripper arm reach position.

The results show that the modeled reach position closely resembles the position of the full-scale reference machine.

The average speed over the entire cycle is found to be $v_{m,sim} = 0.0511 \; \frac{m}{s}$ by integrating the absolute velocities:

$$v_{m,sim} = \int_{t=0s}^{t=65s} |v_m(t)| \, dt. \tag{42}$$

The average load over the entire cycle is found to be $F_{m,sim} = 25.845 \; kN$ by integrating the absolute forces:
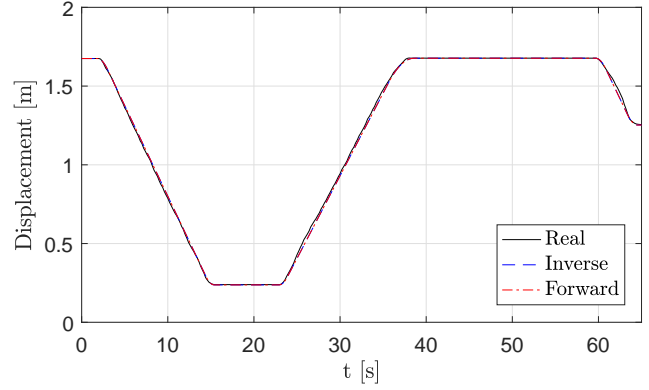
Figure 13: Lifting cylinder displacement.

$$F_{m,sim} = \int_{t=0s}^{t=65s} |F_m(t)| \, dt. \tag{43}$$

The resulting reaction force in the y-direction of the longitudinal driver constraint is derived from Equation 10 and shown in Figure 14.
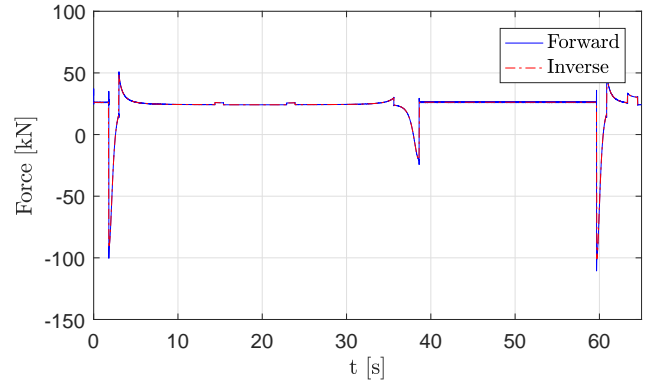
Figure 14: Lifting cylinder axial force.

The magnitude of the largest force produced by the longitudinal driver is read from Figure 14 to be $F_{max} = 100.8 \; kN$ at $59.7s$.

From the simulated average speed and load value from Equations 42 and 43:

$$P_{app,sim} = v_{m,sim} F_{m,sim} \tag{44}$$

the required amount of power is calculated to be $P_{app,sim} = 1319.6 \; W$.

5.2 EMC Drivetrain Components Selection

For stroke lengths greater than $1.5m$, the PRS is the only available screw transmission in the EMC-HD series from Bosch Rexroth (2015). The relevant catalog

71

Table 2: EMC-HD-180 transmission system catalog data (Bosch Rexroth, 2015).

No.	P_{PRS} [m]	i_{gear}	F_{max} [kN]	T_p [Nm]	η	$T_{f,emc}$ [Nm]	v_{max} $[\frac{m}{s}]$	a_{max} $[\frac{m}{s^2}]$
1	0.01	1	250.0	497.4	0.80	17.0	0.33	30
2	0.01	3	250.0	174.5	0.76	19.7	0.19	30
3	0.01	5	250.0	104.7	0.76	12.4	0.12	30
4	0.01	7	250.0	74.8	0.76	9.2	0.08	30
5	0.01	3	250.0	170.9	0.78	23.7	0.19	30
6	0.01	5	250.0	102.5	0.78	12.9	0.12	30
7	0.02	1	133.2	530.0	0.80	19.0	0.67	30
8	0.02	1	136.4	650.0	0.80	19.0	0.67	30
9	0.02	3	178.5	249.1	0.76	20.3	0.39	30
10	0.02	5	178.5	149.5	0.76	12.8	0.23	30
11	0.02	7	178.5	106.8	0.76	9.5	0.17	30
12	0.02	3	290.0	396.5	0.78	24.3	0.39	30
13	0.02	5	290.0	237.9	0.78	13.3	0.23	30

data used for selection of the various transmission system combinations are listed in Table 2, and the relevant servo motor data are listed in Table 3.

The EMC drivetrain parameters used here are for motor attachment via flange and coupling. Three different mounting configurations (without gearbox) are illustrated in Figure 15 to compare the size of the different drivetrain configurations with the EHC system used on the full-scale reference machine.
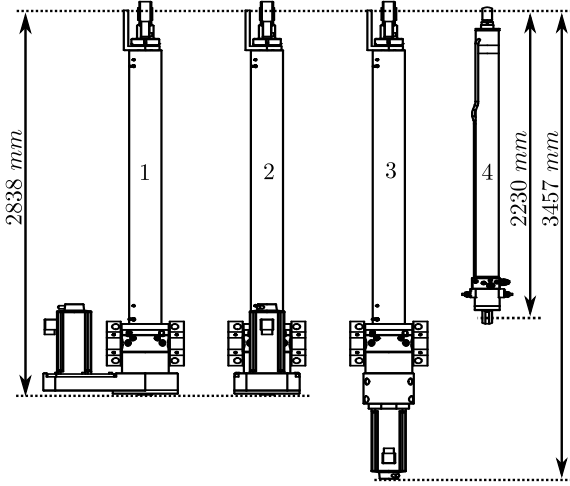
Figure 15: 1-2: motor attachment via timing belt side drive. 3: motor attachment via flange and coupling. 4: existing hydraulic cylinder.

From the servo motor pre-selection procedure described in Section 4.2, the EMC drivetrain combination that satisfies the three conditions is obtained based on the simulation results from the inverse dynamic analysis. As shown in Table 4, combination No. 3 and servo motor MSK101E-300 is the only EMC drivetrain

Table 3: IndraDyn S - servo motor MSK data (Bosch Rexroth, 2015).

Motor	$\omega_{m,max}$ $[\frac{rad}{s}]$	T_0 [Nm]	T_{max} [Nm]
101D-300	481.7	50	160
101E-300	481.7	70	231
101E-300[1]	481.7	105	231
133D-300[1]	314.2	152	320
133E-300[1]	314.2	250	520

[1] With fan

combination which does not require an external cooling system and satisfies the pre-selection procedure.

From the catalog (Bosch Rexroth, 2015), the dynamic load capacity of the selected EMC drivetrain is found to be $C = 470$ kN. Based on the average load and the presented motion cycle (Figure 11), the estimated nominal life of the EMC drivetrain in number of revolutions and hours is determined from Equations 14-16 to be $L_{10} \approx 6.0 \cdot 10^9$ revolutions, and $L_{10h} \approx 3.3 \cdot 10^5$ hours, respectively.

All considered EMC drivetrain combinations in Table 2 satisfy the maximum permissible axial force $F_{max} = 100.8\ kN$. The maximum permissible transmitted power of the EMC-HD-180 is from the catalog (Bosch Rexroth, 2015) found to be 970 W for $P_p = 0.01\ m$ and 1240 W for $P_p = 0.02\ m$, both smaller than the required amount of power $P_{app,sim} = 1319.6\ W$. Combination No. 4 does not satisfy the required linear speed from the desirable motion cycle (Figure 11), where the linear reference speeds are $v_{ref} = 0.115\ \frac{m}{s}$ when retracting and $v_{ref} = 0.105\ \frac{m}{s}$ when extending.

Table 4: EMC drivetrain pre-selection results.

No.	Motor	$\omega_{ts} \left[\frac{rad}{s}\right]$	J_r	T_r
1	133E-300[1]	72.26	1.04	0.56
2	101E-300[1]	216.77	1.01	0.59
3	101E-300	361.28	0.42	0.55
3	101E-300[1]	361.28	0.42	0.36
5	133D-300[1]	216.77	0.29	0.43
5	133E-300[1]	216.77	0.21	0.26
12	133E-300[1]	108.38	0.23	0.42
13	133D-300[1]	180.64	0.13	0.42
13	133E-300[1]	180.64	0.10	0.25

[1] With fan

5.3 Forward Dynamic Analysis

The forward dynamic analysis is used to verify that the selected EMC drivetrain can provide the required power and motion performance of the full-scale reference machine.

Based on the components selection in Section 5.2, the model parameters of combination No. 3, summarized in Table 2, and servo motor MSK101E-300 are obtained from the manufacturer catalogs: (Bosch Rexroth, 2015) and (Bosch Rexroth, 2006). For the servo motor model, the following parameters are used: winding resistance $R = 0.11\Omega$, winding inductance $L = 0.19mH$ and number of pole pairs $P_p = 4$.

In the simulation, the reference speed profile v_{ref} as shown in Figure 11 is given as a reference speed input $\omega_{e,ref}$ to the closed loop PI speed controller illustrated in Figure 10. The simulated speed v_{EMC} of the EMC drivetrain is compared with v_{ref} and the results are shown in Figure 11. The deviation between v_{EMC} and v_{ref} is presented in Figure 16.
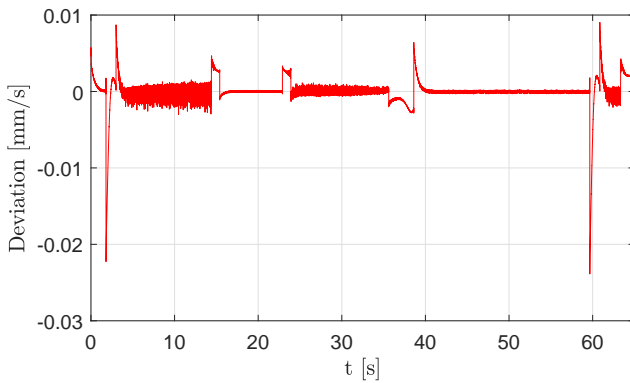
Figure 16: EMC drivetrain speed deviation.

The simulated EMC drivetrain displacement x_{EMC} is compared in Figure 13 against the displacement of the EHC logged from the offshore rig in operation.

The axial force provided by the EMC drivetrain is shown in Figure 14, and the highest occurring force is $F_{EMC} = 110.6\ kN$. The highest torque provided by the servo motor is $T_e = 54.04\ Nm$, as shown in Figure 17.
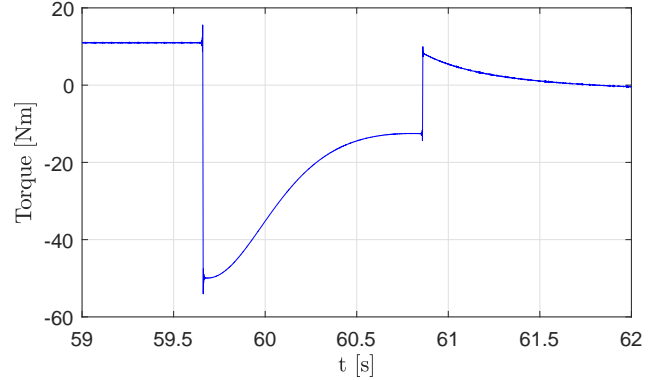

Figure 17: Electromagnetic torque of the servo motor.

The obtained results indicate that both the kinematics and dynamics of the modeled system correspond well to the performance of the full-scale reference machine. In addition, the required actuator force profiles are identical regardless if using inverse or forward dynamic analysis to determine the force/torque demand coming from the multibody system.

6 Feasibility Analysis

Today, the experience and knowledge of using EMC drivetrains in OMS are very subjective, and the skepticism regarding reliability is high, due to e.g. the risk of breakdown (jamming) of the transmission screw due to unexpected impact forces (shock) and overloads. Also, the availability of commercial off-the-shelf EMC drivetrains that satisfy both the explosive atmospheres (Ex) certification (i.e. complies with the ATEX Directive 2014/34/EU (European Commission, 2014)), power, motion, and safety requirements of OMS is limited. However, many manufacturers of EMC drivetrains can deliver tailor-made solutions that have potential to meet these, if not now, then most likely in the future due to research and development of EMC drivetrains design for OMS applications. Furthermore, the durability of tailor-made solutions is difficult to estimate due to lack of manufacturers experience with a customized drive.

6.1 Motion Performance

With a focus on the motion performance, numerical modeling and simulation based on information pro-

vided in the manufacturer catalog (Bosch Rexroth, 2015) are used when sizing and selecting the components of the considered EMC drivetrain.

The forward dynamic analysis verifies that the selected EMC drivetrain can provide the required force, displacement, velocity, and acceleration of the full-scale reference machine. Also, the highest values obtained for axial force, motor torque, motor speed, linear speed and acceleration are within the limits of the maximum permissible values of the selected EMC drivetrain - see Figure 11-17. However, the total power required for the considered motion cycle is higher than the maximum permissible power of all the EMC drivetrain combinations listed in Table 4. Therefore, based on the recommendation of the manufacturer (Bosch Rexroth, 2015), avoidance of overheating cannot be guaranteed for the EMC drivetrain combinations investigated for the case study presented in this paper. Hence, to avoid overheating, the average speed of the motion cycle must be decreased. From the catalog (Bosch Rexroth, 2015) the permissible power is found to be higher for the transmission screw with lead $P_p = 0.02\ m$ (1240 W) compared to $P_p = 0.01\ m$ (970 W). Therefore, by using an EMC drivetrain combination with $P_p = 0.02\ m$ and a servo motor with external cooling (e.g. combination No. 12 and servo motor MSK133E-300[1]) the permissible power would be closer to match the demanded power (1319.6 W) than the EMC drivetrain combination simulated in Section 5.3.

6.2 Reliability and Safety

Research on replacing traditional hydraulic or electro-hydraulic actuation in centralized hydraulic power systems with EMCs with a decentralized power system in aircraft flight control and aerospace systems are well documented in the literature, specially regarding reliability and safe operations - see for instance the work done by Bodden et al. (2007), Garcia et al. (2008), Balaban et al. (2009), and Narasimhan et al. (2010).

Replacing EHC systems with EMCs while maintaining the same level of safety is, according to Garcia et al. (2008), a major challenge when considering decreasing production and maintenance costs, the size of drives, energy consumption, and pollution emissions. Furthermore, when considering to replace EHC systems with EMCs, special attention has to be paid to avoid jamming, that is, when the screw transmission becomes stuck. However, as demonstrated by Garcia et al. (2008), safe operation and reliability of an EMC drivetrain mainly depends on the motor and the electronics, especially the inverter. Finally, Garcia et al. (2008) conclude that early failure detection, independent and fault-tolerant configurations, and high reliability of motors and electronics will allow EMCs to be

used also in primary flight actuators.

In case of breakdown, OMS demand functional features that allow the drive systems to be manually controlled out of the operation zone so that the process can continue with alternative equipment. According to Schinstock and Haskew (1996), it is difficult to design an EMC drivetrain where a failed transmission screw can be disengaged from the load to allow redundant drives to take over. In comparison with the EHC system used in OMS where counterbalance valves serve safety functions for load holding, EMC drivetrains need to use fail-safe brakes to hold the load when the electrical power is lost. Also, self-ventilated electrical motors are not be be continuously operated at high loads and low speeds due to reduced cooling capacity and risk of stall conditions (Pawlus, 2016).

The ATEX Directive (European Commission, 2014) regulates usage of electrical equipment in the hazardous areas, e.g. area around the well center, and it also defines health and safety requirements of OMS. Consequently, this limits the number of available EMC drivetrain components e.g. electrical motors, converters, gearboxes, transmissions screws, hydraulic valves, hydraulic pumps, etc. Since only components that are Ex certified can be used in OMS, the design process becomes more challenging, and it might turn out that the solutions which satisfy the performance requirements and design criteria do not comply with the ATEX Directive, according to Pawlus (2016).

6.3 Durability

A test performed by Schinstock and Haskew (1996) demonstrates that roller screws (SKF set with a non-preloaded nut, a 48mm nominal diameter screw, and 20mm lead) may be damaged by dynamic loading with load magnitudes well within the static load rating of the screw. Schinstock and Haskew (1996) concludes that while this damage is not catastrophic, it would defeat one of the main goals of the replacement of the EHC system with EMC drivetrain. Furthermore, it would be expected that the damaged portions of the thread face would begin to flake and deteriorate and substantially decrease the life of the screw. However, the results presented by Schinstock and Haskew (1996) do not prohibit the use of roller screws in harsh applications. Rather, they emphasize the critical importance of good dynamic analysis of the loads generated by an application and good controller design. Also, Schinstock and Haskew (1996) emphasizes the point that the actuator must be back-drivable and include some sort of force limiting control in such applications.

According to Garcia et al. (2008), condition monitoring is receiving a remarkable deal of attention in the field of aeronautics, as it can detect incipient faults

74

at an early stage. This reduces the maintenance and down-time expense, and also improves operation safety. This is why carriers and flight companies are more interested than ever in the adoption of new condition-monitoring techniques. Preferably, online techniques for predictive maintenance, to check and evaluate performance conditions of both the rotating electrical machines and the whole electronics.

The speed reference control signal used in the analysis presented in this paper is of trapezoidal shape - see Figure 11. According to Pawlus et al. (2016b), trapezoidal profiles cause overshoots, induce residual vibrations and can generate high peak loads. As an alternative reference profile, trigonometric profiles are investigated by Pawlus et al. (2016b) and prove to reduce torque peak values by up to 50 %, remove jerk discontinuities and provide smoother machine operation. Jerk control allows to ensure smooth accelerations, vibrations mitigation and decreased maintenance. This is particularly important from the practical point of view, since the solution to lower the associated fatigue and vibration damage is to use smooth motion profiles which are tailor-made for a given application, rather than invest in costly condition based maintenance (CBM) schemes or implement hardware modifications to the machine.

6.4 Summary

Based on the above literature survey, it is concluded that an EMC drivetrain:

- offers good energy-efficiency, simple installation (plug and play), low maintenance, high stiffness (accuracy) and low space requirements in comparison to EHC systems with HPU and power lines (Michel and Weber, 2012)

- has low durability at high load force due to wear, and has little overload protection against shock loads (Michel and Weber, 2012)

- is an appealing alternative to EHC system, since it allows for the elimination of local hydraulic circuits, implying a significant maintenance cost reduction due to the absence of wearing parts such as seals, hence, eliminates fluid spills (Garcia et al., 2008)

- demands electric power just when it is needed, compared to centralized powered EHC systems where a continuous load on the HPU must be ensured regardless if the hydraulic power is used for actuation or not (Garcia et al., 2008)

- is relatively compact and can offer high power-to-weight ratios and motion velocities (Balaban et al., 2009)

- with a roller screw can be used for both highly and less accurate movement with flexible leads and desired precision (Hojjat and Mahdi Agheli, 2009)

- has high static load capabilities, however, the permissible transmitted power causes limitations on the allowable linear speed at high loads

- with large displacement and high load capabilities certified for explosive atmosphere areas is limited in availability.

7 Conclusion

This paper presents a feasibility study of the implementation of an EMC drivetrain in an offshore vertical pipe handling machine. The EMC-HD from Bosch Rexroth (2015) is considered as one of the commercial off-the-shelf EMC drivetrains which closely can match the power (static and dynamic force) and motion performance (displacement length and speed) demand of the case study machine.

From the inverse dynamic analysis, the EMC drivetrain components are selected based on the sizing principles and selection procedure of the manufacturer. The forward dynamic analysis verifies that the performance of the selected EMC drivetrain satisfies the requirements of the full-scale reference machine. The highest values obtained for axial force, motor torque, motor speed, linear speed and acceleration are within the limits of the maximum permissible values of the selected EMC drivetrain. However, the permissible transmitted power of the EMC drivetrain is lower than the power required by the motion cycle. Hence, based on the manufacturers recommendations, avoidance of overheating in the EMC drivetrain cannot be guaranteed. To avoid overheating, the average speed of the motion cycle must be decreased. Alternatively, external cooling or temperature monitoring and control system that prevents overheating could be implemented. Also, a transmission screw designed with larger lead can increase the permissible power of the EMC drivetrain.

Commercial off-the-shelf EMC drivetrains with large displacement and high load capabilities certified for explosive atmosphere areas are very limited or do not currently exist in the form that would allow to meet the requirements of a typical offshore drilling equipment. Where, design criteria such as temperature condition (typically $+40°C$ to $-20°C$), IP protection class, reliability, safety, and durability need to be satisfied.

75

Even though these systems are not commercially available, this paper shows that once the power and Ex-approval problems are solved, EMC drivetrains might become strong competitors to hydraulic cylinders in offshore drilling equipment systems where centralized hydraulic power is not available.

Acknowledgments

References

Austigard, A. Robotic Drilling Systems. http://rds.no, 2016. Accessed: 2017-03-03.

Bak, M. K. *Model Based Design of Electro-Hydraulic Motion Control Systems for Offshore Pipe Handling Equipment.* Ph.D. thesis, University of Agder, 2014.

Bak, M. K. and Hansen, M. R. Analysis of Offshore Knuckle Boom Crane - Part One: Modeling and Parameter Identification. *Modeling, Identification and Control: A Norwegian Research Bulletin*, 2013. 34(4):157–174. doi:10.4173/mic.2013.4.1.

Balaban, E., Bansal, P., Stoelting, P., Saxena, A., Goebel, K. F., and Curran, S. A diagnostic approach for electro-mechanical actuators in aerospace systems. In *2009 IEEE Aerospace conference*. IEEE, pages 1–13, 2009. doi:10.1109/AERO.2009.4839661.

Bodden, D. S., Clements, N. S., Schley, B., and Jenney, G. Seeded Failure Testing and Analysis of an Electro-Mechanical Actuator. In *2007 IEEE Aerospace Conference*. IEEE, pages 1–8, 2007. doi:10.1109/AERO.2007.352880.

Bosch Rexroth. IndraDyn S - MSK Project Planning Manual. 2006.

Bosch Rexroth. Electrical Mechanical Cylinder EMC-HD Catalog. 2015.

Couper, J. R., Penney, W. R., Fair, J. R., and Walas, S. M. *Chemical Process Equipment – Selection and Design.* Elsevier, 3rd edition edition, 2012.

European Commission. Directive 2014/34/EU of the European Parliament and of the Council. *Official Journal of the European Union L96*, 2014.

Frischemeier, S. Electrohydrostatic actuators for aircraft primary flight control-types, modelling and evaluation. In *5th Scandinavian International Conference on Fluid Power, SICFP '97, Linköping, Sweden, May 28. -30.* pages 1–16, 1997. doi:10.15480/882.236.

Fu, Y., Wang, D., Chen, J., Yang, R., and Qi, X. Nonlinear Modeling and System Analysis of the Linear Electromechanical Actuators Deviation of Nonlinear Dynamic Modeling. *Journal of Computational Information Systems*, 2015. 6(11):1983–1995. doi:10.12733/jcis13671.

Gallant, T. A. and Andrews, K. M. Large cage induction motors for offshore machinery drive applications. In *Petroleum and Chemical Industry Conference.* pages 1155–1159, 2006.

Garcia, A., Cusido, J., Rosero, J., Ortega, J., and Romeral, L. Reliable electro-mechanical actuators in aircraft. *IEEE Aerospace and Electronic Systems Magazine*, 2008. 23(8):19–25. doi:10.1109/MAES.2008.4607895.

Hoevenaars, A. H., Evans, I. C., and Desai, B. Preventing AC drive failures due to commutation notches on a drilling rig. *IEEE Transactions on Industry Applications*, 2013. 49(3):1215–1220. doi:10.1109/TIA.2013.2253078.

Hojjat, Y. and Mahdi Agheli, M. A comprehensive study on capabilities and limitations of roller-screw with emphasis on slip tendency. *Mechanism and Machine Theory*, 2009. 44(10):1887–1899. doi:10.1016/j.mechmachtheory.2009.04.001.

Holm, R. K., Berg, N. I., Walkusch, M., Rasmussen, P. O., and Hansen, R. H. Design of a magnetic lead screw for wave energy conversion. *IEEE Transactions on Industry Applications*, 2013. 49(6):2699–2708. doi:10.1109/TIA.2013.2264272.

Isermann, R., Schwarz, R., and Stolzl, S. Fault-tolerant drive-by-wire systems. *IEEE Control Systems*, 2002. 22(5):64–81. doi:10.1109/MCS.2002.1035218.

Kandukuri, S. T., Klausen, A., Karimi, H. R., and Robbersmyr, K. G. A review of diagnostics and prognostics of low-speed machinery towards wind turbine farm-level health management. *Renewable and Sustainable Energy Reviews*, 2016. 53:697 – 708. doi:10.1016/j.rser.2015.08.061.

Lemor, P. The roller screw, an efficient and reliable mechanical component of electro-mechanical actuators. In *IECEC 96. Proceedings of the 31st Intersociety Energy Conversion Engineering Conference*, volume 1. IEEE, pages 215–220, 1996. doi:10.1109/IECEC.1996.552873.

76

Michel, S. and Weber, J. Energy-efficient electrohydraulic compact drives for low power applications. *Fluid Power and Motion Control (FPMC 2012)*, 2012. pages 94–108.

Narasimhan, S., Roychoudhury, I., Balaban, E., and Saxena, A. Combining Model-Based and Feature-DrivenFeature-Driven Diagnosis Approaches A Case Study on Electromechanical Actuators. *21st International Workshop on Principles of Diagnosis*, 2010. pages 1–9.

Neleman, K. Motor controls for Ex motors in hazardous areas: An application guide! In *2009 Conference Record PCIC Europe*. pages 132–145, 2009.

Nikravesh, P. E. *COMPUTER-AIDED ANALYSIS OF MECHANICAL SYSTEMS*. Prentice Hall, 1988.

Nikravesh, P. E. *PLANAR MULTIBODY DYNAMICS*. CRC Press - Taylor & Francis Group, 2008.

Ottestad, M., Nilsen, N., and Hansen, M. Reducing the static friction in hydraulic cylinders by maintaining relative velocity between piston and cylinder. In *International Conference on Control, Automation and Systems*. pages 764–769, 2012.

Parker. Extreme Force Electromechanical Cylinder Catalog. 2013.

Pawlus, W. *Design and Analysis of Electric Powertrains for Offshore Drilling Applications*. Ph.D. thesis, University of Agder, 2016.

Pawlus, W., Choux, M., and Hansen, M. R. Hydraulic vs. electric: A review of actuation systems in offshore drilling equipment. *Modeling, Identification and Control*, 2016a. 37(1):1–17. doi:10.4173/mic.2016.1.1.

Pawlus, W., Frick, D., Morari, M., Hovland, G., and Choux, M. Drivetrain design optimization for electrically actuated systems via Mixed Integer Programing. In *Industrial Electronics Society, IECON 2015 - 41st Annual Conference of the IEEE*. pages 1465–1470, 2015. doi:10.1109/IECON.2015.7392307.

Pawlus, W., Hansen, M. R., Choux, M., and Hovland, G. Mitigation of fatigue damage and vibration severity of electric drivetrains by systematic selection of motion profiles. *IEEE/ASME Transactions on Mechatronics*, 2016b. 21(6):2870–2880. doi:10.1109/TMECH.2016.2573587.

Pawlus, W., Khang, H. V., and Hansen, M. Temperature rise estimation of induction motor drives based on loadability curves to facilitate design of electric powertrains. *IEEE Transactions on Industrial Informatics*, 2016c. doi:10.1109/TII.2016.2641454. In Press.

Pillay, P. and Krishnan, R. Modeling, simulation, and analysis of permanent-magnet motor drives. The permanent-magnet synchronous motor drive. *Industry Applications, IEEE Transactions on*, 1989. 25(2):265–273. doi:10.1109/28.25541.

Rahimi, M., Rausand, M., and Wu, S. Reliability prediction of offshore oil and gas equipment for use in an Arctic environment. In *International Conference on Quality, Reliability, Risk, Maintenance, and Safety Engineering*. pages 81–86, 2011.

Sakuraba, J., Hata, F., Kung, C. C., Sotooka, K., Mori, H., and Takarada, N. Development of superconducting electric ship propulsion system. In *The Second International Offshore and Polar Engineering Conference*. pages 1–7, 1992.

Schinstock, D. and Haskew, T. Dynamic load testing of roller screw EMAs. In *IECEC 96. Proceedings of the 31st Intersociety Energy Conversion Engineering Conference*, volume 1. IEEE, pages 221–226, 1996. doi:10.1109/IECEC.1996.552874.

Sørensen, J. K. *Reduction of Oscillations in Hydraulically Actuated Knuckle Boom Cranes*. Ph.D. thesis, University of Agder, 2016.

Ummaneni, R. B., Nilssen, R., and Brennvall, J. E. Force analysis in design of high power linear permanent magnet actuator with gas springs in drilling applications. In *Electric Machines Drives Conference, 2007. IEMDC '07. IEEE International*. pages 285–288, 2007. doi:10.1109/IEMDC.2007.382680.

Wang, Z., Chen, J., Cheng, M., and Chau, K. T. Field-oriented control and direct torque control for paralleled vsis fed pmsm drives with variable switching frequencies. *IEEE Transactions on Power Electronics*, 2016. 31(3):2417–2428. doi:10.1109/TPEL.2015.2437893.

Yadav, P., Kumar, R., Panda, S. K., and Chang, C. S. Optimal thrust allocation for semisubmersible oil rig platforms using improved harmony search algorithm. *IEEE Journal of Oceanic Engineering*, 2014. 39(3):526–539. doi:10.1109/JOE.2013.2270017.

Paper B

Study of a Self-Contained Electro-Hydraulic Cylinder Drive

Daniel Hagen, Damiano Padovani, and Morten K. Ebbesen

Study of a Self-Contained Electro-Hydraulic Cylinder Drive

Daniel Hagen
Department of Engineering Sciences
University of Agder
Grimstad, Norway
daniel.hagen@uia.no

Damiano Padovani
Department of Engineering Sciences
University of Agder
Grimstad, Norway
damiano.padovani@uia.no

Morten K. Ebbesen
Department of Engineering Sciences
University of Agder
Grimstad, Norway
morten.k.ebbesen@uia.no

Abstract—Self-contained electro-hydraulic cylinders that can be powered just by an electrical wire will be popular in the coming years. Combining electrical-drives and hydraulic cylinders exploits some excellent properties of these two technologies and enables flexible implementation. To fully benefit from such a drive solution, there is the need to develop electro-hydraulic cylinders capable of operating independently as opposed to standard hydraulic systems that are connected to a central power supply. Therefore, this paper presents a numerical investigation of a self-contained electro-hydraulic cylinder with passive load-holding capability. The corresponding dynamic model is proposed and used to predict the system behavior with a view to future implementation. The simulations show the proposed drive guarantees proper functioning in four-quadrant operations.

Index Terms—compact electro-hydraulic cylinders, valve-less systems, electric-drives, load-holding

I. INTRODUCTION

During the last years, electro-mechanical drives are increasingly replacing standard valve-controlled hydraulic actuators due to the easy installation on the machine and the higher energy efficiency [1]. These electro-mechanical solutions are unsuitable in several applications such as primary aircraft flight control or offshore oil drilling mainly due to the limited reliability [2]. For this reason, there is an ongoing interest in developing self-contained electro-hydraulic cylinders (SCCs) since they represent a valid alternative to electro-mechanical systems. SCCs are compact and self-sufficient drives connected to an electrical power supply that enable plug-and-play installation (Fig. 1). A limited number of commercial SCCs have been introduced to the market mainly using single-rod cylinders [3]. Employing a valve-less architecture to control the hydraulic actuator is popular in many applications since higher energy efficiency is possible. For instance, a displacement-controlled excavator showed a 40% efficiency improvement in a truck loading cycle when compared to a state-of-the-art load-sensing machine [4]. Research focus related to SCCs is primarily on cost efficiency and low power applications, i.e. below 5 kW [5]. For instance, Michel et al. derived specific conclusions about the best approach for SCCs without passive load-holding functions [6]. This means there is need for more generic SCCs capable of delivering higher power and providing features such as passive load-

holding. Countless applications will benefit from such a drive solution. A few examples are gripper arms for offshore pipe handling machines [2], hydraulic presses, trailer lifts, marine jack plates, scissors tables, positioning systems for solar panels, Stewart platforms, single-boom cranes, etc. Thus, this paper takes advantage of a comprehensive literature study on electro-hydraulic architectures to discuss a concept for a self-contained cylinder. The target is on the evaluation of an electro-hydraulic self-contained single-rod cylinder in closed-circuit configuration with sealed tank suitable for power levels above 5 kW. The mathematical model of the proposed system is presented together with a numerical investigation intended to evaluate the performance in view of a future implementation.
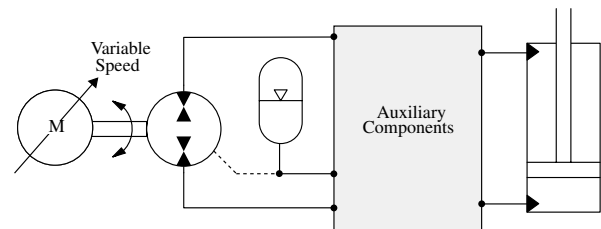

Fig. 1: Standard system architecture for self-contained electro-hydraulic cylinders (simplified schematic).

II. LITERATURE SURVEY

The majority of valve-less systems in closed-circuit configuration makes use of the following approaches to control the motion of linear actuators.

1) Systems with a variable-displacement pump driven at fixed speed. The amount of flow directed to the actuator is controlled by the pump displacement setting while the flow direction is changed by adjusting the swash-plate overcenter. Figure 2 shows the system in closed-circuit configuration presented in [7]. This control approach is mainly used for multi-actuator construction machines, e.g. [4], since a dedicated pressure source is needed to adjust the unit displacements.

2) Systems with a variable-speed electric motor driving the fixed-displacement pump. The actuator motion is controlled
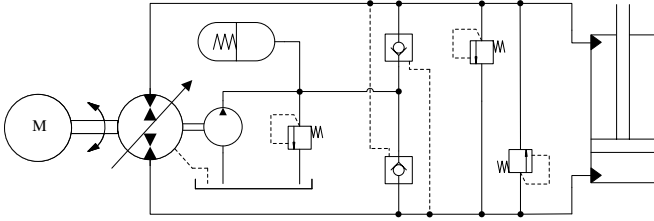
Fig. 2: Displacement-controlled pump driving a single-rod cylinder according to the architecture proposed in [7].

by adjusting both speed and direction of the motor rotation [6], [8], [9], [10], (Fig. 3). The electric motor can either be an asynchronous machine [11] or a synchronous machine [8].
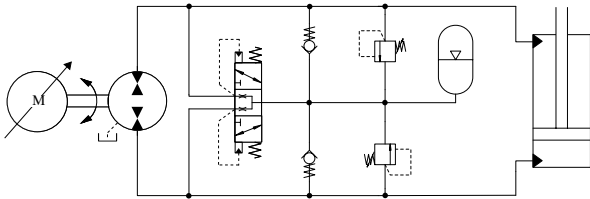

Fig. 3: Speed-controlled pump driving the cylinder according to the architecture proposed in [10].

3) Systems with a combined control method. The variable-speed prime mover drives the variable-displacement servo-pump meaning that both components are actively controlling the actuator motion [12].

Only layouts with a variable-speed electric motor and a fixed-displacement pump have been consistently used for SCCs in the past. This minimizes the number of control elements and the number of hydraulic components, i.e. the additional pressure source of the variable-displacement pump is not needed. Concerning the actuator type, double-rod cylinders are almost exclusively used in aircraft flight controls [13], [14], [15], [16] and [17]. The double-rod configuration increases the installation space while the symmetrical piston areas reduce the maximum available force with the same maximum pressure. Consequently, single-rod cylinders are the most popular actuators for at least 80% of electro-hydraulic drives [18]. Balancing the differential flow due to the asymmetric areas is necessary when the closed-circuit configuration is implemented. Multiple flow compensation methods were proposed in the past mainly involving pilot operated check valves (Fig. 2), flushing valves (Fig. 3), or electrically operated on/off valves [19]. Some issues related to instability and uncontrolled pressure oscillations were mentioned [10] and [20]. However, this is the case under high dynamic excitations of the system [3], i.e. an operating condition that might be representative for low-power applications. Other approaches have also been explored such as using hydraulic transformers, tandem pumps, 3-port axial-piston pumps, asymmetric gear pumps, or two pumps connected to each actuator port (Fig. 4). Table I provides a synthesis of these options.
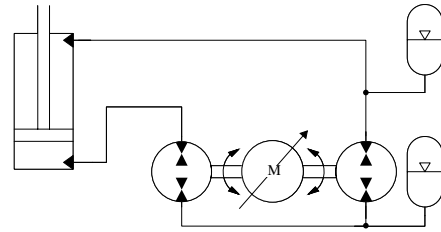
Fig. 4: Simplified architecture according to [8] of a SCC with two gear units that balance the differential cylinder flow.

Moreover, very few researches addressed the passive load-holding capability of SSCs. This feature is intended to maintain a fixed piston position without delivering power to the system. A first solution is a commercialized system [21] that has been patented in 2008 [22]. Pilot operated check valves are installed between the pump and the actuator while each opening pilot is sensing the pressure of the opposite pump side, see Fig. 5. A similar approach is also addressed in [23] and [24]. Alternative load-holding systems were presented in [9] and [25]. Both solutions make use of counter-balance valves that are operated differently. Some of these load-holding systems are also equipped with manual pressure release valves that can be used in case of failure to manually modify the actuator position.
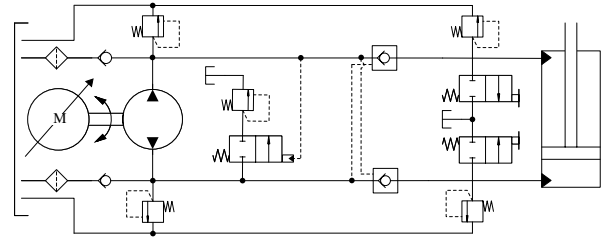

Fig. 5: Closed-circuit configuration with passive load-holding according to [21].

TABLE I: Differential flow compensation methods

Method:	Reference:
Hydraulic transformers	[26], [27], [28]
Pilot operated check valves	[7], [24], [29], [30], [31]
Shuttle valve	[6], [32], [33]
Tandem pumps	[34]
3-port asymmetric piston pump	[35], [36], [37], [38]
Asymmetric gear pump	[39]
Two pumps with equal displacement	[40]
Two pumps with different displacement	[6], [41], [42]
Two single rod cylinders in parallel	[43]

Table II summarizes the architectures of the SCCs addressed in this survey. Details about the possibility of performing four quadrant (4Q) operations are listed as well as the passive load-holding (PLH) capability.

In conclusion, the idea behind electro-hydraulic self-contained cylinders is combining the advantages of standard

hydraulic actuators such as reliability, and high power-to-weight ratio, with the benefits of electro-mechanical drives such as energy efficiency, minimal maintenance, and easy plug-and-play commissioning. Additional requirements such as compactness, robustness, and reduced costs are also of interest due to their relevance in both industrial and mobile applications [3] and [39].

TABLE II: List of considered SCC concepts

SCCs:	4Q:	PLH:	Reference:
Double gear pump	YES	NO	[6]
Direct driven hydraulic drive	YES	NO	[8]
Differential gear pump	NO	NO	[39], [44]
Inverse shuttle valve	YES	NO	[3], [6], [45]
Compact electro-hydraulic actuator	NO	YES	[9], [25]
Pump controlled single rod actuator	YES	NO	[10], [46]
Compact electro-hydraulic actuator	NO	YES	[21], [22]

III. SYSTEM ARCHITECTURE

The target of this research is to study a self-contained cylinder that operates in four quadrants, includes passive load-holding devices, and can deal with power levels above 5 kW. According to the literature survey presented in the previous section, published solutions that meet all these requirements are not available. Several systems represent a partial fit (Tab. II). Therefore, some features coming from them were combined accordingly to generate the architecture depicted in Fig. 6.
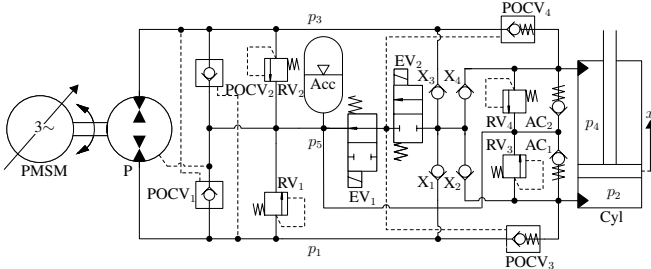
Fig. 6: Schematic of the SCC under investigation.

The combination of a variable-speed servo-motor (PMSM) and a fixed-displacement hydraulic pump was chosen to drive a single-rod cylinder arranged in closed-circuit configuration. Two pilot operated check valves (POCV$_{1,2}$) balance the differential cylinder flow as in the system discussed before [7]. Their low-pressure ports are connected to the accumulator (Acc) that represents the sealed tank of the SCC. The remaining pilot operated check valves (POCV$_{3,4}$) take care of the passive load-holding as in [21] and [23]. The opening pilot pressure is selected as the highest system pressure by some check valves (X$_{1,2,3,4}$) to deal properly with aided loads (i.e. when the load is acting in the same direction as the motion). This solution has been inspired by [47] where a 3/2 valve controls the opening pilot of the load-holding POCVs by using an external pressure signal always high enough. The passive load-holding is enabled or disabled by two electrically operated

on/off valves (EV). When actuator motion is desired, the EVs are energized resulting in the opening pilot pressure equal to the highest system pressure. Conversely, when the EVs are not energized the pilot pressure is equal to the accumulator pressure that maintains POCV$_{3,4}$ closed. Pressure relief valves (RV$_{1,2,3,4}$) are installed on the pump ports and on the actuator ports to avoid overpressurizations during normal functioning and load-holding, respectively. An anti-cavitation valve (AC) is connected to each actuator side. Finally, a manually operated valve intended to release the actuator in case of electric failure is not showed in the schematic but can be easily included in the real system.

Figure 7 shows the functioning of the system under investigation depending on the operating condition. Low-pressure sides (LP) and high-pressure sides (HP) are highlighted in all four quadrants as well as the direction of the flows. The two on/off valves are always energized to disable the load-holding capability.

The size of the components has been chosen from catalogues available on the market according to a conventional static sizing that guarantees maximum piston speed of 150 $\frac{mm}{s}$ and maximum output force of 40 kN. This target is met assuming system pressure up to 200 bar in combination with a cylinder characterized by dimensions 65x35x500 mm. The resulting axial-piston pump has displacement of 10 $\frac{cm^3}{rev}$ since the selected servo-motor can run up to 4200 $\frac{rev}{min}$. This unit is a permanent magnet synchronous machine. Lastly, accumulator has a volume of 3.5 $liters$ whereas the load-holding valves have area ratio of 1:3 and cracking pressure of 5 bar.

IV. SYSTEM MODELING

The hydraulics has been modeled using a well-established approach successfully tested in the past, e.g. by Rahmfeld [19]. The effective magnitudes of the pump are evaluated using flow and torque losses ($Q_S \geq 0$ and $T_S \geq 0$, respectively) measured from steady-state experimental data [48] with a reference unit. The same losses have been assumed for all quadrants and scaled to the desired pump displacement according to (1) and (2). The shaft speed as been scaled via (3).

$$Q_S = \lambda^2 \cdot Q_{S,ref} \tag{1}$$
$$Q_T = \lambda^3 \cdot Q_{T,ref} \tag{2}$$
$$n = \lambda^3 \cdot n_{ref} \tag{3}$$

The scaling factor λ is computed in (4) as function of the pump displacement D_P used in the simulation.

$$\lambda = \sqrt[3]{\frac{D_P}{D_{P,ref}}} \tag{4}$$

The effective unit flow rate is evaluated in (5) according to the machine operation, i.e. pumping or motoring mode. The flow losses are completely attributed to internal losses.

$$Q_P = \begin{cases} (|D_P \cdot n| - Q_S) \cdot sign(n), & \text{if pumping,} \\ (|D_P \cdot n| + Q_S) \cdot sign(n), & \text{otherwise.} \end{cases} \tag{5}$$

(a) Out-stroke, resistant load.

(b) In-stroke, aided load.

(c) Out-stroke, aided load.

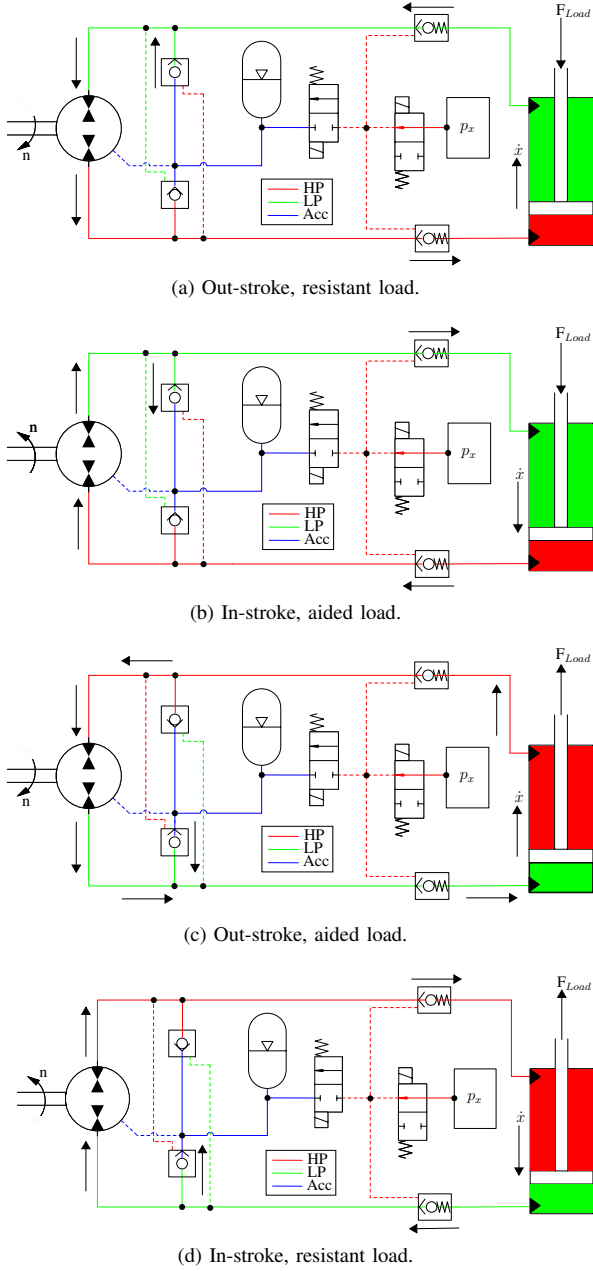(d) In-stroke, resistant load.

Fig. 7: Four quadrant operations for the considered SCC (simplified schematics).

Equation (6) provides the effective shaft torque T_e.

$$T_e = \left(D_P \cdot \frac{\Delta p}{2\pi} + T_S\right) \cdot sign(n) \qquad (6)$$

The mechanical powers measured at the unit shaft P_{Unit} and at the actuator rod P_{Cyl} are defined in (7) and (8).

$$P_{Unit} = T_e \cdot n \cdot sign(n) \qquad (7)$$
$$P_{Cyl} = F_{Load} \cdot \dot{x} \qquad (8)$$

Evaluating the pressures in the different sections of the system is crucial, and they are labeled in Fig. 6. The pressure

build-up equation (9) that involves the fluid bulk modulus β, the volume of the hydraulic capacitance V and the flow balance has been used.

$$\dot{p} = \frac{\beta}{V} \cdot \sum_i Q_i \qquad (9)$$

The pressure gradients related to every hydraulic capacitance are shown in details in (10), (11), (12), (13) and (14).

$$\dot{p}_1 = \frac{\beta}{V_1} \cdot (Q_{POCV_1} + Q_P - Q_{POCV_3} - Q_{RV_1}) \qquad (10)$$

$$\dot{p}_2 = \frac{\beta}{V_2} \cdot (Q_{POCV_3} + Q_{AC_1} - \dot{x} \cdot A_A - Q_{RV_3}) \qquad (11)$$

$$\dot{p}_3 = \frac{\beta}{V_3} \cdot (Q_{POCV_2} - Q_{POCV_4} - Q_P - Q_{RV_2}) \qquad (12)$$

$$\dot{p}_4 = \frac{\beta}{V_4} \cdot (Q_{POCV_4} + Q_{AC_2} + \dot{x} \cdot A_B - Q_{RV_4}) \qquad (13)$$

$$\dot{p}_5 = \frac{\beta}{V_5} \cdot (Q_{RV_{1,2,3,4}} - Q_{POCV_{1,2}} - Q_{AC_{1,2}}) \qquad (14)$$

Constant volumes V_0 have been assumed for the transmission lines V_1 and V_3. The definitions of the volumes V_2 and V_3 are shown in (15) and (16) respectively. The influence of the hydro-pneumatic accumulator is showed in (17), where γ is the polytrophic coefficient, $V_{0,Acc}$ the accumulator volume, and $p_{0,Acc}$ the pre-charge pressure.

$$V_2 = V_{0,2} + A_A \cdot x \qquad (15)$$
$$V_4 = V_{0,4} + A_B \cdot (x_{max} - x) \qquad (16)$$

$$V_5 = V_{0,5} + \left(\beta \cdot \frac{V_{0,Acc}}{\gamma} \cdot \frac{p_{0,Acc}^{\frac{1}{\gamma}}}{p_5^{\frac{\gamma+1}{\gamma}}}\right) \qquad (17)$$

The flow rates of the anti-cavitation valves ($i = AC_{1-2}$) and of the pressure relief valves ($i = RV_{1-4}$) are defined in (18). The characteristic valve flow gain K_i is introduced as well as the inlet pressure p_{In}, the outlet pressure p_{Out}, and the cracking pressure p_{Cr}.

$$Q_i = \begin{cases} K_i \cdot (p_{In} - p_{Out} - p_{Cr}), & \text{if } (p_{In} - p_{Out}) \geq p_{Cr}, \\ 0, & \text{otherwise.} \end{cases}$$
$$(18)$$

The flow rate through the pilot-operated check valves ($i = POCV_{1-4}$) is found with the orifice equation (19). The different terms are the discharge coefficient C_d, the seat diameter d, the lift of the poppet y, the pressure differential across the valve Δp and the fluid density ρ.

$$Q_i = C_d \cdot (\pi \cdot d_i \cdot y_i) \cdot sign(\Delta p_i) \cdot \sqrt{\frac{2}{\rho} \cdot |\Delta p_i|} \qquad (19)$$

The lift results from the force equilibrium of the poppet where the poppet dynamics have been neglected. The pilot pressure p_x, the area of the poppet seat A_{Seat}, the area of the pilot stage A_x, the pre-load force of the spring $F_{S,0}$, and the spring stiffness k_S are involved. Two operating modes are emphasized: normal flow (20) when the pilot stage is separated

from the poppet (i.e. $p_{In} > p_x$) and reverse flow direction (21) if the pilot stage is in contact with the poppet (i.e. $p_{In} < p_x$).

$$y_i = \frac{1}{k_S} \cdot (\Delta p_i \cdot A_{Seat} - F_{S,0}) \qquad (20)$$

$$y_i = \frac{1}{k_S} \cdot ((p_x - p_{In}) \cdot A_x + \Delta p_i \cdot A_{Seat} - F_{S,0}) \qquad (21)$$

The governing equation for the actuator motion is pointed out in (22) from the Newton's second law. A simplified scenario characterized by a horizontal sliding mass m_{Eq} loaded by an external force F_{Load} is accounted.

$$\ddot{x} = \frac{1}{m_{Eq}} \cdot (p_2 \cdot A_A - p_4 \cdot A_B - F_{Fric} - F_{Load}) \qquad (22)$$

The actuator pressures and areas (piston-side area A_A and rod-side area A_B) describe the force coming from the hydraulics while the actuator friction F_{Fric} is given in (23) according to the Stribeck model. The different coefficients account the viscous friction coefficient f_V, the Coulomb friction F_C, and the static friction coefficient f_S.

$$F_{fric} = \dot{x} \cdot f_V + sign(\dot{x}) \cdot \left(F_C + f_S \cdot e^{-\frac{|\dot{x}|}{\tau_S}} \right) \qquad (23)$$

The pressure losses in the transmission lines have been neglected due to the compact configuration of the drive. The valves used to enable/disable the load-holding capability have been simulated as an equivalent logic function. Finally, the dynamics of the electric motor have been simulated using a second-order transfer function from commanded to simulated speed. Due to the fast response of the machine, this simplified approach is sufficient at this stage of the investigation.

V. Simulation Results

Understanding if the proposed SCC is a feasible approach to meet the aforementioned requirements represents the target of the following simulations. Operations in four quadrants are tested by varying the direction of the external load accordingly. The controller implemented in MATLAB-Simulink takes care of generating the commanded motor speed in order to track the desired actuator position. The logic emerges from Fig. 8. The command directed to the on/off valves (not shown in the block diagram) is activated when non-zero actuator velocity is wanted.
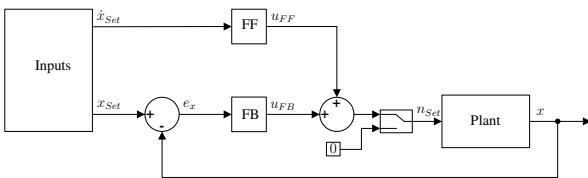
Fig. 8: The control logic for the proposed SCC.

If actuator motion is not desired, the switch logic sets the commanded motor speed to zero. Contrariwise, the motor speed is defined as follows. The feedforward term (FF) estimates the necessary motor speed depending if the HP is on the piston-side or on the rod-side (24).

$$u_{FF} = \begin{cases} \dot{x}_{Set} \cdot \left(\frac{A_A}{D_P} \right), & \text{if HP} \rightarrow \text{piston-side,} \\ \dot{x}_{Set} \cdot \left(\frac{A_B}{D_P} \right), & \text{otherwise.} \end{cases} \qquad (24)$$

The feedback element (FB), originated by a constant gain K_P acting on the position error e_x, corrects the prediction of the feedforward element. The resulting speed command n_{Set} is propagated to the plant according to (25).

$$n_{Set} = e_x \cdot K_P + u_{FF} \qquad (25)$$

Figure 9 depicts the actuator position in combination with the position error and the external load acting on the actuator. The results show good agreement between commanded and simulated position. This is the case for system operations in all four quadrants (OUT $\rightarrow$ cylinder out-stroke, IN $\rightarrow$ cylinder in-stroke, R $\rightarrow$ resistant load, and A $\rightarrow$ aided load).
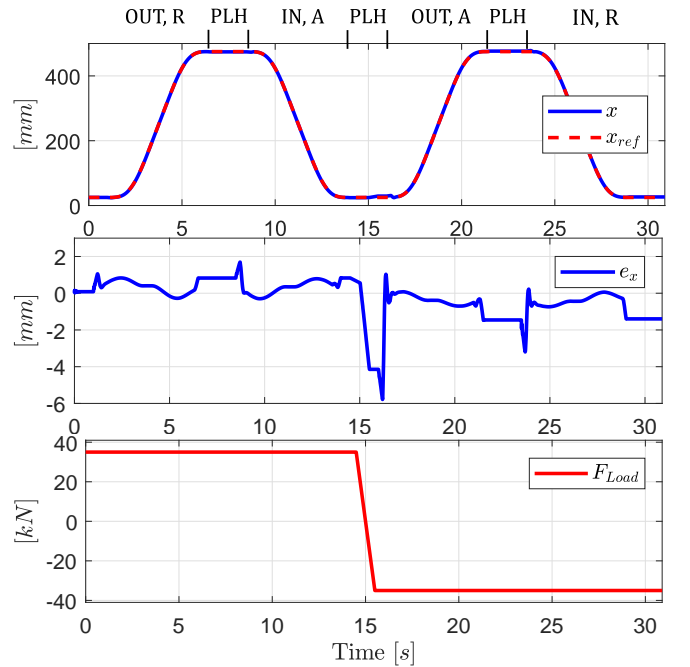

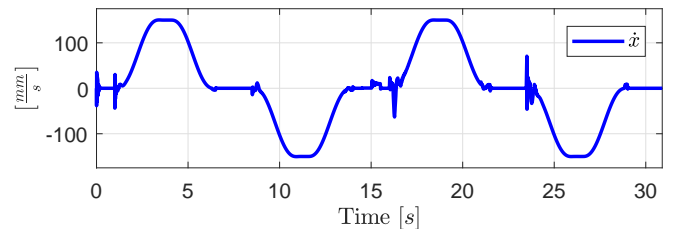Fig. 9: Simulation cycle: piston position, position error, and load force.

Fig. 10: Simulated actuator velocity.

The reference position has been generated to achieve the maximum piston velocity, i.e. $150 \frac{mm}{s}$. Figure 10 proves

the system sizing is satisfactory. The control effort, i.e. the commanded motor speed, is presented in Fig. 11. The speed variation is generally very smooth and well within the upper limit of the electric machine. A few reduced spikes are induced by the zero-velocity switch logic that kicks in. The system pressures are visible in Fig. 12. They behave as expected, especially the accumulator pressure that is characterized by limited variations. Figure 13 highlights the poppet position of the load-holding pilot operated check valves POCV$_{3,4}$. The electric signal directed to the EVs to supervise the load-holding capability is included as well. The POCVs do not introduce unpleasant oscillations during motion. Most importantly, they maintain the piston position (Fig. 9) when the electric motor is not operating.

Fig. 13: Load-holding: poppet lift, and EV signal.
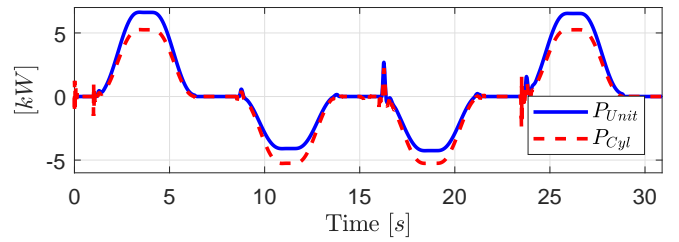
Fig. 14: Actuator and pump power.

is modified accordingly. Finally, these power trends provide some preliminary indications about the efficiency of the hydraulic sub-system. When the actuator is driven, this efficiency is about 80%.

VI. Conclusion

This paper discussed in first place a detailed literature review about electro-hydraulic self-contained cylinders characterized by being a sealed system. The survey pointed out a missing solution to drive SCCs that comprise passive load-holding devices, operate in four quadrants, and are suitable for power levels above 5 kW. Hence, a specific concept was presented and modeled. The numerical simulations showed that the system behaves properly in four quadrant operations and can hold the external load passively. Plans for future investigations include both the design of a more advanced control algorithm and the implementation of this SCC on a real test-bed.

Fig. 11: Commanded and simulated motor speed.

Fig. 12: System pressures: actuator, pump, and accumulator.

Figure 14 illustrates the mechanical power measured both at the unit shaft and at the actuator rod. According to the sign convention, positive values mean the power flow is from the hydraulic unit to the actuator and vice versa for negative values. The power levels presented are relatively low because they refer to a compact system meant for laboratory testing. Nevertheless, this system architecture can successfully deal with much higher power levels if the size of the components

References

[1] E. Jalayeri, A. Imam, Z. Tomas, and N. Sepehri, "A throttle-less single-rod hydraulic cylinder positioning system: Design and experimental evaluation," *Advances in Mechanical Engineering*, vol. 7, no. 5, pp. 1–14, 2015.

[2] D. Hagen, W. Pawlus, M. K. Ebbesen, and T. O. Andersen, "Feasibility Study of Electromechanical Cylinder Drivetrain for Offshore Mechatronic Systems," *Modeling, Identification and Control*, vol. 38, no. 2, pp. 59–77, 2017.

[3] S. Michel and J. Weber, "Electrohydraulic Compact-drives for Low Power Applications considering Energy-efficiency and High Inertial Loads," *The 7th FPNI PhD Symposium on Fluid Power*, pp. 1–18, 2012.

[4] J. Zimmerman, E. Busquets, and M. Ivantysynova, "40% Fuel Savings by Displacement Control Leads to Lower Working Temperatures – A Simulation Study and Measurements," in *52nd National Conference on Fluid Power*, 2011.

[5] J. Weber, B. Beck, E. Fischer, G. Kolks, J. Lübbert, S. Michel, M. Schneider, R. Ivantysyn, L. Shabi, M. Kunkis, A. Sitte, H. Lohse, and J. Weber, "Novel System Architectures by Individual Drives," in *10th International Fluid Power Conference*, 2016, pp. 29–62.

[6] S. Michel and J. Weber, "Energy-efficient electrohydraulic companct drives for low power applications," *ASME/BATH 2012 Symposium on Fluid Power and Motion Control*, pp. 93–107, 2012.

[7] R. Rahmfeld and M. Ivantysynova, "Energy saving hydraulic actuators for mobile machines," in *1st Bratislavian Fluid Power Symposium*, 1998, pp. 177–186.

[8] T. a. Minav, P. Sainio, and M. Pietola, "Direct Driven Hydraulic Drive Without Conventional Oil Tank," in *ASME/BATH 2014 Symposium on Fluid Power and Motion Control*, no. September, 2014, pp. 1–6.

[9] G. Altare and A. Vacca, "A design solution for efficient and compact electro-hydraulic actuators," in *Procedia Engineering*, vol. 106. Elsevier Ltd, 2015, pp. 8–16.

[10] H. Çalışkan, T. Balkan, and B. E. Platin, "A Complete Analysis for Pump Controlled Single Rod Actuators," in *10th International Fluid Power Conference*, 2016, pp. 119–132.

[11] S. H. Cho and R. Burton, "Position control of high performance hydrostatic actuation system using a simple adaptive control (SAC) method," *Mechatronics*, vol. 21, pp. 109–115, 2011.

[12] J. Willkomm, M. Wahler, and J. Weber, "Potentials of Speed and Displacement Variable Pumps in Hydraulic Applications," in *10th International Fluid Power Conference*, 2016, pp. 379–391.

[13] S. Croke and J. Herrenschmidt, "More Electric Initiative Power-By-Wire Actuation Alternatives," in *Proceedings of National Aerospace and Electronics Conference (NAECON'94)*, 1994, pp. 1338–1346.

[14] S. Frischemeier, "Electrohydrostatic Actuators for Aircraft Primary Flight Control - Types, Modelling and Evaluation," in *5th Scandinavian International Conference on Fluid Power*, 1997, pp. 1–16.

[15] B. Kazmeier, "Energieverbrauchsoptimierte Regelung eines elektrohydraulischen Linearantriebs kleiner Leistung mit drehzahlgeregeltem Elektromotor und Verstellpumpe," Ph.D. dissertation, TU Hamburg-Harburg, 1998.

[16] L. Jun, F. Yongling, Z. Guiying, G. Bo, and M. Jiming, "Research on fast response and high accuracy control of an airborne brushless DC motor," in *Proceedings of the 2004 IEEE International Conference on Robotics and Biomimetics*, 2004, pp. 807–810.

[17] D. van den Bossche, "The A380 Flight Control Electrohydrostatic Actuators, Achievements and Lessons Learnt," in *25th International Congress of the Aeronautical Sciences*, 2006, pp. 1–8.

[18] Z. Quan, L. Quan, and J. Zhang, "Review of energy efficient direct pump controlled cylinder electro-hydraulic technology," *Renewable and Sustainable Energy Reviews*, vol. 35, pp. 336–346, 2014.

[19] R. Rahmfeld, "Development and Control of Energy Saving Hydraulic Servo Drives for Mobile Systems," Ph.D. dissertation, TU Hamburg-Harburg, 2002.

[20] C. Williamson and M. Ivantysynova, "Stability and Motion Control of Inertial Loads with Displacement Controlled Hydraulic Actuators," in *6th FPNI - PhD Symposium*, West Lafayette, 2010, pp. 499–514.

[21] Parker Hannifi, "Compact EHA - Electro-Hydraulic Actuators for high power density applications." [Online]. Available: https://goo.gl/t2FMw2

[22] T. Sweeney, P. T. Kubinski, and D. J. Anderson, "Electro-hydraulic actuator mounting, Patent US 8161742 B2," 2008.

[23] Bosch Rexroth, "Advantages of electrification and digitalization technology for hydraulics." [Online]. Available: https://goo.gl/4G6Jxn

[24] G. Li, H. Wang, X. Huang, and H. Yang, "Research on the Control Scheme of Direct Drive Electro-hydraulic Position Servo System," in *Proceedings of 2011 International Conference on Electronic and Mechanical Engineering and Information Technology, EMEIT 2011*, vol. 6, 2011, pp. 3221–3224.

[25] G. Altare, A. Vacca, and C. Richter, "A Novel Pump Design for an Efficient and Compact Electro-Hydraulic Actuator," in *IEEE Aerospace Conference*, 2014, pp. 1–8.

[26] J. Lodewyks, "Differenzialzyliner im geschlossenen hydrostatischen Getriebe," *O + P "Ölhydraulik und Pneumatik" 34 Nr.5*, pp. 394–401, 1993.

[27] ——, "Der Differentialzylinder im geschlossenen hydrostatischen Kreislauf," Ph.D. dissertation, RWTH Aachen, 1994.

[28] G. Vael, P. Achten, and J. Potma, "Cylinder Control With Floating Cup Hydraulic Transformer," pp. 175–190, 2003.

[29] Vickers Inc., "Electrohydraulic system and apparatus with bidirectional electric-motor hydraulic-pump unit, Patent WO 1998011358 A1," 1998.

[30] J.-m. Zheng, S.-d. Zhao, and S.-g. Wei, "Application of self-tuning fuzzy PID controller for a SRM direct drive volume control hydraulic press," *Control Engineering Practice*, vol. 17, no. 12, pp. 1398–1404, 2009.

[31] S. G. Wei, S. D. Zhao, J. M. Zheng, and Y. Zhang, "Self-tuning dead-zone compensation fuzzy logic controller for a switched-reluctance-motor direct-drive hydraulic press," *Proceedings of the Institution of Mechanical Engineers, Part I: Journal of Systems and Control Engineering*, vol. 223, no. 5, pp. 647–656, 2009.

[32] A. J. Hewett, "Hydraulic circuit flow control, Patent US 5329767 A," 1994.

[33] L. Wang, W. J. Book, and J. D. Huggins, "A Hydraulic Circuit for Single Rod Cylinders," *Journal of Dynamic Systems, Measurement, and Control*, vol. 134, no. 1, pp. 1–11, 2012.

[34] K. Cleasby and A. Plummer, "A novel high efficiency electrohydrostatic flight simulator motion system," *ASME/BATH 2008 Symposium on Fluid Power and Motion Control*, pp. 437–449, 2008.

[35] R. L. Kenyon, D. Scanderbeg, M. E. Nolan, and W. D. Wilkerson, "Electro-hydraulic actuator, Patent EP0395420 A2," 1990.

[36] L. Quan, "Current State, Problems and the Innovative Solution of Electro-hydraulic Technology of Pump Controlled Cylinder," *Chinese Journal of Mechanical Engineering*, vol. 44, no. 11, pp. 87–92, 2008.

[37] X. Zhang, L. Quan, Y. Yang, C. Wang, and L. Yao, "Output Characteristics of a Series Three-port Axial Piston Pump," *Chinese Journal Of Mechanical Engineering*, vol. 25, no. 3, 2012.

[38] J. Huang, L. Quan, and X. Zhang, "Development of a dual-acting axial piston pump for displacement-controlled system," *Proceedings of the Institution of Mechanical Engineers, Part B: Journal of Engineering Manufacture*, vol. 228, no. 4, pp. 606–616, 2014.

[39] B. Brahmer, "CLDP - Hybrid Drive using Servo Pump in Closed Loop," in *Proceedings of 8th International Fluid Power Conference*, 2012, pp. 93–102.

[40] S. Helduser, "Electric-hydrostatic drive—an innovative energy-saving power and motion control system," *Proceedings of the Institution of Mechanical Engineers, Part I: Journal of Systems and Control Engineering*, vol. 213, no. 5, pp. 427–437, 1999.

[41] H. C. Pedersen, L. Schmidt, T. O. Andersen, and M. H. Brask, "Investigation of New Servo Drive Concept Utilizing Two Fixed Displacement Units," *JFPS International Journal of Fluid Power System*, vol. 8, no. 1, pp. 1–9, 2014.

[42] T. Minav, C. Bonato, P. Sainio, and M. Pietola, "Direct Driven Hydraulic Drive," in *The 9th International Fluid Power Conference*, 2014.

[43] T. Wiens and D. Bitner, "An Efficient, High Performance And Low-Cost Energy Recovering Hydrostatic Linear Actuator Concept," in *ASME/BATH 2016 Symposium on Fluid Power and Motion Control*, 2016, pp. 1–10.

[44] VOITH, "Servo Drive CLDP - Technical Data Sheet." [Online]. Available: https://goo.gl/mAHm4X

[45] S. Michel and J. Weber, "Prediction of the thermo-energetic behaviour of an electrohydraulic compact drive," in *10th International Fluid Power Conference*, 2016, pp. 219–234.

[46] H. Çalışkan, T. Balkan, and B. E. Platin, "A Complete Analysis and a Novel Solution for Instability in Pump Controlled Asymmetric Actuators," *Journal of Dynamic Systems, Measurement, and Control*, vol. 137, no. 9, pp. 1–14, 2015.

[47] T. I. Hwang, "Hydraulic circuit with load holding valves operated by external pilot pressure , Patent EP 2071195 A2," 2009.

[48] C. Williamson and M. Ivantysynova, "The Effect of Pump Efficiency on Displacement-Controlled Actuator Systems," in *The Tenth Scandinavian International Conference on Fluid Power*, 2007, pp. 301–326.

Paper C

A Self-Contained Electro-Hydraulic Cylinder with Passive Load-Holding Capability

Damiano Padovani, Søren Ketelsen, Daniel Hagen, and Lasse Scmhidt

A Self-Contained Electro-Hydraulic Cylinder with Passive Load-Holding Capability

Damiano Padovani [1],*, Søren Ketelsen [2], Daniel Hagen [1] and Lasse Schmidt [2]

[1]   Department of Engineering Sciences, University of Agder, 4879 Grimstad, Norway; daniel.hagen@uia.no
[2]   Department of Energy Technology, Aalborg University, 9220 Aalborg East, Denmark; sok@et.aau.dk (S.K.); lsc@et.aau.dk (L.S.)
*   Correspondence: damiano.padovani@uia.no; Tel.: +47-37233020

Abstract: Self-contained electro-hydraulic cylinders have the potential to replace both conventional hydraulic systems and the electro-mechanical counterparts enhancing energy efficiency, plug-and-play installation, and reduced maintenance. Current commercial solutions of this technology are limited and typically tailor-made, whereas the research emphasis is primarily on cost efficiency and power applications below five [kW]. Therefore, there is the need of developing more flexible systems adaptable to multiple applications. This research paper offers a contribution in this regard. It presents an electro-hydraulic self-contained single-rod cylinder with passive load-holding capability, sealed tank, capable of recovering energy, and scalable up to about eighty [kW]. The system implementation on a single-boom crane confirms its feasibility: The position tracking error remains well within ± 2 [mm], oscillations are limited, and the overall energy efficiency is about 60 [%] during actuation. Concerning the passive load-holding devices, it is shown that both vented and non-vented pilot-operated check valves achieve the desired functioning and can hold the actuator position without consuming energy. Additional observations about the size and the arrangement of the load-holding valves are also provided. In conclusion, this paper demonstrates that the proposed self-contained cylinder can be successfully extended to several practical applications, especially to those characterized by overrunning external loads and the need of securing the actuator position.

Keywords: Self-contained cylinders; electro-hydraulic systems; load-holding valves; modeling

1. Introduction

Linear actuators capable of delivering high forces to perform heavy-duty operations are commonplace in many fields of industry. Lifters, earth-moving or construction machines, manufacturing processes, and oil drilling applications are a few examples. Since energy efficiency, plug-and-play installation, and reduced maintenance are becoming crucial characteristics in these areas, there is an ongoing tendency to replace standard valve-controlled hydraulic cylinders with the electro-mechanical counterparts (e.g., roller-screw actuators directly driven by electric motors [1]). Nevertheless, these electro-mechanical solutions are unsuitable in several applications such as offshore oil drilling [2], mainly due to the limited reliability (i.e., unexpected impact forces and overloads damage the screw). An alternative approach makes use of self-contained electro-hydraulic cylinders (SCCs). They are, according to the definition used in this paper, self-sufficient linear hydraulic actuators controlled by a local hydraulic unit that is driven by a dedicated electric motor. A sealed tank is essential and additional components such as flow balancing valves and load-holding valves might be required. Figure 1 provides a simplified example of a SCC, even though multiple system architectures are conceivable. More in general, this approach intends to:

- Ensure high energy efficiency (i.e., suitable hydraulic layouts are chosen),

- Achieve compactness (i.e., the built-in components are arranged ad hoc),
- Allow plug-and-play commissioning (i.e., the system only requires a wired connection to the electrical power source),
- Enhance flexible installation (i.e., a centralized hydraulic power supply is not required anymore, long hydraulic transmission lines are removed, and the closed-circuit layout characterized by a sealed reservoir can be tilted without leaking out fluid).

Countless applications will benefit from such a drive solution. A few examples are cranes, presses, gripper arms for offshore pipe handling, marine jack plates, trailer lifts, scissors tables, positioning systems for solar panels, and Stewart platforms.
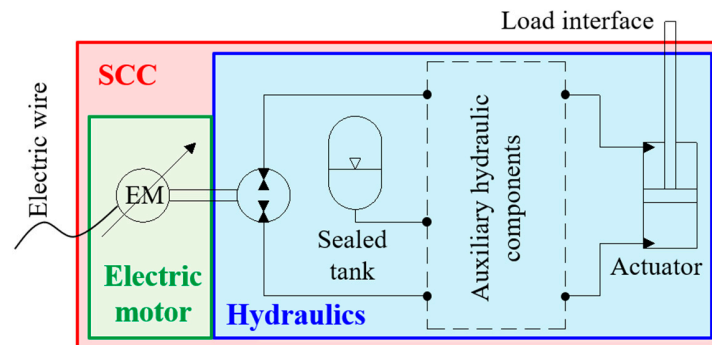
Figure 1. Simplified illustration of a self-contained electro-hydraulic cylinder.

In regard to what has been done so far, a limited number of commercial SCCs were introduced to the market, mainly using single-rod cylinders [3]; those are typically tailor-made solutions restricted to some niche applications because exceptional design effort is needed. It is the authors' opinion that this circumscribed use of SCCs is mainly due to the lack of consistent investigations aimed at identifying cost-effective system architectures adaptable to multiple applications.

Concerning the research activities connected to SCCs, emphasis is primarily on cost efficiency [4], thermal behavior [5], and low power applications below 5 [kW] [6,7]. Employing valve-less architectures to control the hydraulic actuators is commonplace since higher energy efficiency is achieved. Scenarios involving passive load-holding capability (i.e., maintaining the piston position without delivering any power) are seldom addressed, as shown in the next section. There is, therefore, the need of developing a SCC adaptable to the changing requirements of multiple applications and sustainable as a valid alternative to electro-mechanical systems.

This research paper presents a system architecture for an electro-hydraulic self-contained single-rod cylinder in closed-circuit configuration with passive load-holding capability, sealed tank, capable of recovering energy, and suitable for power levels above 5 [kW] representative of many hydraulic machines. Effort is dedicated to motivating the introduction of such a system, to experimentally confirm that the desired performance is achieved in terms of both actuator's position tracking and energy efficiency, and to better understanding the load load-holding capability (insight on the design of the load-holding valves and on their settings is given as well as on their arrangement in the hydraulic layout). This work significantly extends a previous conference publication [8] where a numerical analysis of a SCC that meets the aforementioned requirements is proposed. Specifically, this paper makes the following novel contributions: An improved system architecture, the implementation of the SCC on a test-bed, the experimental validation of the proposed dynamic model, the analysis of the system performance, and noteworthy considerations about the load-holding valves not traced in the technical literature.

2. Literature Survey

Due to the limited literature on SCCs, this survey also covers generic valve-less systems that might be converted into self-contained solutions. The main reason for focusing on valve-less layouts is

their potential for high energy efficiency (i.e., throttle-related losses in control valves are removed and energy recovery can be easily implemented). In fact, conventional valve-controlled systems waste a considerable percentage of the input energy in control valves (e.g., about 35 [%] in working cycles of load-sensing excavators [9]). Previous investigations about throttle-less concepts showed fuel savings up to 40 [%] in comparison to standard hydraulics [10].

Relevant valve-less systems that drive linear actuators can be classified depending on the following closed-circuit layouts:

1. Variable-displacement hydraulic unit and fixed-speed prime mover. The actuator motion is controlled by varying the displacement of the hydraulic pump/motor. This approach is prevalent among multi-actuator machines (e.g., compact excavators [10]) since a unique charge pump supplies the displacement adjustment system of each unit. The prime mover can be either a combustion engine or an electric motor.
2. Fixed-displacement hydraulic unit and variable-speed prime mover. Regulating both the angular speed and the direction of rotation of the prime mover's shaft controls the actuator motion [3,11–13]. The electric prime mover can be either a synchronous machine [11] or an asynchronous machine [14].
3. Variable-displacement hydraulic unit and variable-speed prime mover. Both the electric prime mover and the hydraulic unit actively control the actuator motion [15].

Narrowing the search field to case #2, this approach minimizes the number of control elements when compared to case #3 (i.e., a much cheaper fixed-displacement hydraulic unit is selected) and simplifies the hydraulics if related to case #1 (i.e., the pressure source dedicated to adjusting the unit displacement is not needed).

Moreover, a competing valve-less solution that does not fall under any of these three categories is gaining ground. It is based on multiple fixed-displacement pumps/motors driven by a common variable-speed prime mover. Alternatives with two hydraulic units [6,16–18] or with three hydraulic units [19–21] exist.

Regarding the hydraulic actuator, double-rod cylinders are almost exclusively used in the aerospace industry [22–26]. When compared to the single-rod design, the double-rod configuration increases the installation space and delivers a reduced output force for a given pressure. Thus, single-rod cylinders are the most popular solution for at least 80% of the electro-hydraulic drives [27]. Balancing the differential flow dictated by the unequal piston areas is, therefore, essential to implement a closed-circuit architecture. Various flow compensation methods were investigated in the past, mainly involving pilot-operated check valves [28], shuttle valves [13], or electrically-operated on/off valves [29]. Some issues related to instability and uncontrolled pressure oscillations were mentioned for shuttle valves [13] and for pilot-operated check valves [30], respectively. However, this is typically the case under high dynamic excitations of the system [3] (i.e., operating conditions that might be representative of some low-power applications). Other flow compensation alternatives were explored such as hydraulic transformers, three-port asymmetric piston pumps, or multiple gear pumps. Table 1 provides a synthesis of these options.

Table 1. Methods for compensating the differential flow.

Methods	References
Hydraulic transformers	[31–33]
Pilot-operated check valves	[10,28,34–38]
Inverse shuttle valve	[3,39,40]
3-port asymmetric pump	[41–44]
Two cylinders in parallel	[45]
Multiple fixed-displacement pumps	[6,16–21,46]

Additionally, limited researches addressed passive load-holding capabilities for SCCs. This feature serves the purpose of maintaining a given actuator position without supplying any power to the system.

A first solution is a commercialized system [47,48] where pilot-operated check valves (POCVs) are installed between the pump and the actuator. The hydraulic connections are arranged in such a manner that each opening pilot line of the POCVs is sensing the pressure of the opposite pump side. A similar approach is also presented in Reference [49]. Then, an interesting method to control the opening pilot of POCVs is discussed in References [37,38] and in Reference [50], even though this technique is not intended for SCCs. Alternatively, passive load-holding systems grounded on counterbalance valves were studied in Reference [12] and References [51,52], but they cannot recover energy.

Table 2 summarizes the system architectures for the SCCs addressed in this survey. Details about the presence of the passive load-holding capability (P_{LH}) are listed, as well as the possibility of performing four quadrant operations (4Q) that refer to piston extension and to piston retraction with both resistant and overrunning external loads acting on the actuator.

Table 2. Self-contained cylinders: concepts and characteristics.

Architectures	4Q	P_{LH}	References
Multiple fixed-displacement pumps	No	No	[27]
Multiple fixed-displacement pumps	Yes	No	[11,20,21]
Inverse shuttle valves	Yes	No	[3,5,6,13,53]
Compact system	Yes [1]	Yes	[12,51]
Electro-hydraulic actuator	No	Yes	[47–49]

[1] No energy recovery.

In conclusion, the idea behind electro-hydraulic self-contained cylinders is to combine the advantages of standard hydraulic actuators (i.e., reliability and high power-to-weight ratio) with the benefits of electro-mechanical drives (i.e., energy efficiency, minimal maintenance, and simple plug-and-play commissioning). Extra requirements such as compactness, robustness, and reduced costs are also of interest due to their relevance in both industrial and mobile applications [3,17].

3. The System under Investigation

According to the literature review, the requirements for SCCs listed in the introduction are not met by previously published solutions (several systems only represent a partial fit according to Table 2). Hence, some of these features were combined accordingly to create the proposed SCC.

3.1. System Architecture

Figure 2 depicts the self-contained cylinder discussed in this investigation. The system operates in four quadrants, includes passive load-holding devices, can recover energy, has a sealed reservoir, and is suitable for power levels up to at least 80 [kW].
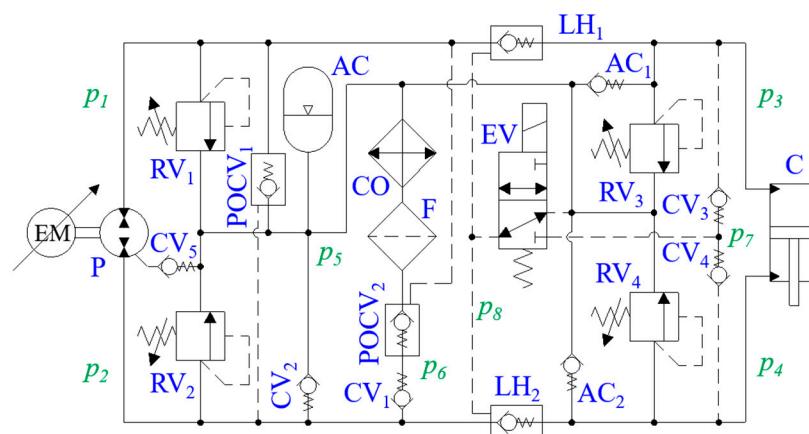

Figure 2. System architecture of the investigated self-contained cylinder.

The combination of an electric servo-motor (EM) and of a fixed-displacement hydraulic unit (P) drives the single-rod double-acting cylinder (C) arranged in a closed-circuit configuration. The differential flow dictated by the piston's unequal areas is balanced by two pilot-operated check valves (POCV$_{1\rightarrow2}$) and by two check valves (CV$_{1\rightarrow2}$). The low-pressure accumulator (AC) represents the sealed reservoir of the SCC. The pilot-operated check valves LH$_1$ and LH$_2$ (i.e., the load-holding valves) create the passive load-holding capability by isolating the actuator when the 3/2 electro-valve (EV) is de-energized. Conversely, energizing the EV results in transferring the highest actuator pressure into the opening pilot line of the two load-holding valves (the check valves CV$_{3\rightarrow4}$ select the dominant value among the pressures in the cylinder chambers); this enables the actuator motion. As can be seen, the EV is repositioned by the spring force in case of power failure, securing the load-holding function. Pressure-relief valves (RV$_{1\rightarrow4}$) are installed on both pump ports and on both actuator ports to avoid over-pressurizations during actuation and throughout passive load-holding. Anti-cavitation valves (AC$_{1\rightarrow2}$) are also connected to the actuator chambers. A cooler (CO) and a filter (F) are comprised in the system. The cooler can be easily removed if it is not necessary.

Figure 3 takes advantage of a simplified system representation to outline the operating condition in each quadrant when the passive load-holding capability is deactivated (i.e., EV is energized). Flow directions and pressure levels are emphasized: The red color denotes the high-pressure side, the blue color designates the low-pressure side, Q_p is the cylinder flow on the bore-side, Q_r is the cylinder flow on the rod-side, and $Q_d = Q_p - Q_r$ represents the differential flow. For a given speed of the servo-motor, the actuator velocity is higher in the left half-plane because the pump/motor flow is going to (or is coming from) the actuator's rod-side chamber that has a smaller piston area than the bore-side. More importantly, it should be noted that this system architecture fits particularly well with applications characterized by frequent overrunning loads acting on the actuator (e.g., cranes); the differential flow is, in fact, forced to go through both the filter and the cooler during operations in the IV quadrant, ensuring proper fluid conditioning.
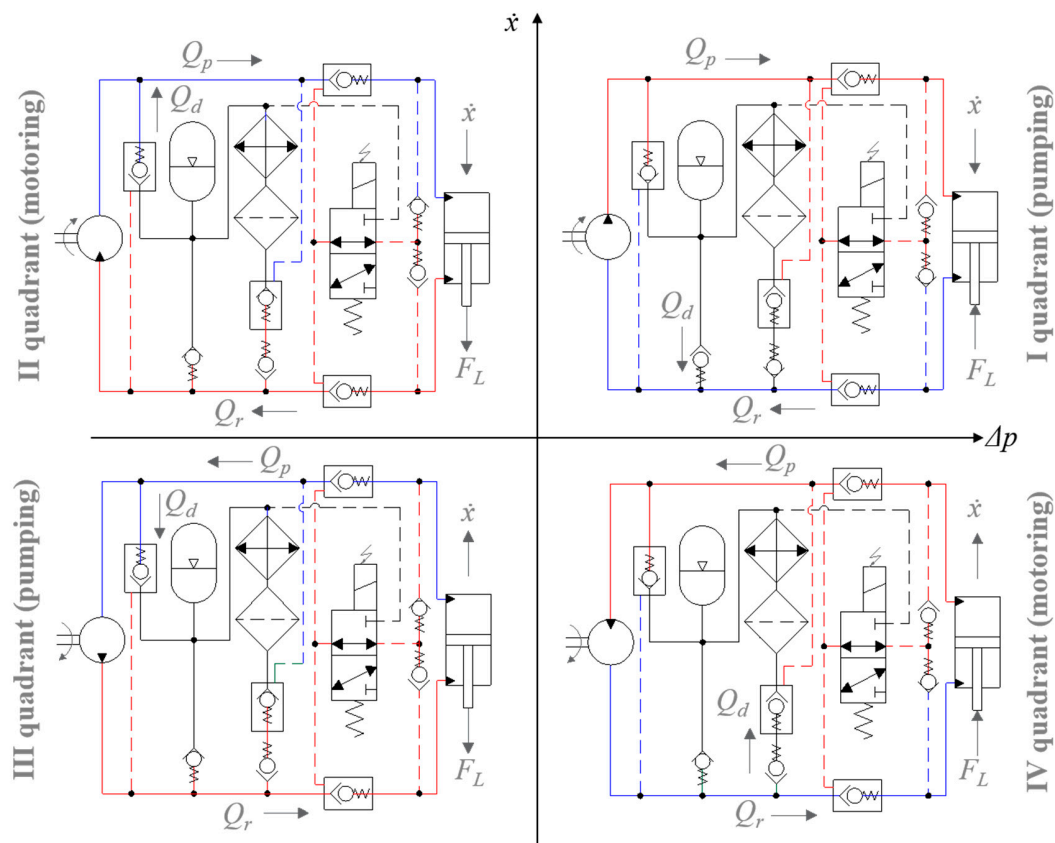

Figure 3. Simplified illustration of the system functioning in four quadrants ($\Delta p = p_1 - p_2$).

3.2. Control Algorithm

The control algorithm designed for this SCC generates a reference speed for the electric servo-motor in order to track the commanded position of the linear actuator. The control logic emerges from the block diagram proposed in Figure 4. A feedforward controller (FF) estimates the required servo-motor speed (u_{FF}) via (1), depending on the operating condition (there are different formulations for each quadrant). The actuator's bore-side area (A_p), the rod-side area (A_r), the pump/motor displacement (D), and a constant volumetric efficiency (e.g., $\eta_v = 0.95$ in motoring mode and $\eta_v = 1$ in pumping mode) are recalled.

$$
u_{FF} = \begin{cases}
\frac{\dot{x}_{Set} \cdot A_p}{D \cdot \eta_v} & \text{if } \dot{x} \geq 0 \text{ \& } \Delta p \geq 0 \quad \text{(i.e., I quadrant)} \\
\frac{\dot{x}_{Set} \cdot A_r \cdot \eta_v}{D} & \text{if } \dot{x} \geq 0 \text{ \& } \Delta p < 0 \quad \text{(i.e., II quadrant)} \\
\frac{\dot{x}_{Set} \cdot A_r}{D \cdot \eta_v} & \text{if } \dot{x} < 0 \text{ \& } \Delta p < 0 \quad \text{(i.e., III quadrant)} \\
\frac{\dot{x}_{Set} \cdot A_p \cdot \eta_v}{D} & \text{if } \dot{x} < 0 \text{ \& } \Delta p \geq 0 \quad \text{(i.e., IV quadrant)}
\end{cases} \tag{1}
$$

The proportional-integral controller (PI) in the position feedback loop corrects the prediction of the feedforward term by manipulating the position error (e_x). The proportional gain $k_P = 90$ [rev/(min·mm)] and the integral gain $k_I = 300$ [rev/(min·mm·s)] generate the corresponding feedback command (u_{FB}).
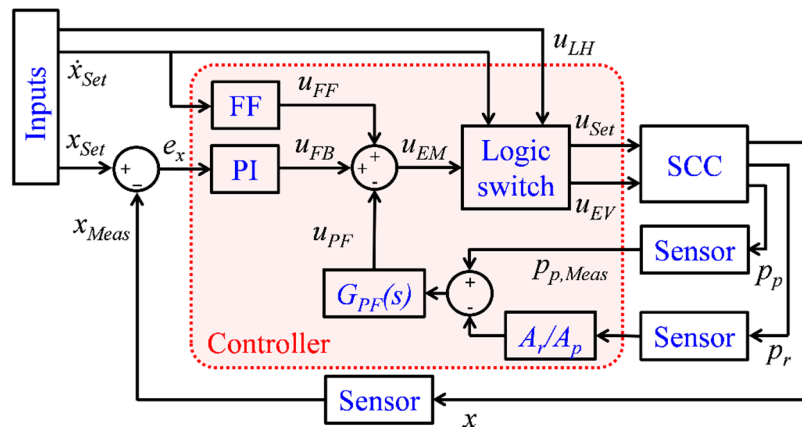
Figure 4. Block diagram of the control algorithm.

Additionally, a negative pressure feedback term (u_{PF}) adds damping to the system by canceling out pressure oscillations. This is done by filtering the measured actuator pressures using a first-order high-pass filter (2). Its cut-off frequency is $\omega_{PF} = 3$ [rad/s], whereas the small filter gain $k_{PF} = 5 \times 10^{-5}$ [rev/min/Pa] is due to the input being [Pa].

$$
G_{PF}(s) = k_{PF} \cdot \frac{s}{s + \omega_{PF}} \tag{2}
$$

The resulting speed command for the servo-motor (u_{EM}) is then sent through the logic switch and finally propagated to the SCC. The logic switch sets the commanded motor speed (u_{Set}) to zero when actuator motion is not desired (i.e., when $|\dot{x}_{Set}| < 0.005$ [mm/s]) otherwise it does not affect the signal. At the same time, the logic switch generates the command (u_{EV}) directed to the 3/2 electro-valve that engages, or disengages, the load-holding capability. If the load-holding enabler (u_{LH}) is active (this means passive load-holding is wanted), then the EV is energized when $\dot{x}_{Set}$ is non-zero or de-energized when $\dot{x}_{Set}$ is zero and the position error is smaller than two [mm]. If passive load-holding is not desired (i.e., u_{LH} is switched off), then the EV is energized independently of $\dot{x}_{Set}$.

4. Experimental Set-Up

An experimental test-bed was commissioned to drive a single-boom crane available at the University of Agder (Figure 5). This representative application was selected since it encompasses different operating conditions such as motion against both resistant external loads (i.e., I quadrant) and overrunning external loads (i.e., IV quadrant). It also offers the opportunity of testing the passive load-holding capability. Furthermore, this crane challenges the performance of the SCC because the mechanical structure was specifically designed to enhance oscillations (originally, the crane was driven by a valve-controlled system [54]). More details about the crane are available in Appendix A.

Regarding the SCC, the selected servo-motor is a PMSM Bosch Rexroth MSK071E-0300 with a dedicated driver IndraDrive HCS02. The axial-piston swashplate unit A10F has a displacement of 10.6 [cm^3/rev]. The cylinder PMC 25CA has piston diameter of 65 [mm], rod diameter of 35 [mm], and stroke of 500 [mm]. The load-holding valves (Sun Hydraulics CVEVXFN) have area ratio 3:1 and cracking pressure of seven [bar], whereas the other POCVs (Sun Hydraulics CKEBXCN) have the same area ratio, but cracking pressure of two [bar]. The opening pilot for the load-holding valves is selected by means of check valves Hawe Hydraulics RB2 with cracking pressure of 0.1 [bar] and of a 3/2 directional control valve Argo Hytos SD1E. The additional check valves Hawe Hydraulic RK4 still have cracking pressure of 0.1 [bar], whereas the pressure-relief valves Sun Hydraulics RDDA have cracking pressure of 200 [bar]. A tailor-made manifold houses these valves. A Bosch Rexroth cooler KOL3N (cooling power up to 3 [kW]) and a filter 50LEN0100 are used to condition the oil ISO VG 46.
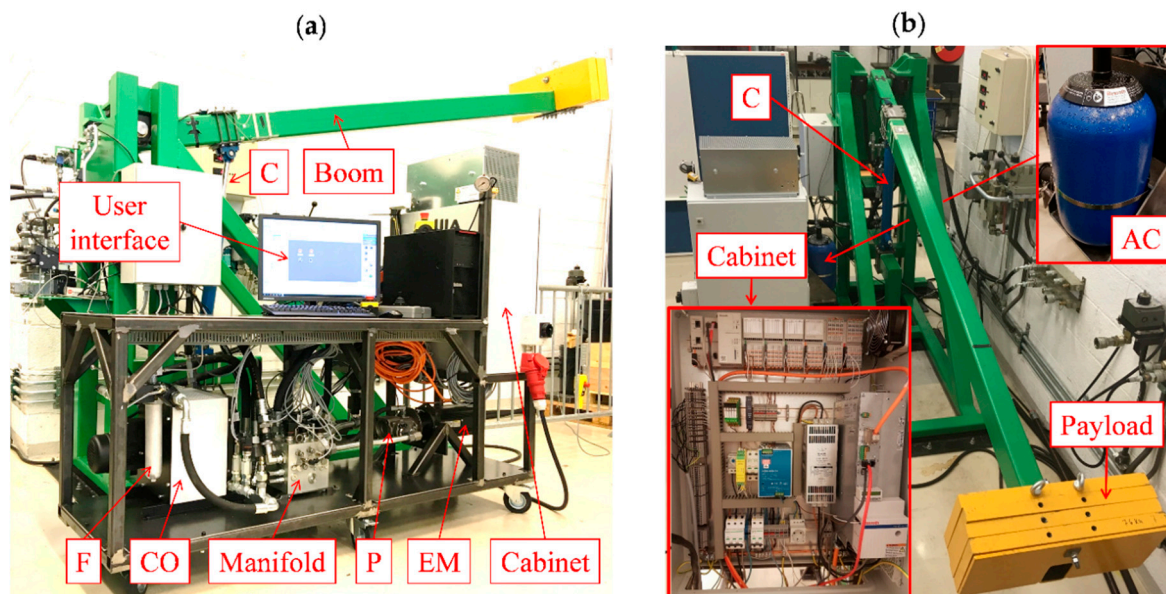
Figure 5. (**a**) Overview of the experimental test-bed; and (**b**) detailed view of the single-boom crane and of the electric cabinet dedicated to the servo-motor.

In terms of sensors, the servo-motor comes standard with an encoder. A position sensor Regal PS6310 monitors the actuator's piston position. Transducers Bosch Rexroth HM20 measure the pressures $p_{1\to5}$. Finally, MATLAB-Simulink®is used for control and data acquisition. The software IndraWorks translates the control algorithm into machine code that runs at a frequency of 1000 [Hz] on the PLC IndraControl XM22.

5. System Modeling and Validation

Multiple dynamic models of the SCC were created and simulated in MATLAB-Simulink®.

5.1. The Dynamic Modeling of the System

The electric servo-motor was modeled using a second-order transfer function (3) from commanded to simulate shaft speed where the natural frequency and the damping ratio are $\omega_n = 5$ [Hz] and $\zeta = 0.99$, respectively.

$$G_{EM}(s) = \frac{\omega_n^2}{s^2 + 2 \cdot \omega_n \cdot \zeta \cdot s + \omega_n^2} \tag{3}$$

The hydraulics was simulated by means of a consolidated approach. The effective fluid's bulk modulus (β_i) in the *i*-th hydraulic capacitance was modeled via Equation (4).

$$\beta_i = \frac{1}{\frac{1}{\beta_O} + \varepsilon_{A,i} \cdot \left(\frac{1}{\beta_{A,i}} - \frac{1}{\beta_O} \right)} \tag{4}$$

The different terms are the oil's bulk modulus ($\beta_O = 7500$ [bar]), the air's bulk modulus ($\beta_{A,i}$) calculated as $\beta_{A,i} = \gamma \cdot p_i$ with γ being the adiabatic air constant and p_i the pressure in the capacitance, and the volumetric air content ($\varepsilon_{A,i}$), which is obtained according to Equation (5). This equation recalls the atmospheric pressure (p_{atm}) and the volumetric air content of the oil at atmospheric pressure ($\varepsilon_{A,0} = 0.015$ [%]).

$$\varepsilon_{A,i} = \frac{1}{\frac{1 - \varepsilon_{A,0}}{\varepsilon_{A,0}} \cdot \left(\frac{p_{atm}}{p_i} \right)^{-\frac{1}{\gamma}} + 1} \tag{5}$$

The well-known pressure build-up equation was applied several times to evaluate the pressures $p_{1 \to 8}$ labeled in Figure 2. The resulting expressions are reported in Equations (6)–(13) where the effective bulk modulus (β_i), the appropriate flow rates (Q_i), and the suitable volumes of the hydraulic capacitances (V_i) are considered accordingly.

$$\dot{p}_1 = \frac{\beta_1 \cdot (Q_{e,P} + Q_{POCV,1} - Q_{LH,1} - Q_{RV,1})}{V_{1,0}} \tag{6}$$

$$\dot{p}_2 = \frac{\beta_2 \cdot (-Q_{e,P} - Q_{CV,1} + Q_{CV,2} - Q_{LH,2} - Q_{RV,2})}{V_{2,0}} \tag{7}$$

$$\dot{p}_3 = \frac{\beta_3 \cdot (Q_{LH,1} - A_p \cdot \dot{x} - Q_{RV,3} + Q_{AC,1} - Q_{CV,3})}{V_{3,0} + A_p \cdot x} \tag{8}$$

$$\dot{p}_4 = \frac{\beta_4 \cdot (Q_{LH,2} + A_r \cdot \dot{x} - Q_{RV,4} + Q_{AC,2} - Q_{CV,4})}{V_{4,0} + A_r \cdot (x_{Max} - x)} \tag{9}$$

$$\dot{p}_5 = \frac{1}{C_{H,5}} \cdot \left(\sum_{i=1}^{4} Q_{RV,i} + Q_{EV} - Q_{POCV,1} - Q_{POCV,2} - Q_{AC,1} - Q_{AC,2} - Q_{CV,2} \right) \tag{10}$$

$$\dot{p}_6 = \frac{\beta_6 \cdot (Q_{CV,1} + Q_{POCV,2})}{V_{6,0}} \tag{11}$$

$$\dot{p}_7 = \frac{\beta_7 \cdot (Q_{CV,3} + Q_{CV,4} - Q_{EV})}{V_{7,0}} \tag{12}$$

$$\dot{p}_8 = \frac{\beta_8 \cdot Q_{EV}}{V_{8,0}} \tag{13}$$

The volumes of the transmission lines ($V_{i,0}$) are assumed constant whereas the equations related to the actuator require the piston areas, the piston position (x), and the cylinder stroke (x_{Max}). The capacitance $C_{H,5}$ used in the pressure build-up equation associated to the hydro-pneumatic accumulator is elucidated in Equation (14). Among other terms, it involves the effective accumulator gas volume ($V_{AC,0} = 9.2$ [L]) and the pre-charge pressure of the accumulator ($p_{AC,0} = 0.05$ [bar]).

$$C_{H,5} = \frac{V_{5,0}}{\beta_5} + \frac{V_{AC,0}}{\gamma} \cdot \frac{p_{AC,0}^{\frac{1}{\gamma}}}{p_5^{\frac{\gamma+1}{\gamma}}} \tag{14}$$

Concerning the flow rates, the contributions ascribed to the different components are clarified in the sequel. The flow rates through the POCVs ($Q_{POCV,i}$) are computed by means of the orifice Equation (15). It comprises the pressure differential across the valve (Δp_i), the discharge coefficient (C_d), the seat diameter (d_i), the poppet lift (y_i), and the fluid density (ρ).

$$Q_{POCV,i} = C_d \cdot \pi \cdot d_i \cdot y_i \cdot sign(\Delta p_i) \cdot \sqrt{\frac{2}{\rho} \cdot |\Delta p_i|} \tag{15}$$

If a POCV is not closed, two operating modes characterize its functioning. The "normal flow" condition takes place when the pilot stage is detached from the poppet. Conversely, the valve is subjected to "reverse flow" if the pilot stage and the poppet are in contact. In the case of a non-vented valve (Figure 6 depicts alternative designs), an opening pilot pressure lower than the inlet pressure is the prerequisite for "normal flow" (i.e., $p_x < p_{In}$). The poppet lift always results from the force equilibrium that is expressed differently and is contingent on "normal flow" (16) or "reverse flow" (17).

$$y_i = \frac{(p_{In,i} - p_{Out,i}) \cdot A_{S,i} - F_{S0,i}}{k_{S,i}} \tag{16}$$

$$y_i = \frac{(p_{x,i} - p_{In,i}) \cdot A_{x,i} + (p_{In,i} - p_{Out,i}) \cdot A_{S,i} - F_{S0,i}}{k_{S,i}} \tag{17}$$

The areas of the poppet seat ($A_{S,i}$) and of the pilot stage ($A_{x,i}$) are introduced in the previous equations as well as the spring stiffness ($k_{S,i}$) and the spring's pre-load force ($F_{S0,i}$). The poppet dynamics is simulated via a first-order transfer function with time constant $\tau = 0.05$ [s].
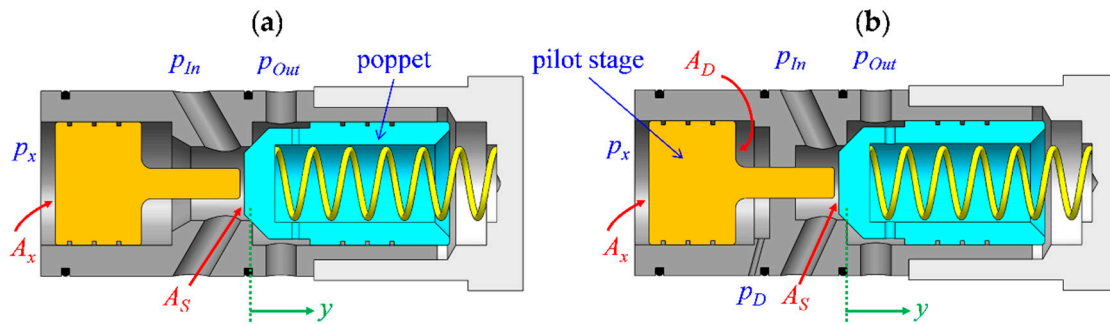
Figure 6. Cross-sectional views of pilot-operated check valves: (**a**) Non-vented design; (**b**) Vented design.

If a POCV comes in the vented version, the previous definition of the operating modes holds true, but the criterion for "normal flow" becomes $p_x \cdot A_x < p_D \cdot A_D + p_{In} \cdot (A_x - A_D)$. The force balance for the "normal flow" condition is still given by Equation (16), whereas it is described in Equation (18) for the other operating mode. The pilot stage's area inside the drain chamber ($A_{D,i}$) and the drain pressure ($p_{D,i}$) are included.

$$y_i = \frac{1}{k_{S,i}} \cdot [(p_{x,i} - p_{In,i}) \cdot A_{x,i} + (p_{In,i} - p_{Out,i}) \cdot A_{S,i} + (p_{In,i} - p_{D,i}) \cdot A_{D,i} - F_{S0,i}] \tag{18}$$

The orifice equation also provides the flow rate through the electro-valve (Q_{EV}). The only difference from the formulation given in Equation (15) is about the flow area that depends on the valve command. Then, the flow rate of both the CVs and the RVs is computed according to Equation (19).

The evoked parameters are the valve flow gain ($k_{v,i}$), the cracking pressure ($p_{c,i}$), the inlet pressure ($p_{In,i}$), and the outlet pressure ($p_{Out,i}$).

$$Q_i = \begin{cases} 0 & \text{if } p_{In,i} < p_{Out,i} + p_{c,i} \\ k_{v,i} \cdot (p_{In,i} - p_{Out,i} - p_{c,i}) & \text{if } p_{In,i} \geq p_{Out,i} + p_{c,i} \end{cases} \tag{19}$$

The effective magnitudes of the pump/motor are evaluated by means of flow losses ($Q_S \geq 0$) and torque losses ($T_S \geq 0$) derived from steady-state experimental data of a reference axial-piston unit with displacement equal to D_{Ref} [55]. The same losses are assumed for all quadrants and are scaled to the desired pump displacement (D) by using the scaling laws elucidated in Equation (20) that refer to the quantities of the reference unit denoted by the subscript "*Ref*". The scaling factor (λ), the unit's shaft speed (ω), and the losses of the reference unit are involved.

$$\lambda = \sqrt[3]{\frac{D}{D_{Ref}}} \quad \rightarrow \quad \begin{cases} \omega_{Ref} = \lambda \cdot \omega \\ Q_S = \lambda^2 \cdot Q_{S,Ref} \\ T_S = \lambda^3 \cdot T_{S,Ref} \end{cases} \tag{20}$$

The effective flow rate of the pump/motor ($Q_{e,P}$) is elucidated in Equation (21) for operations in the I quadrant and in the IV quadrant (the sign convention accounts for the functioning in pumping or in motoring mode). The flow losses are completely attributed to internal leakages.

$$Q_{e,P} = D \cdot \omega - Q_S \tag{21}$$

The computation of the pump/motor's effective shaft torque ($T_{e,P}$) expressed in Equation (22) requires the pressure differential across the unit (Δp).

$$T_{e,P} = \begin{cases} \dfrac{D \cdot \Delta p}{2 \cdot \pi} + T_S \text{(I quadrant)} \\ -\dfrac{D \cdot \Delta p}{2 \cdot \pi} + T_S \text{(IV quadrant)} \end{cases} \tag{22}$$

The pressure losses in the transmission lines and in the cooling/filtering unit are neglected mainly due to the compact configuration of the drive. Moreover, Equation (23) describes the actuator's force balance where the hydraulic force (F_H) and the friction force (F_F) are clarified in Equations (24) and (25), respectively.

$$F_H = F_F + G(x) + M(x) \cdot \ddot{x} \tag{23}$$

$$F_H = p_3 \cdot A_p - p_4 \cdot A_r \tag{24}$$

$$F_F = f_v \cdot \dot{x} + \tanh(\dot{x} \cdot a) \cdot \left(F_C + F_S \cdot e^{\frac{-\dot{x} \cdot \tanh(\dot{x} \cdot a)}{k_C}} \right) \tag{25}$$

The different terms represent the pressure in the bore-side chamber (p_3), the pressure in the rod-side chamber (p_4), the viscous friction coefficient ($f_v = 4 \times 10^3$ [kg/s]), the Coulomb force ($F_C = 75$ [N]), the static friction force ($F_S = 500$ [N]), the static friction force's constant ($k_C = 0.02$ [m/s]), the equivalent mass of the system $M(x)$, and the gravitational load $G(x)$ on the actuator. The friction in the joint of the crane is lumped into the friction of the linear actuator whereas the hyperbolic tangent is used to prevent numerical issues such as discontinuities (the dimensionless tuning parameter is set equal to a = 250). Figure 7 depicts the variation of both $G(x)$ and $M(x)$ as a function of the piston position (Appendix A); the Coriolis and the centripetal terms are neglected due to their minimal influence.

Regarding the overall system efficiency (η_{SCC}), the mechanical power at the load/actuator interface (P_C) and the servo-motor's electrical power (P_{EM}) are addressed. The latter term involves

the armature current (i_A) and the torque constant of the machine (k_T = 2.05 [N·m/A]). The ratio of the output energy over the input energy of the SCC is calculated via Equation (26).

$$\eta_{SCC} = \begin{cases} \frac{P_C}{P_{EM}} = \frac{(F_H - F_F) \cdot \dot{x}}{i_A \cdot k_T \cdot \omega} & \text{if} \quad P_{EM} \geq 0 \\ \frac{P_{EM}}{P_P} = \frac{i_A \cdot k_T \cdot \omega}{(F_H - F_F) \cdot \dot{x}} & \text{if} \quad P_{EM} < 0 \end{cases} \tag{26}$$

Diverse formulations are used if the electrical energy is supplied, or if the regenerative functioning is taking place (i.e., $P_{EM} < 0$).
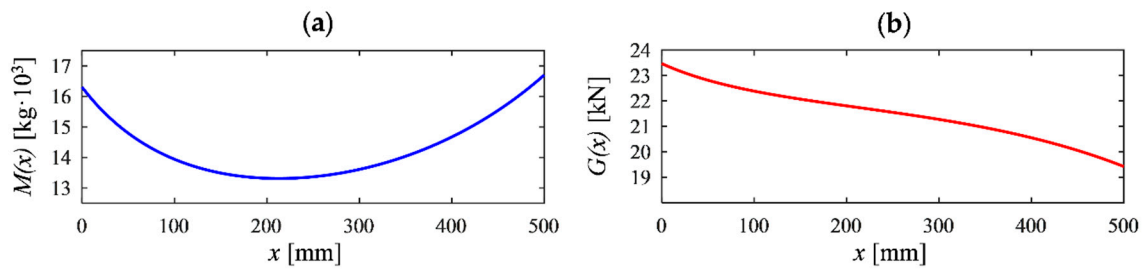
Figure 7. (**a**) Variation of the equivalent system's mass as function of the piston position; (**b**) and variation of the gravitational load acting on the actuator as function of the piston position.

5.2. Open-Loop Model Validation

The complete dynamic model of the SCC was validated against experimental data. The applied open-loop command (i.e., the desired speed for the electric motor) generates typical working conditions such as extension and retraction of the actuator. The results proposed in Figure 8 show good agreement among measured and simulated quantities, confirming the high-fidelity nature of the model. Consequently, it represents a meaningful tool for further analyses.
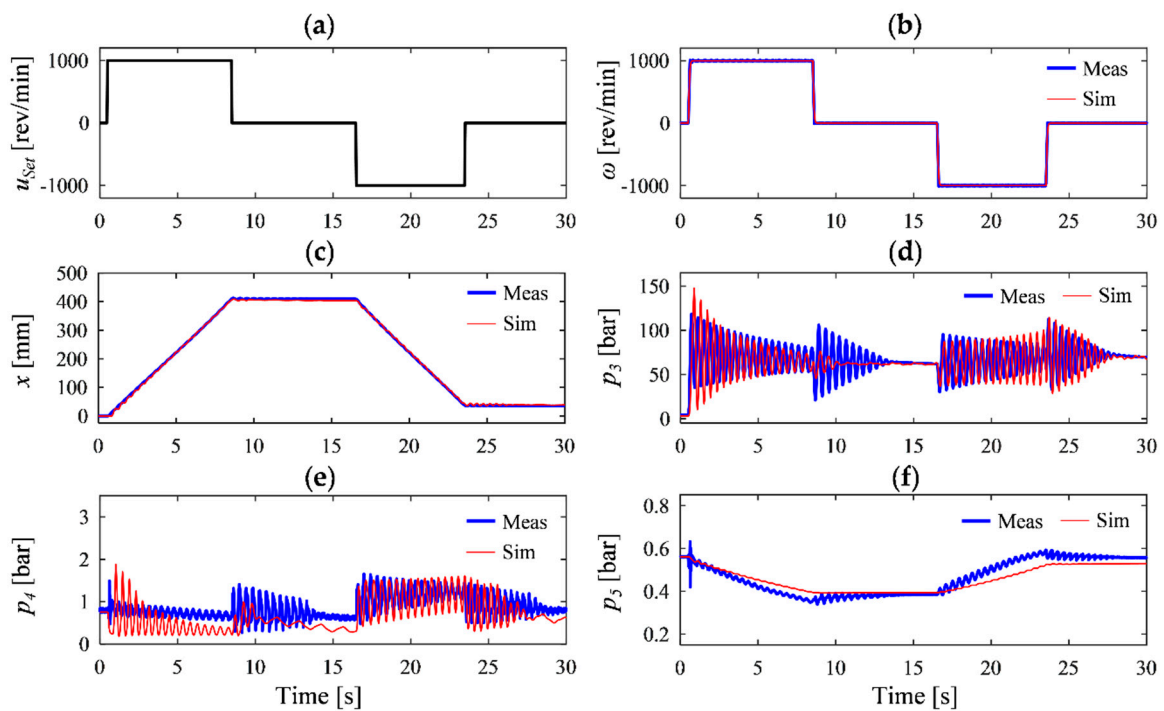
Figure 8. Experimental model validation: (**a**) Commanded motor speed; (**b**) motor speed; (**c**) piston position; (**d**) actuator's bore-side pressure; (**e**) actuator's rod-side pressure; and (**f**) accumulator pressure.

6. Closed-Loop System Performance

A representative working cycle with both active load-holding operations (A_{LH}) and passive load-holding operations (P_{LH}) serves the purpose of analyzing the system performance when the SCC is controlled in closed-loop according to the algorithm illustrated in Figure 4. The trend of the commanded position selected for this test implies a piston velocity equal to 150 [mm/s] during actuation, that represents the upper limit for the experimental set-up.

The agreement between the commanded and the measured actuator position presented in Figure 9 is satisfactory since the error falls well within ±2 [mm]. In fact, the expected accuracy for hydraulic cranes is typically worse as the maximum position error is frequently higher than 15 [mm] [56,57].
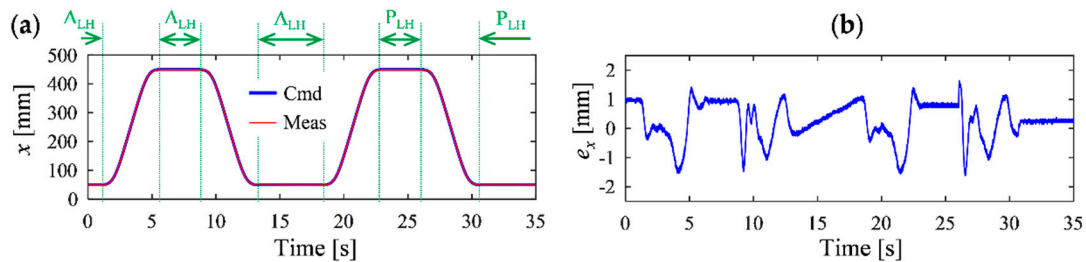
Figure 9. (**a**) Commanded and measured piston position; (**b**) Position error.

The servo-motor speed shown in Figure 10 (i.e., the control effort of this electro-hydraulic system) remains within the recommended limits of the machine (about ±3200 [rev/min]) and its variation is mostly smooth.
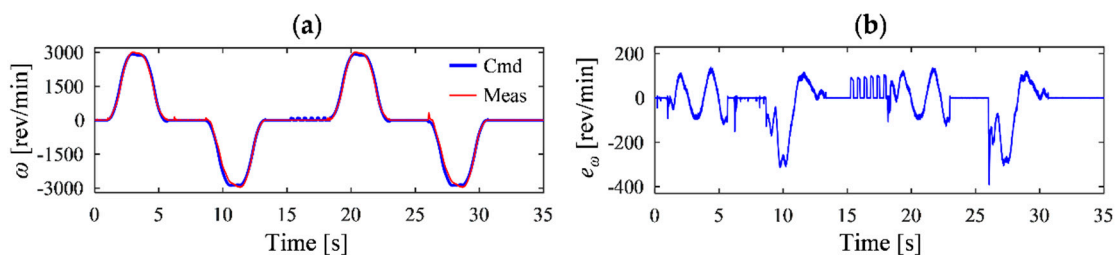
Figure 10. (**a**) Commanded and measured servo-motor speed; (**b**) Speed error.

The relevant system pressures are presented in Figure 11. They vary, as expected, showing stable behavior and smooth transitions between different operating conditions; this result is a key aspect because standard hydraulic cranes equipped with load-holding valves are usually characterized by a disturbing oscillatory behavior (this is also the case for the crane used in this investigation when powered by a conventional load-sensing system [54]). Regarding the pressures in the bore-side of the SCC, the difference between p_1 and p_3 during passive load-holding is due to the leakages across the pump/motor.
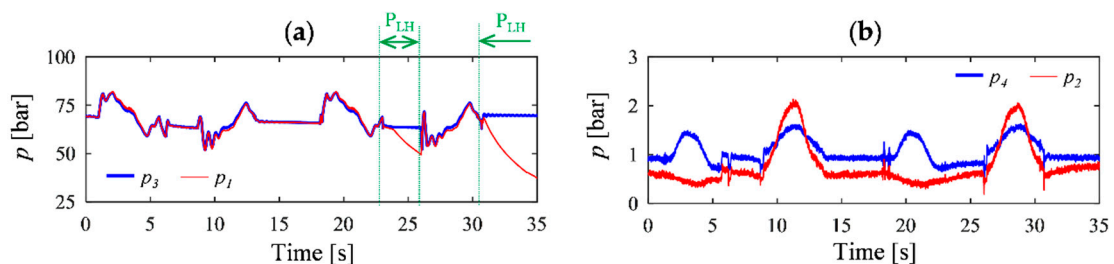
Figure 11. (**a**) Measured pressures in the bore-side of the system; and (**b**) measured pressures in the rod-side of the system.

Concerning the load-holding valves, Figure 12 highlights the poppet position and the command directed to the on/off electro-valve that supervises the load-holding devices (the passive load-holding function is activated when the signal is equal to zero).
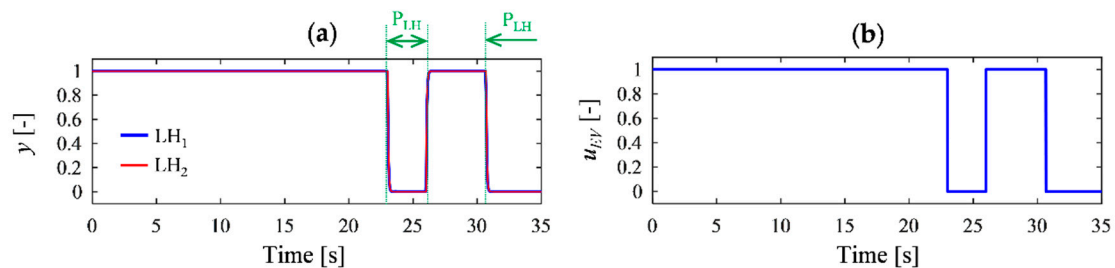

Figure 12. (**a**) Simulated poppet lift of the vented load-holding valves; (**b**) Electro-valve command.

These POCVs do not introduce any unpleasant oscillations during motion. Most importantly, they maintain the piston position when the servo-motor is not active (this is the case between about 23–27 seconds and 31–35 seconds).

Finally, the overall energy efficiency of the system is addressed in Figure 13. The average value during actuation runs in the neighborhood of 60 [%], with a slightly worse performance during regenerative functioning. This means the SCC can be considered efficient when compared to conventional valve-controlled circuits (e.g., [9]). Furthermore, the SCC is regenerating energy during piston retraction. This means the electric machine is outputting electrical energy that can be returned to the grid or can be stored in a dedicated device (in the case of the test-bed, the recovered electrical energy is dissipated by a resistor). The measured current (filtered signal) was used to calculate the electrical power, whereas a zero efficiency was arbitrarily assigned if $|P_{EM}| < 0.25$ [kW] to avoid numerical issues.
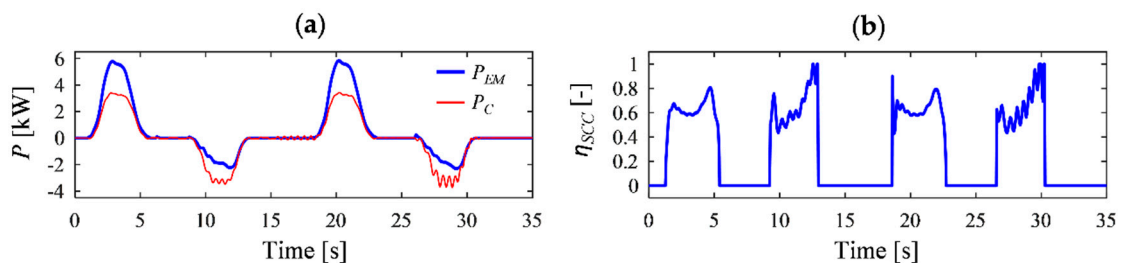
Figure 13. (**a**) Measured input power and simulated output power of the self-contained cylinder; (**b**) and simulated overall energy efficiency of the self-contained cylinder.

7. Discussion about the Load-Holding Valves

It is worth recalling that the load-holding valves represent a peculiarity of this SCC. Discussing, therefore, both their design and their arrangement is invaluable to gain deeper insight.

7.1. Design of the Pilot-Operated Check Valves

The experimental results were obtained by utilizing vented load-holding POCVs. This is the most conservative approach since the total effort required to open the poppet in a given operating condition is reduced, if compared to non-vented valves. Thus, this sub-section is about understanding how the valve design (i.e., vented or non-vented valve configuration) affects the overall system response (Figure 14).

The outcomes displayed in Figure 14 were derived by simulating non-vented load-holding POCVs where diverse values of the area ratio and of the seat diameter were considered, specifically: the "original" settings of the experimental set-up (i.e., area ratio 3:1 and seat diameter 5 [mm]), a first

alternative with area ratio increased to 7:1 and seat diameter 5 [mm], and another solution with area ratio 3:1 and seat diameter raised to 9 [mm].
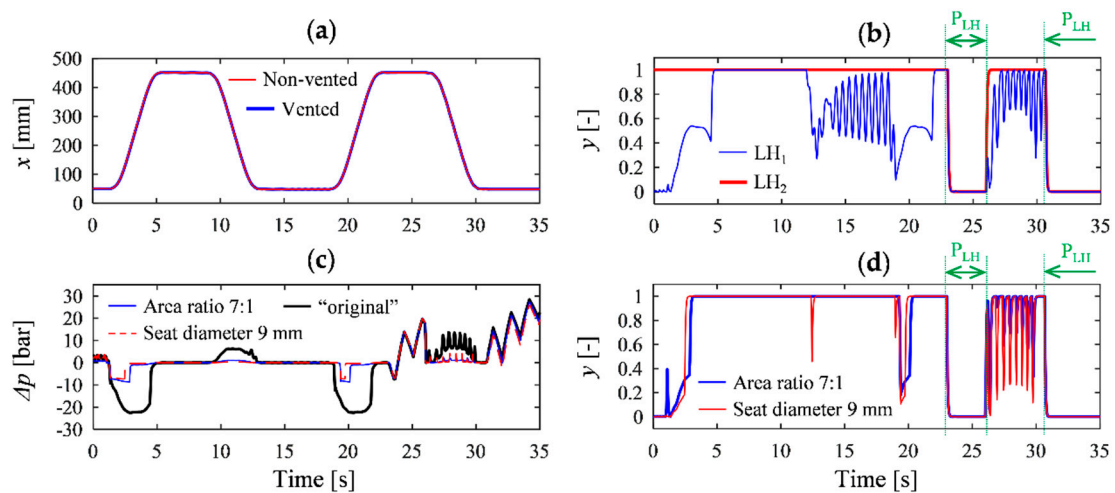

Figure 14. (**a**) Simulated piston position with vented and non-vented load-holding valves (area ratio 3:1 and seat diameter 5 [mm]); (**b**) simulated poppet lift using non-vented load-holding valves (area ratio 3:1 and seat diameter 5 [mm]); (**c**) simulated pressure drop across LH_1 using non-vented POCVs; and (**d**) simulated poppet lift of LH_1 using non-vented POCVs with modified settings.

Choosing the vented design is not strictly necessary, even though it is advisable. The piston position is, in fact, indistinguishable if non-vented POCVs are preferred to the vented counterparts (plot a) in Figure 14). Nevertheless, the poppet of the non-vented valve LH_1, located on the bore-side of the actuator, is not completely lifted from its seat when the hydraulic cylinder is actuated (plot b) in Figure 14); this aspect does not affect the position tracking, but results in an increased pressure drop across the valve that turns out in a higher energy consumption. This drawback related to energy efficiency is mitigated if non-vented load-holding valves with enlarged nominal flow (i.e., bigger seat diameter) and/or increased pilot ratio are introduced (plot c) in Figure 14). Using these modified settings, the actuator's position tracking is still equivalent to the reference scenario established by vented POCVs and the oscillations of the poppet diminish (plot d) in Figure 14).

7.2. Arrangement of the Pilot-Operated Check Valves

The other aspect that deserves further debate is the arrangement of the load-holding valves. The proposed SCC takes their opening pilot pressures from the actuator chambers, when the EV is energized. This approach is in contrast with some references that mention POCVs utilized as load-holding devices: In fact, the opening pilot pressures in these systems are taken from the pump/motor ports according to the diagram given in Figure 15.

The dynamic model of the SCC was adapted congruently to reflect the alteration in the configuration of the load-holding POCVs' pilot lines and to remove the sub-system dedicated to the selection of their pilot pressure (i.e., the EV and $CV_{3\rightarrow4}$). After simulating this transformed hydraulic architecture, it is therefore relevant to stress that such an approach leads to an unwanted system functioning when overrunning loads are acting on the actuator (Figure 16).

When the actuator load becomes overrunning between about 9.5–14 seconds and 27–31.5 seconds, then the load-holding valves do not stay open as desired (plot d) in Figure 16). This causes an oscillatory behavior that undermines both the position tracking (plot a) in Figure 16) and the operational safety. Enormous pressure fluctuations (plot c) in Figure 16) arise up to the maximum admitted value (a pressure-relief valve located on the bore-side is regulating, namely this solution is also characterized by inefficient functioning). Then, the control input (i.e., the commanded speed of the electric servo-motor) varies abruptly trying to match the commanded actuator position.
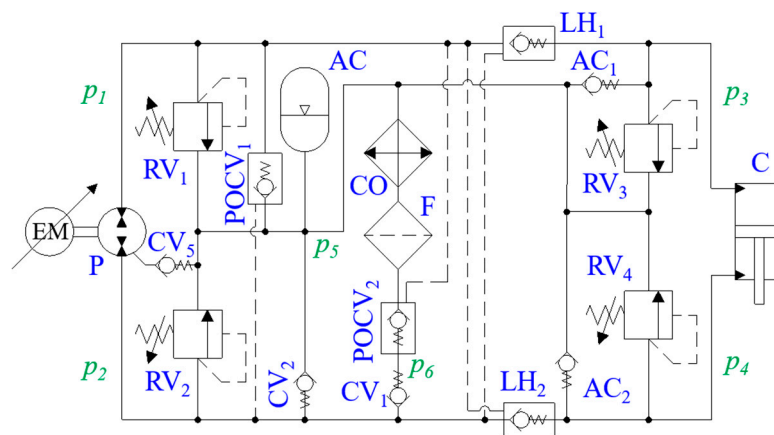
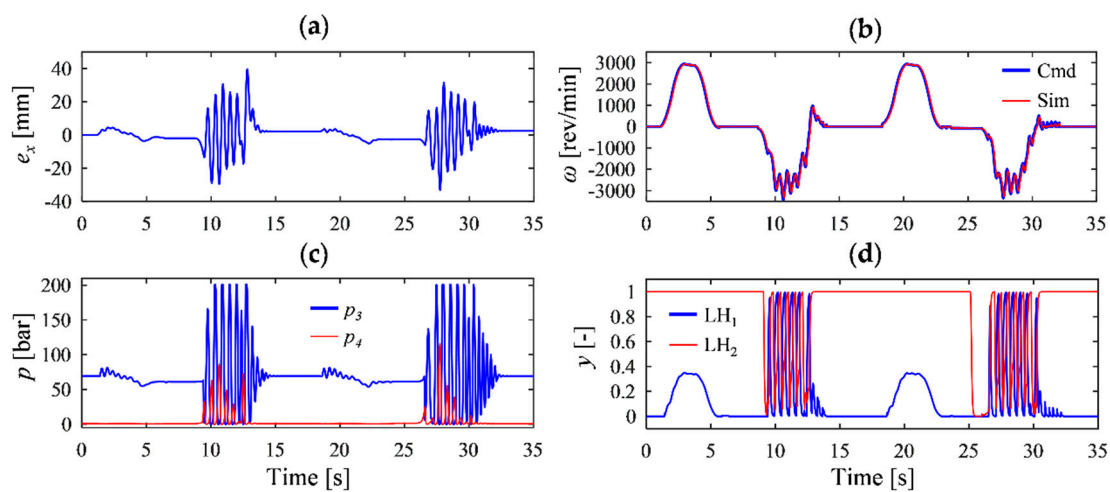**Figure 15.** Alternative system with the load-holding valves arranged according to References [47–49].

Figure 16. Simulation of the system depicted in Figure 15: (**a**) Actuator's position error; (**b**) speed of the servo-motor; (**c**) Pressures in the actuator chambers; and (**d**) poppet lift of the load-holding valves.

A similar undesirable system behavior takes place if the pilot ratio of the load-holding valves is increased (e.g., from 3:1 up to 7:1), meaning that this modified layout does not properly manage overrunning loads. Additionally, vented load-holding valves were assumed, even though non-vented components lead to equivalent results not reported for the sake of brevity.

8. Conclusions

An in-depth literature survey emphasized the need for self-contained cylinders that operate in four quadrants, include passive load-holding devices, and can deal with power levels above 5 [kW]. Consequently, this research paper gives a contribution to bridge this gap as follows:

1. A novel system architecture (i.e., a solution not found in literature) of an electro-hydraulic self-contained cylinder was presented and implemented on a test-bed.
2. Experimental evidence proves the expected system functioning; the maximum position error ranges well within ± 2 [mm] and the passive load-holding capability maintains the actuator position when needed.
3. A dynamic model of the system was developed and experimentally validated; it provides a sizing and simulation tool for future implementations.
4. Insight about key parameters was given; the overall system efficiency results highly satisfactory being about 60 [%] during actuation.

5. It was shown that both vented and non-vented load-holding valves achieve the desired system functioning; however, choosing the vented design is advisable.
6. The drastic limitations caused by an alternative arrangement of the load-holding pilot-operated check valves traced in the technical literature were highlighted.

For these reasons, the proposed self-contained system can be successfully extended to several practical applications. Those including overrunning external loads and the need of securing the actuator position represent the natural field of application (e.g., cranes, presses, gripper arms for offshore pipe handling, marine jack plates, trailer lifts, scissors tables, positioning systems for solar panels, and Stewart platforms). Future work will cover the system implementation in real-world environments, the thermal analysis of this hydraulic architecture to minimize the cooler size, and considerations about the life estimation of key components. In particular, emphasis will be placed on scaling up the system to deal with higher power levels. It is expected to deliver up to about eighty [kW] by simply replacing some components with alternative off-the-shelf parts selected from the same catalogues used during the design of the experimental test-bed.

Conflicts of Interest: The authors declare no conflict of interest.

Nomenclature

Abbreviations

4Q	Four quadrant operations
A_{LH}	Active load-holding
AC	Anti-cavitation valve
C	Actuator (i.e., hydraulic cylinder)
CO	Cooler
CV	Check valve
EM	Electric servo-motor
EV	3/2 electro-valve
F	Filter
FF	Feedforward controller
LH	Load-holding valve
P_{LH}	Passive load-holding
POCV	Pilot-operated check valve
RV	Pressure-relief valve
SCC	Self-contained electro-hydraulic cylinder

Symbols

a	Tuning parameter for the friction force of the actuator and of the crane joint
A_D	Pilot stage's area inside the drain chamber of pilot-operated check valves
A_p	Cylinder area on the bore-side
A_r	Cylinder area on the rod-side
A_S	Poppet seat's area of pilot-operated check valves
A_x	Pilot stage's area of pilot-operated check valves
C_d	Discharge coefficient
C_H	Hydraulic capacitance
D	Pump/motor displacement
d	Seat diameter of pilot-operated check valves

D_{Ref}	Displacement of the reference unit used to derive the loss model of the pump/motor
e_x	Position error of the hydraulic actuator
F_C	Coulomb force of the actuator and of the crane joint
F_F	Friction force of the actuator and of the crane joint
F_H	Hydraulic force of the actuator
F_S	Static friction force of the actuator and of the crane joint
F_{S0}	Spring's pre-load force of pilot-operated check valves
f_v	Viscous friction coefficient of the actuator and of the crane joint
$G(x)$	Gravitational load acting on the actuator
i_A	Armature current of the servo-motor
k_C	Static friction force's constant of the actuator and of the crane joint
k_I	Integral gain of the PI controller
k_P	Proportional gain of the PI controller
k_{PF}	Filter gain of the high-pass pressure filter
k_S	Spring stiffness of pilot-operated check valves
k_T	Torque constant of the servo-motor
k_v	Flow gain of check valves and of pressure-relief valves
$M(x)$	Equivalent mass of the system acting on the actuator
p	Pressure
p_1	Pressure at the pump/motor port on the bore-side of the actuator
p_2	Pressure at the pump/motor port on the rod-side of the actuator
p_3	Actuator's bore-side pressure
p_4	Actuator's rod-side pressure
p_5	Accumulator pressure
$p_{AC,0}$	Pre-charge pressure of the accumulator
p_{atm}	Atmospheric pressure
p_c	Cracking pressure of check valves and of pressure-relief valves
P_C	Mechanical power at the load/actuator interface
p_D	Drain pressure in pilot-operated check valves
P_{EM}	Electrical power of the servo-motor
p_{In}	Pressure at the inlet port of hydraulic valves
p_{Out}	Pressure at the outlet port of hydraulic valves
p_x	Opening pilot pressure of pilot-operated check valves
Q	Volume flow rate
Q_d	Differential actuator's volume flow rate
$Q_{e,P}$	Effective flow rate of the pump/motor
Q_{EV}	Volume flow rate through the electro-valve
Q_p	Actuator's volume flow rate on the bore-side
Q_{POCV}	Flow rate through pilot-operated check valves
Q_r	Actuator's volume flow rate on the rod-side
Q_S	Flow losses of the pump/motor
$T_{e,P}$	Effective shaft torque of the pump/motor
T_S	Torque losses of the pump/motor
u_{EM}	Commanded servo-motor speed
u_{EV}	Command directed to the 3/2 electro-valve
u_{FF}	Commanded servo-motor speed from the feedforward term
u_{LH}	Load-holding enabler command
u_{PF}	Commanded servo-motor speed from the pressure feedback term
$V_{AC,0}$	Effective accumulator gas volume
V	Volume
x	Piston position
x_{Max}	Actuator stroke
$\dot{x}_{Set}$	Commanded piston velocity
Greek symbols	
y	Poppet lift of pilot-operated check valves
β	Effective bulk modulus of the working fluid

β_A	Air's bulk modulus
β_O	Oil's bulk modulus
γ	Adiabatic air constant
Δp	Pressure differential
ε_A	Volumetric air content of the working fluid
$\varepsilon_{A,0}$	Volumetric air content of the working fluid at atmospheric pressure
ζ	Damping term used in the servo-motor's transfer function
η_{SCC}	Overall system efficiency of the self-contained cylinder
η_v	Pump/motor's volumetric efficiency
λ	Scaling factor used in the loss model of the pump/motor
ρ	Oil density
τ	Time constant of the poppet dynamics in pilot-operated check valves
ω	Shaft speed of the pump/motor
ω_n	Natural frequency used in the servo-motor's transfer function
ω_{PF}	Cut-off frequency of the high-pass pressure filter

Appendix A

This appendix presents the specifications of the single-boom crane involved in the experimental testing. The relevant dimensions used to define the crane kinematics are highlighted in Figure A1. The boom pivots around point A whereas the actuator is connected to point B and to point C. The distances between the points A, B, C, and G (i.e., the center of mass) are evaluated via Equation (A1) whereas the effective length of the hydraulic cylinder (L_{Cyl}) is expressed in (A2).

$$L_{ij} = \sqrt{L_{ij_x}^2 + L_{ij_y}^2} \tag{A1}$$

$$L_{Cyl} = x + L_{Min} \tag{A2}$$

The equivalent mass of the system and the gravitational load acting on the actuator are elucidated in (A3) and (A4), respectively. These formulae give the trends presented in Figure 7.

$$M(x) = -\frac{4 \cdot \left(L_{AG_x}^2 \cdot L_{Cyl}^2 \cdot m + L_{AG_y}^2 \cdot L_{Cyl}^2 \cdot m + L_{Cyl}^2 \cdot J \right)}{\left(L_{AB} - L_{Cyl} - L_{AC} \right) \cdot \left(L_{AB} - L_{Cyl} + L_{AC} \right) \cdot \left(L_{AB} + L_{Cyl} + L_{AC} \right) \cdot \left(L_{AB} + L_{Cyl} - L_{AC} \right)} \tag{A3}$$

$$G(x) = -\frac{L_{Cyl}}{L_1} \cdot \left\{ 2 \cdot \sqrt{-L_1} \cdot g \cdot m \cdot \cos[\arccos(L_2) + \alpha] \cdot L_{AG_x} - \sin[\arccos(L_2) + \alpha] \cdot L_{AG_y} \right\}$$
$$\begin{cases} \text{where :} \\ \alpha = \arctan\left(\frac{L_{AG_y}}{L_{AG_x}}\right) - \arctan\left(\frac{L_{AB_y}}{L_{AB_x}}\right) + \arctan\left(\frac{L_{AC_y}}{L_{AC_x}}\right) \\ L_1 = \left(L_{Cyl} - L_{AB} + L_{AC}\right) \cdot \left(L_{Cyl} - L_{AB} - L_{AC}\right) \cdot \left(L_{Cyl} + L_{AB} - L_{AC}\right) \cdot \left(L_{Cyl} + L_{AB} + L_{AC}\right) \\ L_2 = \frac{1}{2} \cdot \frac{L_{AB}^2 + L_{AC}^2 - L_{Cyl}^2}{L_{AC} \cdot L_{AB}} \end{cases} \tag{A4}$$
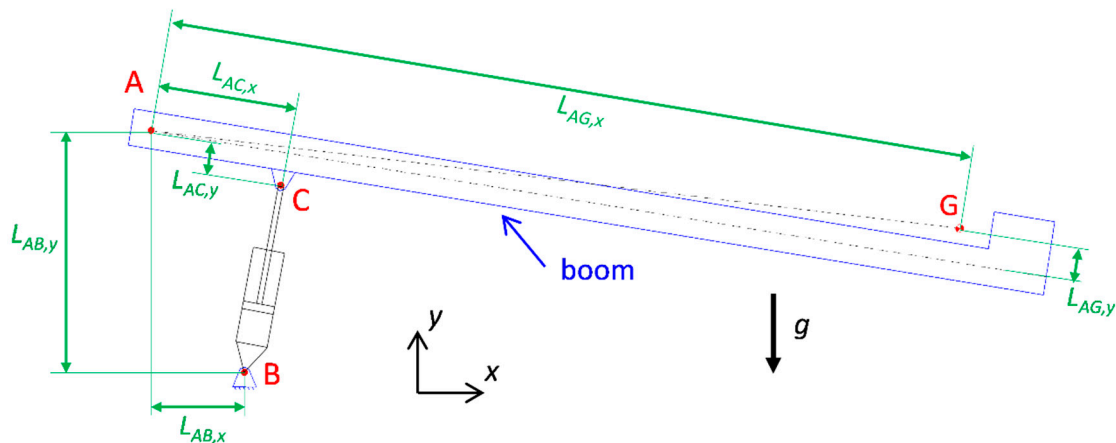

Figure A1. Kinematics of the single-boom crane used for the experimental testing.

Lastly, Table A1 collates the key parameters of the crane. These quantities are the aforementioned distances, the minimum length (L_{Min}) between point B and point C, the acceleration of gravity (g), the payload mass (m), and the moment of inertia of the crane (J) about its center of mass.

Table A1. Key parameters of the single-boom crane.

Magnitude	Value	Unit	Magnitude	Value	Unit
$L_{AG,x}$	3.139	[m]	$L_{AB,y}$	1.055	[m]
$L_{AG,y}$	0.064	[m]	L_{Min}	0.772	[m]
$L_{AC,x}$	0.550	[m]	g	9.82	[m/s^2]
$L_{AC,y}$	0.130	[m]	m	402	[kg]
$L_{AB,x}$	0.420	[m]	J	288.518	[kg·m^2]

References

1. Garcia, A.; Cusido, J.; Rosero, J.; Ortega, J.; Romeral, L. Reliable Electro-Mechanical Actuators in Aircraft. *IEEE Aerosp. Electron. Syst. Mag.* **2008**, *23*, 19–25. [CrossRef]
2. Hagen, D.; Pawlus, W.; Ebbesen, M.K.; Andersen, T.O. Feasibility Study of Electromechanical Cylinder Drivetrain for Offshore Mechatronic Systems. *Model. Identif. Control* **2017**, *38*, 59–77. [CrossRef]
3. Michel, S.; Weber, J. Electrohydraulic Compact-drives for Low Power Applications considering Energy-efficiency and High Inertial Loads. In Proceedings of the 7th FPNI PhD Symposium on Fluid Power, Reggio Emilia, Italy, 27–30 June 2012; pp. 1–18.
4. Schneider, M.; Koch, O.; Weber, J. Green Wheel Loader—Improving fuel economy through energy efficient drive and control concepts. In Proceedings of the 10th International Fluid Power Conference, Dresden, Germany, 8–10 March 2016.
5. Michel, S.; Weber, J. Prediction of the Thermo-Energetic Behaviour of an Electrohydraulic Compact Drive. In Proceedings of the 10th International Fluid Power Conference, Dresden, Germany, 8–10 March 2016.
6. Michel, S.; Weber, J. Energy-efficient Electrohydraulic Compact Drives for Low Power Applications. In Proceedings of the Fluid Power Motion Control (FPMC 2012), Bath, UK, 12–14 September 2012; pp. 93–107.
7. Weber, J.; Beck, B.; Fischer, E.; Ivantysyn, R.; Kolks, G.; Kunkis, M.; Lohse, H.; Lübbert, J.; Michel, S.; Schneider, M.; Shabi, L. Novel System Architectures by Individual Drives. In Proceedings of the 10th International Fluid Power Conference, Dresden, Germany, 8–10 March 2016.
8. Hagen, D.; Padovani, D.; Ebbesen, M.K. Study of a Self-Contained Electro-Hydraulic Cylinder Drive. In Proceedings of the Global Fluid Power Society PhD Symposium (GFPS), Samara, Russia, 18–20 July 2018.
9. Zimmerman, J.; Pelosi, M.; Williamson, C.; Ivantysynova, M. Energy Consumption of an LS Excavator Hydraulic System. In Proceedings of the ASME International Mechanical Engineering Congress & Exposition, Seattle, WA, USA, 11–15 November 2007.
10. Zimmerman, J.; Busquets, E.; Ivantysynova, M. 40% Fuel Savings by Displacement Control Leads to Lower Working Temperatures—A Simulation Study and Measurements. In Proceedings of the 52nd National Conference on Fluid Power, Las Vegas, NV, USA, 23–25 March 2011.
11. Minav, T.; Panu, S.; Matti, P. Direct-Driven Hydraulic Drive Without Conventional Oil Tank. In Proceedings of the ASME/BATH Symposium on Fluid Power & Motion Control, Bath, UK, 10–12 September 2014; pp. 1–6.
12. Altare, G.; Vacca, A. A Design Solution for Efficient and Compact Electro-hydraulic Actuators. *Procedia Eng.* **2015**, *106*, 8–16. [CrossRef]
13. Çalışkan, H.; Balkan, T.; Platin, B.E. A Complete Analysis for Pump Controlled Single Rod Actuators. In Proceedings of the 10th International Fluid Power Conference, Dresden, Germany, 8–10 March 2016; pp. 119–132.
14. Cho, S.H.; Burton, R. Position control of high performance hydrostatic actuation system using a simple adaptive control (SAC) method. *Mechatronics* **2011**, *21*, 109–115. [CrossRef]
15. Willkomm, J.; Wahler, M.; Weber, J. Potentials of Speed and Displacement Variable Pumps in Hydraulic Applications. In Proceedings of the 10th International Fluid Power Conference, Dresden, Germany, 8–10 March 2016; pp. 379–392.

16. Pedersen, H.C.; Schmidt, L.; Andersen, T.O.; Brask, M.H. Investigation of New Servo Drive Concept Utilizing Two Fixed Displacement Units. *JFPS Int. J. Fluid Power Syst.* **2014**, *8*, 1–9. [CrossRef]

17. Brahmer, B. Hybrid Drive using Servo Pump in Closed Loop. In Proceedings of the 8th International Fluid Power Conference, Dresden, Germany, 26–28 March 2012; pp. 93–102.

18. Minav, T.; Bonato, C.; Sainio, P.; Pietola, M. Direct Driven Hydraulic Drive. In Proceedings of the 9th International Fluid Power Conference, Aachen, Germany, 24–26 March 2014.

19. Schmidt, L.; Roemer, D.B.; Pedersen, H.C.; Andersen, T.O. Speed-Variable Switched Differential Pump System for Direct Operation of Hydraulic Cylinders. In Proceedings of the ASME/BATH 2015 Symposium on Fluid Power and Motion Control, Chicago, IL, USA, 12–14 October 2015.

20. Schmidt, L.; Groenkjaer, M.; Pedersen, H.C.; Andersen, T.O. Position Control of an Over-Actuated Direct Hydraulic Cylinder Drive. *Control Eng. Pract.* **2017**, *64*, 1–14. [CrossRef]

21. Ketelsen, S.; Schmidt, L.; Donkov, V.H.; Andersen, T.O. Energy Saving Potential in Knuckle Boom Cranes using a Novel Pump Controlled Cylinder Drive. *Model. Identif. Control* **2018**, *39*, 73–89. [CrossRef]

22. Croke, S.; Herrenschmidt, J. More Electric Initiative Power-By-Wire Actuation Alternatives. In Proceedings of the National Aerospace and Electronics Conference, Dayton, OH, USA, 23–27 May 1994; pp. 1338–1346.

23. Frischemeier, S. Electrohydrostatic Actuators for Aircraft Primary Flight Control—Types, Modelling and Evaluation. In Proceedings of the Fifth Scandinavian International Conference on Fluid Power (SICFP'97), Linköping, Sweden, 28–30 May 1997; pp. 1–16.

24. Kazmeier, B. *Energieverbrauchsoptimierte Regelung eines Elektrohydraulischen Linearantriebs Kleiner Leistung mit Drehzahlgeregeltem Elektromotor und Verstellpumpe*; VDI-Verl: Düsseldorf, Germnay, 1998.

25. Jun, L.; Yongling, F.; Guiying, Z.; Bo, G.; Jiming, M. Research on Fast Response and High Accuracy Control of an Airborne Brushless DC Motor. In Proceedings of the 2004 IEEE International Conference on Robotics and Biomimetics, Shenyang, China, 22–26 August 2004; pp. 807–810.

26. van den Bossche, D. The A380 Flight Control Electrohydrostatic Actuators, Achievements and Lessons Learnt. In Proceedings of the 25th International Congress of the Aeronautical Sciences, Hamburg, Germany, 3–8 September 2006; pp. 1–8.

27. Quan, Z.; Quan, L.; Zhang, J. Review of Energy Efficient Direct Pump Controlled Cylinder Electro-Hydraulic Technology. *Renew. Sustain. Energy Rev.* **2014**, *35*, 336–346. [CrossRef]

28. Rahmfeld, R.; Ivantysynova, M. Energy Saving Hydraulic Actuators for Mobile Machines. In Proceedings of the 1st Bratislavian Fluid Power Symposium, Častá-Píla, Slovakia, 2–3 June 1998; pp. 177–186.

29. Rahmfeld, R. *Development and Control of Energy Saving Hydraulic Servo Drives for Mobile Systems*; VDI-Verlag: Hamburg, Germany, 2002.

30. Williamson, C.; Ivantysynova, M. Stability and Motion Control of Inertial Loads with Displacement Controlled Hydraulic Actuators. In Proceedings of the 6th FPNI-PhD Symposium, West Lafayette, IN, USA, 15–19 June 2010; pp. 499–514.

31. Lodewyks, J. Differenzialzyliner im Geschlossenen Hydrostatischen Getriebe. *Ölhydraulik und Pneumatik* **1993**, *186*, 394–401.

32. Lodewyks, J. *Der Differentialzylinder im Geschlossenen Hydrostatischen Kreislauf*; RWTH Aachen: Aachen, Germany, 1994.

33. Vael, G.; Achten, P.; Potma, J. Cylinder Control with Floating Cup Hydraulic Transformer. In Proceedings of the Scandinavian International Conference on Fluid Power (SICFP), Tampere, Finland, 7–9 May 2003; pp. 175–190.

34. Bloomquist, J.V.; Niemiec, A.J.; Vickers Inc. Electrohydraulic system and apparatus with bidirectional electric-motor/hydraulic-pump unit. U.S. Patent 5778671A, 19 March 1998.

35. Zheng, J.; Zhao, S.; Wei, S. Application of Self-Tuning Fuzzy PID Controller for a SRM Direct Drive Volume Control Hydraulic Press. *Control Eng. Pract.* **2009**, *17*, 1398–1404. [CrossRef]

36. Wei, S.; Zhao, S.; Zheng, J.; Zhang, Y. Self-Tuning Dead-Zone Compensation Fuzzy Logic Controller for a Switched-Reluctance-Motor Direct-Drive Hydraulic Press. *Proc. Inst. Mech. Eng. Part I J. Syst. Control Eng.* **2009**, *223*, 647–656. [CrossRef]

37. Schneider, M.; Koch, O.; Weber, J.; Bach, M.; Jacobs, G. Green Wheel Loader –Development of an Energy Efficient Drive and Control System. In Proceedings of the 9th International Fluid Power Conference, Aachen, Germany, 24–26 March 2014.

38. Schneider, M.; Koch, O.; Weber, J. *Green Wheel Loader -Operating Strategy of an Energy Efficient Hybrid Drive Train*; SAE Commercial Vehicle Engineering Congress, Paper 2014-01-2400M; Rosemont, IL, USA, 2014.

39. Hewett, A.J. Hydraulic Circuit Flow Control. U.S. Patent 5,329,767A, 19 July 1994.

40. Wang, L.; Book, W.J.; Huggins, J.D. A Hydraulic Circuit for Single Rod Cylinders. *J. Dyn. Syst. Meas. Control* **2012**, *134*, 011019. [CrossRef]

41. Kenyon, R.L.; Scanderberg, D.; Nolan, M.E.; Wilkerson, W.D. Electro-Hydraulic Actuator. E.P. Patent 0,395,420A2, 31 October 1990.

42. Quan, L. Current State, Problems and the Innovative Solution of Electro-hydraulic Technology of Pump Controlled Cylinder. *Chin. J. Mech. Eng.* **2008**, *44*, 87–92. [CrossRef]

43. Zhang, D.; Li, W.; Lin, Y.; Bao, J. An Overview of Hydraulic Systems in Wave Energy Application in China. *Renew. Sustain. Energy Rev.* **2012**, *16*, 4522–4526. [CrossRef]

44. Huang, J.; Quan, L.; Zhang, X. Development of a Dual-acting AxialPiston Pump for Displacement-Controlled System. *Proc. Inst. Mech. Eng. Part B J. Eng. Manuf.* **2014**, *228*, 606–616. [CrossRef]

45. Wiens, T.; Bitner, D. An Efficient, High Performance and Low-Cost Energy Recovering Hydrostatic Linear Actuator Concept; In Proceedings of the BATH/ASME 2016 Symposium on Fluid Power and Motion Control, Bath, UK, 7–9 September 2016.

46. Cleasby, K.G.; Plummer, A.R. A Novel High Efficiency Electrohydrostatic Flight Simulator Motion System. In Proceedings of the Fluid Power Motion Control (FPMC 2008), Bath, UK, 10–12 September 2008; pp. 437–449.

47. Parker, H. Compact EHA—Electro-Hydraulic Actuators for High Power Density Applications. 2013. Available online: https://goo.gl/t2FMw2 (accessed on 17 December 2018).

48. Sweeney, T.; Kubinski, P.T.; Anderson, D.J. Electro-hydraulic Actuator Mounting. U.S. Patent 8161742 B2, 24 April 2012.

49. Rexroth, B. Advantages of Electrification and Digitalization Technology for Hydraulics. 2018. Available online: https://goo.gl/4G6Jxn (accessed on 17 December 2018).

50. Bing, X.; Xiaoping, O.; Yang, H. Energy-Saving System Applying Pressure Accumulators for VVVF Controlled Hydraulic Elevators. In Proceedings of the ASME International Mechanical Engineering Congress, Washington, DC, USA, 15–21 November 2003.

51. Altare, G.; Vacca, A.; Richter, C. A Novel Pump Design for an Efficient and Compact Electro-Hydraulic Actuator. In Proceedings of the 2014 IEEE Aerospace Conference, Big Sky, MT, USA, 2014.

52. Jalayeri, E.; Imam, A.; Tomas, Z.; Sepehri, N. A throttle-less single-rod hydraulic cylinder positioning system: Design and experimental evaluation. *Adv. Mech. Eng.* **2015**, *7*, 1–14. [CrossRef]

53. Çalışkan, H.; Balkan, T.; Platin, B.E. A Complete Analysis and a Novel Solution for Instability in Pump Controlled Asymmetric Actuators. *J. Dyn. Syst. Meas. Control* **2015**, *137*. [CrossRef]

54. Sørensen, J.K.; Hansen, M.R.; Ebbesen, M.K. Numerical and Experimental Study of a Novel Concept for Hydraulically Controlled Negative Loads. *Model. Identif. Control* **2016**, *37*, 195–211. [CrossRef]

55. Williamson, C.; Ivantysynova, M. The Effect of Pump Efficiency on Displacement-Controlled Actuator Systems. In Proceedings of the Eight Scandinavian International Conference on Fluid Power, Tampere, Finland, 21–23 May 2007.

56. Kjelland, M.B.; Hansen, M.R. Numerical and Experiential Study of Motion Control Using Pressure Feedback. In Proceedings of the 13th Scandinavian International Conference on Fluid Power, Linköping, Sweden, 3–5 June 2013.

57. Kjelland, M.B.; Hansen, M.R. Offshore Wind Payload Transfer Using Flexible Mobile Crane. *Model. Identif. Control* **2015**, *36*, 1–9. [CrossRef]

Paper D

Enabling Energy Savings in Offshore Mechatronic Systems by using Self-Contained Cylinders

Daniel Hagen, Damiano Padovani, and Martin Choux

Enabling Energy Savings in Offshore Mechatronic Systems by using Self-Contained Cylinders

Daniel Hagen [1]   Damiano Padovani [1]   Martin Choux [1]

[1]*Department of Engineering Sciences, University of Agder, N-4898 Grimstad, Norway.*
E-mail: daniel.hagen@uia.no

Abstract

This paper proposes a novel actuation system for an offshore drilling application. It consists of three self-contained electro-hydraulic cylinders that can share and store regenerated energy. The energy saving potential of the proposed solution is analyzed through a multibody system simulation. The self-contained system demonstrates superior energy efficiency compared to the benchmark system representing the state-of-the-art approach used today (i.e., valve-controlled cylinders by means of pressure-compensated directional control valves and counter-balance valves, supplied by a centralized hydraulic power unit). Due to the "power on demand" capability, the cancellation of the throttling losses, and the opportunity to recover energy in motoring quadrants, the self-contained system consumes 83.44% less energy without affecting the system's performance.

Keywords: Electrification of hydraulics, linear actuator, offshore mechatronic systems, self-contained electro-hydraulic cylinder, proportional directional control valve, passive load-holding, energy savings

1. Introduction

With the increasing focus on the environmental impact, such as CO_2 emission and hydraulic fluid pollution, of the oil and gas industry, traditionally used hydraulically-actuated systems tend to be replaced by electric drives (Pawlus et al., 2016). However, force densities available from linear hydraulic actuators are still typically higher than those of electric actuators. Therefore, after the electrification of all rotational actuations, hydraulic power is still needed to actuate some hydraulic cylinders controlled by throttling valves. A relevant Offshore Mechatronic System (OMS) example is the pipe handling equipment (Fig. 1) implemented on state-of-the-art drilling rigs (Bak, 2014), where AC motors with a variable speed drive and a gearbox, here referred to as AC drivetrains, have successfully replaced all hydraulic motors. However, for some of the linear actuators included in the operational motion cycle, hydraulic Valve-Controlled

Cylinders (VCCs) are still state-of-the-art, although an electro-mechanical counterpart has been used in other industry fields for many years. For electro-mechanical cylinders, the predominant challenges are low reliability under high load operating conditions. In Hagen et al. (2017) an offshore case-study was carried out, demonstrating that the permissible transmitted power of the most promising available off-the-shelf electro-mechanical cylinder was lower than the power required by the motion cycle of the existing hydraulic actuation system. Typically in OMSs, the hydraulic source is supplied from a centralized Hydraulic Power Unit (HPU) consisting of multiple pumps driven by large electric motors. The required electric power is generated by diesel generators that are running continuously, supplying the entire offshore installation with electricity.

An alternative solution to the inefficient VCC is a "valve-less" pump controlled (electro-hydraulic) cylinder drive. Pump-controlled concepts using standard

differential cylinders are classified and reviewed in Ketelsen et al. (2019). In literature, research related to compact electro-hydraulic cylinders is primarily on cost efficiency and low power applications (less than 5 $[kW]$). In this paper, these solutions are referred to as Self-Contained Cylinders (SCCs), namely self-sufficient and sealed systems that only consume energy when motion is demanded. For instance, Michel and Weber (2012) derived specific conclusions about the best approach for SCCs. However, passive load-holding capability was not considered. An alternative approach based on a triple pump solution which enables higher stiffness and good energy efficiency was also considered (Schmidt et al., 2015, 2017; Ketelsen et al., 2018). However, the hydraulic circuits of typically offshore load-carrying applications must contain passive load-holding devices to meet safety regulations. Hence, a literature survey and simulation study of an SCC concept that can operate in four quadrants, including passive load holding, suitable for power levels above 5 $[kW]$, is presented in Hagen et al. (2018). In Padovani et al. (2019), a similar SCC concept, also including a filter and cooling circuit, was successfully implemented on a single-boom crane and tested in two quadrant operations; the proper functioning of the passive load-holding capability and an overall energy efficiency of about 60% during actuation were demonstrated. Therefore, applying such a drive technology to a multi-actuator OMS and demonstrating the resulting benefits over the more traditional valve-controlled hydraulic cylinders is the target of this investigation.

To fully benefit from the great energy efficiency of SCCs, the entire operation cycle of a pipe handling equipment with periods of motoring, load holding and regenerative braking must be considered together with different solutions for storing energy. Inspired by the principles introduced and explained in Ristic and Wahler (2018), this paper proposes an actuation system consisting of three SCCs that can share energy with other electric-drives and store regenerated energy in a battery, instead of using brake resistors to dissipate the recovered energy as heat to the surrounding.

Section (2) presents the offshore drilling application case study. A conventional offshore VCC system used as a benchmark is explained in Section (3) whereas the proposed SCC system is addressed in Section (4). Section (5) contains an inverse dynamic analysis of the energy recovery potential of the case study, and identifies the design requirements for the actuation systems. Furthermore, it presents the simulated system performance, power consumption, energy efficiency, and a comparison of the two actuation systems regarding the energy consumption. Finally, section (6) discusses the simulation results and some practical challenges that
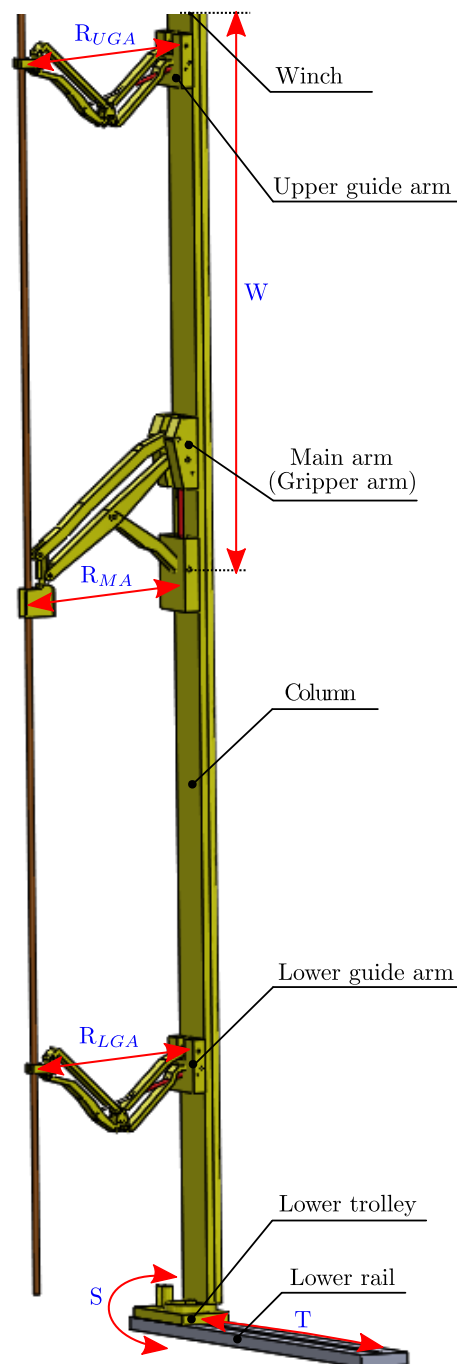
must be considered in future works.

Figure 1: Considered offshore mechatronic system (simplified CAD model of the multibody system).

2. The Considered Case-Study

An offshore Pipe Racking Machine (PRM), as shown in Fig. 1, is used as an OMS case study for analyzing the energy saving potential when replacing the cen-

tralized VCCs of the reach arms (i.e., the upper guide arm, the main arm, and the lower guide arm) with SCCs. The PRM is a column-type multipurpose pipe handling machine (drill-pipe, drill-collar and casings) that combines the functionality of several traditional types of pipe handling equipment in one machine.

The PRM can perform the following tasks according to Hagen et al., 2017:

- moving stands (two or more joints of pipe connected) between the Well Center (WC) and the desired Finger Board (FB) slot

- building of stands for storage inside the FB while drilling

- handling of a single pipe from horizontal to vertical position and vice versa

- lifting operation on drill floor, i.e., the main arm can be used as a crane.

By rack and pinion systems, the column is supported at the upper beam (not shown) and at the lower rail. The lower rail is mounted directly on the drill floor, whereas the upper beam is connected to the structure of the derrick. The column includes an upper and a lower Guide Arm (GA) that are designed to guide the stand, i.e., guide the top and bottom of the drill-stand being in motion. The arm located in the middle is the Main Arm (MA), responsible for holding the pipe in a secure grip (gripper arm). All arms are equipped with a VCC which allows for the extension and retraction (i.e., horizontal Reach (R) motion) in order to position a stand in the desired FB slot or at the WC. Redundant AC drivetrains are located both on the upper and lower Trolleys (T), controlling the horizontal movement of the column along the tracks. The Winch (W) located on top of the column is used to hoist and lower the MA (i.e., the stand) using redundant AC drivetrains. Finally, the redundant AC drivetrains located on the lower trolley make it possible for the column to Slew (S) (rotate) about its vertical axis.

2.1. The Considered Operation Sequence

The operation sequence considered in this study is the so-called tripping sequence. It takes place when the drill-string is assembled or disassembled during a well-construction process. During this sequence, the PRM continually moves between the WC and the FB where the stands are stored. The leading specification rating of these machines is the tripping speed, i.e., how many stands can be moved between the WC and the FB per hour. The motion steps of the PRM for the considered sequence are illustrated in Fig. 2.
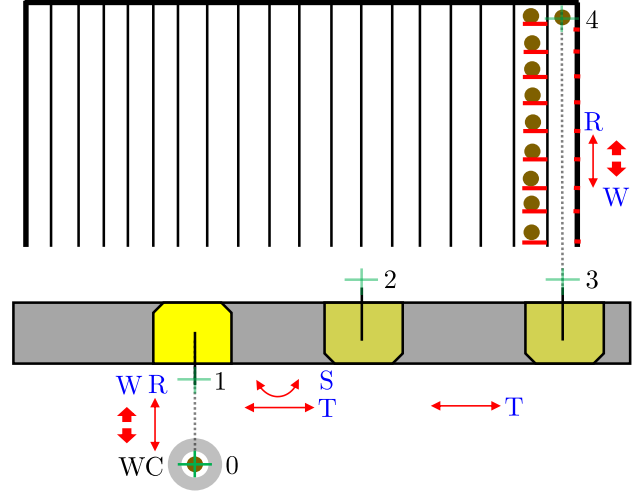

Figure 2: Operation sequence steps of the arms reach (R), winch (W), trolley (T), and slew (S), when moving a drill-stand from the well-center to the desired fingerboard slot (simplified top-view).

The PRM starts at the WC and a stand is ready for being moved to the desired FB slot. The sequence consists of the following steps:

0-1; the MA gripper and GAs guide close around the stand, the winch lifts the MA (the stand) for 1 $[m]$ and the arms retract from the WC position to the inner reach position

1-2; the PRM starts to trolley and rotates 180 $[°]$

2-3; the PRM continues to trolley until reaching the set-point (a 9 $[m]$ traveling is performed)

3-4; the three arms extend until the set-point of 4 $[m]$ is reached, the stand is lowered for 2 $[m]$ to the floor, and the MA gripper and GAs guide open while the machine returns back to WC in reverse steps.

2.2. Motion Reference Generator

An motion profile with a constant jerk S-curve, represented by a second-order polynomial function in velocity (3rd order in position), is used for all motion references. As an example, a motion profile for the MA cylinder extending and retracting is shown in Fig. 3 for position set-point $x_{C_{SP}} = 400$ $[mm]$, velocity set-point $v_{C_{SP}} = 120$ $[\frac{mm}{s}]$, and acceleration set-point $a_{C_{SP}} = 80$ $[\frac{mm}{s^2}]$.

The maximum jerk is found as:

$$j_{C_{SP}} = \frac{a^2_{C_{SP}}}{v_{C_{SP}} - v_{C_0}}. \quad (1)$$
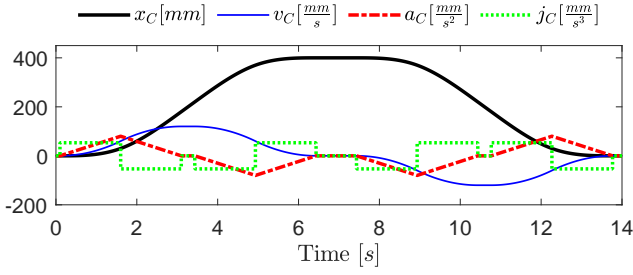
91

Figure 3: Main arm cylinder motion profile example.

The time period with constant velocity necessary to reach the desired position may be estimated as:

$$t_{cst} = \frac{x_{C_{SP}} - 2s_a}{v_{C_{SP}}} \quad (2)$$

where

$$s_a = \frac{v_{C_{SP}} - v_{C_0}}{a_{C_{SP}}} \quad (3)$$

is the travel distance during the acceleration phase.

2.2.1. Reach Arm Kinematics

During the considered operation cycle, the reach motion (position (x_R) and velocity (v_R)) of the MA and of the GAs must be operated synchronously when the stand is moved. The main control input are depicted in Fig. 4, for defining the desired motion reference (i.e., cylinder position and the velocity) of the MA cylinder. Furthermore, the GAs follow the calculated reach motion based on the desired MA cylinder motion trajectory.
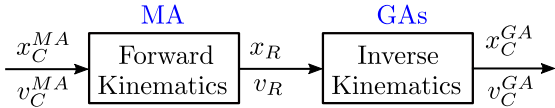
Figure 4: Reach arms motion reference conversion.

The reach length/position of the MA with respect to the effective cylinder stroke length (x_C^{MA}), i.e., the forward kinematics, is derived using the Pythagoras theorem, as illustrated in Fig. 5, and calculated as:

$$x_R = \underbrace{\sqrt{c^2 - a^2}}_{b} + x_{R_0} \quad (4)$$

where c (the hypotenuse) is the known length of the arm, a (the opposite side) is the sum of effective cylinder displacement and the cylinder's initial length ($a = x_C^{MA} + x_{C_0}^{MA}$), and x_{R_0} is the offset from the revolute joint (RJ_{bc}) to the center of the pipe. The reach velocity is calculated as:

$$v_R = -\frac{a}{b} v_C^{MA}. \quad (5)$$
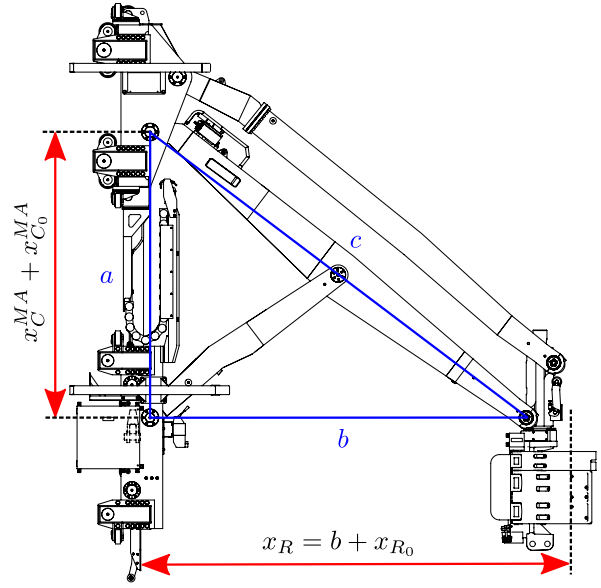
Figure 5: Main arm at max reach ($x_R = 4\,[m]$ and $x_C^{MA} = 0\,[m]$).
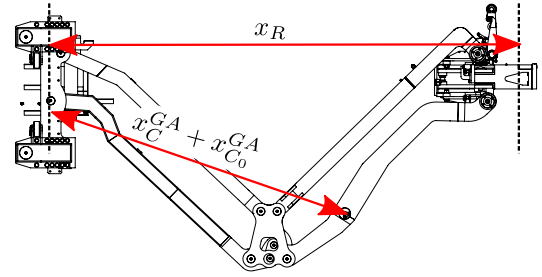
Figure 6: Guide arm at max reach ($x_R = 4\,[m]$ and $x_C^{GA} = 1.04\,[m]$).

An efficient solvable analytical expression is not obtained for the GA's inverse kinematics with sufficient accuracy because of the height variation of the tool point when the mechanism extends or retract. Hence, the required cylinder positions of the GAs (x_C^{GA}), as illustrated in Fig. 6, to follow the desired reach position are calculated using the polynomial function:

$$x_C^{GA} = p_5 x^5 + p_4 x^4 + p_3 x^3 + p_2 x^2 + p_1 x + p_0 \quad (6)$$

where x is the input (reach position) minus an offset ($x = x_R - x_{R_0}^{GA}$), and $p_{0...5}$ are coefficients identified using curve fitting on simulated position values of x_R and x_C^{GA}. The maximum error between the reference position and the measured reach position is 1 [mm] (i.e., below 0.04% of the total reach length). Finally, the velocity of the GAs cylinders are calculated as:

$$v_C^{GA} = (5p_5 x^4 + 4p_4 x^3 + 3p_3 x^2 + 2p_2 x + p_5 x)v_R. \quad (7)$$

2.3. Multibody System Model

The mechanical system of the PRM is modeled using the multibody system (MBS) library in MATLAB-Simulink®. The MBS is modeled based on the work in Hagen et al. (2017), where a similar MBS of the MA is mathematically represented and simulated. In this paper, in addition to the MA (consisting of 9 bodies, a payload and 8 RJs), two GAs (consisting of 2·10 bodies and 2·12 RJs), the column (1 body), the lower trolley (1 body), and the lower rail (1 body) are modeled, as shown in Fig. 7, to simulate the considered operation sequence. The input of the MBS model depends on if an inverse or forward dynamic analysis is carried out. Either the desired position reference is used as an input and the output force/torque is analyzed (inverse dynamics), or the force/torque from the actuation system model (e.g., the hydraulic force from the cylinders) is used as input to the actuated joints and the output motion are analyzed (forward dynamics).

2.3.1. Friction Models

The combined friction (F_f^i) of both the actuator (i.e., the hydraulic cylinders and the AC drivetrains) and the mechanical system (i.e., the revolute joints) is modeled according to an equivalent Stribeck model:

$$F_f^i = f_v^i \dot{x} + \tanh(\dot{x}a)\left(F_C^i + f_S^i e^{-\frac{\dot{x}\tanh(\dot{x}a)}{\tau_S}}\right) \qquad (8)$$

where $\dot{x}$ is the velocity of the ith actuator, a is the constant value used in the tanh function, while the different coefficients account the viscous friction (f_v^i), the Coulomb friction (F_C^i), the static friction (f_S^i) and the friction force's constant ($\tau_S = 0.02[\frac{s}{m}]$). The parameters used for each actuator are listed in Table 1. In case of rotary motions, the angular velocity is used, resulting in a friction torque (T_f^i).

Table 1: Friction parameters.

Actuator	f_v^i	F_C^i	f_S^i
F_f^{MA}:	$60[\frac{kNs}{m}]$	$1.13\ [kN]$	$1.25\ [kN]$
F_f^{GA}:	$20[\frac{kNs}{m}]$	$0.38\ [kN]$	$0.75[kN]$
F_f^{W}:	$30[\frac{kNs}{m}]$	$0.56\ [kN]$	$0.88[kN]$
F_f^{T}:	$40[\frac{kNs}{m}]$	$0.75\ [kN]$	$0.1\ [kN]$
T_f^{S}:	$16[kNs]$	$0.30\ [kNm]$	$0.05[kNm]$

2.4. Specifications

The PRM consists of four main degrees of freedom, as highlighted in Figs. 1-2. In Table 2 the requirements for the considered actuators are described.
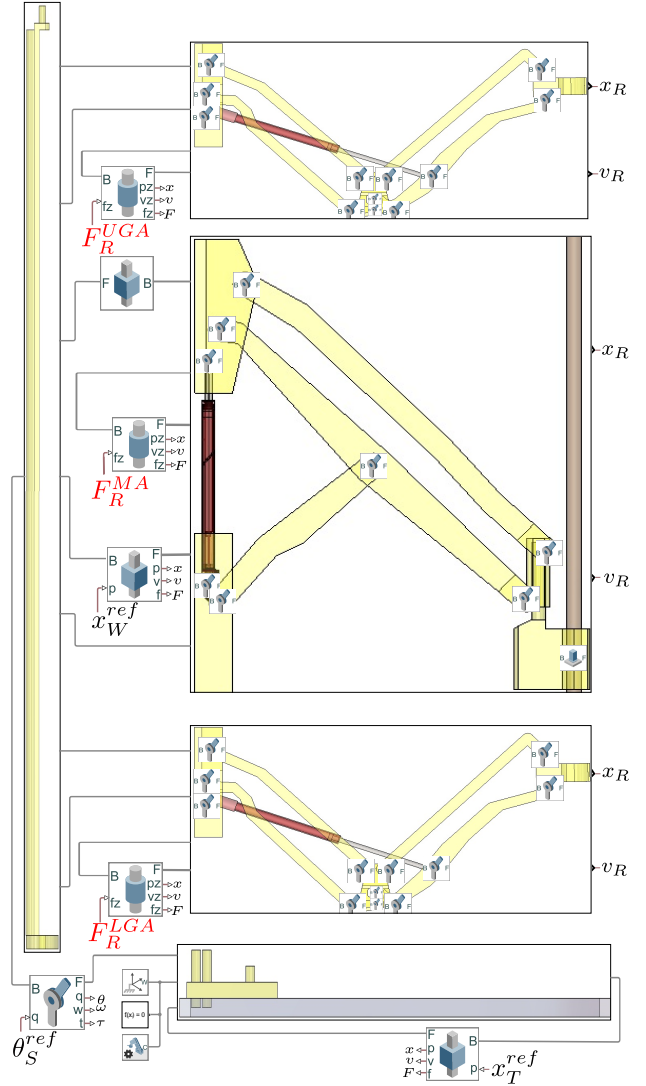

Figure 7: The MATLAB-Simulink® MBS model.

3. Benchmark System

State-of-the-art hydraulically-actuated systems used in offshore drilling equipment and cranes are introduced and explained in the works of Bak (2014), Kjelland (2016), Sørensen (2016), and Hagen et al. (2017). This paper presents a synthesis of the hydraulic actuation system together with the numerical simulation models of the MA and the GAs reach motion.

The considered benchmark system is based on state-of-the-art hydraulic load-sensing valves (i.e., pressure compensated proportional directional control valves) including passive load-holding valves on both cylinder ports. The individual actuators are powered by a central HPU ensuring a constant supply pressure (p_S^i) and a fixed return pressure (p_R^i). Fig. 8 shows the layout of the benchmark system and the general architecture

Table 2: Actuator requirements of the PRM.

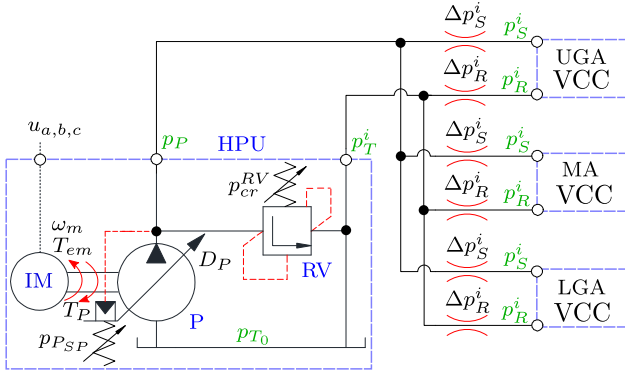|	
R – reach distance	4.0 [m]
MA – cylinder speed	0.12 $[\frac{m}{s}]$
W – max lifting capacity	14 [mT]
W – hoisting speed	1.0 $[\frac{m}{s}]$
W – vertical travel distance	25 [m]
T – horizontal travel distance	10 [m]
T – travel speed	0.5 $[\frac{m}{s}]$
S – column rotate angle	360 [°]
S – rotational speed	5 [rpm]

Figure 8: Benchmark system layout (simplified schematic).

of the VCC is shown in Fig. 10.

The HPU consists of an Induction Motor (IM) connected to the 50 $[Hz]$ AC grid:

$$\begin{bmatrix} u_a \\ u_b \\ u_c \end{bmatrix} = \begin{bmatrix} A_{peak} \sin(\omega_F t) \\ A_{peak} \sin(\omega_F t - 2/3\pi) \\ A_{peak} \sin(\omega_F t - 4/3\pi) \end{bmatrix} \quad (9)$$

where

$$A_{peak} = \frac{V_L}{\sqrt{3}}\sqrt{2} \quad (10)$$

and $V_L = 690$ $[V]$ is the RMS voltage, rotating the hydraulic pump at a constant angular velocity (ω_m), a variable axial-piston Pump (P) with max displacement D_P, a hydraulic tank with pressure p_{T_0}, and a pressure Relief-Valve (RV) ($p_{cr}^{RV} = 210$ $[bar]$) for safety purpose. The transmission lines between the HPU and the VCCs represent the supply and return flows. The equivalent pressure losses across the lines (Δp_S^i and Δp_R^i) are estimated in Section (3.3).

3.1. Actuator Requirements

From the inverse dynamic analysis, the minimum actuator requirements of the MA and GAs cylinders are identified. In addition to the minimal values from the considered drive cycle, the cylinders must deliver some

extra force ($\pm$ 5 $[kN]$) to account for potential forces distributed from wind and additional centripetal accelerations. The requirements considered when sizing the VCCs are listed in Table 3.

Table 3: Actuator requirements.

Description	MA	GAs
Displacement:	1.70 [m]	1.04 [m]
Velocity:	$\pm$ 0.12 $[\frac{m}{s}]$	$\pm$ 0.106 $[\frac{m}{s}]$
Extension force:	62 [kN]	15 [kN]
Retraction force:	2.5 [kN]	3 [kN]

The dominating design value when sizing the hydraulic cylinders is the buckling factor, and according to regulations (DNVGL-CG-0128), the accepted criterion for buckling in hydraulic cylinders is to use a safety factor $f_s = 4$, unless a more accurate analysis of the buckling load is carried out. The minimum rod diameter is determined by:

$$D_r^i \geq \sqrt[4]{\frac{64 f_s L_{C_{tot}}^{i2} F_{C_{max}}^i}{\pi^3 E}} \quad (11)$$

where $L_{C_{tot}}^i$ is the total length of the cylinder in extended position, $F_{C_{max}}^i$ is the maximum force acting on the cylinder (Table 3), and E is the elasticity modulus (206 $[GPa]$). The piston diameter may be selected based on:

$$D_p^i \geq \sqrt{\frac{4}{\pi} \frac{F_{C_{max}}^i}{p_A - p_B \varphi^i}} \quad (12)$$

where p_A is the piston side pressure typically set to 20...30 $[bar]$ below the maximum pump pressure ($p_P = 210$ $[bar]$), p_B is the rod side pressure, and φ^i the ratio between rod and piston area.

Based on eq. (11-12) assuming $f_s = 2.7$ $[-]$, $p_A = 180$ $[bar]$, and $p_B = 5$ $[bar]$, the dimensions in Table 4 are chosen for the MA and GAs cylinders according to the ISO 6022 standard.

Table 4: Selected cylinder dimensions and max induced load pressures.

Description	MA	GAs
Rod diameter:	70 [mm]	40 [mm]
Piston diameter:	100 [mm]	63 [mm]
Max load pressure:	81.5 [bar]	51.1 [bar]

3.2. Hydraulic Power Unit

The HPU's pump is sized based on the required flow of the MA and GAs cylinders:

$$Q_{max}^i = \begin{cases} v_C^i A_A^i, & v_C^i \geq 0 \\ v_C^i A_B^i, & v_C^i < 0 \end{cases} \quad (13)$$

during the considered motion cycle and the required pump pressure $p_{P_{SP}} = p_{Lmax} + \Delta p_{Smax} + 30 \ [bar]$, where $p_{Lmax} = 81.5 \ [bar]$ is the highest load induced pressure in the inlet chamber of the cylinders (Table 4) and Δp_{Smax} is the highest pressure loss between the HPU and the VCCs. The total flow demand for the pump ($Q_{Pmax} = (Q_{MA} + 2 \cdot Q_{GA})_{max}$) is approximately 84.6 $[\frac{l}{min}]$ when using the velocity values in Table 3. The maximum flows for each actuator are $Q_{max}^{MA} \approx 57 \ [\frac{l}{min}]$ and $Q_{max}^{GA} \approx 20 \ [\frac{l}{min}]$.

The effective pump losses are evaluated using the flow losses (Q_S) and torque losses (T_S) measured from steady-state experimental data in Williamson and Ivantysynova (2007) using a reference unit equivalent to the considered pump. The losses are scaled to the desired pump displacement according to:

$$Q_S = \lambda^2 \cdot Q_S^{ref} \quad (14)$$

$$T_S = \lambda^3 \cdot T_S^{ref} \quad (15)$$

$$\lambda = \sqrt[3]{\frac{D_P}{D_P^{ref}}} \quad (16)$$

where the quantities of the reference unit is denoted by the subscript ref and λ is a scaling factor as a function of the displacement of the considered pump (D_P) and the reference unit (D_P^{ref}).

Selecting a 690 $[V]$, 50 $[Hz]$, 3-phase IM with 4 poles gives in general a rotational speed of $n_m = 1450...1500 \ [rpm]$, depending on the external load.

From:

$$D_P > \frac{Q_{max}}{n_m} \quad (17)$$

the required pump displacement must be greater than 54.7 $[\frac{cm^2}{rev}]$ (assuming $n_m = 1450 \ [rpm]$), and according to:

$$T_P > \frac{p_P D_P}{2\pi} \quad (18)$$

the available torque from the IM must be greater than $T_P = 104.4 \ [Nm]$.

Considering the maximum pump pressure $p_P = 210 \ [bar]$, a displacement $D_P = 60 \ [\frac{cm^3}{rev}]$ and rotational speed $n_m = 1500 \ [rpm]$, the volumetric (leakage) loss ($Q_S = 4.3 \ [\frac{l}{min}]$) and the hydro-mechanical (friction) loss ($T_S = 20.81 \ [Nm]$) are estimated based on the

scaled measurements. Hence, when accounting for the estimated leakages in the pump, a variable displacement pump with $D_P = 60 \ [\frac{cm^3}{rev}]$ is sufficient. Finally, an electric motor can be selected based on the estimated maximum power ($\dot{E}_{IM}^{Mech} = \omega_m(T_P + T_S)$) of 21.05 $[kW]$ that the IM must deliver continuously.

3.3. Hydraulic Transmission Lines

Between the HPU and the VCCs, the hydraulic flow in the transmission lines is restricted through flexible drag chains between the moving elements of the PRM, i.e., between the upper beam and the upper trolley, between the upper trolley and the column, and between the column and the VCC of the individual arms. Also, in the supply line, a filter and a shut-off valve are included, as illustrated in Fig. 9.
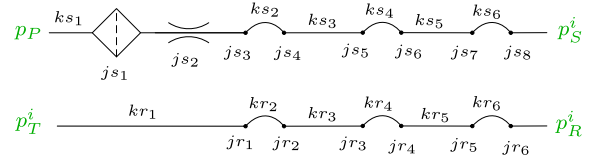

Figure 9: Considered supply and return line loss elements.

Equations for turbulent flow are used according to Stecki and Garbacik (2002). The losses are the pressure drop (Δp_L^i) in the supply line ($p_P - p_S^i$) and in the return line ($p_R^i - p_T^i$). In detail, line losses occur due to the large ratio between length and diameter of the lines and hoses, and all local losses, i.e., disturbances in the shut-off valve, inlet-filter and changes in flow area between lines, hoses, and fittings. For the hoses in each drag-chains, a 90° bend accounts for the local loss coefficients. The total flow loss may be estimated by:

$$\Delta p_L^i = \left(\underbrace{\sum \lambda_{ki} \frac{l_{ki}}{d_{ki} A_{ki}^2}}_{K_{ki} \ (line)} + \underbrace{\sum \xi_{ji} \frac{1}{A_{ji}^2}}_{K_{ji} \ (local)} \right) \frac{\rho}{2} Q_L^{2i} \quad (19)$$

where the subscript i denotes the actuator, L the transmission line type (supply or return), k the line or hose number, and j the local loss element number according to Fig. 9. In eq. (20) the coefficient of line pressure losses (λ_{ki}), assuming heat transfer between the fluid and the environment, is defined. Depending on the Reynold's Number in eq. (21), ξ_{ji} is the coefficient of local losses obtained from Stecki and Garbacik (2002), l_{ki} is the length of the line, d_{ki} is the diameter of the line, A_{ki} and A_{ji} is the effective flow area, and $\rho = 860 \ [\frac{kg}{m^3}]$

is the density of the hydraulic fluid.

$$\lambda_{ki} = \frac{75}{Re_{ki}} \quad (20)$$

$$Re_{ki} = \frac{v_{ki}d_{ki}}{\nu} \quad (21)$$

v_{ki} is the average flow velocity ($v_{ki} = Q_{avg}/A_{ki}$), and $\nu = 46 \cdot 10^{-6} \left[\frac{m^2}{s}\right]$ is the kinematic viscosity of the fluid.

The flow loss coefficients are combined as the gain $K_{L,i}$, and eq. (19) may be rewritten as:

$$\Delta p_L^i = K_L^i \frac{\rho}{2} Q_L^{2i} \quad (22)$$

where the estimated gains are listed Table 5.

Table 5: Transmission line loss gains.

Gain	UGA	MA	LGA
K_S^i [−]:	$9.97 \cdot 10^8$	$1.52 \cdot 10^9$	$1.31 \cdot 10^9$
K_R^i [−]:	$4.92 \cdot 10^8$	$7.81 \cdot 10^8$	$8.10 \cdot 10^8$

Finally, the effective back pressure from the HPU's tank (p_T^i) is estimated:

$$p_T^i = p_{T_0} + \rho g h^i \quad (23)$$

where p_{T_0} is the local tank pressure, g is the gravitational acceleration, and h^i is the height between the machine interface located on the upper beam and the ith VCC.

3.4. Control Valves

Pressure compensated Proportional Directional Control Valves (PDCVs) are popular in the offshore industry since the flow characteristics are load independent, and disturbance from other actuators connected to the same transmission line is avoided. A PVG32 from SauerDanfoss is selected according to the flow required by the actuators. From the available sizes, PDCVs with a flow capacity of 100 $\left[\frac{l}{min}\right]$ and 40 $\left[\frac{l}{min}\right]$ are selected for the MA and GAs, respectively.

3.5. Load-Holding Valves

The size of the Counter-Balance Valves (CBVs) is chosen to match the rated flow of the PDCVs. CBVs with a flow capacity of 120 $\left[\frac{l}{min}\right]$ for the MA and 60 $\left[\frac{l}{min}\right]$ for the GAs are selected from SUNhydraulics. The Check Valve (CV) cracking pressures is $p_{crC}^{CV} = 1.7$ [bar] for all CBVs.

To avoid unintended opening of the CBVs, it is recommended (Bak and Hansen, 2013) to set the cracking pressure of the Poppet Valve (PV) to a factor of 1.3 above the maximum load induced pressure (p_{Lmax}):

$$p_{cr,i}^{PV} \geq 1.3 \cdot p_{Lmax} \quad (24)$$

The cracking pressures of the MA and GAs PVs are set, based on the maximum load pressures identified in Table 4, to 105.5 [bar] and 66.5 [bar], respectively.

The combination of PDCV and CBVs tends to induce oscillatory behavior or even instability (Sørensen, 2016; Hagen et al., 2019). Hence, the most critical design consideration when selecting the CBV is to choose the best pilot area ratio (α_p) for the considered system. Based on experience on similar applications, a pilot ratio $\alpha_p = 3$ [−] is often chosen as a compromise between stability and energy efficiency.

3.6. System Modeling

A 22 [kW] double squirrel cage IM from ABB is selected, and modeled according to Krause et al. (2002).

The VCC circuit for the MA and GAs are modeled based on Hagen et al. (2019) where a similar hydraulic system is validated on a single-boom crane. The equations used in the numerical model of the benchmark system are listed in Section (A.1). The force balance of the piston in eq. (41), that are interfacing with the MBS, is considered as well as the well-known pressure build-up equation that is applied several times to evaluate the system pressures elucidated in Fig. 10.

The following equations are used to simulate the power of the different elements of the benchmark system considered in the Sankey diagram in Fig. 26: electrical power from the AC grid;

$$\dot{E}_{In}^{El} = u_a i_a + u_b i_b + u_c i_c \quad (25)$$

mechanical power of the motor's shaft;

$$\dot{E}_{IM}^{Mech} = T_{em}\omega_m \quad (26)$$

hydraulic power of the pump;

$$\dot{E}_P^{Hyd} = Q_P \Delta_{p_P}. \quad (27)$$

hydraulic power delivered to the individual VCCs;

$$\dot{E}_L^{Hyd} = Q_L p_L \quad (28)$$

hydraulic power delivered by the PDCVs;

$$\dot{E}_V^{Hyd} = Q_{V_{In}} p_{LS} \quad (29)$$

hydraulic power in the cylinder;

$$\dot{E}_C^{Hyd} = F_C v_C \quad (30)$$

and, finally, the mechanical power delivered by the arms;
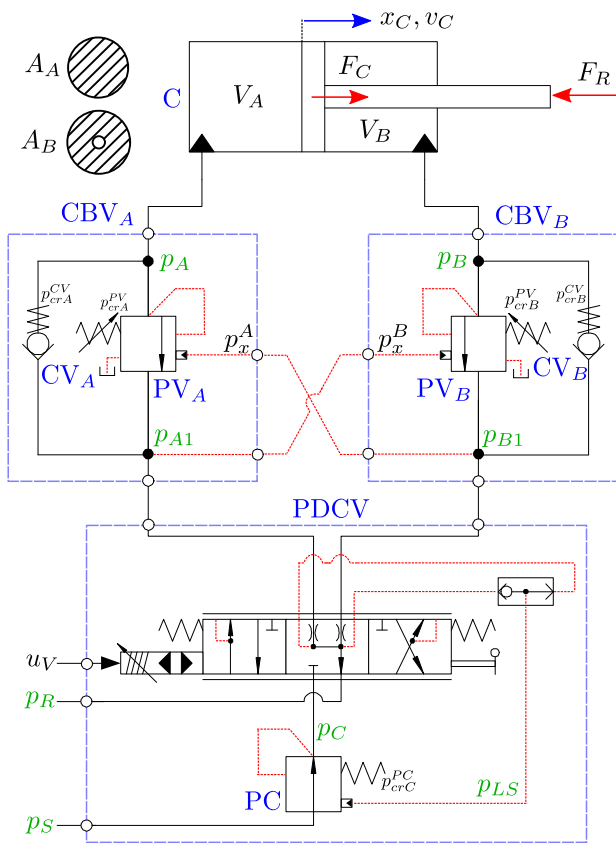
$$\dot{E}_{Out}^{Mech} = F_R v_C. \quad (31)$$

96

Figure 10: Valve-controlled cylinder architecture.

4. Self-Contained System

The self-contained electro-hydraulic cylinder drive concept investigated in Hagen et al. (2018) and successfully implemented and tested in Padovani et al. (2019) is scaled to the MA and GAs cylinders dimensions selected for the benchmark system. The combination of a Servo-Motor (SM) and a fixed-displacement hydraulic machine (P) drives the cylinder arranged in a closed-circuit configuration, as illustrated in Fig. 11.
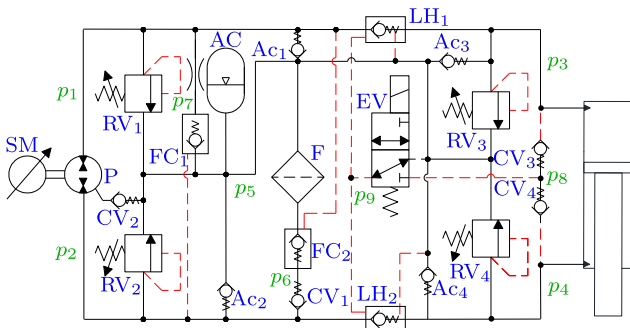

Figure 11: Self-contained cylinder architecture.

The differential flow dictated by the cylinder's unequal areas is balanced by two pilot-operated check

valves (FC$_{1-2}$), by the Anti-cavitation valves (Ac$_{1-2}$) and the Check Valve CV$_1$. The bladder accumulator (AC) represents the sealed reservoir of the SCC. The Pilot-Operated Check Valves (POCV) LH$_1$ and LH$_2$ are used for passive load-holding purposes by isolating the cylinder when the 3/2 electro-valve (EV) is not actuated. To enable motion, the EV is actuated resulting in transferring the highest cylinder pressure, selected through the CV$_3$ and CV$_4$, into the opening pilot line of LH$_1$ and LH$_2$. Pressure Relief Valves (RV$_{1-4}$) are installed on both pump ports and on both cylinder ports to avoid over-pressurizations. Ac valves (Ac$_{3-4}$) are also connected to the cylinder chambers. Finally, the low pressure filter (F) is comprised in the system.

To benefit from the energy recovery capability of the SCC, this paper proposes the system layout as shown in Fig. 12 to drive the MA and GAs of the considered PRM.
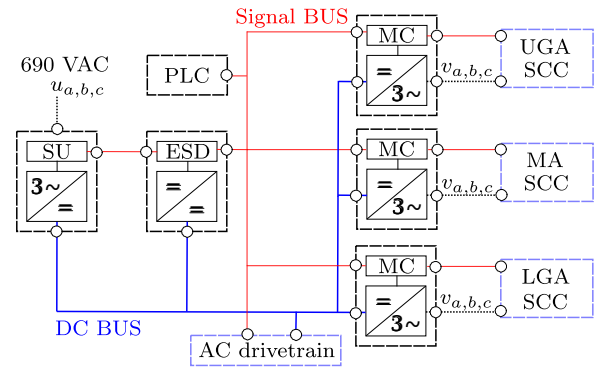
Figure 12: Proposed electric power distribution layout when using self-contained cylinders together with existing AC drivetrains (simplified schematic).

The Supply Unit (SU) converts the AC voltage from the electric grid to a DC bus voltage that is shared with the individual DC to AC PWM inverters controlled by a Motion Controller (MC). The MC includes a cascaded controller that takes care of cylinder position, pressure-feedback, and the servo-motor's speed through a space vector PWM controller (field oriented control). For additional energy storage (i.e., when the winch is lowering, the travel or slew motors are braking) and for emergency operation, in case of power shut down, a Electrochemical Storage Device (ESD) (i.e., a battery) is connected to the DC bus through a DC/DC converter. An industrial Programmable Logic Controller (PLC) is used, in combination with emergency stop modules, for safety functionalities, motion trajectory generators, and is communicating with the SCC's I/Os and the MCs, SU, and ESD, using a standard bus communication protocol (e.g, Profinet, Profibus, Sercos, etc.).

4.1. Sizing of Components

Equivalent components to the ones used in the reference concept (Padovani et al., 2019) are scaled according to the flow and pressure (power) requirements used when sizing the benchmark system. The selected SMs are suitable for potentially explosive environments.

Table 6: Selected components for the SCCs.

	Description	MA	GAs
SM:	Rexroth MKE	118B-024	098B-047
P:	Rexroth A10FZG	18 $[cm^3]$	6 $[cm^3]$
F:	Rexroth 10 TEN	95 $[\frac{l}{min}]$	62 $[\frac{l}{min}]$
AC:	Rexroth HAB-CE	20 $[l]$	10 $[l]$
EV:	Argo-H. SD1E-A3	30 $[\frac{l}{min}]$	30 $[\frac{l}{min}]$
LH:	SUN CVEV XFN	120 $[\frac{l}{min}]$	60 $[\frac{l}{min}]$
FC:	SUN CKEB XCN	120 $[\frac{l}{min}]$	60 $[\frac{l}{min}]$
CV$_1$:	Hawe RB2	50 $[\frac{l}{min}]$	50 $[\frac{l}{min}]$
CV$_2$:	Hawe RK4	120 $[\frac{l}{min}]$	120 $[\frac{l}{min}]$
CV$_{3-4}$:	Hawe RK2	50 $[\frac{l}{min}]$	50 $[\frac{l}{min}]$
Ac$_{1-2}$:	Hawe RK4	120 $[\frac{l}{min}]$	120 $[\frac{l}{min}]$
Ac$_{3-4}$:	Hawe RB2	50 $[\frac{l}{min}]$	50 $[\frac{l}{min}]$
RV$_{1-4}$:	SUN RD	95 $[\frac{l}{min}]$	45 $[\frac{l}{min}]$

4.2. System Modeling

The servo-motor, a surface mounted permanent magnet synchronous motor, and the variable speed driver, using field-oriented control (vector control), is modeled based on the work of Harnefors (2003). The hydraulic circuit for the MA and GAs SCCs, are modeled based on Padovani et al. (2019) where a similar system is modeled and validated on a single-boom crane. The equations used in the numerical model of the SCCs are listed in Section (A.2). The force balance of the piston in eq. (60), that are interfacing with the MBS, is considered as well as the well-known pressure build-up equation that is applied several times to evaluate the system pressures elucidated in Fig. 11.

5. Simulation Results

First, an inverse dynamic analysis is carried out for design purpose and the driving cycles (i.e., the motion and load cycle) for the desired operational sequence (reach, winch, slew and trolley motion) are formulated. The MA and GAs kinematics are thereafter validated, and the output power that each actuator must deliver is estimated, together with an analysis of the mechanical energy of the arms that have potential to be regenerated when using SCCs. Secondly, the motion performance, power consumption, and efficiency of the

benchmark system and the self-contained system are presented, and finally, the energy consumptions of both systems are compared.

5.1. Inverse Dynamic Analysis

5.1.1. Actuator Force

It was found that the scissor mechanism of the MA tends to have high gearing ratio in the inner position ($x_C^{MA} = 1.5 - 1.7$ [m]), causing high peaks in the reaction force when accelerating or decelerating. Fig. 13 demonstrates the actuator force for maximum load and with the considered operational load, i.e., a quadruple stand of $5\frac{7}{8}$ [Inch] (149.3 [mm] in diameter) drill-pipes.
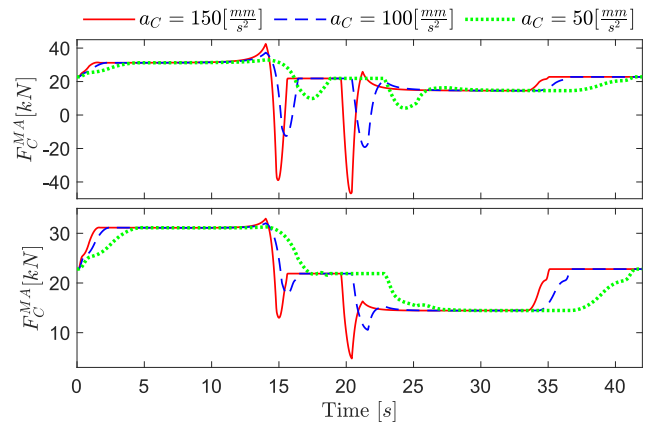

Figure 13: MA cylinder force at different acceleration profiles: (top) with max payload (14 [mT]); (bottom) with normal operational payload (1.5 [mT]).

To reduce the force peak, the acceleration set-point ($a_{C_{SP}} = 50 \left[\frac{mm}{s^2}\right]$, green line in Fig. 13) is chosen as low as possible for the given stroke length and velocity.

5.1.2. Considered Motion Cycles

The generated motion trajectories for the MA cylinder and the GAs cylinders for the considered operation sequence are plotted in Fig. 14. The generated motion trajectories for the reach arms, winch actuator (x_W [m] and v_W [$\frac{m}{s}$]), trolley actuator (x_T [m] and v_T [$\frac{m}{s}$]), and the slew actuator (θ_S [rad] and ω_S [$\frac{rad}{s}$]) are plotted in Fig 15.

5.1.3. Load Cycles

The resulting actuator load cycles from the inverse dynamics are demonstrated in Fig. 16 for the reach arms cylinders, and in Fig. 17 for the winch, trolley and slew actuators. From Fig. 16, it can be seen that the highest force in the MA cylinder is when the PRM is slewing
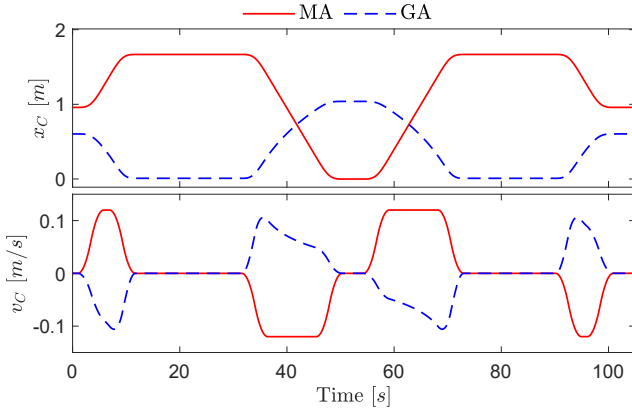
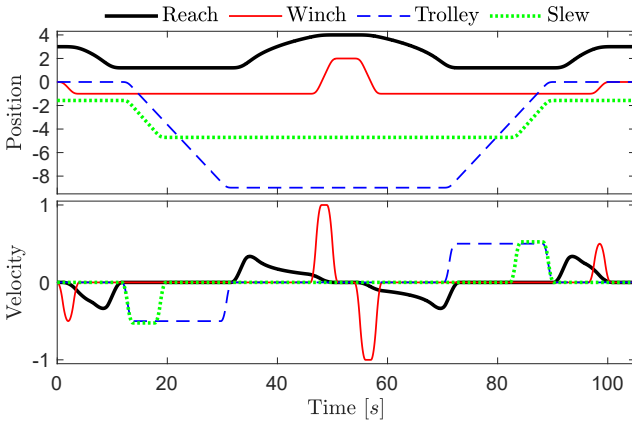Figure 14: MA and GAs motion reference: (top) position; (bottom) velocity.

Figure 15: Generated motion trajectories: (top) position reference x_R [m], x_W [m], x_T [m], and θ_S [rad]; (bottom) velocity reference v_R [$\frac{m}{s}$], v_W [$\frac{m}{s}$], v_T [$\frac{m}{s}$], and ω_S [$\frac{rad}{s}$].
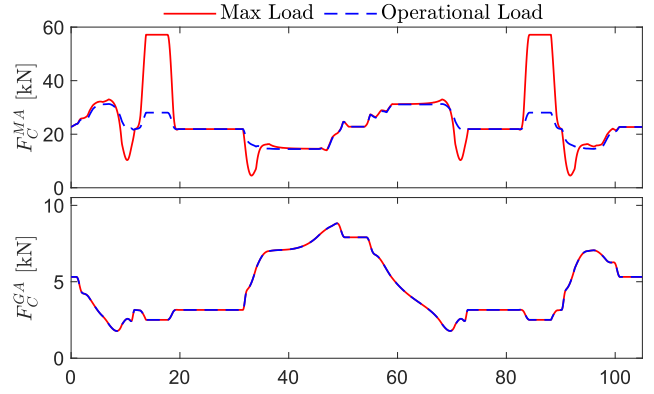

Figure 16: Actuator load cycle at max load and operational load: (top) main arm; (bottom) guide arms.
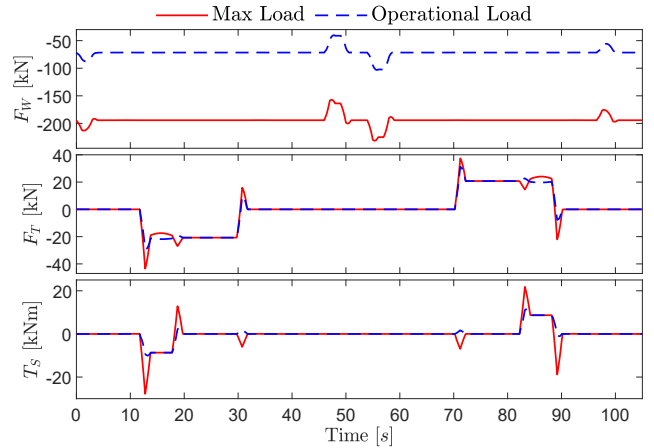
Figure 17: Actuator load cycle at max load and operational load: (top) winch; (middle) trolley; (bottom) slew.

with maximum load. This is because of the resulting centripetal force from the moving drill-stand.

5.1.4. Energy Saving Potential

The simulated actuators output power in Figs. 18-19 gives an indication of the energy recovery potential during the considered operational sequence. When the output power has a negative sign then the actuator is exposed to overrunning load (i.e., velocity and force/torque have the same direction) and the SCC have the potential to recover energy.

From Fig. 20 it is demonstrated that the energy consumed to actuate the PRM during the considered motion sequence is 888 [kJ] without energy recovery, and 644 [kJ] if considering 100% efficient regeneration. Hence, the potential energy that can be regenerated is 244 [kJ] (27.5%).

Based on the considered operational sequence, Table 7 displays at which steps the actuators are in use

or not during the different cycle steps and specifies if an actuator can potentially regenerate energy (overrunning load), highlighted using green letters or consuming energy (resistant load), highlighted in red.

Table 7: Actuation overview.

Step:	0-1	1-2	2-3	3-4	4-3	3-2	2-1	1-0
R_{MA}:	on	off	off	on	on	off	off	on
R_{GAs}:	on	off	off	on	on	off	off	on
W:	on	off	off	on	on	off	off	on
T:	off	on	on	off	off	on	on	off
S:	off	on	off	off	off	off	on	off

From the presented inverse dynamic analysis, it is clear that the actuators that can potentially regenerate energy are the MA, the GAs, and the winch. Additionally, when the trolley and slew actuators are braking (decelerating), there is a short period when the actuators can regenerate energy. Furthermore, when the MA
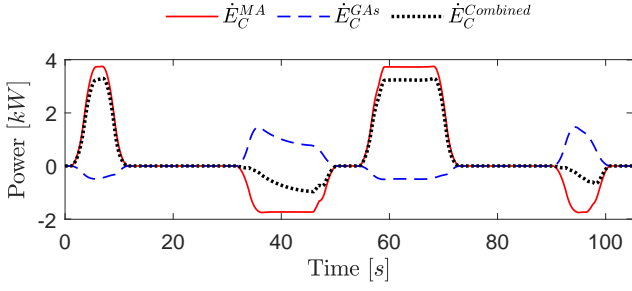
99

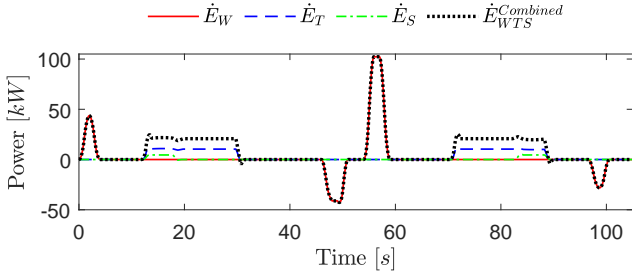Figure 18: Main arm and guide arms; actuator output power.

Figure 19: Winch, trolley and slew; actuator output power.

Figure 20: The total energy consumption of all actuators.
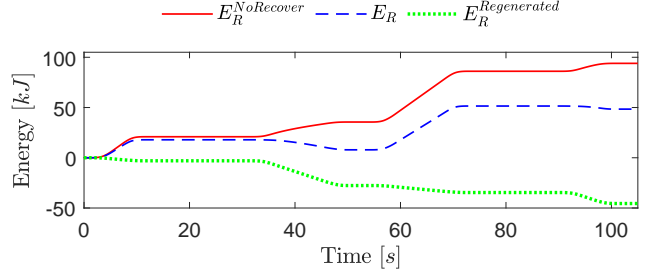
Figure 21: Energy consumption of the reach arm actuators.

regenerates energy the GAs consume energy and vice versa. Hence, by introducing self-contained electro-hydraulic cylinders connected to a common DC bus (Fig. 12) there is potential to directly supply electrical power to the GAs when the MA is regenerating, and when the GAs is regenerating, the demanded power from the grid to actuate the MA may be reduced.

When considering the reach motion separately, it can be seen from Fig. 21, that by sharing the energy between the MA and the GAs, the energy consumption of the reach motion, potentially, can be reduced with almost 50%.

Furthermore, using an external storage device, i.e., a battery pack, the regenerated energy from the winch during other operations not detailed in this study and the remaining energy from the MA can be stored and reused, resulting in further energy savings.

5.2. Benchmark System

The numerical model of the induction motor and of the hydraulic system (Appendix (A.1)) representing the benchmark system is simulated according to the motion reference of the considered operational cycle (Figs. 14-15) evaluated in the inverse dynamic analysis. The performance of the different subsystems (i.e, the hydraulic power unit, the transmission lines, the main arm VCC, and the two guide arms VCCs) are demonstrated.

In Fig. 22, the effective magnitudes of the HPU when idling (i.e., when no motion is demanded) is for the
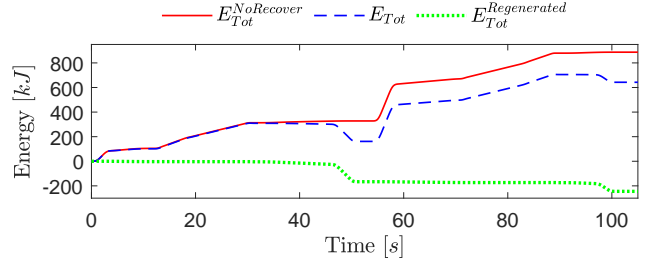
pump pressure $p_P = 125$ $[bar]$, pump displacement $D_P = 1.9$ $[\frac{cm^3}{rev}]$, pump flow $Q_P = 0$ $[\frac{l}{min}]$, and pump torque $T_P = 19.7$ $[Nm]$.

When maximum velocity is demanded, the pump displacment increases up to about $D_P = 56$ $[\frac{cm^3}{rev}]$ resulting in an output flow of $Q_P = 80$ $[\frac{l}{min}]$ and in a required torque of $T_P = 125.4$ $[Nm]$.
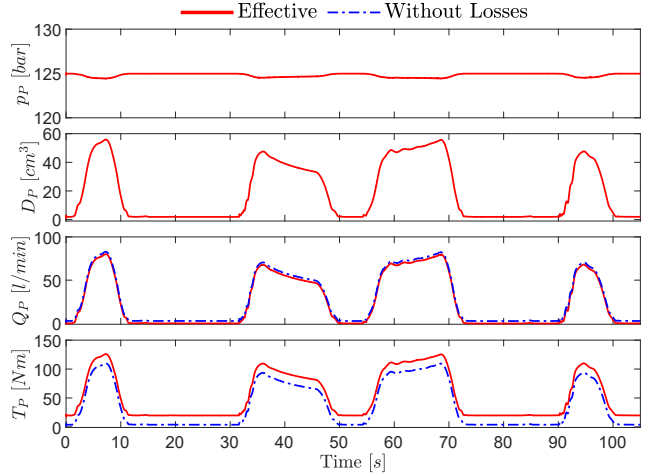

Figure 22: Hydraulic power unit performance.

In Fig. 23, the highest pressure drop of the supply and return lines are for the main arm $\Delta p_S^{MA} = 12.6$ $[bar]$ and $\Delta p_R^{MA} = 5.9$ $[bar]$, the upper guide arm $\Delta p_S^{UGA} = 8.0$ $[bar]$ and $\Delta p_R^{UGA} = 3.7$ $[bar]$, and the lower guide arm $\Delta p_S^{LGA} = 10.3$ $[bar]$ and $\Delta p_R^{LGA} = 6.0$ $[bar]$.

From Fig. 24, the highest error of the reach position
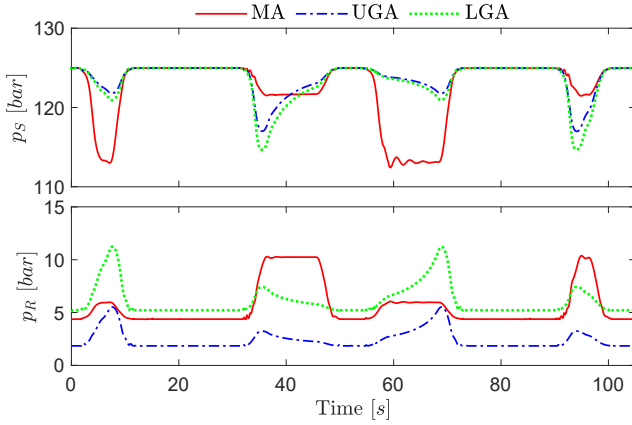
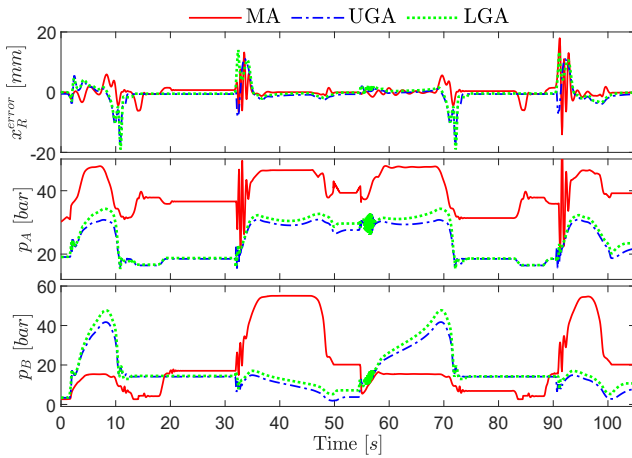Figure 23: Transmission line pressures.

Figure 24: Reach arms performance.

is 14 $[mm]$ for the main arm, 17.5 $[mm]$ for the upper guide arm, and 19 $[mm]$ for the lower guide arm. The resulting accuracy is acceptable since the drill-stand can move freely within a tolerance of 50 $[mm]$ when guided during the reach motion. The pressures in the cylinders behave as expected, and there are limited fluctuations when the cylinder starts to move.

The power consumption of the different elements of the benchmark subsystems are highlighted in Fig. 25.

The dominating losses of the benchmark system are illustrated in Fig. 26 and consist of the following terms:

- Induction motor – electric and mechanical losses (copper, Eddy current, hysteresis and viscous friction)

- Hydraulic pump – volumetric losses (leakage) eq. (14) and hydro-mechanical losses (friction) eq. (15)

- Transmission lines – hydraulic friction losses (pressure drop) eq. (19)
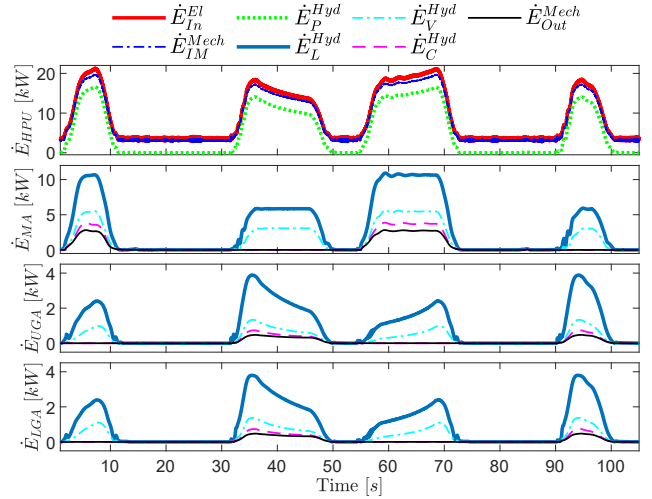
- Control valves – throttling losses eq. (53)

Figure 25: Power consumption of hydraulic power unit, main arm, upper guide arm, and lower guide arm.

- Load-holding valves – throttling losses eq. (53)

- Cylinder and arm mechanism – combined friction losses of the cylinders and the mechanical system eq. (8).

The average hydraulic efficiency when considering the VCCs separately, using the power from the supply line as input, is 21.6% for the main arm and 11.5% for the guide arms.

5.3. Self-Contained System

The numerical model of the self-contained system (Appendix (A.2)), includes the electro-hydraulic model of the main arm's SCC and two identical SCCs for the two guide arms.

The effective magnitudes of the SCC's motor-pump unit when idling are for the pump supply pressures $p_1^{MA} = 0.23$ $[bar]$ and $p_1^{GA} = 0.51$ $[bar]$ (Fig. 27), the suction pressure $p_2^{MA} = 0.25$ $[bar]$ and $p_2^{GA} = 0.53$ $[bar]$ (Fig. 28). From Fig. 29, the rotational speed of the SMs is 0 $[rpm]$, the supply flow is 0 $[\frac{l}{min}]$, and the torque of the pumps are 0 $[Nm]$. It is shown that the SCCs do not demand any power when not moving, compared to the benchmark system where the HPU is constantly supplying flow to maintain the desired pressure level. The system pressures behave as expected when the SCCs are delivering maximum velocity.

In Fig. 30, the highest error for the reach position are 10.2 $[mm]$ for the main arm, 4.4 $[mm]$ for the upper guide arm, and 3.9 $[mm]$ for the lower guide arm.

The power consumptions of all elements (components) of the SCCs are plotted in Fig. 31, and in Fig. 26 the Sankey diagram is illustrating the energy distri-
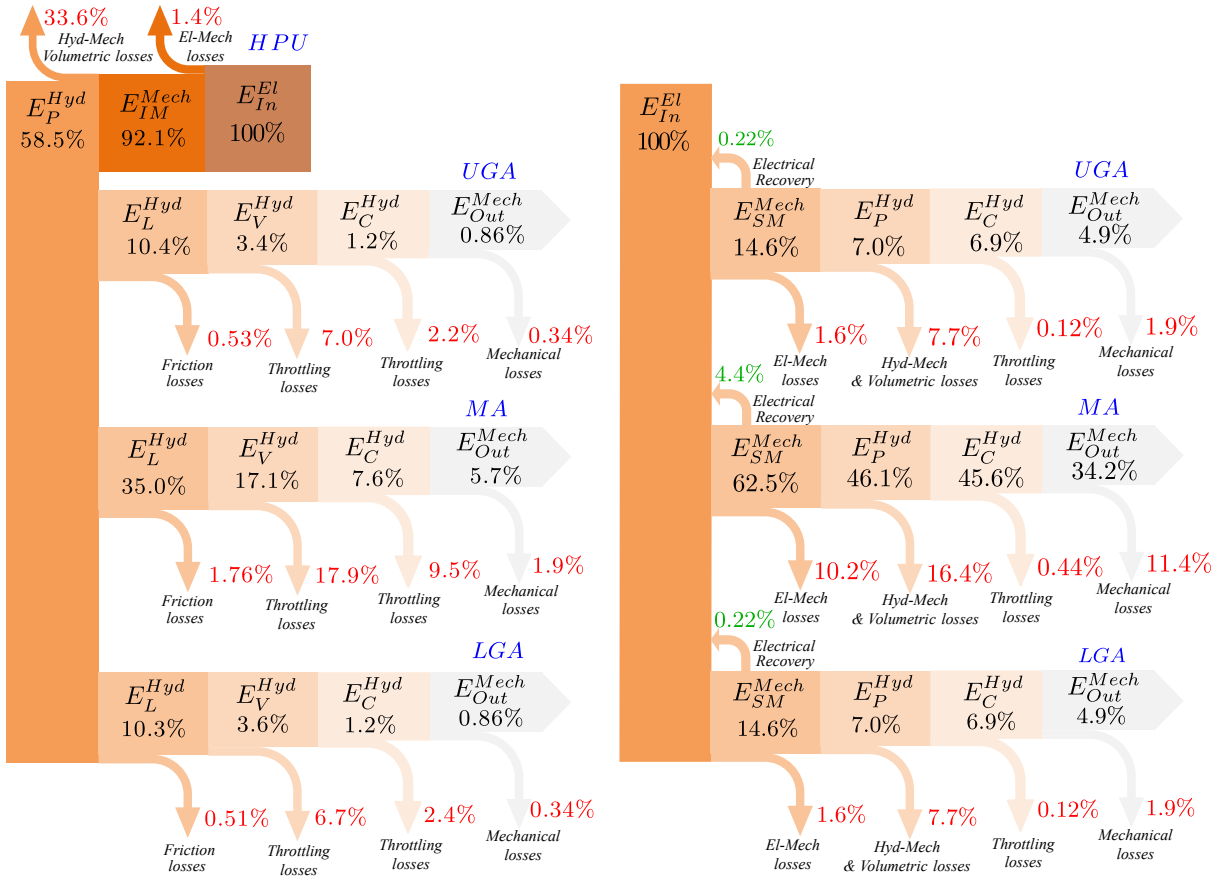
101

Figure 26: Sankey diagrams showing the energy distribution from electrical input to mechanical output: (left) benchmark system; (right) self-contained system.

bution from electrical input to mechanical output together with the following losses:

- Servo-motor – electric and mechanical losses (copper, Eddy current, hysteresis and viscous friction)

- Hydraulic pump – volumetric losses (leakage) eq. (14) and hydro-mechanical losses (friction) eq. (15)

- Load-holding valves: throttling losses eq. (71)

The average electro-hydraulic efficiency when considering the SCCs separately is 62.8% for the main arm and 42.7% for the guide arms.

The input power when the arms extend into the fingerboard (Fig. 31 between 31-52 [s]), is for the MA -1.06 [kW] at the highest, meaning that up to 1.06 [kW] can be recovered, i.e., shared with the two GAs that are consuming 1.50 [kW] each at its maximum. When the arms retract the power consumption is for the MA 5.86 [kW] and for each of the GAs 0.49 [kW].

5.4. Energy Comparison

In Fig. 32, the overall power and energy consumption of the benchmark system and self-contained system are compared. The energy saving potential using self-contained electro-hydraulic cylinders versus centralized valve-controlled cylinders is 83.44%.

Moreover, the total consumption of the self-contained system is highlighted in Fig. 33, comparing the electric power and the energy consumption when energy recovery is applied or not for the considered system. From Fig. 33, it is clear that by enabling energy sharing between the main arm's SCC and the guide arm's SCCs, the overall energy consumption is improved by 6%. However, if pumps with a better efficiency were available (e.g., a constant hydro-mechanical efficiency of 90%) energy recovery would also be enabled for the guide arms SCCs, resulting in 45% less energy consumption compared to the considered self-contained cylinders with higher simulated pump losses.
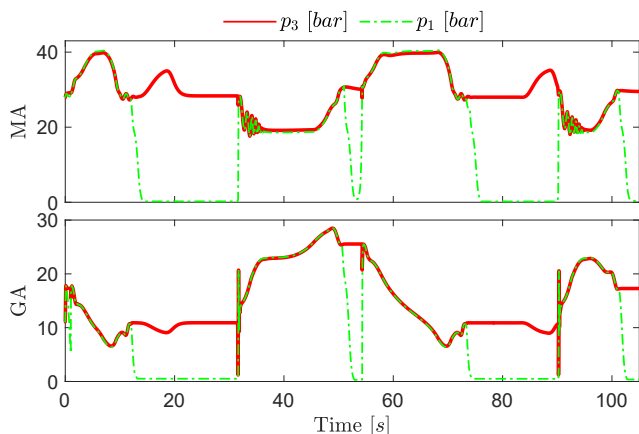
Figure 27: SCC's high pressures: (red) piston-side chamber; (green) pump supply.
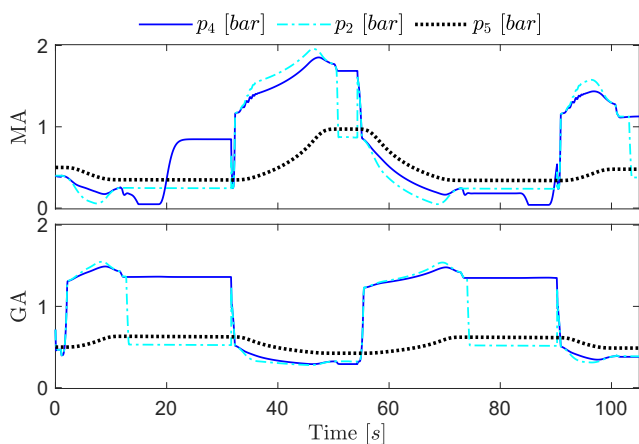

Figure 28: SCC's low pressures: (blue) rod-side chamber; (light blue) pump's suction-side; (black) accumulator.
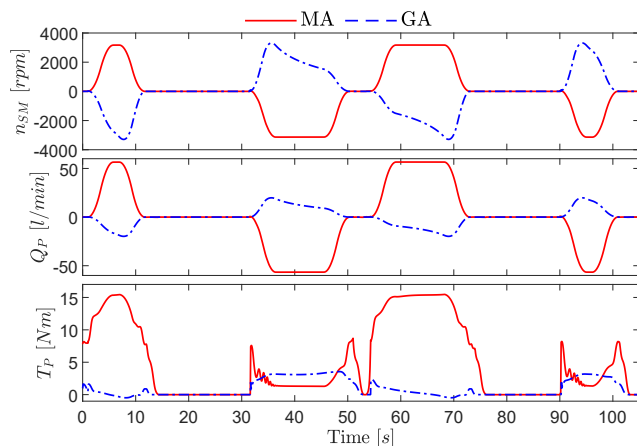

Figure 29: Performance of motor-pump unit: (top) rotational speed of the servo-motors; (middle) supplied flow to the cylinders; (bottom) torque demand of the pumps.
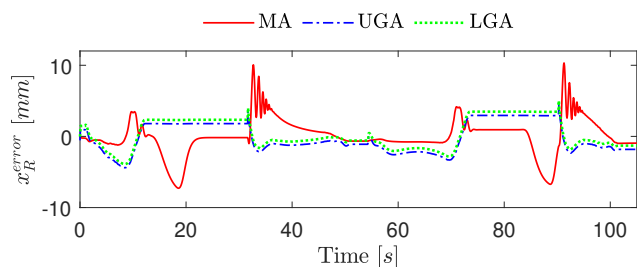

Figure 30: Reach arms position error using SCCs.

6. Discussion

For the considered case-study, both the benchmark system and the self-contained system can follow the desired motion profile with acceptable position errors for the reach arms that are moving synchronously. The self-contained system has approximately 37% lower maximum position error. Moreover, this section discusses the energy saving potential and some practical challenges that must be considered in future works.

6.1. Energy Saving Potential

When considering the power from the mechanical system, and assuming 100% efficient energy recovery, there is a potential for the considered offshore drilling application to regenerate 27.5% during the operational sequence. However, due to the hydro-mechanical losses of the hydraulic axial piston machine (65-92% depending on the rotational speed and pressure drop across

the pump), the potential power from the mechanical system is dissipating in the hydraulic machine. Consequently, only 6% of the total energy (when considering the energy consumption of the reach motion separately) can potentially be recovered, compared to 45%, if a hydraulic machine with a constant hydromechanical efficiency of 90% is used.

Compared to the benchmark system representing the hydraulic actuation system used today, applying the considered self-contained cylinders instead of centralized valve-controlled cylinders to drive the reach arms, the energy saving potential is 83.44% without affecting the system's performance (e.g., the position tracking results even better). Furthermore, applying more efficient pumps to the self-contained system results in an energy saving potential of 91.1%, and 88.33% when considering a more efficient pump for the benchmark system as well. The superior energy efficiency of the self-contained system is also due the "power on demand" capability: when the cylinders are idling (i.e., when the PRM moves between the WC and FB), then the passive load-holding valves are activated and the electric-drive is switched off. Conversely, the hydraulic power unit of the benchmark system is always running to maintain a constant supply pressure. Also, us-
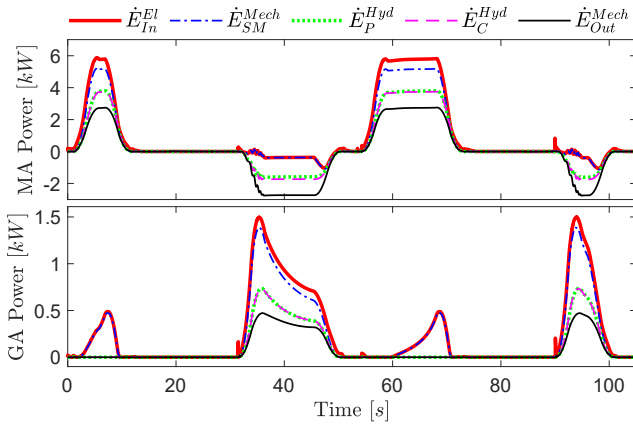
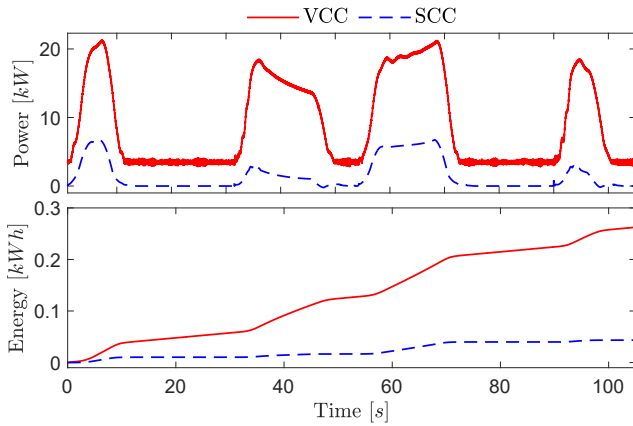Figure 31: Power consumption of the main arm and guide arms SCCs.

Figure 32: Energy comparison between benchmark system and self-contained system.
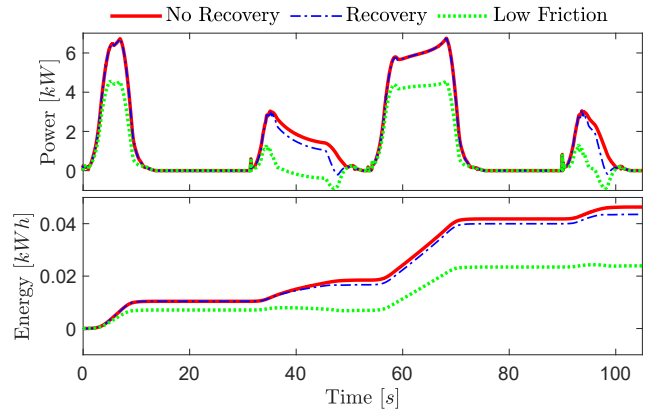

Figure 33: Comparison of the total energy consumption of the self-contained system without and with energy recovery, and with increased efficiency of the pump.

ing pilot-operated check valves as load-holding valves is much more energy efficient since flow throttling is almost negligible during motion. This is not the case for the counter-balance valves that waste approximately 134 $[kJ]$ to enable the main arm cylinder to retract, while the SCC can regenerate energy.

6.2. Challenges

The scissor mechanism used in the main arm introduces high force peaks in the inner position when accelerating or decelerating. Consequently, the desired dynamic response of the actuation system is a trade-off between cost and motion cycle time. Higher accelerations require an electric-drive with higher torque, and current limits, while the reaction force acting on the hydraulic cylinder will require a larger rod diameter due to the buckling factor criterion. Hence, designing the actuation system for the maximum load results in a non-optimal solution because of the oversized cylinder (due to the buckling safety factor) and

the high friction pump (during the operational load cycle, the required cylinder pressure is low, and hydraulic pumps, in general, have low hydro-mechanical efficiency when the pressure drop across the pump is low at high speed). Furthermore, energy efficiency may be further improved by designing the application so that the relation between actuator pressures and pump efficiency is optimal.

Currently, the motor drivers (frequency converters) of the AC drivetrains are located away from the machine. For each drivetrain, there is one electric power cable between the driver located in a centralized control-cabinet and the electric motor. In the proposed layout, as seen in Fig. 12, the motor drivers are located on the machine close to the actuator and there is only one power cable interfacing with the machine. Furthermore, on the machine, there is a common DC bus shared between the individual DC to AC inverters. This solution has the potential to save much space on the rig, and there will be fewer cables on the machine, compared to using a centralized control-cabinet. However, in explosive environments (Ex), such as on a drilling rig, all components need to be ATEX certified according to European Commission (2014). Consequently, the inverters (that today are not available for Ex environments) need to be located in ATEX certified junction boxes that take some extra space.

Furthermore, the AC drivetrains used today consist of induction motors that are well proved for the offshore end Ex environment. In SCCs the permanent magnet synchronous motors are preferred, mainly because of the superior power density, better efficiency, and controllability, compared to IMs.

Finally, the size and weight of the actuator itself (i.e., the cylinder) will increase using the self-contained concept compared to the conventional system. An example
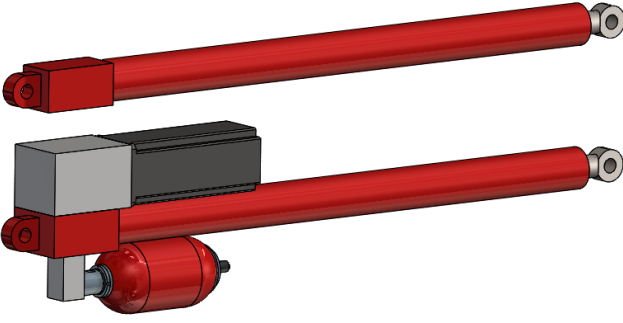
104

Figure 34: Size comparison – main arm cylinder (simplified CAD models).

is illustrated in Fig. 34 where the main arm's SCC is compared against the VCC using the same cylinder dimensions, when selecting the servo-motor, pump, and auxiliary-valves according to Table 6.

Depending on the application, it may be challenging to install the SCC without doing re-design of the mechanical system. Hence, the whole machine design should be optimized around the SCC system when designing new applications.

7. Conclusion

This paper presents a simulation study to identify the energy saving potential when self-contained electro-hydraulic cylinders are applied to an offshore pipe racking machine. This approach is an alternative to conventional valve-controlled cylinders used nowadays. To have a fair comparison between the energy consumption of the benchmark system and the new self-contained system, both actuation systems have been designed based on the same requirements identified from an inverse dynamic analysis of the considered case-study. Numerical models representing all dominating loss elements of the actuation systems, from electrical input to the desired motion of the mechanical system, are considered.

This paper proposes an actuation system consisting of three self-contained cylinders that can share energy. Due to the "power on demand" capability, the cancellation of the throttling losses, and the opportunity to recover energy in motoring quadrants, the self-contained system demonstrates a superior energy efficiency compared to the benchmark system without affecting the system's performance. For the selected driving cycle, the benchmark system consumes 0.26 $[kWh]$ of electrical energy, while the self-contained system consumes 0.044 $[kWh]$ (i.e., 83.44% less energy) if ideal energy sharing is assumed.

This result suggests that potential for significant energy savings exists when using the proposed self-contained system for actuating the reach arms of the pipe racking machine. On an offshore drilling rig, reduced electric energy consumption will result in reduced consumption of fossil fuel of the diesel generators supplying the offshore installation with electricity. Additionally, by introducing the proposed actuation system that is self-sufficient and completely sealed, offshore mechatronic applications can reduce the risk of oil pollution to the ocean environment when compared to using centralized hydraulic power units.

Acknowledgments

Nomenclature

Symb.	Description	Unit
V_L	RMS voltage	$[V]$
A_{peak}	Peak amplitude	$[V]$
v_s^s	Stator-voltage	$[V]$
T_{32}	Clarke transformation	
i_s^s	Stator-current	$[A]$
Ψ_{r1}^s	Rotor fluxes cage 1	$[Vs]$
Ψ_{r2}^s	Rotor fluxes cage 2	$[Vs]$
j	Imaginary unit	
ω_m	Mech. angular velocity	$\left[\frac{rad}{s}\right]$
ω_r	Electrical angular velocity	$\left[\frac{rad}{s}\right]$
T_{em}	Electromagnetic torque	$[Nm]$
p	Number of poles	$[-]$
L_{r1}	Rotor inductance cage 1	$[H]$
L_{r2}	Rotor inductance cage 2	$[H]$
L_m	Mutual inductance	$[H]$
L_λ	Total inductance	$[H]$
T_P	Pump torque	$[Nm]$
B_f	Viscous friction coefficient	$\left[\frac{Nms}{rad}\right]$
J_{tot}	Combined inertia	$\left[\frac{rad}{s}\right]$
$i_{a,b,c}$	Stator currents	$[V]$
T_{23}	Inv. Clarke transformation	
a_i	State space constant	$[W]$
F_R	Force delivered to the MBS	$[N]$
F_C	Hydraulic cylinder force	$[N]$
A_A	Piston area of the cylinder	$[m^2]$
A_B	Annulus area of the cylinder	$[m^2]$
p_i	Hydraulic pressure	$[Pa]$
$\dot{p}_i$	Pressure buildup	$\left[\frac{Pa}{s}\right]$

Continued from previous column

Symb.	Description	Unit
p_{cr}	Crack pressure	$[Pa]$
Q_{Vi}	Flow through valve	$[\frac{m^3}{s}]$
k_S	Flow loss gain supply line	$[-]$
k_R	Flow loss gain return line	$[\frac{m^3}{s}]$
p_{LS}	Load-sensing pressure	$[Pa]$
v_C	Cylinder velocity	$[\frac{m}{s}]$
V_i	Volume	$[m^3]$
B_i	Effective bulk modulus	$[Pa]$
x_C	Effective cylinder displacement	$[m]$
h_C	Max piston displacement	$[m]$
β_0	Bulk modulus	$[Pa]$
κ_{air}	Adiabatic air constant	$[-]$
p_{atm}	Atmospheric pressure	$[Pa]$
η_{air}	Volumetric air constant	$[\%]$
Δ_{pV}	Pressure drop across the valve	$[Pa]$
k_V	Flow constant of the valve	$[\frac{m^3}{s\sqrt{Pa}}]$
ξ_V	Effective valve opening	$[-]$
$G_V(s)$	Valve dynamic of the PDCV	$[-]$
ω_V	Natural frequency of the PDCV	$[\frac{rad}{s}]$
ζ_V	Damping ratio of the PDCV	$[-]$
p_{cr}	Cracking pressure of the valve	$[Pa]$
p_{fo}	Pressure to fully open the valve	$[Pa]$
α_i	Pilot ratio of the CBV	$[Pa]$
p_x	Pilot pressure of the CBV	$[Pa]$
L_s	Stator inductance	$[H]$
R_s	Stator resistance	$[Ohm]$
Ψ_R	Rotor flux	$[Vs]$
E^s	Back emf	$[V]$
θ	Flux angle	$[rad]$
K	Space vector scaling constant	$[-]$
i_q	Torque generating current	$[A]$
V_{AC_0}	AC pre-charge pressure	$[Pa]$
C_i	Hydraulic capacitance	$[\frac{Pa}{m^3}]$
C_d	Discharge coefficient	$[-]$
ξ_{NF}	Poppet lift normal flow	$[-]$
ξ_{RF}	Poppet lift reverse flow	$[-]$
A_S	Poppet seat area	$[m^2]$
F_{S_0}	Spring's pre-load force	$[N]$
k_S	Spring stiffness	$[\frac{N}{m}]$
A_x	Pilot stage area	$[m^2]$

A. Appendices

A.1. Benchmark System

The following equations represent the numerical model of the hydraulic power supply and the valve-controlled cylinders as depicted in Fig. 8 and 10.

$$\frac{d\mathrm{i}_s^s}{dt} = (a_{32b} + a_{32a}j\omega_r)\Psi_{r2}^s + a_{21}\Psi_{r1}^s + a_{33}\mathrm{i}_s^s \\ + b_3\mathrm{v}_s^s + (a_{31b} + a_{31a}j\omega_r)\Psi_{r1}^s \tag{32}$$

$$\mathrm{v}_s^s = \begin{bmatrix} \mathrm{Re}(v_\alpha) \\ \mathrm{Im}(v_\beta) \end{bmatrix} = \begin{bmatrix} u_a \\ u_b \\ u_c \end{bmatrix} T_{32} \tag{33}$$

$$\frac{d\Psi_{r1}^s}{dt} = (a_{11} + j\omega_r)\Psi_{r1}^s + a_{12}\Psi_{r2}^s + a_{13}\mathrm{i}_s^s \tag{34}$$

$$\frac{d\Psi_{r2}^s}{dt} = (a_{22} + j\omega_r)\Psi_{r2}^s + a_{21}\Psi_{r1}^s + a_{23}\mathrm{i}_s^s \tag{35}$$

$$T_{em} = \mathrm{Im}(\Psi_{r1}^s \mathrm{i}_s^s)\frac{pL_{r2}L_m}{3L_\lambda} + \mathrm{Im}(\Psi_{r2}^s \mathrm{i}_s^s)\frac{pL_{r1}L_m}{3L_\lambda} \tag{36}$$

$$\frac{d\omega_m}{dt} = \frac{T_{em} - T_P - B_f\omega_m}{J_{tot}} \tag{37}$$

$$T_P = \frac{D_P\Delta_{p,i}}{2\pi} + T_S sign(\omega_m) \tag{38}$$

$$\omega_r = \frac{p}{2}\omega_m \tag{39}$$

$$\begin{bmatrix} i_a \\ i_b \\ i_c \end{bmatrix} = \begin{bmatrix} \mathrm{Re}(i_\alpha) \\ \mathrm{Im}(i_\beta) \end{bmatrix} T_{23} = \mathrm{i}_s^s T_{23} \tag{40}$$

$$F_R^{VCC} = \underbrace{p_A A_A - p_B A_B}_{F_C} - F_f \tag{41}$$

$$\dot{p}_P = \frac{\beta_P(Q_P - Q_{RV})}{V_{P_0}} \tag{42}$$

$$Q_P = D_P\omega_m - Q_S sign(\omega_m) \tag{43}$$

$$\dot{p}_{A1} = \frac{\beta_{A1}(Q_{V_{In}} - Q_{CV_A} + Q_{PV_A})}{V_{A1_0}} \tag{44}$$

$$\dot{p}_A = \frac{\beta_A(Q_{CV_A} - A_A v_C - Q_{PV_A})}{A_A x_C + V_{A_0}} \tag{45}$$

$$\dot{p}_{B1} = \frac{\beta_{B1}(Q_{V_{Out}} - Q_{CV_B} + Q_{PV_B})}{V_{B1_0}} \tag{46}$$

106

$$\dot{p}_B = \frac{\beta_B(Q_{CV_B} + A_B v_C - Q_{PV_B})}{A_B(h_C - x_C) + V_{B_0}} \quad (47)$$

$$\dot{p}_S = \frac{\beta_S(\sqrt{\frac{1}{k_S}\frac{2}{\rho}|p_P - p_R|} - Q_{V_{In}})}{V_{S_0}} \quad (48)$$

$$\dot{p}_R = \frac{\beta_R(Q_{V_{Out}} - \sqrt{\frac{1}{k_R}\frac{2}{\rho}|p_R - p_T|})}{V_{R_0}} \quad (49)$$

$$p_C = \begin{cases} p_{LS} + p_{crC}^{PC}, & p_{crC}^{PC} \le (p_S - p_{LS}) \\ p_S - p_{LS}, & 0 < (p_S - p_{LS}) < p_{crC}^{PC} \\ p_{LS}, & (p_S - p_{LS}) \ge 0 \end{cases} \quad (50)$$

$$p_{LS} = \begin{cases} p_{A1}, & \xi_V < 0 \\ p_R, & \xi_V = 0 \\ p_{B1}, & \xi_V > 0 \end{cases} \quad (51)$$

$$\beta_i = \frac{1}{\frac{1}{\beta_0} - \frac{1}{\kappa_{air}(p_i + p_{atm})\left(\frac{\eta_{air}-1}{\eta_{air}(\frac{p_{atm}}{p_i - p_{atm}})^{\frac{1}{\kappa_{air}}}} - 1\right)}} \quad (52)$$

$$Q_V = k_V \xi_V \sqrt{|\Delta_{pv}|} sign(\Delta_{pV}) \quad (53)$$

$$G_V(s) = \frac{\xi_V}{u_V} = \frac{\omega_V^2}{s^2 + 2\omega_V\zeta_V s + \omega_V^2} \quad (54)$$

$$\xi_{CV} = \frac{\Delta_{pCV} - p_{cr,CV}}{p_{fo,CV}} \quad (55)$$

$$\xi_{PV} = \frac{p_{In,PV} + \alpha_i p_x - p_{cr,PV}}{p_{fo,PV}} \quad (56)$$

A.2. Self-Contained System

The following equations represent the numerical model of the self-contained electro-hydraulic cylinders as depicted in Fig. 11.

$$L_s \frac{d\mathrm{i}_s^s}{dt} = \mathrm{v}_s^s - R_s \mathrm{i}_s - \underbrace{j\omega_r \Psi_R e^{j\theta}}_{E^s} \quad (57)$$

$$T_{em} = \frac{3p}{2K^2} \mathrm{Im}(\Psi_R i_q) \quad (58)$$

$$J_{tot} \frac{d\omega_m}{dt} = \frac{3p}{2K^2} T_{em} - T_P \quad (59)$$

$$F_R^{SCC} = \underbrace{p_3 A_A - p_4 A_B}_{F_{C,i}} - F_{f,i} \quad (60)$$

$$\dot{p}_1 = \frac{\beta_1(Q_P + Q_{FC_1} - Q_{LH_1} - Q_{RV_1} - Q_{Ac_1})}{V_{1_0}} \quad (61)$$

$$\dot{p}_2 = \frac{\beta_2(-Q_P - Q_{CV_1} + Q_{Ac_2} - Q_{LH_2} - Q_{RV_2})}{V_{2_0}} \quad (62)$$

$$\dot{p}_3 = \frac{\beta_3(Q_{LH_1} - A_A v_C - Q_{RV_3} + Q_{Ac_3} - Q_{CV_3})}{V_{3_0} + A_A x_C} \quad (63)$$

$$\dot{p}_4 = \frac{\beta_4(Q_{LH_2} + A_B v_C - Q_{RV_4} + Q_{Ac_4} - Q_{CV_4})}{V_{4_0} + A_B(h_C - x_C)} \quad (64)$$

$$\dot{p}_5 = \frac{Q_{RV_{1-4}} + Q_{EV} - Q_{FC_{1-2}} - Q_{Ac_{1-4}}}{C_5} \quad (65)$$

$$\dot{p}_6 = \frac{\beta_6(Q_{CV_1} + Q_{FC_2})}{V_{6_0}} \quad (66)$$

$$\dot{p}_7 = \frac{\beta_7(Q_{OR} - Q_{FC_1})}{V_{7_0}} \quad (67)$$

$$\dot{p}_8 = \frac{\beta_8(Q_{CV_3} + Q_{CV_4} - Q_{EV})}{V_{8_0}} \quad (68)$$

$$\dot{p}_9 = \frac{\beta_9 Q_{EV}}{V_{9_0}} \quad (69)$$

$$C_5 = \frac{V_{5_0}}{\beta_5} + \frac{V_{AC_0}}{\kappa_{air}} \frac{p_{AC_0}^{\frac{1}{\kappa_{air}}}}{p_5^{\frac{\kappa_{air}+1}{\kappa_{air}}}} \quad (70)$$

$$Q_{POCV} = C_d \pi d \xi_j \sqrt{\frac{2}{\rho}|\Delta_p|} sign(\Delta_p) \quad (71)$$

$$\xi_{NF} = \frac{(p_{In} - p_{Out})A_S - F_S}{k_S} \quad (72)$$

$$\xi_{RF} = \frac{(p_x - p_{In})A_x + (p_{In} - p_{Out})A_S - F_{S_0}}{k_S} \quad (73)$$

$$Q_V = \begin{cases} 0, & \text{if } p_{In} < p_{Out} + p_c \\ k_V(p_{In} - p_{Out} - p_c), & \text{if } p_{In} \ge p_{Out} + p_c \end{cases} \quad (74)$$

107

References

Bak, M. K. *Model Based Design of Electro-Hydraulic Motion Control Systems for Offshore Pipe Handling Equipment.* Ph.D. thesis, University of Agder, 2014. doi:10.16373/j.cnki.ahr.150049.

Bak, M. K. and Hansen, M. R. Model based design optimization of operational reliability in offshore boom cranes. *International Journal of Fluid Power*, 2013. 14(3). doi:10.1080/14399776.2013.10801413.

European Commission. Directive 2014/34/EU of the European Parliament and of the Council. Technical report, Official Journal of the European Union L96, 2014.

Hagen, D., Padovani, D., and Choux, M. Design and Implementation of Pressure Feedback for Load-Carrying Applications With Position Control [Accepted]. In *The Sixteenth Scandinavian International Conference on Fluid Power*. 2019.

Hagen, D., Padovani, D., and Ebbesen, M. K. Study of a Self-Contained Electro-Hydraulic Cylinder Drive. *2018 Global Fluid Power Society PhD Symposium, GFPS 2018*, 2018. doi:10.1109/GFPS.2018.8472360.

Hagen, D., Pawlus, W., Ebbesen, M. K., and Andersen, T. O. Feasibility Study of Electromechanical Cylinder Drivetrain for Offshore Mechatronic Systems. *Modeling, Identification and Control*, 2017. 38(2). doi:10.4173/mic.2017.2.2.

Harnefors, L. *Control of Variable-Speed Drives.* Mälardalen University, 2003.

Ketelsen, S., Padovani, D., Andersen, T., Ebbesen, M., and Schmidt, L. Classification and Review of Pump-Controlled Differential Cylinder Drives. *Energies*, 2019. 12(7). doi:10.3390/en12071293.

Ketelsen, S., Schmidt, L., Donkov, V., and Andersen, T. Energy saving potential in knuckle boom cranes using a novel pump controlled cylinder drive. *Modeling, Identification and Control*, 2018. 39(2). doi:10.4173/mic.2018.2.3.

Kjelland, M. B. *Offshore Wind Turbine Access Using Knuckle Boom Cranes.* Ph.D. thesis, University of Agder, 2016.

Krause, P., Wasynczuk, O., and Sudhoff, S. *Analysis of Electric Machinery.* IEEE® Press, 2002.

Michel, S. and Weber, J. Energy-efficient electrohydraulic companct drives for low power applications. *ASME/BATH 2012 Symposium on Fluid Power and Motion Control*, 2012.

Padovani, D., Ketelsen, S., Hagen, D., and Schmidt, L. A Self-Contained Electro-Hydraulic Cylinder with Passive Load-Holding Capability. *Energies*, 2019. 12(2):292. doi:10.3390/en12020292.

Pawlus, W., Choux, M., and Hansen, M. R. Hydraulic vs. electric: A review of actuation systems in offshore drilling equipment. *Modeling, Identification and Control*, 2016. 37(1). doi:10.4173/mic.2016.1.1.

Ristic, M. and Wahler, M. Electrification of Hydraulics Opens New Ways for Intelligent Energy-Optimized Systems. In *11th International Fluid Power Conference*. 2018.

Schmidt, L., Groenkjaer, M., Pedersen, H. C., and Andersen, T. O. Position Control of an OverActuated Direct Hydraulic Cylinder Drive. *Control Engineering Practice*, 2017. 64. doi:10.1016/j.conengprac.2017.04.003.

Schmidt, L., Roemer, D. B., Pedersen, H. C., and Andersen, T. O. Speed-Variable Switched Differential Pump System for Direct Operation of Hydraulic Cylinders. In *ASME/BATH 2015 Symposium on Fluid Power and Motion Control*. 2015. doi:10.1115/FPMC2015-9575.

Sørensen, J. K. *Reduction of Oscillations in Hydraulically Actuated Knuckle Boom Cranes.* Ph.D. thesis, University of Agder, 2016.

Stecki, J. S. and Garbacik, A. *Design and Steady-state Analysis of Hydraulic Control Systems.* Fluid Power Net Publications, 2002.

Williamson, C. and Ivantysynova, M. The effect of pump efficiency on displacement-controlled actuator systems. In *Tenth Scandinavian International Conference on Fluid Power, Tampere, Finland*. 2007.

Paper E

Design and Implementation of Pressure Feedback for Load-Carrying Applications with Position Control

Daniel Hagen, Damianio Padovani, and Martin Choux

DESIGN AND IMPLEMENTATION OF PRESSURE FEEDBACK FOR LOAD-CARRYING APPLICATIONS WITH POSITION CONTROL

Daniel Hagen, Damiano Padovani, Martin Choux
University of Agder, Department of Engineering Sciences
Jon Lilletunsvei 9, 4879 Grimstad, NORWAY
E-mail: daniel.hagen@uia.no

ABSTRACT

This research paper presents the design and implementation of pressure feedback on a hydraulically actuated single-boom crane operated in closed-loop position control. It is well known that systems with pressure compensated proportional valves in combination with over-center valves tend to induce instability, especially when the external load is overrunning (e.g., while lowering a load). However, in some applications pressure oscillations arise also with resistant external loads (e.g., while lifting a load). Hence, a pressure feedback capable of stabilizing the system functioning in both operations using the pressures from both actuator chambers (i.e., piston-side and rod-side) is proposed and compared against the conventional solution using only the rod-side chamber pressure. The investigation demonstrates that the implementation of a proposed "inverse valve dynamic" algorithm is needed in order for the control valve to stabilize the system when introducing the piston-side pressure in the pressure feedback. With this new method, the experimental tests demonstrate a satisfactory reduction of the pressure fluctuations in closed-loop motion control and a good position tracking (the average position error while lowering the load is reduced by almost 90% compared to the original system without pressure feedback). Finally, simulated results show that the proposed pressure feedback allows for potential energy savings of about 50% when lowering the load.

KEYWORDS: Over-center valves, pressure compensated proportional valves, active-damping, pressure feedback, position control, energy saving.

1. INTRODUCTION

The hydraulic circuits of load-carrying applications must contain passive load-holding devices to meet safety regulations. A popular load-carrying solution makes use of pressure-compensated Proportional Directional Control Valves (PDCVs) in combination with Over-Center Valves (OCVs). This is considered state-of-the-art in many industrial fields (e.g., in knuckle-boom cranes for offshore applications) due to the load-independent flow control and reduced system cost. Nevertheless, this approach tends to introduce an oscillatory behavior, or even instability, that undermines both performance and operational safety. Several investigations were carried out to mitigate this issue, especially when dealing with overrunning loads. Optimizing the design parameters [1] is today a common approach that often requires hardware reconfiguration [2] (e.g., adjusting the pilot ratio of the OCV's, increasing the volumes in hydraulic lines related to the OCV pilot pressure and/or the load-sensing pilot pressure of the PDCV's compensator). An alternative is introducing active damping to compensate for oscillations. An overview of active damping focused on hydraulically actuated mobile applications is presented in [3]. This solution is usually referred to as Pressure Feedback (PF) and may involve closed-loop control of the PDCV's spool position [4]. In [5], a high-pass filter is implemented in the PF of a

mobile-crane and demonstrates a clear reduction of the oscillatory behavior. More advanced control strategies using PF are proposed in [6-8] (i.e., adaptive control, frequency-based control and auto tuning). However, according to [9], these methods are complex and less general compared to the approach first described in [4], referred to as the "classical approach". Recently, Pedersen and Andersen demonstrated that there is an optimum range for the high-pass filter parameters that affects both the obtainable damping and the dynamic response [9]. A guideline for adjusting the filter parameters is proposed in [10] for systems with pressure-compensated PDCVs in combination with OCVs. However, the low bandwidth of PDCVs may have essential limitations on the damping effect [9-11], especially when using PDCVs that have a much lower bandwidth compared to servo-valves. Moreover, pressure feedback is typically implemented in combination with open-loop velocity control where the machine operator closes the loop (operator in the control loop). However, in some applications (e.g., automated offshore oil drilling machinery [12]) a fully automated closed-loop position control is applied for more efficient operations. In the offshore environment, these machines are subjected to disturbances such as strong wind and relevant wave motion that may excite resonance modes of the mechanical structure and restrict the dynamic performance of the actuation system. These factors, when combined with the intrinsic oscillatory behavior of the hydraulic system reduce the system productivity. Consequently, there is an on-going trend of replacing hydraulic actuators with electric drives that results in increased energy efficiency and controllability [12-13].

For these reasons, this paper aims to design and implement pressure feedback on a standard valve-controlled actuator equipped with an over-center valve. The main focus is on a pressure feedback algorithm that uses both actuator pressures instead of only the pressure of the rod-side chamber, like [5] and [10-11]; this idea is inspired by a solution successfully implemented on a self-contained electro-hydraulic cylinder with passive load-holding capability that drives a single-boom crane in two quadrant operations [14]. The considered system under investigation is explained in detail in Section 2. A non-linear model is described and validated against experimental data in Section 3.1, and further simplified and linearized in Section 3.2. The linear model is in Section 4 used to analyze the stability of the original system and when implementing the considered pressure feedback methods. In Section 5, the proposed algorithm with pressure feedback is tested on a high-fidelity non-linear model before the final implementation on the experimental test-bed. The last section contains the conclusion.

2. THE CONSIDERED SYSTEM

The considered system is the hydraulically-actuated, single-boom crane visible in Figure 2 that is built specifically for having a flexible structure in the boom with the purpose of inducing pressure oscillations in the hydraulic system depicted in Figure 1. The OCV serves multi-functional purposes such as leak tight load-holding and shock absorption [11]. A state-of-the-art pressure compensated PDCV is connected to a centralized Hydraulic Power Unit (HPU) providing a constant supply pressure (p_S) and a fixed return pressure (p_R) to the actuation system. The motion of the hydraulic cylinder (C) is controlled by the PDCV that receives the control input u_V from the control system.
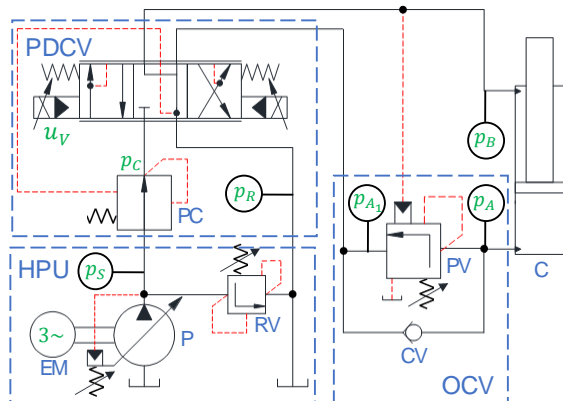

Figure 1. The hydraulic system of the experimental setup.
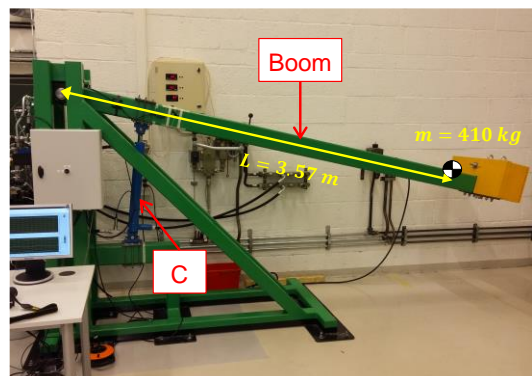

Figure 2. The single-boom crane.

The key components for the experimental setup consist of the following eight elements in addition to the instrumentation: the electric motor (EM) drives the variable-displacement, axial-piston pump (P) with displacement of 75 cm³/rev. The supply pressure is controlled by the absolute pressure limiter of the pump while a pressure-Relief Valve (RV) is installed for safety. The PDCV, a Danfoss PVG32, consists of two key parts, namely the main spool with integrated closed-loop position control and the Pressure Compensator (PC) that guarantees a load independent flow across the metering edge. The vented OCV, a Sun Hydraulics CWCA with pilot ratio 3:1, contains a by-pass Check Valve (CV) and a pilot-operated Poppet Valve (PV) for controlling the overrunning load when lowering the crane boom. The hydraulic cylinder has piston diameter $D_P = 65\ mm$, rod diameter $D_R = 35\ mm$, and stroke length $h_C = 500\ mm$. Finally, the system is instrumented with sensors for measuring the pressures labeled in Figure 1 as well as the cylinder position (x_C).

3. SYSTEM MODELING AND VALIDATION

This paper makes use of a dynamic model of the valve-controlled system that drives the single-boom crane: the MATLAB-Simulink® environment was chosen to perform the numerical simulations. In this section both a high-fidelity, non-linear model and a simplified linear model are introduced.

3.1. The High-fidelity Model

The mechanical system including the crane boom is modeled using the finite segment method [15-16] (Figure 3), which serves the purpose of representing the relevant flexibility of the structure.
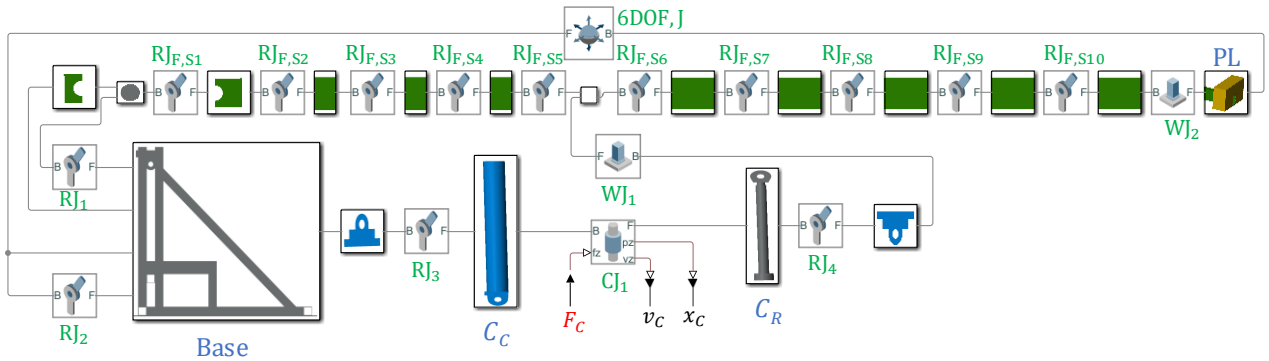

Figure 3. MATLAB-Simulink® multibody model of the flexible boom.

The multibody system (MBS) consists of two revolute joints (RJ1-2) connecting the flexible boom to the base of the crane and two RJ3-4 connecting the cylinder body (C_C) to the base and the rod (C_R) to the boom, respectively. A cylindrical joint (CJ) is applied between C_C and C_R interfacing the hydraulic system through the cylinder piston force (F_C), velocity (v_C) and position (x_C). In the finite segment method, the boom is modeled by a number of smaller boom segments connected together using RJs with an internal torsional spring/damper (RJF,S1-10) to simulate the bending of the structure. The torsional springs have equivalent stiffness ($k_{eq,i}$) and damping ($C_{eq,i}$) related to the segment number i, as expressed in (1) and (2), where E is the bulk modulus of the boom material, I_Z is the second moment of inertia for the cross section of the boom, $L_{S,i}$ is the length of the segment, and $J_{S,i}$ is the moment of inertia of the segment.

$$k_{eq,i} = \frac{E I_Z}{L_{S,i}}$$
(1)

$$C_{eq,i} = \sqrt{2 J_{S,i} k_{eq,i}}$$
(2)

Concerning the hydraulics, equation (3) elucidates the actuator force transferred to the MBS.

$$F_C = p_A A_A - p_B A_B - F_F \tag{3}$$

The actuator pressures (p_A and p_B) and areas (A_A for the piston-side and A_B for the rod-side) describe the hydraulic force while the friction force (F_F) is given in (4), according to the Stribeck model.

$$F_F = B_{vf} \dot{x} + \tanh(\dot{x}a)\left(F_{Cf} + F_{Sf} e^{-\frac{\dot{x} \cdot \tanh(\dot{x}a)}{\tau_{Sf}}}\right) \tag{4}$$

The different terms identified with experiments are the viscous friction coefficient ($B_{vf} = 1.5 \cdot 10^4$ kg/s), the Coulomb force ($F_{Cf} = 75$ N), the static friction force ($F_{Sf} = 1450$ N), and the static friction force's constant ($\tau_{Sf} = 0.02$ m/s). The hyperbolic tangent is introduced to prevent numerical issues, where the dimensionless tuning parameter is set as $a = 250$.

The well-known pressure build-up equation is then applied to evaluate the pressures labeled in Figure 1 (both the supply pressure $p_S = 180$ bar and the return pressure $p_R = 1.1$ bar are assumed constant). The resulting expressions are given in (5)-(7).

$$\dot{p}_{A1} = \frac{1}{C_{A1}}\left(Q_{V,In} - Q_{CV} + Q_{PV}\right), \qquad where \; C_{A1} = \frac{V_{A1,0}}{\beta_{A1}} \tag{5}$$

$$\dot{p}_A = \frac{1}{C_A}\left(Q_{CV} - A_A v_C - Q_{PV}\right), \qquad where \; C_A = \frac{A_A x_C + V_{A,0}}{\beta_A} \tag{6}$$

$$\dot{p}_B = \frac{1}{C_B}\left(Q_{V,Out} + A_B v_C\right), \qquad where \; C_B = \frac{A_B(h_C - x_C) + V_{B,0}}{\beta_B} \tag{7}$$

The hydraulic capacitances related to the actuator chambers (C_i) are defined recalling the piston position when needed, the cylinder stroke, the volumes of the transmission lines ($V_{i,0}$) that are assumed constant, and the effective fluid's bulk modulus (β_i). This parameter is modeled differently for each capacitance via equation (8).

$$\beta_i = \frac{1}{\dfrac{1}{\beta_0} - \dfrac{1}{\kappa_{air}(p_i + p_{atm})\left(\dfrac{\eta_{air} - 1}{\eta_{air}\left(\dfrac{p_{atm}}{p_i + p_{atm}}\right)^{\frac{1}{\kappa_{air}}}} - 1\right)}} \tag{8}$$

The terms are the oil's bulk modulus ($\beta_0 = 12000$ bar), the adiabatic air constant ($\kappa_{air} = 1.4$), the pressure in the capacitance (p_i), the atmospheric pressure (p_{atm}) and the volumetric air content of the oil ($\eta_{air} = 0.007$ %). Additionally, the flow rates through the OCV are computed using a simplified approach (9) that involves the valve flow gain ($k_{V,i}$), the cracking pressure ($p_{Cr,i}$), the inlet pressure ($p_{In,i}$), and the outlet pressure ($p_{Out,i}$).

$$Q_i = \begin{cases} 0, & p_{In,i} < p_{Out,i} + p_{Cr,i} \\ k_{V,i}(p_{In,i} - p_{Out,i} - p_{Cr,i}), & p_{In,i} \geq p_{Out,i} + p_{Cr,i} \end{cases} \tag{9}$$

On the contrary, the flow rates through the PDCV are modeled using the orifice equation (10).

$$Q_i = \xi_V C_d A_d \sqrt{\frac{2}{\rho}|\Delta p_i|} \; sign(\Delta p_i) \tag{10}$$

It comprises the valve opening (ξ_V) (i.e., a dimensionless number ranging between -1 and 1 with zero being the center position of the spool), the discharge coefficient (C_d), the maximum flow area (A_d), the fluid density (ρ), and the pressure differential across the spool (Δp_i). The valve opening characteristics, such as the maximum flow areas as well as the spool overlaps (dead-bands) are taken from [17]. The spool position is related to the valve command (u_V) via a second order transfer function ($G_V(s)$ in (11)) that accounts for the valve dynamics. The natural frequency is $\omega_V = 30 \; \frac{rad}{s}$ as identified in [18] while the damping ratio is adjusted equal to $\zeta_V = 0.7$ after validation against experimental data.

$$G_V(s) = \frac{\xi_V}{u_V} = \frac{\omega_V^2}{s^2 + 2\omega_V \zeta_V s + \omega_V^2} \qquad (11)$$

The PDCV's upstream pressure (p_C) is modeled according to (12); the nominal pressure drop across the spool's metering edge (i.e., the equivalent pressure setting of the compensator $p_0 = 7\ bar$) and the load-sensing pressure (p_{LS}) are introduced. The latter term is selected by a logic function so that $p_{LS} = p_A$ when the spool position is negative, $p_{LS} = p_B$ when the spool position is positive, and $p_{LS} = p_R$ when the spool is centered.

$$p_C = \begin{cases} p_{LS} + p_0, & p_0 \le (p_S - p_{LS}) \\ p_S - p_{LS}, & 0 < (p_S - p_{LS}) < p_0 \\ p_{LS}, & (p_S - p_{LS}) \le 0 \end{cases} \qquad (12)$$

The relative opening of the poppet (ξ_{PV}) in the OCV is given in (13), where α_p is the pilot area ratio, $p_{PV,cr}$ is the cracking pressure, and $p_{PV,fo}$ is the extra pressure required to fully open the valve.

$$\xi_{PV} = \frac{\alpha_p \cdot p_B + p_A - p_{PV,cr}}{p_{PV,fo}} \qquad (13)$$

The dynamics of the poppet and the dynamics of the pressure compensator are simulated via a first-order transfer function with a time constant $\tau_i = 0.001\ s$.

Finally, validation against experimental data was carried out and the results are reported in Figure 4. The comparison shows a good match (except the pressure peak that occurs when the PDCV closes after 20s in Figure 4 (d)) between simulated and measured data, especially, with regards to the oscillatory behavior.
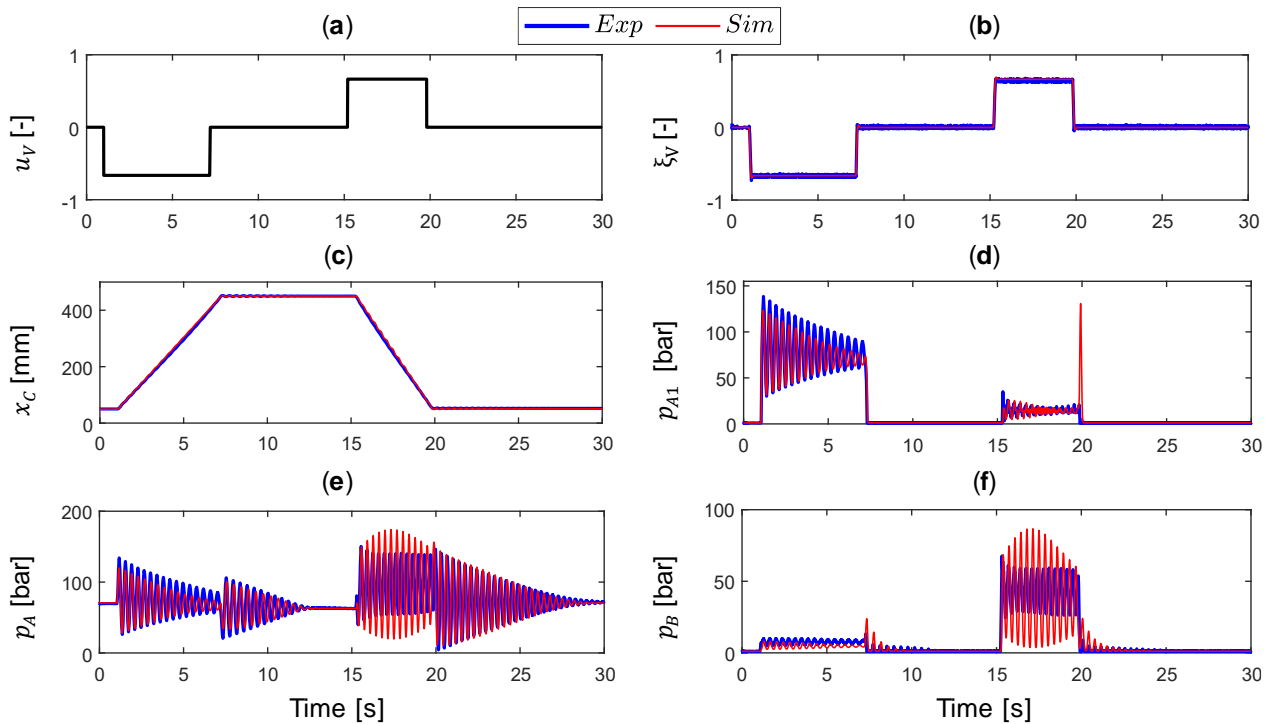

Figure 4. Validation of the non-linear model against experimental data: (a) Input command; (b) PDCV spool position; (c) Cylinder position; (d)-(f) Relevant system pressures.

3.2. The Linear Model

A simplified model emphasizing the cylinder retraction (i.e., the most critical operating condition) was derived for a linear analysis. The flow through the CV elucidated in (5)-(6) is neglected and all capacitances are considered constant and defined by the cylinder position $x_{C,0} = 0.45m$. The resulting force balance on the piston is given in (14).

$$p_A A_A - p_B A_B - B_v v_C = M_{eq}(x_{C,0}) \dot{v}_C + G_{eq}(x_{C,0}) \tag{14}$$

The equivalent mass (m_{eq}) is considered as a constant contribution $m_{eq} = M_{eq}(x_{C,0})$. Then, the external load acting on the actuator is the equivalent gravitational term $(G_{eq}(x_{C,0}))$ that is assumed as a disturbance.

The general expression (15) is used to find a linear approximation of the PDCV at steady-state (ss).

$$\tilde{Q}_i = \left.\frac{\partial Q_i}{\partial p_i}\right|_{ss} \tilde{p}_i + \left.\frac{\partial Q_i}{\partial u_i}\right|_{ss} \tilde{u}_i = k_{qp,i}\tilde{p}_i + k_{q,i}\tilde{\xi}_i$$
$$\tilde{p}_i = p_i - p_i^{ss} \tag{15}$$
$$\tilde{\xi}_i = \xi_i - \xi_i^{ss}$$

The model is linearized around the operating point where the cylinder is almost fully extended and at rest $(v_C = 0 \, m/s)$ with the PDCV centered $(\xi_V^{ss} = 0)$ and the PV closed $(\xi_{PV}^{ss} = 0)$. The steady-state values for the pressures (p_i^{ss}) are obtained from experimental data. The flow-pressure gains $k_{qA1,PV}$ and $k_{qA,PV}$ become zero when the PV is considered closed at steady-state. The numerical values for the linearized gains are listed in Table 1. From now on, the "tilde" prescript resulting from the linearization is omitted and, generally, only deviations from the operating point are considered.

Table 1. Parameters used for the linearized model.

$k_{qA,PV}$ $[m^4 s/kg]$	$k_{qB,PV}$ $[m^4 s/kg]$	$k_{qA1,V_{Out}}$ $[m^4 s/kg]$	$k_{q,V_{In}}$ $[m^2/s]$	$k_{q,V_{Out}}$ $[m^2/s]$	$k_{qB,V_{In}}$ $[m^2/s]$	$k_{q,PV}$ $[m^2/s]$
$2.86 \cdot 10^{-8}$	$8.57 \cdot 10^{-8}$	$1.01 \cdot 10^{-10}$	$5.83 \cdot 10^{-4}$	$1.21 \cdot 10^{-4}$	$1.67 \cdot 10^{-11}$	$1.30 \cdot 10^{-3}$
m_{eq} [kg]	μ_C [-]	A_B $[m^2]$	B_v $[Ns/m]$	C_{A1} $[m^3/Pa]$	C_A $[m^3/Pa]$	C_B $[m^3/Pa]$
$1.55 \cdot 10^4$	1.41	$2.4 \cdot 10^{-3}$	$1.5 \cdot 10^4$	$1.52 \cdot 10^{-13}$	$3.78 \cdot 10^{-12}$	$3.59 \cdot 10^{-12}$

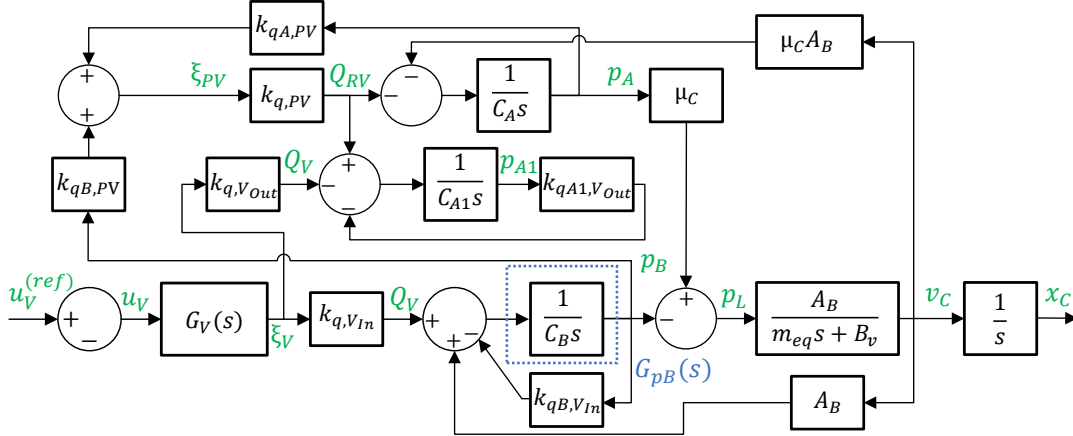A block diagram of the linear model is shown in Figure 5.

Figure 5. Block diagram of the linearized system model.

Finally, the validation against experimental data is presented for a step command with valve opening $u_V = 10\%$. The results in Figure 6 show a satisfactory agreement between measurements and simulated magnitudes (it should be noted the real system is highly non-linear and the crane has some flexibility). Most importantly, the oscillatory behavior of the pressures is captured at the same amplitude and frequency.
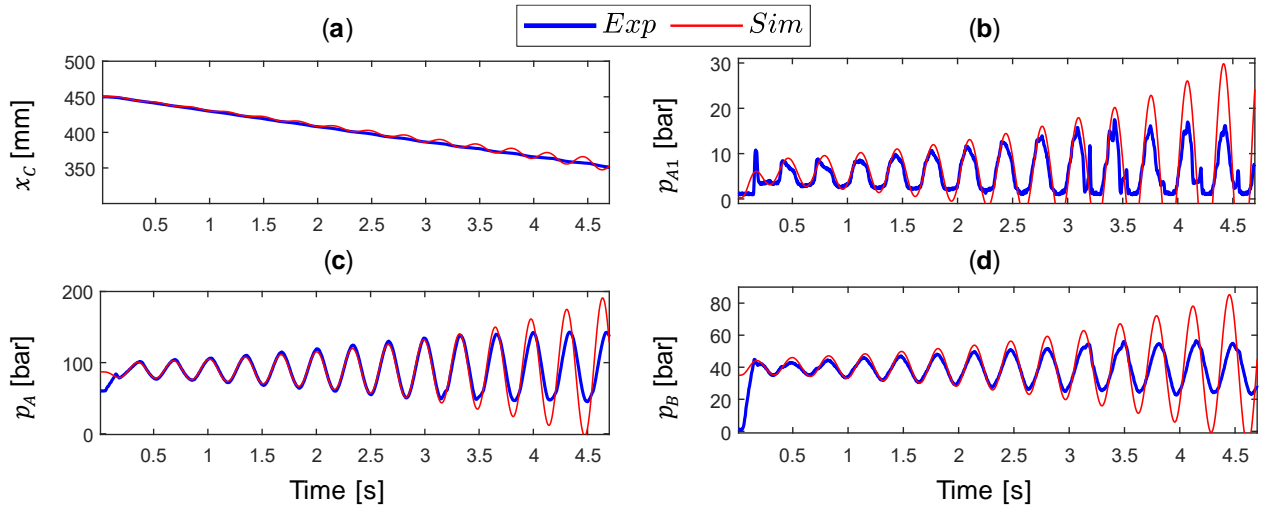
Figure 6. Validation of the linear model against experimental data: (a) Cylinder position; (b)-(d) System pressures.

4. PRESSURE FEEDBACK

Implementing high-pass filtered pressure feedback is proven to increase the system damping for cranes when lowering the load [5]. A first-order high-pass filter (16) is chosen.

$$G_f(s) = \frac{Q_{PF}}{p_i} = \frac{k_f s}{\tau_f s + 1} \tag{16}$$

The two following methods of PF are investigated in this paper.

4.1. The Rod-side Pressure Feedback

First, the rod-side pressure (p_B) is used as feedback element (PF_{pB}) in accordance to the approach chosen in [5], [10] and [11] as shown in Figure 7.
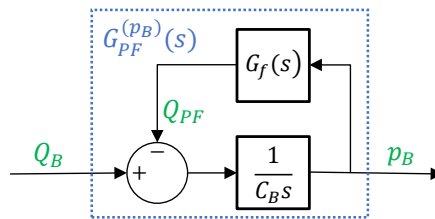

Figure 7. Block diagram of rod-side pressure feedback.

By using the high-passed pressure feedback, the open-loop transfer function $G_{pB}(s)$ of the original system (Figure 5) becomes the compensated open-loop transfer function $G_{PF}^{(p_B)}(s)$ according to (17).

$$G_{PF}^{(p_B)}(s) = \frac{1}{(C_B + k_f)s} \frac{\tau_f s + 1}{\frac{C_B}{C_B + k_f}\tau_f s + 1} \tag{17}$$

For the implementation of this PF on a real application (Figure 8), the non-negligible dynamics of the PDCV should be accounted for when selecting the filter parameters. The inverse of the valve flow gain $(k_{q,V_{In}})$ is, therefore, included to estimate the required valve opening.
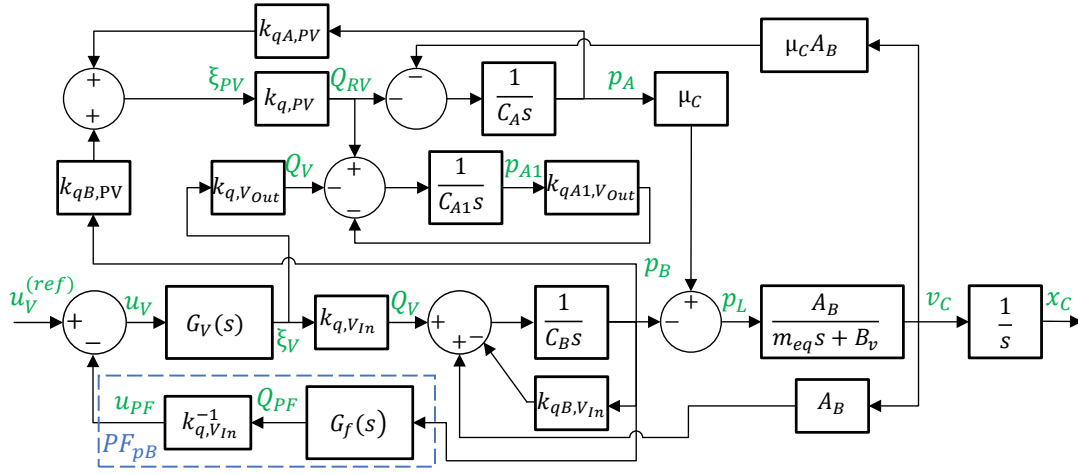
Figure 8. Pressure feedback implemented on the valve side using rod-side pressure.

A state space model (18) is used to generate the transfer function representing the desired system.

$$
\begin{bmatrix} v_C \\ \dot{v}_C \\ \dot{p}_{A1} \\ \dot{p}_A \\ \dot{p}_B \\ \dot{\xi}_V \\ \ddot{\xi}_V \\ \dot{Q}_{PF} \end{bmatrix} =
\begin{bmatrix}
0 & 1 & 0 & 0 & 0 & 0 & 0 & 0 \\
0 & \dfrac{-B_v}{m} & 0 & \dfrac{A_B\mu_C}{m} & \dfrac{-A_B}{m} & 0 & 0 & 0 \\
0 & 0 & \dfrac{-k_{qA1,V}}{C_{A1}} & \dfrac{k_{q,PV}k_{qA,PV}}{C_{A1}} & \dfrac{k_{q,PV}k_{qB,PV}}{C_{A1}} & \dfrac{-k_{q,V_{Out}}}{C_{A1}} & 0 & 0 \\
0 & \dfrac{-A_B\mu_C}{C_A} & 0 & \dfrac{-k_{q,PV}k_{qA,RV}}{C_A} & \dfrac{-k_{q,PV}k_{qB,PV}}{C_A} & 0 & 0 & 0 \\
0 & \dfrac{A_B}{C_B} & 0 & 0 & \dfrac{-k_{qB,V_{In}}}{C_B} & \dfrac{k_{q,V_{In}}}{C_B} & 0 & 0 \\
0 & 0 & 0 & 0 & 0 & 0 & 1 & 0 \\
0 & 0 & 0 & 0 & 0 & -\omega_V^2 & -2\zeta_V\omega_V & -\omega_V^2 k_{q,V_{In}}^{-1} \\
0 & \dfrac{A_B k_f}{C_B\tau_f} & 0 & 0 & 0 & \dfrac{k_{q,V_{In}}k_f}{C_B\tau_f} & 0 & \dfrac{-1}{\tau_f}
\end{bmatrix}
\begin{bmatrix} x_C \\ v_C \\ p_{A1} \\ p_A \\ p_B \\ \xi_V \\ \dot{\xi}_V \\ Q_{PF} \end{bmatrix} +
\begin{bmatrix} 0 \\ 0 \\ 0 \\ 0 \\ 0 \\ 0 \\ -\omega_V^2 \\ 0 \end{bmatrix} u_V^{(ref)}
\quad (18)
$$

Pedersen et al. [9-10] recommend selecting the filter's time constant (τ_f) reasonably high and then adjusting the filter gain (k_f) until sufficient damping is achieved. The high-pass filter time constant should be selected so that $\frac{1}{\tau_f} < \omega_n$, where ω_n is the natural eigenfrequency of the undamped system. According to the absolute stability criteria (19) derived in [11], increasing the rod-side capacitance (C_B) (i.e., increasing the rod-side volume), and/or decreasing the CBV pilot ratio (α_p) can stabilize the system.

$$
\frac{C_B}{C_A} > \frac{\alpha_p}{\mu_C}
\quad (19)
$$

The bore-side capacitance ($C_A \gg C_B$) is chosen as a reference when adjusting the filter gain ($k_f = \lambda_f C_A(x_{C,0})$), where λ_f is a tuning parameter [9-10]. The actuator capacitances depend on the cylinder position (6)-(7), thus to be conservative, k_f is selected when the actuator is close to full extension ($x_{C,0} = 0.45m$) and the volume of the rod-side (V_B) is low. Therefore, $\tau_f = \frac{2}{\omega_n}$ is chosen for $\omega_n = 19.1 \, rad/s$, that has been identified from the linear analysis, and $\lambda_f = 2$.

To analyze the stability of the resulting system, Bode plots and a pole-zero plot of the open-loop transfer function in (20) are derived with pressure feedback (PF_{pB}) and also without pressure feedback (PF_{Off}) to have a benchmark. As a side note, the gain $k_{q,V_{In}}^{-1}$ in (18) is selected equal to zero when PF is not desired.

$$
G_{x_C}^{(p_B)}(s) = \frac{x_C}{u_V^{(ref)}} = \boldsymbol{C}_{x_C}\left(\boldsymbol{I}s - \boldsymbol{A}^{(p_B)}\right)^{-1}\boldsymbol{B}, \qquad where \; \boldsymbol{C}_{x_C} = [1 \quad 0 \quad 0 \quad 0 \quad 0]
\quad (20)
$$

Figure 9 (a) shows a clear increase in damping when PF is added. Figure 9 (b) suggests that the system without PF is stable when the cylinder position is below 0.313m. Figure 9 (c) displays that the two positive complex poles of PF_{Off} move to the negative side when adding pressure feedback (PF_{pB}) in the worst-case scenario (i.e., $x_C = 0.45\ m$), resulting therefore in a stable system.
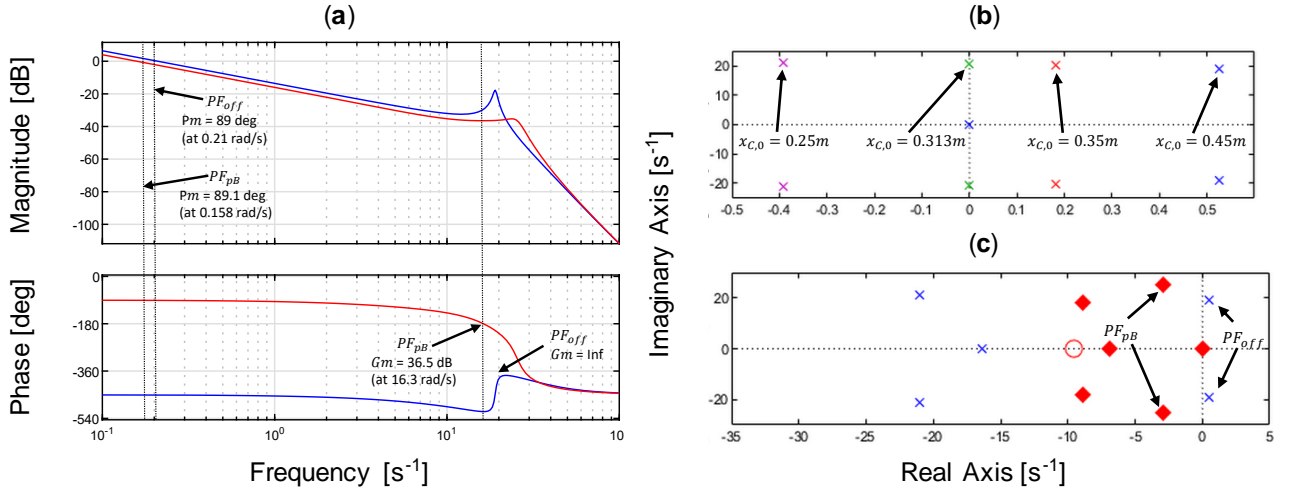

Figure 9. Stability analysis of $G_{x_C}^{(p_B)}(s)$: (a) Bode plots; (b) Plot PF_{Off} at different cylinder positions; (c) Poles and zeros PF_{Off} (blue) and PF_{pB} (red) at $x_{C,0} = 0.45m$.

4.2. The Load Pressure Feedback

A different approach for the pressure feedback based on the "load pressure" (i.e., the difference between the bore chamber pressure multiplied by the area ratio of the cylinder and the rod chamber pressure, $p_L = p_A \mu_c - p_B$) is addressed in order to get rid of the undesired pressure oscillations identified during piston extension (Figure 12). Achieving this result benefits those systems characterized by a flexible mechanical structure like the single-boom crane under investigation.

The row eight of matrix $\boldsymbol{A}$, in (18) is modified according to (21) when including the piston-side chamber pressure.

$$\boldsymbol{A}^{(p_L)} = \begin{bmatrix} \cdots & \cdots & \cdots & \cdots & \cdots & \cdots & \cdots & \cdots \\ 0 & \dfrac{-k_f A_B \left(\dfrac{\mu_c^2}{C_A} + \dfrac{1}{C_B} \right)}{\tau_f} & 0 & \dfrac{-k_f \mu_c k_{q,PV} k_{qA,RV}}{C_A \tau_f} & \dfrac{-k_f \mu_c k_{q,PV} k_{qB,PV}}{C_B \tau_f} & \dfrac{-k_{q,VIn} k_f}{C_B \tau_f} & 0 & \dfrac{-1}{\tau_f} \end{bmatrix} \quad (21)$$

The open-loop transfer function from valve command to position output ($G_{x_C}^{(p_L)}(s)$) elucidated (22) and the transfer function from valve command to velocity output ($G_{v_C}^{(p_L)}(s)$) elucidated (23) are used to analyze the system stability using load pressure feedback (PF_{pL}, Figure 10). The filter's time constant $\tau_f = \dfrac{2}{\omega_n}$ and the filter gain tuning parameter $\lambda_f = 0.7$ are used.

$$G_{x_C}^{(p_L)}(s) = \frac{x_C}{u_V^{(ref)}} = \boldsymbol{C}_{x_C} \left(\boldsymbol{I}s - \boldsymbol{A}^{(p_L)} \right)^{-1} \boldsymbol{B}, \quad where \ \boldsymbol{C}_{x_C} = \begin{bmatrix} 1 & 0 & 0 & 0 & 0 \end{bmatrix} \quad (22)$$

$$G_{v_C}^{(p_L)}(s) = \frac{v_C}{u_V^{(ref)}} = \boldsymbol{C}_{v_C} \left(\boldsymbol{I}s - \boldsymbol{A}^{(p_L)} \right)^{-1} \boldsymbol{B}, \quad where \ \boldsymbol{C}_{v_C} = \begin{bmatrix} 0 & 1 & 0 & 0 & 0 \end{bmatrix} \quad (23)$$
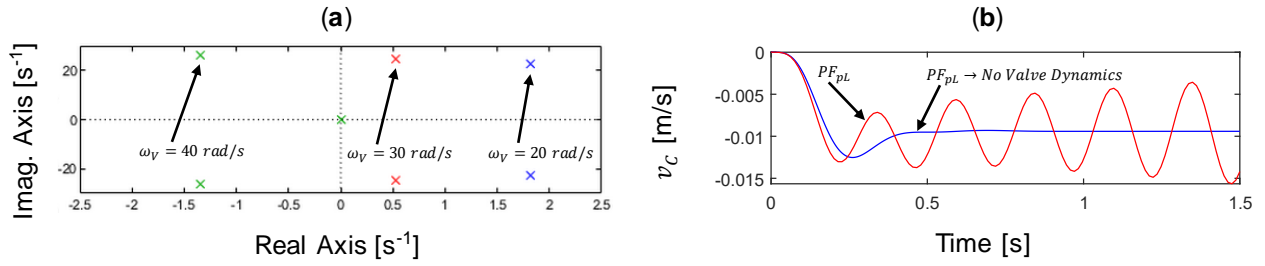
169

Figure 10. Stability analysis $x_{C,0} = 0.45m$: (a) Pole-zero plot of $G_{x_C}^{(p_L)}(s)$; (b) Step response of $G_{v_C}^{(p_L)}(s)$.

Figure 10 (a) shows that the system with PF_{p_L} is unstable with the considered valve ($\omega_V = 30\ rad/s$); however, increasing the natural eigenfrequency of the valve (e.g., up to $\omega_V = 40\ rad/s$) makes the system stable. Figure 10 (b) compares a step response of $G_{v_C}^{(p_L)}$ with command $u_V = 10\%$ to highlight that the steady-state piston velocity is not achieved when considering the valve dynamics. The latter scenario, as discussed in [9-11], is because of the low bandwidth of PDCVs, and in [9] it is seen that when $\omega_V \geq 3\omega_n$ the effect diminishes. Consequently, the inverse of the valve dynamics ($G_V^{-1}(s)$) must be included in the pressure feedback according to the block diagram in Figure 11.
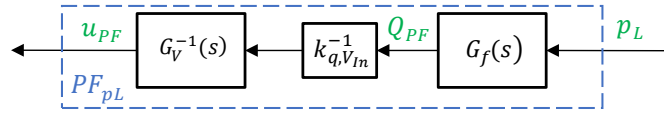

Figure 11. Pressure feedback using the load pressure and including the inverse valve dynamics.

To get a proper transfer function (i.e., the degree of the numerator does not exceed the degree of the denominator), a pseudo transfer function (24) is added assuming $k = 5$.

$$G_V^{-1}(s) = \frac{k^2 s^2 + 2\omega_V \zeta_V k^2 s + \omega_V^2 k^2}{s^2 + 2\omega_V k s + \omega_{n,V}^2 k^2} \tag{24}$$

5. RESULTS

First, the high-fidelity model is used to test the PF based on the rod-side pressure when compared against the original system. Secondly, the load pressure feedback is also evaluated before implementation and testing on the experimental setup. Finally, the proposed pressure feedback is simulated for different OCV's pilot ratios to understand if there is room for potential energy savings.

5.1. The Rod-side Pressure Feedback

To evaluate the performance of this pressure feedback, positive and negative step inputs at 40% of the maximum valve opening are simulated by means of the non-linear dynamic model (Figure 12).
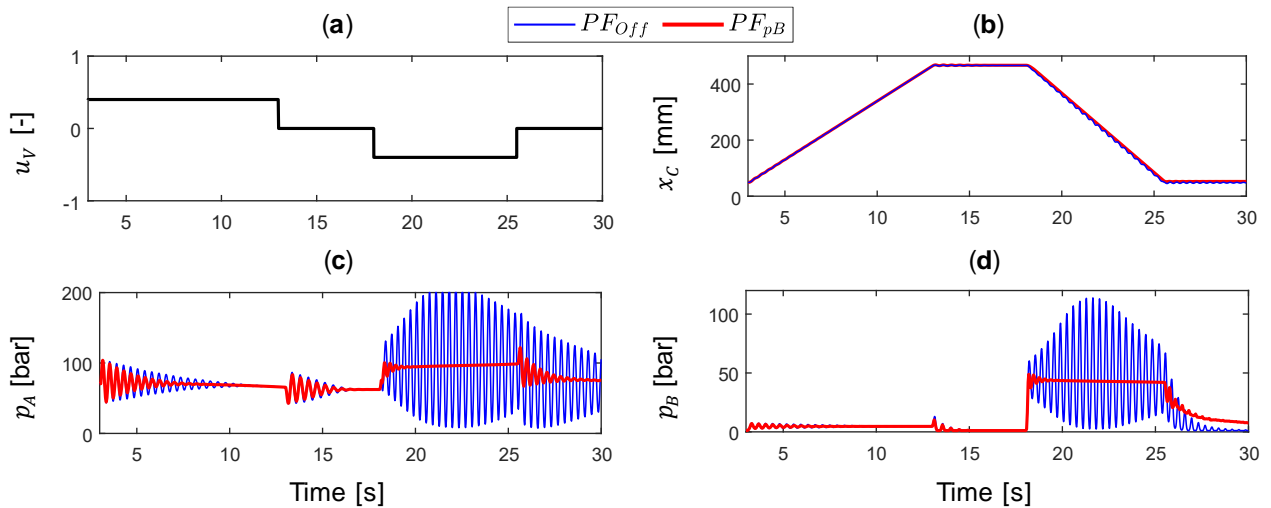
Figure 12. Simulated results with (PF_{pB}) *and without* (PF_{Off}) *pressure feedback: (a) System input; (b) Piston position; (c) Pressure in the bore chamber; (d) Pressure in the rod chamber.*

The results in Figure 12 demonstrate a significant improvement when pressure feedback is used since the pressure oscillations are greatly reduced in comparison to the undamped system. This is especially true during piston retraction (i.e., from about 17 to 26 seconds) with an overrunning external load. However, when the cylinder is extending, the pressure feedback based on the rod chamber pressure is not able to mitigate the pressure oscillations (i.e., before 5 seconds). For this reason, the following feedback method involving both actuator pressures is investigated.

5.2. The Load Pressure Feedback

The performance of the proposed pressure feedback (PF_{pL}) is compared in Figure 13 against the conventional feedback approach (PF_{pB}) while simulating a step input.
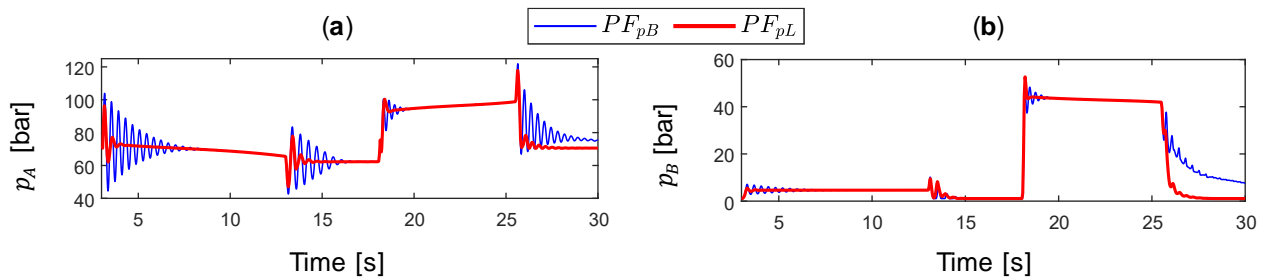

Figure 13. Simulated results of pressure feedback based on rod-side pressure and on load pressure when including $G_V^{-1}(s)$: *(a) Pressure in the bore chamber; (b) Pressure in the rod chamber.*

The results show a clear improvement of the load pressure feedback in reducing the unwanted pressure oscillations when the piston is extending (i.e., from 0 up to about 12 seconds). In addition, the performance is also improved during piston retraction.

5.3. Experimental Tests – The Closed Loop Position Control

The investigated load pressure feedback is tested experimentally on the considered application and compared to the conventional system that is used as a reference after selecting the filter parameters properly. Figure 14 illustrates the block diagram representing the implemented control algorithm.
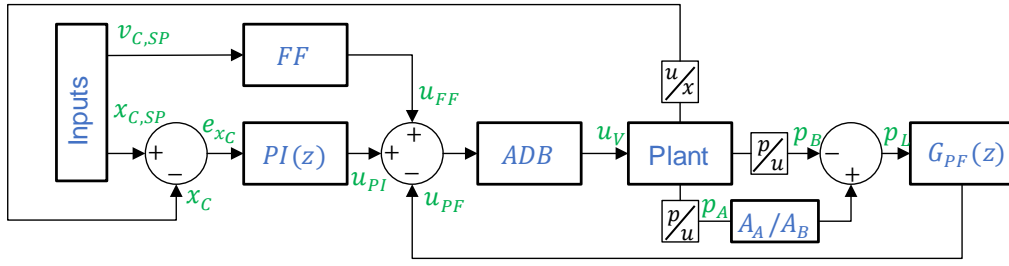
171

Figure 14. Block diagram of the considered control algorithm.

It consists of a position controller based on a closed-loop PI contribution (u_{PI}) and a feed forward (FF) term elucidated in (25), in addition to the pressure feedback in (26). Anti-dead-band logic is also implemented to compensate for the effective dead-band of the PDCV, as explained in [17].

$$u_{FF} = \frac{A_A v_C}{k_{Q_{max}}} \ if \ v_C \geq 0; \ u_{FF} = \frac{A_B v_C}{k_{Q_{max}}} \ otherwise \tag{25}$$

$$G_{PF}(z) = \frac{u_{PF}}{p_L} = G_V^{-1}(z) k_{q,V_{ln}}^{-1} G_f(z) \tag{26}$$

This controller was first developed in a Simulink® model and then converted to IEC 61131-3 Structured Text code using the Simulink-PLC-Coder®. The generated PLCopen XML file was then uploaded to IndraWorks® and executed on an embedded controller XM22 from Bosch Rexroth that runs at a frequency of 1000 Hz. The Simulink-PLC-Coder® requires discrete blocks, hence all transfer functions in the s-domain were converted to the z-domain.

A setpoint S-curve trajectory with a resulting piston velocity $v_{C,SP} = 20 \ mm/s$ was generated and used as input to the position controller (a low velocity is assumed since it is the worst condition due to reduced damping). The measured position error for three different approaches are compared in Figure 15, namely a controller without PF, a control algorithm with PF based on p_B, and a control logic with PF grounded on p_L.
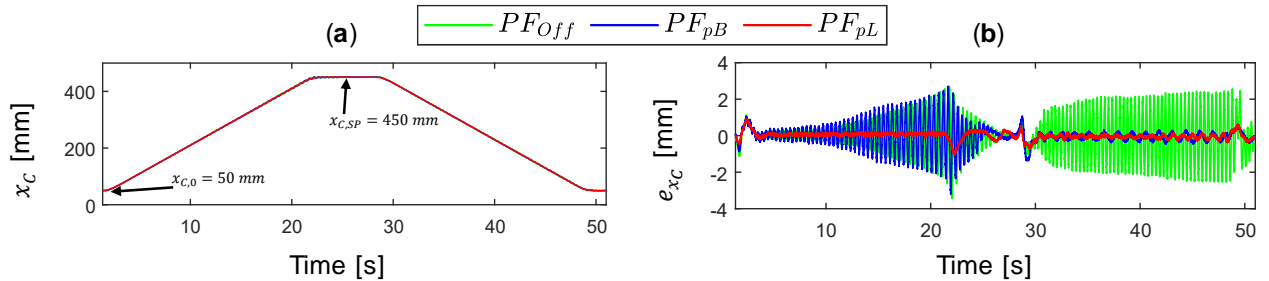

Figure 15. Experimental closed-loop position tracking for different control algorithms.

These experiments demonstrate that adding pressure feedback plays a major role in improving the system performance, even though the induced oscillations make the system with rod-side pressure feedback (PF_{pB}) unstable when the cylinder is extending. Conversely, the system with load pressure feedback (PF_{pL}) stabilizes the system during both piston extension and retraction. This approach results in a much smaller average position error during piston extension (the maximum error is 1.0 mm at about 22 s when the system is decelerating); in comparison to the system without pressure feedback, the improvement in terms of position tracking is close to 2 mm during piston retraction.

The smoother system behavior is clearly reflected in the pressures trends proposed in Figure 16: implementing load pressure feedback removes the oscillatory nature in both quadrants when closed-loop position control is desired.
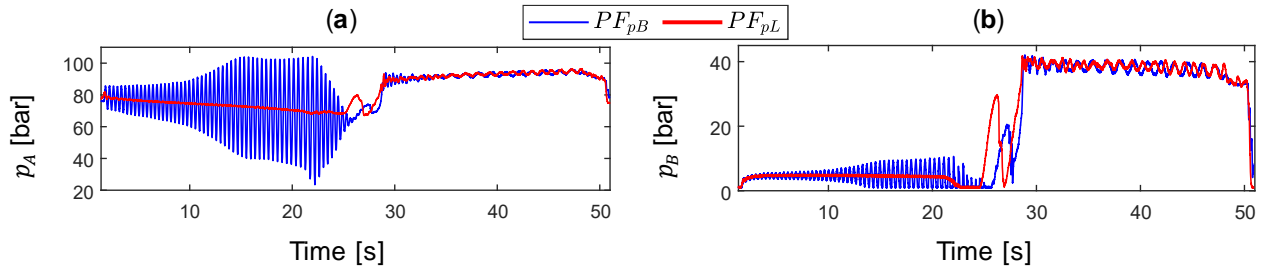
172

Figure 16. Experimental results comparing PF_{pL} and PF_{pB}: (a) Piston-side pressure; (b) Rod-side pressure.

A similar test for a higher piston velocity ($v_{C,SP} = 120\ mm/s$) that represents the upper limit in terms of velocity requirement for this system is also carried out showing similar behavior (the results are not reported for the sake of brevity).

Lastly, Table 2 provides a synthesis of the system performance for closed-loop position control: the simpler implementation of the rod-side pressure feedback is highlighted (i.e., including the valve dynamics is not strictly necessary) as well as the improved performance of the load pressure feedback (i.e., smoother functioning is achieved in every operation).

Table 2. Performance summary.

Pressure Feedback	$G_V^{-1}(s)$	Lifting	Lowering
Off		-	-
p_B	No	-	+
p_L	Yes	+	+

5.4. The Energy Saving Potential

The OCV's pilot ratio affects both the system stability and the energy efficiency. From the stability criterion given in (19), it is clear that it is not possible to achieve stability for the whole cylinder stroke when standard values of the pilot ratio (i.e., $\alpha_p = 2 \dots 8$) are used [11]. However, implementing pressure feedback can make the system stable. Solving this issue, provides an opportunity to emphasize the system's energy consumption that can potentially be improved by selecting a higher pilot ratio of the OCV. Energy savings can be achieved when lowering the crane if the pressure required to open the OCV is reduced; Figure 17 shows the effects of replacing the reference pilot ratio ($\alpha_p = 3$) with $\alpha_p = 5$ and $\alpha_p = 10$, respectively. The results are derived via the non-linear model simulated in closed-loop position control; the considered scenario is similar to the one discussed in Figure 16 but for a higher piston velocity ($v_{C,SP} = 120\ mm/s$) during piston retraction (i.e., when the OCV regulates).
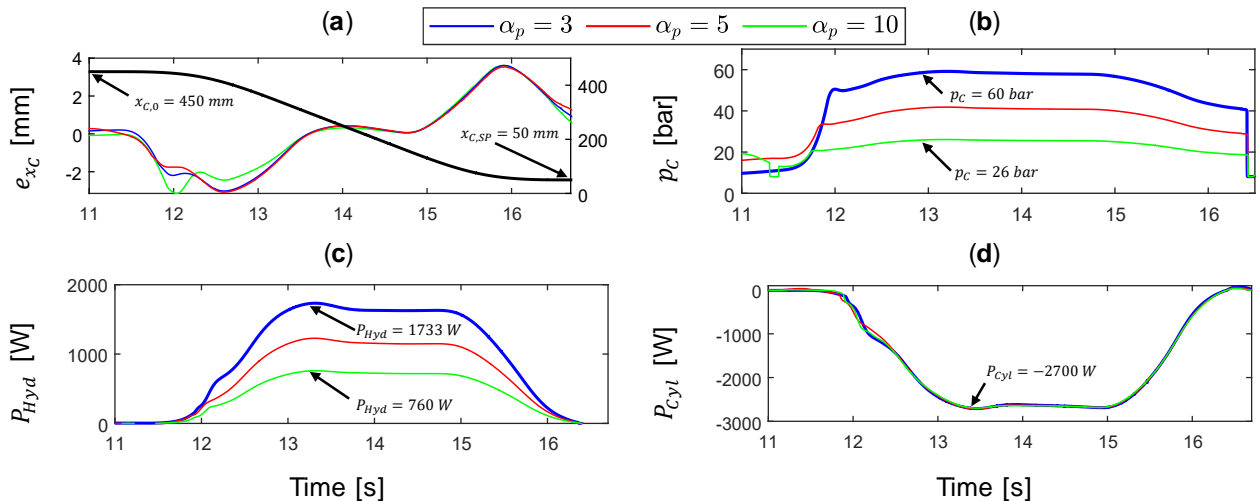

Figure 17. Simulated results with PF_{pL} and different pilot ratios of the OCV: (a) Position error; (b) Rod-side pressure; (c) Consumed hydraulic power; (d) Mechanical power at the actuator.

It can be concluded from Figure 17 (a) that varying the OCV's pilot ratio has little or no effect on the position tracking while the motion remains smooth. This is also confirmed by the trends of the pressure p_C sensed upstream the main spool of the PDCV that are depicted in Figure 17 (b); a lower value of this magnitude translates into energy savings since the required hydraulic power, defined via (27), drops down as visible in Figure 17 (c). In particular, increasing the pilot ratio up to $\alpha_p = 10$ reduces the power consumption to about 50% with respect to the case where $\alpha_p = 3$.

$$P_{Hyd} = p_C \, Q_B \tag{27}$$

The modifications that enable these energy savings do not affect the system performance because the mechanical power outputted by the actuator expressed in (28), remains about constant for every scenario (Figure 17 (d)).

$$P_{Cyl} = F_C \, v_C \tag{28}$$

6. CONCLUSION

The benefits of pressure feedback discussed in the technical literature are often demonstrated on simplified linear models, moreover these references do not show how the pressure feedback algorithm is implemented and tested on real applications using standard directional proportional control valves.

This paper investigates the implementation of pressure feedback on a hydraulically-actuated, single-boom crane operated in closed-loop position control. In comparison to conventional pressure feedback only based on the rod-side chamber pressure, the use of both actuator pressures achieves improved stabilization in both piston extension and retraction. To enable closed-loop stability without compromising the motion performance (i.e., settling time and tracking error), it is necessary to include the piston-side pressure for the considered application. However, adding the piston-side pressure to the pressure feedback induce instability due to the low bandwidth of the directional control valve. One solution presented in this paper is to account for the valve dynamics in the pressure feedback. The experimental results show relevant reduction of the oscillatory behavior of the actuator pressures in closed-loop motion control, the maximum position error during lifting of the payload is reduced from 3.5 mm to 1.0 mm, and the average position error when the payload is lowered is approximately 0.2 mm (in comparison to the system without pressure feedback, this is an improvement of almost 2 mm). Finally, this study demonstrates that the recommended pressure feedback allows the pilot-ratio of the over-center valve to be increased which results in a significant potential for energy savings.

Concerning the future work, the energy saving potential will be experimentally validated and the proposed pressure feedback will be tested on a hydraulic circuit with load-holding valves on both actuator ports in applications where the direction of the external load is changing (i.e., four quadrant operations).

REFERENCES

[1]   M. R. Hansen and T. O. Andersen, "A Design Procedure for Actuator Control Systems Using Optimization Methods," in *The 7th Scandinavian International Conference on Fluid Power*, 2001.

[2]   P. A. Nordhammer, M. K. Bak, and M. R. Hansen, "A Method for Reliable Motion Control of Pressure Compensated Hydraulic Actuation with Counterbalance Valves," *Control. Autom. Syst. (ICCAS), 2012 12th Int. Conf.*, 2012.

[3]   R. Rahmfeld and M. Ivantysynova, "An overview about active oscillation damping of mobile machine structure," *Int. J. Fluid Power*, vol. 5, no. 2, 2004.

[4]   P. Krus and J.-O. Palmberg, "Damping of mobile systems in machines with high inertia loads," in *JFPS Int. Symp. Fluid Power*, 1989.

[5]   M. R. Hansen and T. O. Andersen, "Improved Functionality and Performance of Mobile Cranes Using Pressure Feedback," in *Drives and Controls/Power Electronics Conferance*, 2001.

[6]   D. Cristofori, A. Vacca, and K. Ariyur, "A Novel Pressure-Feedback Based Adaptive Control Method to Damp Instabilities in Hydraulic Machines," *SAE Int. J. Commercial Vehicles*, vol. 5, no. 2, 2012.

[7]   R. Bianchi, G. F. Ritelli, A. Vacca, and M. Ruggeri, "A Frequency-Based Control Methodology for the Reduction of Payload Oscillations in Hydraulic Load Handling Machines," in *ASME/BATH 2015 Symposium on Fluid Power and Motion Control*, 2015.

[8]   G. F. Ritelli and A. Vacca, "A General Auto-Tuning Method for Active Vibration Damping of Mobile Hydraulic Machines," in *8th FPNI Ph.D Symposium on Fluid Power*, 2014.

[9]   H. C. Pedersen and T. O. Andersen, "Pressure Feedback in Fluid Power Systems - Active Damping Explained and Exemplified," *IEEE Trans. Control Syst. Technol.*, vol. 26, no. 1, 2018.

[10]   H. C. Pedersen, T. O. Andersen, and M. R. Hansen, "Guidelines For Properly Adjusting Pressure Feedback In Systems With Over-Centre Valves," in *Proceedings of BATH/ASME Symposium on Fluid Power & Motion Control FPMC2016*, 2016.

[11]   M. R. Hansen and T. O. Andersen, "Controlling a Negative Loaded Hydraulic Cylinder Using Pressure Feedback," in *29th IASTED International Conference on Modelling, Identification and Control, MIC*, 2010.

[12]   D. Hagen, W. Pawlus, M. K. Ebbesen, and T. O. Andersen, "Feasibility Study of Electromechanical Cylinder Drivetrain for Offshore Mechatronic Systems," *Model. Identif. Control*, vol. 38, no. 2, 2017.

[13]   W. Pawlus, M. Choux, and M. R. Hansen, "Hydraulic vs. Electric: A Review of Actuation Systems in Offshore Drilling Equipment," *Model. Identif. Control A Nor. Res. Bull.*, vol. 37, no. 1, 2016.

[14]   D. Padovani, S. Ketelsen, D. Hagen, and L. Schmidt, "A Self-Contained Electro-Hydraulic Cylinder with Passive Load-Holding Capability," *Energies, 12(2), 292*, 2019.

[15]   R. L. Huston and Y. Wang, "Flexibility Effects in Multibody Systems," in *Computer-Aided Analysis of Rigid and Flexible Mechanical Systems*, Dordrecht: Springer Netherlands, 1994.

[16]   J. K. Sørensen, M. Hansen, Rygaard, and M. K. Ebbesen, "Numerical and Experimental Study of a Novel Concept for Hydraulically Controlled Negative Loads," *Model. Identif. Control*, 2016.

[17]   M. K. Bak and M. R. Hansen, "Model based design optimization of operational reliability in offshore boom cranes," *Int. J. Fluid Power*, vol. 14, no. 3, 2013.

[18]   M. K. Bak and M. R. Hansen, "Modeling , Performance Testing and Parameter Identification of Pressure Compensated Proportional Directional Control Valves," in *The 7th FPNI PhD Symposium on Fluid Power Modeling*, 2012.

Paper F

A Comparison Study of a Novel Self-Contained Electro-Hydraulic Cylinder versus a Conventional Valve-Controlled Actuator – Part 1: Motion Control

Daniel Hagen, Damianio Padovani, and Martin Choux

A Comparison Study of a Novel Self-Contained Electro-Hydraulic Cylinder versus a Conventional Valve-Controlled Actuator—Part 1: Motion Control

Daniel Hagen * [iD]**, Damiano Padovani**[iD] **and Martin Choux**

Department of Engineering Sciences, University of Agder, 4879 Grimstad, Norway;
damiano.padovani@uia.no (D.P.); martin.choux@uia.no (M.C.)
* Correspondence: daniel.hagen@uia.no

Abstract: This research paper presents the first part of a comparative analysis of a novel self-contained electro-hydraulic cylinder with passive load-holding capability against a state of the art, valve-controlled actuation system that is typically used in load-carrying applications. The study is carried out on a single-boom crane with focus on the control design and motion performance analysis. First, a model-based design approach is carried out to derive the control parameters for both actuation systems using experimentally validated models. The linear analysis shows that the new drive system has higher gain margin, allowing a considerably more aggressive closed-loop position controller. Several benefits were experimentally confirmed, such as faster rise time, 75% shorter settling time, 61% less overshoot, 66% better position tracking, and reduction of pressure oscillations. The proposed control algorithm is also proven to be robust against load variation providing essentially the same position accuracy. In conclusion, the novel self-contained system is experimentally proven to be a valid alternative to conventional hydraulics for applications where passive load-holding is required.

1. Introduction

Compact and self-contained electro-hydraulic cylinders (SCCs) have received considerable attention in the last decade [1–9]. They are, according to the definition used in this paper, self-sufficient linear hydraulic actuators controlled by a dedicated hydraulic unit that is driven by an electric prime mover. A sealed tank is essential and additional components, such as flow balancing valves, are required when using single-rod cylinders that are preferred in many applications due to the excellent force density. Furthermore, SCCs have shown the potential to replace both conventional hydraulics as well as linear electro-mechanical systems in low-power applications (i.e., below 5 kW) enhancing energy efficiency, modular design, plug-and-play installation, and reduced maintenance [1]. Current commercial solutions of the SCC technology are limited and typically tailor-made [8], especially the ones developed for load-carrying applications that are required to contain passive load-holding devices, according to the safety regulations (e.g., ISO 17096 and DNVGL-ST-0378). Then, the research emphasis is primarily on different electro-hydraulic configurations [10–13], for low-power servo applications [14–17]. There is, therefore, a lack of experimental studies comparing state-of-the-art, valve-controlled technology for load-carrying applications to self-contained hydraulic cylinders in the technical literature, both in terms of motion performance and energy efficiency. Hence, the first part of this research aims to experimentally assess the motion performance of a novel self-contained electro-hydraulic cylinder

against a conventional valve-controlled approach (as a side note, the second part of this study [18] focuses on the energy efficiency). This goal is achieved by modeling the SCC (Section 2), recalling the valve-controlled cylinder (Section 3), and designing a suitable control algorithm (Section 4). Finally, the comparison between the two architectures is given, in terms of motion performance, in Section 5. A single-boom crane built explicitly for having a flexible structure of the boom that induces pressure oscillations is chosen as case-study since it represents a worst-case scenario within load-carrying applications typically used in an offshore environment. The comparison study will show that the novel self-contained system is a valid alternative to conventional hydraulics for applications where passive load-holding is required in combination with precise position tracking in harsh environments.

2. The Self-Contained Electro-Hydraulic Cylinder

The combination of an electric drive and a fixed-displacement axial piston machine (P) drives the hydraulic cylinder (C) arranged in a closed-circuit configuration, as illustrated in Figure 1.
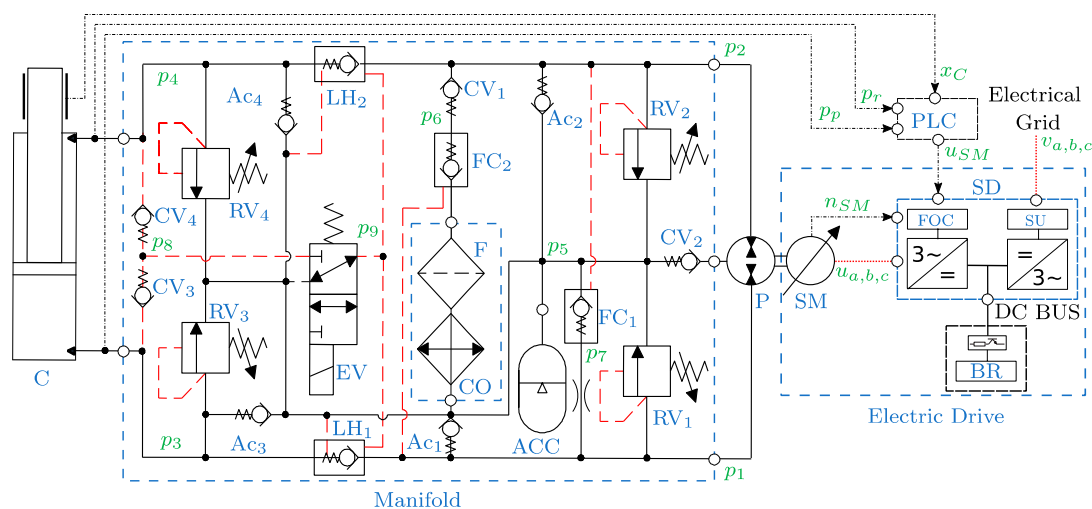

Figure 1. The self-contained electro-hydraulic cylinder addressed in this paper.

The auxiliary hydraulic components are implemented in a manifold, and the bladder-type accumulator (ACC) represents the sealed reservoir. The differential flow dictated by the cylinder's unequal areas is balanced by the two pilot-operated check valves FC_1 and FC_2, the check valves Ac_1 and Ac_2, and the check valve CV_1. The pilot-operated check valves LH_1 and LH_2 are used for passive load-holding purposes by isolating the cylinder when the 3/2 electro-valve (EV) is not actuated. The EV must be activated to enable the actuator motion, resulting in transferring the highest cylinder pressure, selected through the CV_3 and CV_4, into the opening pilot line of LH_1 and LH_2. Anti-cavitation valves (Ac_3 and Ac_4) are installed between the actuator sides and the ACC to avoid cavitation in the cylinder chambers. Pressure-relief valves (RV_1–RV_4) on both pump ports and on both cylinder ports avoid over-pressurizations. Finally, a cooler (CO) and a low-pressure filter (F) complete the hydraulics.

The electric drive consists of two main components, namely the servo-motor (SM) and the servo-drive (SD). The supply unit (SU) of the driver converts the AC voltage from the electrical grid to a DC bus voltage. The DC bus voltage is further shared with the PWM inverter, controlling the speed of the prime mover based on the field-oriented controller (FOC). A closed-loop position controller is implemented on the programmable logic controller (PLC) controlling the motion of the hydraulic cylinder by sending the control signal u_{SM} (i.e., the desired rotational speed of the prime mover) to the variable speed controller embedded in the servo-drive. An external brake resistor (BR) is connected to the DC bus to dissipate the regenerated power as heat.

2.1. Nonlinear Model of the System

A high-fidelity, dynamic model of the considered SCC driving the single-boom crane depicted in Figure 2a is presented and validated in [9]. This paper introduces the simplified system model that is used for linear control design. All models are created, simulated, and analyzed in MATLAB-Simulink®. Since the SCC used in this application only operates in two quadrants, the rod-side chamber is always connected to the low-pressure accumulator as visible in Figure 2b. (It is assumed that the 3/2 electro-valve is energized to enable motion).
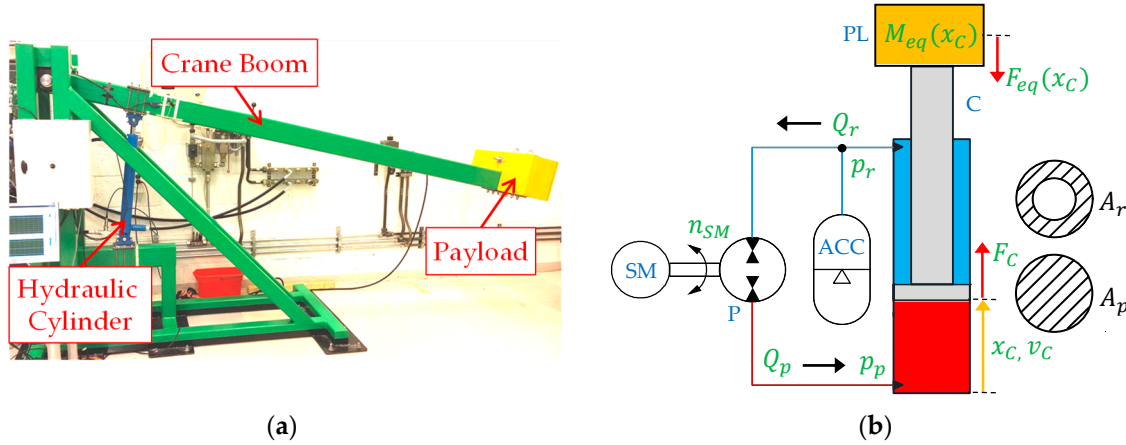

Figure 2. The considered application and the electro-hydraulic linear actuator: (**a**) single-boom crane; (**b**) simplified electro-hydraulic cylinder's circuit.

The nonlinear model of the simplified mechanical-hydraulic system is described using the Newton's second law to extract the actuator dynamics:

$$M_{eq}(x_C) \cdot \ddot{x}_C = F_C - F_{eq}(x_C). \tag{1}$$

This equation is based on the equivalent mass (M_{eq}) and on the equivalent gravitational force (F_{eq}) of the single-boom crane. Their trends were derived in Padovani et al. [9] as a function of the piston position (x_C). The mechanical force delivered by the hydraulic cylinder:

$$F_C = A_p \cdot p_p - A_r \cdot p_r - B \cdot v_C, \tag{2}$$

involves the piston-side area (A_p), the piston chamber pressure (p_p), the rod-side area (A_r), the rod chamber pressure (p_r), the viscous friction coefficient (B), and the piston velocity (v_C). The well-known pressure buildup equations for the dynamics of the actuator pressures result as:

$$\dot{p}_p = \frac{1}{C_p} \cdot \left(Q_{P,e} - A_p \cdot v_C - Q_{C,L} \right), \tag{3}$$

$$\dot{p}_r = \frac{1}{C_r} \cdot \left(A_r \cdot v_C + Q_{C,L} - Q_{P,e} \right). \tag{4}$$

They include the effective pump flow ($Q_{P,e}$), the internal leakage in the cylinder ($Q_{C,L}$), the piston-side capacitance (C_p), and the rod-side capacitance (C_r) specified below:

$$Q_{P,e} = D_p \cdot \omega_{SM} - Q_S, \tag{5}$$

$$C_p = \frac{A_p \cdot x_C + V_{p,0}}{\beta}, \tag{6}$$

$$C_r = \frac{A_r \cdot (h_C - x_C) + V_{r,0}}{\beta} + \frac{V_{AC,0}}{\kappa_{air}} \cdot \frac{p_{AC,0}^{\frac{1}{\kappa_{air}}}}{p_r^{\frac{\kappa_{air}+1}{\kappa_{air}}}}. \tag{7}$$

The effective pump flow in Equation (5) is based on the pump displacement (D_p), on the angular speed of the servo-motor (ω_{SM}), and on the pump's flow losses (Q_S), as explained in [9]. It should be noted that a positive sign of the motor speed denotes operations in pumping mode (i.e., throughout piston extension), whereas a negative sign refers to motoring mode (i.e., during piston retraction). The two capacitances in Equations (6) and (7) include the effective volume of the actuator chambers (h_C represents the maximum stroke length of the cylinder), the transmission lines' volumes ($V_{p,0}$, $V_{r,0}$), and the bulk modulus of the hydraulic fluid (β) assumed constant. The rod-side capacitance also accounts the hydro-pneumatic accumulator by recalling the effective accumulator gas volume ($V_{AC,0}$), the pre-charge pressure of the accumulator ($p_{AC,0}$), and the adiabatic air constant (κ_{air}).

2.2. Linear Model of the System

The simplified model of the SCC has been linearized and is now investigated when its natural-frequency is low (i.e., when the hydraulic cylinder is extended) because it limits the performance and represents the worst-case scenario. The resulting block diagram illustrated in Figure 3 has been obtained by considering the capacitance and the equivalent mass constant and calculated with the piston almost fully extended ($x_C = 0.45$ m). Additionally, the rod-side pressure is assumed constant and equal to $p_r = 0$ bar due to its extremely low value [9], while the external force has been considered as a disturbance that is not included in the linear model.
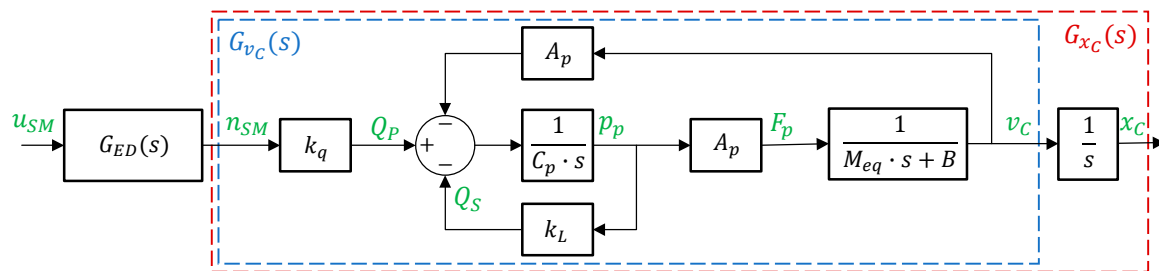

Figure 3. Block diagram representing the linear model of the uncompensated self-contained electro-hydraulic cylinder.

The transfer function of the electric drive from commanded speed (u_{SM}) to actual speed (n_{SM}) is described by the following open-loop, second-order transfer function including the natural-frequency ($\omega_{n,ED}$) and the damping ratio (ζ_{ED}):

$$G_{ED}(s) = \frac{n_{SM}(s)}{u_{SM}(s)} = \frac{\omega_{n,ED}^2}{s^2 + 2 \cdot \omega_{n,ED} \cdot \zeta_{ED} \cdot s + \omega_{n,ED}^2}. \tag{8}$$

The velocity output of the uncompensated mechanical-hydraulic system is described by the second-order, open-loop transfer function $G_{v_C}(s)$ using the gain (K_{MH}), the natural-frequency ($\omega_{n,MH}$), and the damping ratio (ζ_{MH}) according to the equations below:

$$G_{v_C}(s) = \frac{v_C(s)}{n_{SM}(s)} = \frac{K_{MH} \cdot \omega_{n,MH}^2}{s^2 + 2 \cdot \omega_{n,MH} \cdot \zeta_{MH} \cdot s + \omega_{n,MH}^2}, \tag{9}$$

$$K_{MH} = \frac{k_q \cdot A_p}{B \cdot k_L + A_p^2}, \tag{10}$$

$$\omega_{n,MH} = \sqrt{\frac{B \cdot k_L + A_p^2}{M_{eq} \cdot C_p}}, \tag{11}$$

$$\zeta_{MH} = \frac{M_{eq} \cdot k_L + B \cdot C_p}{2 \cdot \sqrt{C_p \cdot M_{eq} \cdot \left(B \cdot k_L + A_p^2\right)}}. \tag{12}$$

These parameters are evaluated using the pump flow gain ($k_q = D_p/60 \text{ m}^3/(\text{s} \cdot \text{rpm})$), and the leakage flow gain (k_L) that includes both the internal leakage in the hydraulic cylinder and the flow losses mentioned in Equation (5). Finally, the transfer function $G_{x_C}(s)$ from the servo-motor speed to piston position is derived by integrating $G_{v_C}(s)$.

The numerical values representative of the system and details about their identification are shared in Appendix A.

3. The Valve-Controlled System

The hydraulic, valve-controlled drive taken into account as the benchmark is used in several industrial applications, such as offshore cranes and oil drilling equipment, and represents the state of the art (e.g., [19–22]). The system consists of a centralized hydraulic power unit (HPU) providing a constant supply pressure (p_S) and a fixed return pressure (p_R) to the valve-controlled cylinder, as illustrated in Figure 4.
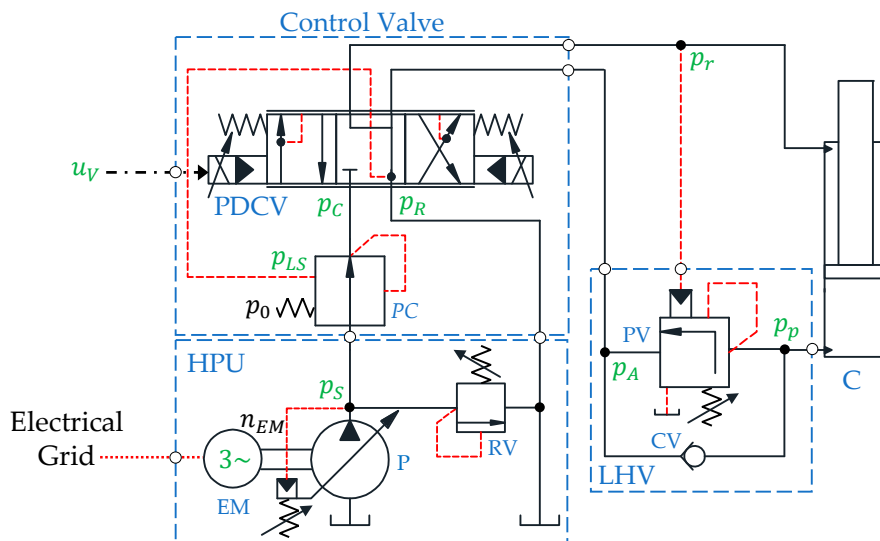

Figure 4. The considered valve-controlled cylinder architecture.

The components of the HPU are the electric motor (EM) running at constant speed and the variable-displacement axial piston pump (P). The supply pressure is controlled by the absolute pressure limiter, while a pressure-relief valve (RV) is installed for safety.

The motion of the hydraulic cylinder is controlled by a pressure-compensated, proportional directional control valve (PDCV) that receives the control input u_V from the embedded controller. The state-of-the-art flow control valve consists of two essential parts, namely the main spool with integrated closed-loop position control and the pressure compensator (PC) that guarantees a load-independent pressure drop across the metering edge. The load-holding valve (LHV), namely a vented counterbalance valve with a pilot ratio 3:1, contains a by-pass check valve (CV) and a pilot-operated poppet valve (PV) for controlling overrunning loads (i.e., when retracting the cylinder). Finally, the system is instrumented with sensors for measuring the pressures labeled in Figure 4 as well as the rod-side flow rate (Q_R) and the piston's position.

4. The Control Design

To have a fair comparison between the considered SCC and the VCC, a common control strategy based on a closed-loop PI position controller in combination with a velocity feedforward and a pressure feedback is implemented according to Figure 5.
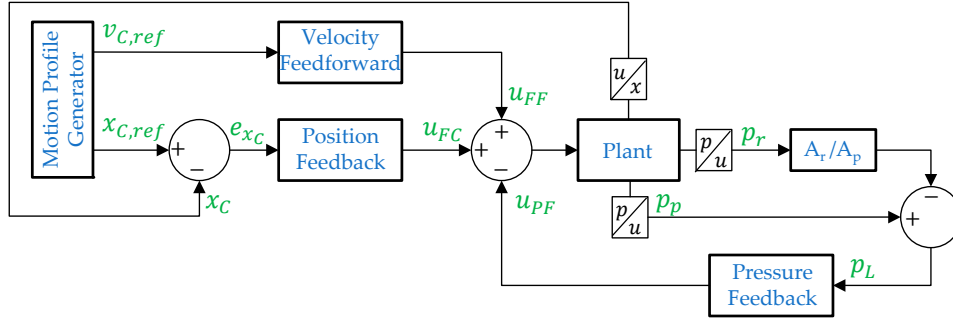

Figure 5. The proposed control structure applied to both actuation systems.

The pressure feedback represents the active-damping term of the hydraulic system that is essential due to the extremely low damping ratio of the uncompensated system ($\zeta_{MH} = 0.052$). Hence, the pressure feedback's parameters are first chosen so that the desired damping ratio of the system is obtained before designing the motion controller for the damped system; a complete explanation of the process used to derive these parameters is included in Appendix B. Further on, the motion profile generator presented in [19] provides reference signals for the desired piston velocity ($v_{C,ref}$) and piston position ($x_{C,ref}$) to the motion controller. The motion controller consists of the combination of two blocks, namely the velocity feedforward and the position feedback. The summation of the feedforward signal (u_{FF}), position feedback signal (u_{FC}), and pressure feedback signal (u_{PF}) represents the desired control input. For the SCC, this input represents the desired rotational speed of the servo-motor (u_{SM}), while it represents the desired valve opening (u_V) in the VCC. Based on the piston area, the pump flow gain, and the reference velocity of the piston, the desired speed of the prime mover is calculated as:

$$u_{FF} = \frac{A_p}{k_q} \cdot v_{C,ref}. \tag{13}$$

The control signal from the position feedback is given as:

$$u_{FC} = e_{x_C} \cdot \left(k_P + k_I \cdot \frac{1}{s}\right), \tag{14}$$

where the proportional gain (k_P) and the integral gain (k_I) are derived in the following equations:

$$k_P = 10^{\frac{Gm(\omega_{pc})}{20}}, \tag{15}$$

$$k_I = 0.1 \cdot \omega_{pc} \cdot k_P, \tag{16}$$

and the gain margin (Gm) and the phase cross over frequency (ω_{pc}) are explained in the next sections.

In addition, the VCC's control algorithm compensates for the overlap in the valve's spool according to [20], while the SCC can be operated using two different load-holding strategies. Passive load-holding (PLH) (i.e., running the prime mover is not desired during load-holding phases) takes place when the load-holding valves are closed by deactivating the electro-valve signal:

$$u_{EV} = \begin{cases} 1, & \left|v_{C,ref}\right| > 0 \text{ and } u_{ED} > 0 \\ 0, & \left|v_{C,ref}\right| = 0 \text{ and } \left|e_{x_C}\right| < 0.5 \text{ mm} \end{cases} \tag{17}$$

and by switching off the signal enabling power to the electric motor according to the logic below:

$$u_{ED} = \begin{cases} 1, & \left| v_{C,ref} \right| > 0 \\ 0, & u_{EV} = 0 \end{cases} \tag{18}$$

Conversely, active load-holding (ALH) is performed by controlling the desired piston position using the prime mover (i.e., the load-holding valves are kept open).

4.1. Control Parameters for the Self-Contained Electro-Hydraulic Cylinder

The proportional and integral gains are derived using the Bode plots according to the procedure proposed in [23]. As explained in this reference, the PI-controller should lead to fast response and only to a small overshoot if the phase margin is chosen around a phase angle of $\phi_m = 40°$. In order to ensure a stable closed-loop controller, the proportional gain in Equation (15) is calculated using the gain margin that corresponds to the phase crossover frequency at which the phase angle of the open-loop transfer function is equal to $(-180° + \phi_m + 5°)$. The identified parameters from the Bode plots and the resulting PI-controller gains are presented in Table 1 for both the uncompensated system ($G_{x_C}(s)$) and the solution that includes the high-pass filtered pressure feedback ($G_{4,HP}(s)$).

Table 1. Identified control parameters used for the PI-controller.

System	Pm (deg)	Gm(ω_{pc}) (dB)	ω_{pc} (rad/s)	k_P (rad/(s·m))	k_I (rad/(s²·m))
$G_{x_C}(s)$	45	89.1	13.3	$2.69 \cdot 10^4$	$3.61 \cdot 10^4$
$G_{4,HP}(s)$	45	102	8.93	$1.26 \cdot 10^5$	$1.19 \cdot 10^5$

Pressure feedback adds artificial damping and increases the gain margin that allows significant higher PI-controller gains while still ensuring a stable system. The approach with a high-pass filtered pressure feedback is selected, where a model-based approach for selecting the gain $k_{f,HP} = 4.77 \cdot 10^{-11}$ m³/(s · Pa) and the time constant $\tau_{f,HP} = 1.04$ s of the filter is used (a complete explanation of the process used to derive these quantities is included in Appendix B.2). This feedback is implemented in the control algorithm illustrated in Figure 5 as:

$$u_{PF} = k_q^{-1} \cdot \frac{k_{f,HP} \cdot s}{\tau_{f,HP} \cdot s + 1} \cdot p_L. \tag{19}$$

4.2. Control Parameters for the Valve-Controlled System

A linear state-space model of the considered VCC was used in Hagen et al. [20] to derive the high-pass filtered pressure feedback parameters. As demonstrated in this reference, additional damping is necessary to achieve smooth operations since the combination of a pressure-compensated control valve and a counterbalance valve makes the system unstable both in open- and closed-loop control, when the load is overrunning. The high-pass filter's parameters were evaluated as $k_{f,HP} = 9.44 \cdot 10^{-13}$ m³/(s · Pa) and $\tau_{f,HP} = 0.1047$ s. Lastly, the Bode plots of the compensated open-loop system presented in [20] are used to identify the gain margin and the phase cross over frequency. This is a necessary step to derive the PI-controller gains in Table 2 that are based on Equations (15) and (16).

Table 2. Identified control design values of the benchmark system.

Pm (deg)	Gm(ω_{pc}) (dB)	ω_{pc} (rad/s)	k_P(1/m)	k_I (1/(m·s))	k_q (m³/s)
45	29.3	6.68	29.17	19.49	$5.83 \cdot 10^{-4}$

5. Results and Discussion

Three closed-loop tests are carried out to analyze the motion performance of the novel self-contained system compared to the valve-controlled solution. Details about the considered test setups are explained in the second part of this study [18]. First, a step response is performed with maximum payload (i.e., load mass equal to 304 kg) to evaluate the closed-loop response time. Then, a working cycle with maximum payload and different piston velocity setpoints is performed to assess the tracking error. Finally, the single-boom crane is also actuated with half payload and without payload to explore the actuation system's robustness against load variations.

5.1. Closed-Loop Step Response

The closed-loop step response of both systems is reported in Figure 6. A relatively small position step from 50 to 75 mm is commanded to avoid flow saturation of the control valve in the VCC. The resulting piston velocity remains within the limits (Figure 6b) since its maximum values are 120 mm/s for the VCC and about 170 mm/s for the SCC.
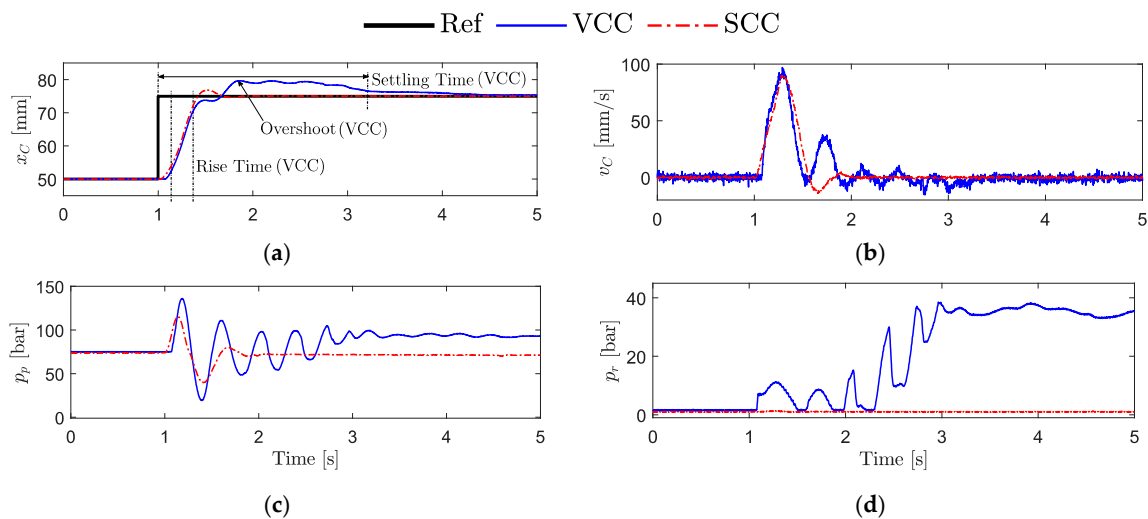

Figure 6. The closed-loop position step response comparison: (**a**) commanded and measured piston positions; (**b**) position tracking errors; (**c**) piston chamber pressures; and (**d**) rod chamber pressures.

The SCC has 10 ms faster rise time, 75% faster settling time (i.e., the time required by the velocity error to fall within 2% of the reference value), and 61% less overshoot than the VCC (Table 3 provides the exact values). The response of the VCC is expected to be slower because the open-loop crossover frequency of the compensated system is 2.25 rad/s lower than that of the SCC. As seen in Figure 6c, the piston-side chamber's pressure of the VCC has more oscillations and higher spikes than the SCC. This pressure in the VCC is about 22 bar higher at steady-state than the SCC; it is the case because the rod-side chamber's pressure (Figure 6d) is about 38 bar higher when compared to the SCC that maintains a stable pressure of about 1.0 bar.

Table 3. Results from the closed-loop position step response test.

System	Rise Time (s)	Settling Time (s)	Overshoot (mm)
VCC	0.27	2.23	4.65
SCC	0.26	0.57	1.83

5.2. Representative Working Cycle

Based on the maximum flow that the two systems can deliver to the cylinder, the highest desired piston velocity ($v_{C,max}$) is assumed equal to 120 mm/s, and the SCC is operated with passive

load-holding in the following tests. A motion profile generator is used at different velocity setpoints equal to 20, 75, and 120 mm/s, starting from the initial piston position $x_{C,0} = 50$ mm to the final position $x_{C,ref} = 450$ mm. Figure 7 shows the position tracking performance of both systems at $v_{C,max} = 120$ mm/s, also indicating when the load-holding valves of the SCC are engaged/disengaged.
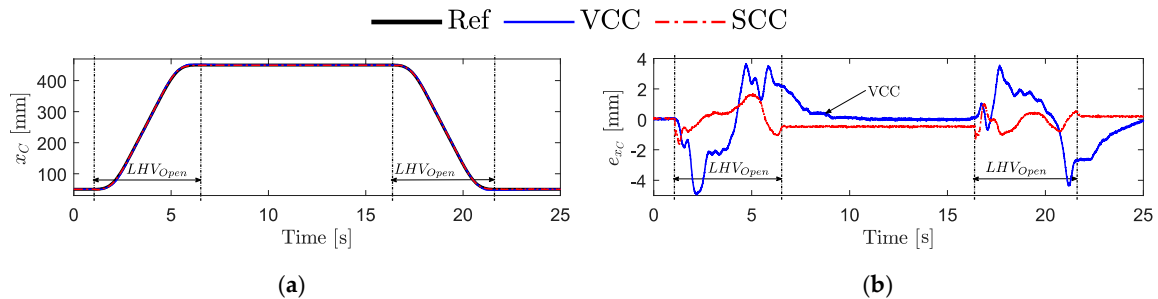

Figure 7. Position tracking performance comparison: (**a**) commanded and measured piston position; (**b**) tracking error.

Both systems can follow the desired motion profile satisfactorily, even though the maximum tracking error results are 5.0 mm for the VCC and only 1.7 mm for the SCC (i.e., 66% less). During passive load-holding, it can be seen that the VCC reaches approximately zero steady-state error. The SCC closes, however, the load-holding valves and switches off the electric motor when the measured position error is within $e_{x_C} = |0.5|$ mm, resulting in a steady-state error of about -0.48 mm. The piston position is maintained constant until the load-holding valves are opened again (i.e., at about 16.5 s). The resulting RMS tracking errors for the different velocities' setpoints are presented in Table 4; it is concluded that the SCC behaves significantly more precisely when medium/high velocity is desired.

Table 4. Resulting RMS position tracking error at max payload.

Velocity SP (mm/s)	20		75		120	
System	VCC	SCC	VCC	SCC	VCC	SCC
RMS error (mm)	0.17	0.25	1.26	0.37	1.5	0.52

Figure 8 illustrates the commanded and measured control inputs of both systems.
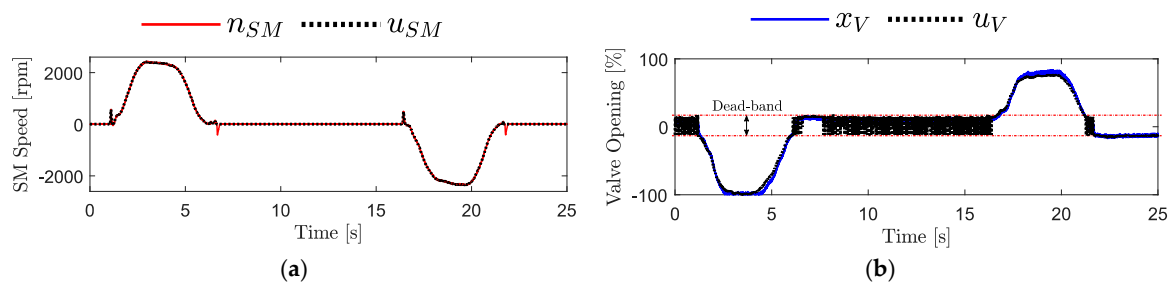

Figure 8. Commanded and measured control inputs: (**a**) self-contained system; (**b**) valve-controlled system.

The measured control signals follow the commanded values fairly well during motion. The measured speed of the servo-motor (Figure 8a) matches the desired one with high accuracy; when the load-holding valves are closing, at about 6.7 and 21.8 s, there is a limited spike due to the drop of the piston-side pump's pressure. The control valve (Figure 8b) has an expected positive overlap in the spool (i.e., a dead-band) between -11.5 and $+14.3\%$ of the opening that is compensated by the motion controller; this is the reason for the, apparently, oscillatory behavior.

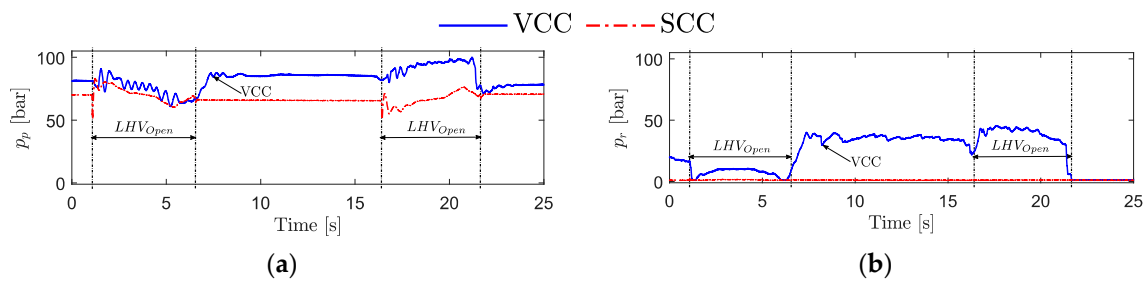Figure 9 provides the actuator pressures of both systems.

Figure 9. Actuator pressures: (**a**) piston-side chamber; (**b**) rod-side chamber.

The VCC has a higher piston-side chamber's pressure (Figure 9a) during the entire working cycle because the rod-side chamber's pressure is higher compared to the SCC (Figure 9b). When the cylinder is lowering the crane boom (i.e., between 16.5 and 22 s), the rod-side chamber's pressure is above 40 bar for the VCC, while it is stable and around 1 bar in the SCC. This condition is the case since the VCC solution needs to build up pressure on the rod-side to open the counterbalance valve and enable motion, while the SCC uses the load pressure taken from the piston-side to maintain the two load-holding valves fully open. In the VCC (Figure 10a), there is a constant supply pressure of 180 bar controlled by the HPU's pump during the entire working cycle, while the pump pressures are about 1 bar for the SCC (Figure 10b) when motion is not desired.
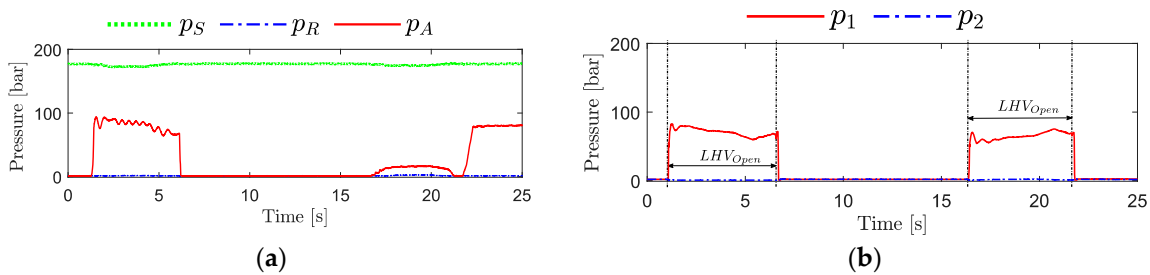

Figure 10. System pressures: (**a**) benchmark system; (**b**) self-contained system.

Consequently, the SCC has the potential to be more energy-efficient during the entire working cycle compared to the VCC, where the HPU continuously consumes power.

5.3. Scenarios with Reduced Payload

Both systems are also tested with different payloads at the velocity setpoint $v_{C,max} = 120$ mm/s to verify if the respective control algorithms are robust against load variations. The results of the tracking errors are shown in Figure 11 whereas the actuator pressures in Figure 12 for the load cases with half payload (i.e., load mass equal to 152 kg) and without payload, respectively.
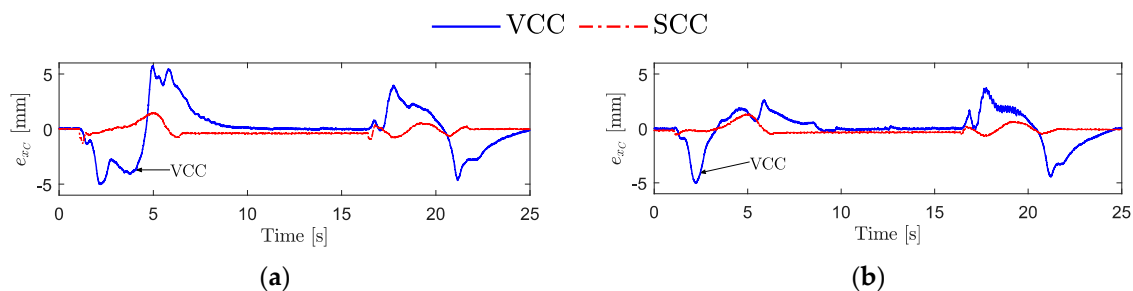

Figure 11. Tracking errors: (**a**) scenario with half payload; (**b**) scenario without payload.

Both systems can track the commanded piston position with similar performance as for the test at maximum payload. Hence, it is proven that the closed-loop position controllers of both systems

are robust enough against load variations. The SCC has less tracking error in both load conditions, confirming the above-mentioned advantages. The VCC has higher tracking error with half payload and less tracking error without payload compared to the test with full payload. The resulting RMS tracking errors are listed in Table 5.

Table 5. Resulting RMS position tracking error at the different load cases.

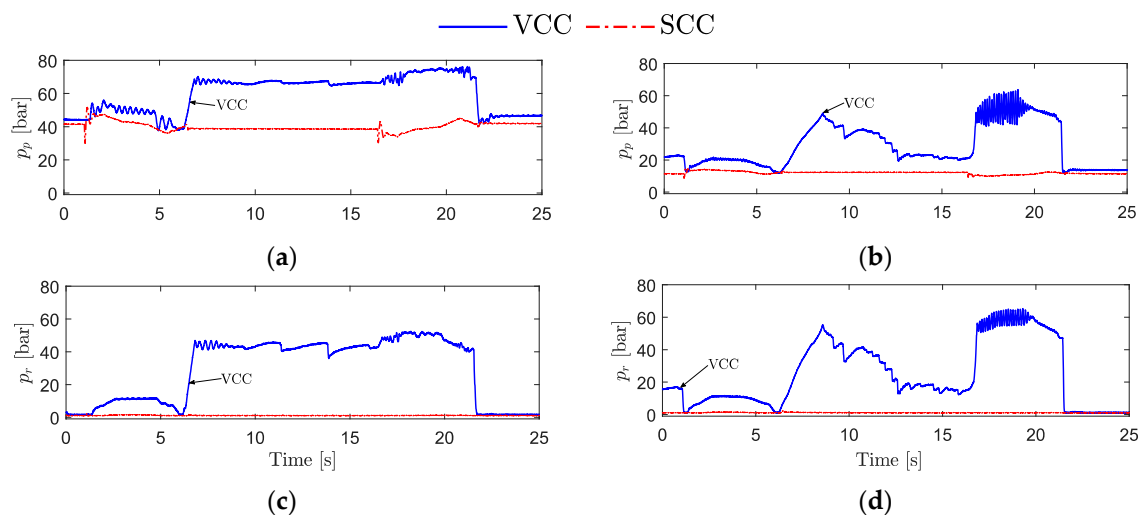| Load Case	Max Payload		Half Payload		No Payload	
System	VCC	SCC	VCC	SCC	VCC	SCC
RMS error (mm)	1.5	0.52	1.94	0.41	1.36	0.37

Figure 12. Actuator pressures: (**a**) piston chamber with half payload; (**b**) piston chamber without payload; (**c**) rod chamber with half payload; and (**d**) rod chamber without payload.

The maximum actuator pressures of both systems are clearly lower in magnitude compared to the tests with maximum payload (Figure 9) due to the decreased force acting on the hydraulic cylinder when reducing the payload. Nevertheless, there are disturbing pressure oscillations in the VCC without payload when lowering the crane boom (Figure 12b,d). This is the case because the bandwidth of the control valve (4.77 Hz) becomes lower than the frequency of the pressure oscillations (8.0 Hz); the natural-frequency of the mechanical-hydraulic system increases when the effective mass is reduced causing, therefore, these issues.

In general, the SCC performs better than the VCC for the considered working cycles. The SCC has faster response (i.e., shorter rise time and settling time) and less tracking error than the VCC. The increased performance is mainly because the SCC has a higher gain margin that allows a more aggressive closed-loop position controller while still ensuring a stable system. The active damping performs better (i.e., it gives a better reduction of the pressure oscillations) in the SCC compared to the VCC. The latter characteristic is motivated by the bandwidth of the SCC's prime mover (up to 87.54 Hz for small input commands) that is 95% higher than that of the VCC's control valve. Finally, the tests also demonstrate that the SCC can safely maintain the piston position when motion is not desired, even in case of a power shutdown. Concerning the engagement of the load-holding valves, there is a reduced pressure spike in the piston-side chamber when the load-holding is commanded. The effect, visible in Figure 9a, results in a position drop up to 1.7 mm that is considered acceptable.

6. Conclusions

This research paper presents both a theoretical and experimental analysis of a novel self-contained electro-hydraulic cylinder with particular focus on motion performance when driving a single-boom

crane. A valve-controlled cylinder was used as a benchmark since it is representative of the state of the art in many fields of industry. A control algorithm was designed based on linear techniques, including pressure feedback to add artificial damping to the system. The experimental results prove that the essential passive load-holding function of the self-contained, electro-hydraulic cylinder (SCC) can safely maintain the piston position when motion is not desired. The proposed control algorithm also seems to be robust against load variation. Further on, the SCC outperforms the benchmark system when driving the single-boom crane on all fronts:

- The SCC achieves significantly better position tracking (up to 66% less tracking error and 61% less overshoot) and faster response (i.e., 10 ms faster rise time and 75% faster settling time);
- The active pressure feedback in the SCC reduces the pressure oscillations more effectively since the electric drive has about 95% higher bandwidth than the control valve.

It is therefore concluded that the novel self-contained system represents a valid alternative to conventional hydraulic systems in terms of motion performance in load-carrying applications where position tracking and reduced oscillations are essential. It is also the case when considering energy efficiency, as presented in a separate paper (i.e., the second part of this study). Lastly, emphasis for future developments will be placed on obtaining a perfectly smooth engagement/disengagement of the passive load-holding functionality.

Conflicts of Interest: The authors declare no conflict of interest.

Nomenclature

Abbreviations

AC	Alternating current
ACC	Accumulator
Ac	Anti-cavitation valve
ALH	Active load-holding
AV	Auxiliary valves
BR	Brake resistor
C	Hydraulic cylinder
CO	Oil cooler
CV	Check valve
DC	Direct current
ED	Electric drive
EM	Electric motor
EV	Electro-valve
F	Low pressure oil filter
FC	Flow compensation valve
FOC	Field-oriented control
Gm	Gain margin
HPU	Hydraulic power unit
HS	Hydraulic system
LHV	Load-holding valve
P	Axial piston machine (pump)
PC	Pressure compensator
PDCV	Proportional directional control valve
PI	Proportional and integral
PLC	Programmable logic controller

PLH	Passive load-holding
PV	Poppet valve
PWM	Pulse-width modulation
RMS	Root mean square
RV	Pressure-relief valve
SBC	Single-boom crane
SCC	Self-contained electro-hydraulic cylinder
SD	Servo-drive
SM	Servo-motor
SU	Supply unit
V	Control valve
VCC	Valve-controlled cylinder

Symbols

A_p	Cylinder area on the piston-side
A_r	Cylinder area on the rod-side
B	Viscous friction coefficient
C_p	Piston-side capacitance
C_r	Rod-side capacitance
D_p	Pump displacement
e_{x_C}	Actuator's piston position error
K_D	Gain of the mechanical-hydraulic system including direct pressure feedback
$k_{f,D}$	Gain of the direct pressure feedback
$k_{f,HP}$	Gain of the high-pass filtered pressure feedback
K_{MH}	Gain of the uncompensated mechanical-hydraulic system
k_L	Combined leakage flow gain
k_I	Integral controller gain
k_q	Pump flow gain
k_P	Proportional controller gain
M_{eq}	Equivalent mass
n_{SM}	Rotational speed of the servo-motor in revolutions per minute
$Q_{C,L}$	Internal leakage in the hydraulic cylinder
Q_P	Actuator's flow demand
$Q_{P,e}$	Effective pump flow
Q_r	Rod-side flow
Q_S	Pump's flow losses
p_0	Fixed pressure-drop across the proportional directional control valve
p_1	Piston-side pump pressure
p_2	Rod-side pump pressure
$p_{AC,0}$	Pre-charge pressure of the accumulator
p_{LS}	Load-sensing pressure
p_p	Actuator's piston chamber pressure
p_r	Actuator's rod chamber pressure
p_R	Return pressure
p_S	Supply pressure
u_{ED}	On/off command to enable power to the servo-motor
u_{EV}	On/off command to open or close the 3/2 electro-valve
u_{FC}	Position feedback control signal
u_{FF}	Velocity feedforward control signal
u_{PF}	Pressure feedback control signal
u_{SM}	Commanded servo-motor speed
u_V	Commanded opening of the control valve's spool position
$V_{AC,0}$	Effective accumulator gas volume
v_C	Actuator's piston velocity
$v_{C,ref}$	Actuator's piston velocity reference command

$V_{p,0}$	Transmission lines' volumes between the pump and the piston-side chamber
$V_{r,0}$	Transmission lines' volumes between the pump and the rod-side chamber
x_C	Actuator's piston position
$x_{C,0}$	Actuator's initial piston position
$x_{C,ref}$	Actuator's piston position reference command

Greek symbols

β	Constant bulk modulus of the hydraulic fluid
κ_{air}	Adiabatic air constant
$\tau_{f,HP}$	Time constant of the high-pass filtered pressure feedback
ϕ_m	Phase angle
ω_{gc}	Gain cross over frequency
$\omega_{n,D}$	Natural-frequency of mechanical-hydraulic system including direct pressure feedback
$\omega_{n,ED}$	Natural-frequency of the electric drive
$\omega_{n,MH}$	Natural-frequency of the uncompensated mechanical-hydraulic system
ω_{pc}	Phase cross over frequency
ω_{SM}	Angular velocity of the servo-motor in radians per second
ζ_D	Damping ratio of the mechanical-hydraulic system including direct pressure feedback
ζ_{ED}	Damping ratio of the electric drive
ζ_{MH}	Damping ratio of the uncompensated mechanical-hydraulic system
ζ_3	Damping ratio of the complex conjugate pole pair in the transfer function $G_{3,HP}(s)$

Appendix A.

This appendix presents the parameter identification and validation of the uncompensated SCC. An open-loop ramp test was carried out, where a ramp time of 0.1 s was used to avoid saturation of the acceleration limiter of the electric drive. Figure A1 shows the given input signal and the corresponding simulated and experimental measurements. The simplified system model was validated when the hydraulic cylinder is almost fully extended (i.e., $x_C = 450$ mm).
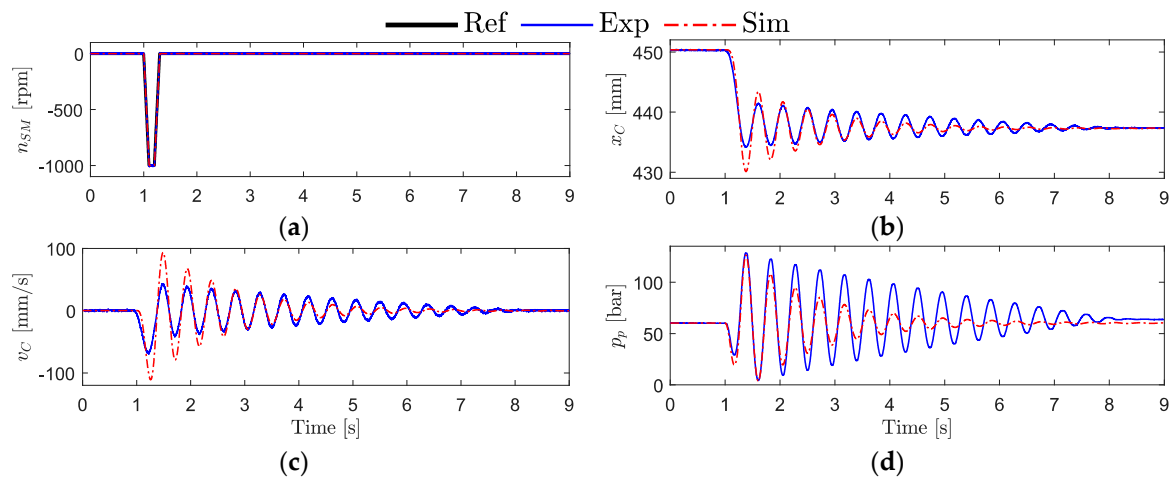
Figure A1. Open-loop validation of the linear system model: (**a**) commanded, simulated, and measured speed of the servo-motor; (**b**) simulated and measured piston position; (**c**) simulated and estimated piston velocity; and (**d**) simulated and measured piston chamber pressure.

The parameters of the linear transfer functions presented in Table A1 are identified by performing a three-step parameter tuning process such that the simulated and measured values in Figure A1 best match each other. First, the natural-frequency and the damping ratio of the electric drive are tuned according to Figure A1a. Secondly, the initial volume, the bulk modulus, and the leakage flow gain are tuned according to Figure A1d. Finally, the pump flow gain is tuned according to Figure A1b.

Table A1. Identified parameters of the transfer functions.

| Parameter	Value	Parameter	Value
$\omega_{n,ED}$	550 (rad/s)	$V_{p,0}$	$0.88 \cdot 10^{-3}$ (m^3)
ζ_{ED}	0.8	k_L	$1.00 \cdot 10^{-15}$ (m^3/(s$\cdot$Pa))
k_q	$2.17 \cdot 10^{-7}$ (m^3/(s$\cdot$rpm))	A_p	0.0033 (m^2)
C_p	$3.60 \cdot 10^{-12}$ (m^3/Pa)	B	22500 (N$\cdot$s/m)
β	$6600 \cdot 10^5$ (Pa)	M_{eq}	15500 (kg)

Appendix B.

This appendix clarifies the definition of the control parameters involved in the pressure feedback of the SCC. Two methods were investigated in this paper to enable active damping, namely direct and high-pass filtered pressure feedback.

Figure A2 illustrates the modified plant model, where the effect of the internal pressure feedback is considered as an equivalent flow rate (Q_{PF}).
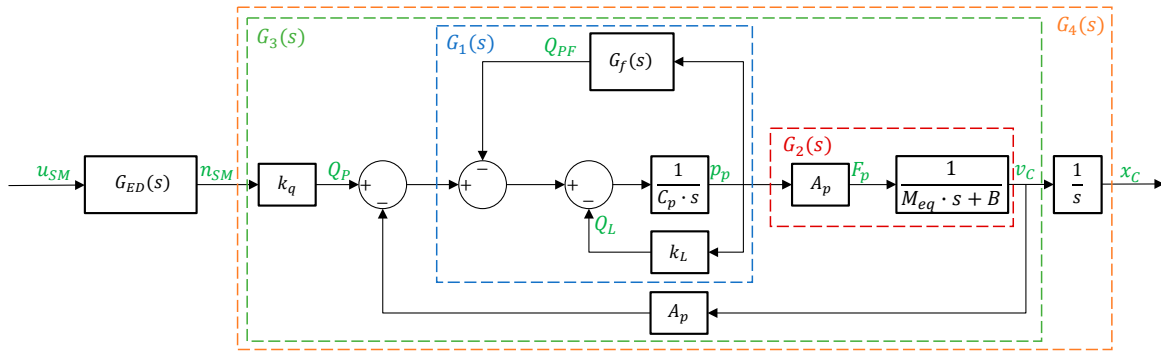
Figure A2. A function block representing the modified plant model that includes the pressure feedback.

Appendix B.1. Direct Pressure Feedback

When applying direct pressure feedback, the transfer function $G_f(s) = G_{f,D}$ consists of a simple gain $k_{f,D}$ According to [24], $k_{f,D}$ should be selected so that the damping ratio of the system is within the range $0.5 < \zeta_D < 0.7$ The open-loop transfer function from servo-motor speed to piston velocity when including direct pressure feedback is given as:

$$G_{3,D}(s) = \frac{v_C(s)}{n_{SM}(s)} = \frac{K_D \cdot \omega_{n,D}^2}{s^2 + 2 \cdot \omega_{n,D} \cdot \zeta_D \cdot s + \omega_{n,D}^2}, \tag{A1}$$

where the resulting gain (K_D), the natural-frequency ($\omega_{n,D}$), and the damping ratio (ζ_D) are:

$$K_D = \frac{k_q \cdot A_p}{B \cdot \left(k_{f,D} + k_L\right) + A_p^2}, \tag{A2}$$

$$\omega_{n,D} = \sqrt{\frac{B \cdot \left(k_{f,D} + k_L\right) + A_p^2}{M_{eq} \cdot C_p}}, \tag{A3}$$

$$\zeta_D = \frac{C_p \cdot \left(k_{f,D} + B\right) + M_{eq} \cdot \left(k_{f,D} + k_L\right)}{2 \cdot \sqrt{C_p \cdot M_{eq} \cdot \left[B \cdot \left(k_{f,D} + k_L\right) + A_p^2\right]}}. \tag{A4}$$

By rewriting Equation (A4), the desired damping ratio of $G_{3,D}(s)$ dictates the following pressure feedback gain:

$$k_{f,D} = \frac{2 \cdot \zeta_D \cdot \sqrt{C_p \cdot M_{eq} \cdot A_p^2 - C_p^2 \cdot B^2 \cdot \left(1 - \zeta_D^2\right)} - C_p \cdot B \cdot \left(1 - 2 \cdot \zeta_D^2\right)}{M_{eq}} - k_L. \tag{A5}$$

Finally, the transfer function $G_{4,D}(s)$ from servo-motor speed to piston position, including the direct pressure feedback, is derived by integrating $G_{3,D}(s)$.

Figure A3 demonstrates the effect of applying direct pressure feedback with the desired damping of 0.5 and 0.7, in comparison to the uncompensated system with the damping ratio 0.052.
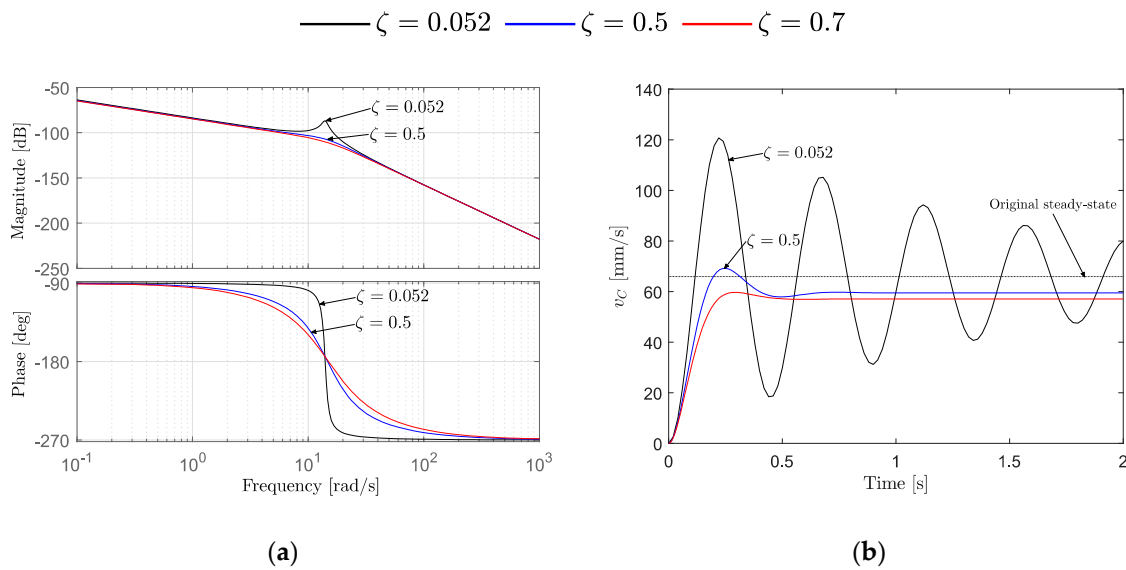

Figure A3. The effect of different damping ratios in comparison to the uncompensated system: (**a**) Bode plots of $G_{4,D}(s)$ and $G_{x_C}(s)$; (**b**) step response ($n_{SM} = 1000$ rpm) of $G_{3,D}(s)$ and $G_{v_C}(s)$.

The control design values such as the gain margin, the cross over frequency, the rise time, the settling time, and the overshoot identified from Figure A3 are presented in Table A2 for different system's damping ratios.

Table A2. Identified control design values when using direct pressure feedback.

ζ	Gm (dB)	ω_{gc} (rad/s)	Rise Time (s)	Settling Time (s)	Overshoot (mm/s)
0.052	86.9	14.0	0.077	5.39	85.02
0.5	108	14.7	0.11	0.55	16.29
0.7	111	15.0	0.14	0.40	4.59

A drawback when implementing direct pressure feedback is that the measured pressure in steady state will yield a signal that commands the prime mover to rotate. Consequently, the steady-state pressure must continuously be updated and subtracted from the measured pressures; this is also the case when implementing a low-pass filtered pressure feedback. Due to the high nonlinearities of the hydraulic system, the load that is changing during the operating cycle, and the noise of the pressure feedback signal, direct pressure feedback is challenging to implement. Hence, a high-pass filter is often used to avoid these problems [25,26]. However, direct pressure feedback is much simpler to use for linear control analysis because a second-order transfer function of the mechanical-hydraulic system is maintained. Therefore, this paper proposes to derive the pressure feedback gain according to Equation (A5) based on the desired damping ratio of the damped second-order system and further use it in the high-pass filtered pressure feedback. A damping ratio $\zeta_D = 0.5$ was chosen because of the faster rise time, resulting in $k_{f,D} = k_{f,HP} = 4.77 \cdot 10^{-11}$ m^3/ (s · Pa).

Appendix B.2. High-Pass Filtered Pressure Feedback

A high-pass filtered pressure feedback was successfully implemented on a SCC in [9] but the filter parameters where experimentally tuned. In this paper, it is proposed a model-based approach for selecting the gain ($k_{f,HP}$) and the time constant ($\tau_{f,HP}$) of the high-pass filter given below:

$$G_{f,HP}(s) = \frac{k_{f,HP} \cdot s}{\tau_{f,HP} \cdot s + 1}. \tag{A6}$$

The open-loop transfer function from motor speed to piston velocity when including high-pass filtered pressure feedback results as:

$$G_{3,HP}(s) = \frac{v_C(s)}{n_{SM}(s)} = \frac{k_q \cdot G_1(s) \cdot G_2(s)}{1 + G_1(s) \cdot G_2(s) \cdot A_p} = \frac{k_q \cdot A_p\big(\tau_{f,HP} \cdot s + 1\big)}{D_3 \cdot s^3 + D_2 \cdot s^2 + D_1 \cdot s + D_0}, \tag{A7}$$

where the different terms that form the denominator are given as follows:

$$D_3 = M_{eq} \cdot C_p \cdot \tau_{f,HP}, \tag{A8}$$

$$D_2 = \big(k_L \cdot \tau_{f,HP} + C_p + k_{f,HP}\big) \cdot M_{eq} + C_p \cdot B \cdot \tau_{f,HP}, \tag{A9}$$

$$D_1 = \big(k_L \cdot \tau_{f,HP} + C_p + k_{f,HP}\big) \cdot B + M_{eq} \cdot k_L + A_p^2 \cdot \tau_{f,HP}, \tag{A10}$$

$$D_0 = B \cdot k_L + A_p^2. \tag{A11}$$

Finally, the transfer function $G_{4,HP}(s)$ from servo-motor speed to piston position, including the high-pass filtered pressure feedback, is derived by integrating $G_{3,HP}(s)$.

Figure A4 demonstrates the effect of varying the filter's time constant while maintaining the same gain.
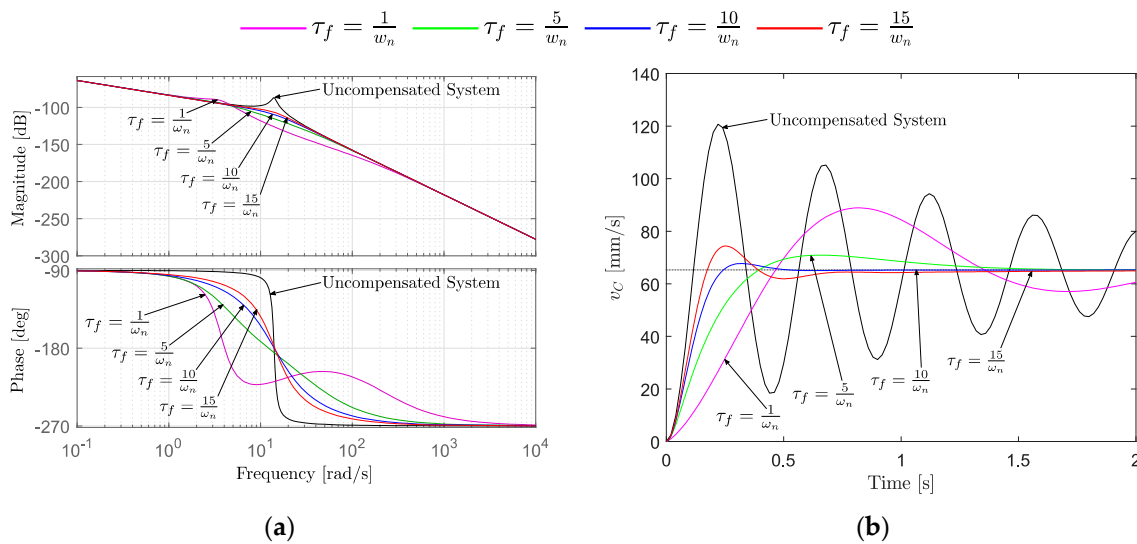

(a)　　　　　　　　　　　　　　　　　　　　**(b)**

Figure A4. The effect of varying the time constant of the high-pass filter: (**a**) Bode plots of $G_{4,HP}(s)$ and $G_{x_C}(s)$; (**b**) step response of $G_{3,HP}(s)$ and $G_{v_C}(s)$.

The control design values, namely the gain margin, the cross over frequency, the damping of the complex conjugate pole pair (ζ_3) of $G_{3,HP}(s)$, the rise time, settling time, and the overshoot, identified from Figure A4 are presented in Table A3 for the different filter's time constants.

Table A3. Identified control design values when using high-pass filtered pressure feedback.

$\tau_{f,HP}$ (s)	Gm (dB)	ω_{gc} (rad/s)	ζ_3	Rise Time (s)	Settling Time (s)	Overshoot (mm/s)
$1/\omega_n$	92.6	4.06	0.319	0.34	2.93	36.14
$5/\omega_n$	113	12.2	0.864	0.27	1.27	8.61
$10/\omega_n$	110	14.1	0.713	0.16	0.41	3.72
$15/\omega_n$	107	14.3	0.486	0.12	0.67	13.99

The filter time constant $\tau_{f,HP} = 14.55/14.03 = 1.04$ s is selected because it corresponds to a damping ratio of the complex conjugate poles $\zeta_3 = 0.5$ with a rise time comparable to the system with direct pressure feedback as demonstrated in Figure A3 and Table A1. The high-pass filtered pressure feedback causes slower rise time and settling time. However, the overshoot is 14% smaller, and the steady-state error, as shown in Figure A3b, is removed.

References

1. Michel, S.; Weber, J. Electrohydraulic Compact-drives for Low Power Applications considering Energy-efficiency and High Inertial Loads. In Proceedings of the 7th FPNI PhD Symposium on Fluid Power, Reggio Emilia, Italy, 27–30 June 2012; pp. 27–30.
2. Minav, T.A.; Sainio, P.; Pietola, M. Direct Driven Hydraulic Drive without Conventional Oil Tank. In Proceedings of the ASME/BATH 2014 Symposium on Fluid Power and Motion Control, Bath, UK, 10–12 September 2014.
3. Altare, G.; Vacca, A.; Richter, C. A Novel Pump Design for an Efficient and Compact Electro-Hydraulic Actuator. In Proceedings of the IEEE Aerospace Conference, Big Sky, MT, USA, 1–8 March 2014.
4. Altare, G.; Vacca, A. A design solution for efficient and compact electro-hydraulic actuators. *Procedia Eng.* **2015**, *106*, 8–16. [CrossRef]
5. Jalayeri, E.; Imam, A.; Tomas, Z.; Sepehri, N. A throttle-less single-rod hydraulic cylinder positioning system: Design and experimental evaluation. *Adv. Mech. Eng.* **2015**, *7*, 1687814015583249. [CrossRef]
6. Rexroth, B. Electrification and Digitalization: The Fitness Program for Hydraulics. 2015. Available online: https://www.boschrexroth.com/en/xc/products/product-groups/industrial-hydraulics/the-fitness-program-for-hydraulics (accessed on 21 September 2019).
7. Helbig, A.; Boes, C. Electric Hydrostatic Actuation-modular building blocks for industrial applications. In Proceedings of the 10th International Fluid Power Conference, Dresden, Germany, 8–10 March 2016; pp. 93–102.
8. Hagen, D.; Padovani, D.; Ebbesen, M.K. Study of a Self-Contained Electro-Hydraulic Cylinder Drive. In Proceedings of the 2018 Global Fluid Power Society PhD Symposium (GFPS), Samara, Russia, 18–20 July 2018.
9. Padovani, D.; Ketelsen, S.; Hagen, D.; Schmidt, L. A Self-Contained Electro-Hydraulic Cylinder with Passive Load-Holding Capability. *Energies* **2019**, *12*, 292. [CrossRef]
10. Weber, I.J.; Schneider, D.I.; Shabi, M.S.; Sitte, D.I.; Weber, D.I.; Willkomm, D.I.; Beck, D.I.; Fischer, D.I.; Ivantysyn, M.S.; Kolks, D.I.; et al. Novel System Architectures by Individual Drives. In Proceedings of the 10th International Fluid Power Conference, Dresden, Germany, 8–10 March 2016; pp. 29–62.
11. Ketelsen, S.; Padovani, D.; Andersen, T.; Ebbesen, M.; Schmidt, L. Classification and Review of Pump-Controlled Differential Cylinder Drives. *Energies* **2019**, *12*, 1293. [CrossRef]
12. Schmidt, L.; Ketelsen, S.; Brask, M.H.; Mortensen, K.A. A class of energy efficient self-contained electro-hydraulic drives with self-locking capability. *Energies* **2019**, *12*, 1866. [CrossRef]
13. Pedersen, H.C.; Schmidt, L.; Andersen, T.O.; Brask, M.H. Investigation of New Servo Drive Concept Utilizing Two Fixed Displacement Units. *9th JFPS Int. J. Fluid Power Syst.* **2014**, *8*, 1–9. [CrossRef]
14. Michel, S.; Weber, J. Energy-efficient electrohydraulic compact drives for low power applications. In Proceedings of the ASME/BATH 2012 Symposium on Fluid Power and Motion Control, Arlington, VA, USA, 31 October–2 November 2012; pp. 93–107.
15. Schmidt, L.; Roemer, D.B.; Pedersen, H.C.; Andersen, T.O. Speed-Variable Switched Differential Pump System for Direct Operation of Hydraulic Cylinders. In Proceedings of the ASME/BATH Symposium on Fluid Power and Motion Control, Chicago, IL, USA, 12–14 October 2015.
16. Schmidt, L.; Ketelsen, S.; Padovani, D.; Mortensen, K.A. Improving the Efficiency and Dynamic Properties of a Flow Control Unit in a Self-Locking Compact Electro-Hydraulic Cylinder Drive. In Proceedings of the ASME/Bath Symposium on Fluid Power and Motion Control, Longboat Key, FL, USA, 7–9 October 2019.
17. Schmidt, L.; Groenkjaer, M.; Pedersen, H.C.; Andersen, T.O. Position Control of an Over-Actuated Direct Hydraulic Cylinder Drive. *Control Eng. Pract.* **2017**, *64*, 1–14. [CrossRef]
18. Hagen, D.; Padovani, D.; Choux, M. A Comparison Study of a Novel Self-Contained Electro-Hydraulic Cylinder versus a Conventional Valve-Controlled Actuator—Part 2: Energy Efficiency. *Actuators* **2019**. on press.
19. Hagen, D.; Padovani, D.; Choux, M. Enabling Energy Savings in Offshore Mechatronic Systems by using Self-Contained Cylinders. *Model. Identif. Control* **2019**, *40*, 89–108. [CrossRef]
20. Hagen, D.; Padovani, D.; Choux, M. Design and Implementation of Pressure Feedback for Load-Carrying Applications with Position Control. In Proceedings of the Sixteenth Scandinavian International Conference on Fluid Power, Tampere, Finland, 22–24 May 2019.

21. Bak, M.K. Model Based Design of Electro-Hydraulic Motion Control Systems for Offshore Pipe Handling Equipment. Ph.D. Thesis, University of Agder, Kristiansand S, Norway, 2014.

22. Kjelland, M.B. Offshore Wind Turbine Access Using Knuckle Boom Cranes. Ph.D. Thesis, University of Agder, Kristiansand S, Norway, 2016.

23. Phillips, C.L.; Harbor, R.D. *Feedback Control System*; Prentice-Hall International Editions: Upper Saddle River, NJ, USA, 1991.

24. Mohieddine, J.; Kroll, A. *Hydraulic Servo-Systems: Modelling, Identification and Control*; Springer: London, UK, 2003.

25. Krus, P.; Palmberg, J.O. Damping of mobile systems in machines with high inertia loads. In *Proceedings of the JFPS International Symposium on Fluid Power*; The Japan Fluid Power System Society: Tokyo, Japan, 1989; Volume 1989, pp. 63–70.

26. Pedersen, H.C.; Andersen, T.O.; Hansen, M.R. Guidelines for Properly Adjusting Pressure Feedback in Systems with Over-Centre Valves. In Proceedings of the BATH/ASME Symposium on Fluid Power & Motion Control, Bath, UK, 7–9 September 2016.

Paper G

A Comparison Study of a Novel Self-Contained Electro-Hydraulic Cylinder versus a Conventional Valve-Controlled Actuator – Part 2: Energy Efficiency

Daniel Hagen, Damianio Padovani, and Martin Choux

A Comparison Study of a Novel Self-Contained Electro-Hydraulic Cylinder versus a Conventional Valve-Controlled Actuator—Part 2: Energy Efficiency

Daniel Hagen *[ID], **Damiano Padovani**[ID] and **Martin Choux**

Department of Engineering Sciences, University of Agder, 4879 Grimstad, Norway;
damiano.padovani@uia.no (D.P.); martin.choux@uia.no (M.C.)
* Correspondence: daniel.hagen@uia.no

Abstract: This research paper presents the second part of a comparative analysis of a novel self-contained electro-hydraulic cylinder with passive load-holding capability against a state of the art, valve-controlled hydraulic system that is typically used in load-carrying applications. After addressing the control design and motion performance in the first part of the study, the comparison is now focused on the systems' energy efficiency. It is experimentally shown that the self-contained solution enables 62% energy savings in a representative working cycle due to its throttleless and power-on-demand nature. In the self-contained drive, up to 77% of the energy taken from the power supply can be used effectively if the recovered energy is reused, an option that is not possible in the state of the art hydraulic architecture. In fact, more than 20% of the consumed energy may be recovered in the self-contained system during the proposed working cycle. In summary, the novel self-contained option is experimentally proven to be a valid alternative to conventional hydraulics for applications where passive load-holding is required both in terms of dynamic response and energy consumption. Introducing such self-sufficient and completely sealed devices also reduces the risk of oil spill pollution, helping fluid power to become a cleaner technology.

Keywords: linear actuators; self-contained cylinders; electro-hydraulic systems; passive load-holding; proportional directional control valves; load-carrying applications; energy recovery; energy efficiency

1. Introduction

Due to the increasing focus on the environmental impact, such as CO_2 emissions and oil spill pollution, inefficient state of the art hydraulic actuation tends to be replaced by electric drives in many industrial environments. This is the case, for instance, in offshore oil drilling [1]. However, hydraulic systems are still needed in load-carrying applications (e.g., knuckle-boom cranes or oil drilling equipment) because their force density is higher than that of their linear electro-mechanical counterparts and they do not present key issues related to reliability (e.g., strong impact forces) [2].

Consequently, compact and self-contained electro-hydraulic cylinders (SCCs) have received considerable attention in the last decade [3–10], showing the potential to replace both conventional hydraulics and linear electro-mechanical systems [11]. SCCs can in fact enhance energy efficiency, modular design, plug-and-play installation, and reduced maintenance [12]. Current commercial solutions of the SCC technology are limited and typically tailor-made, whereas the research emphasis is primarily on different electro-hydraulic configurations [13–16], energy-efficiency [17–21], thermal analysis [22–24], and low-power servo applications [25]. According to the survey presented in [10], compact and self-contained solutions comprising passive load-holding devices, able to operate in four quadrants, and suitable for power levels above 5 kW are missing, both on the market and

in the technical literature. Moreover, the lack of experimental comparisons in terms of energy consumption and efficiency between SCCs and conventional solutions for load-carrying applications is evident. Only a limited number of simulation studies applying the SCC technology to load-carrying applications and investigating the energy-saving potentials compared to existing hydraulic systems were identified [26,27].

　　　Hence, this research paper aims to experimentally evaluate and compare the energy consumption and the energy efficiency of a self-contained electro-hydraulic cylinder versus a conventional approach. A SCC concept able to operate in four quadrants, including passive load holding, and suitable for power levels above 5 kW was proposed in [10] and implemented on a single-boom crane in [12]. A further analysis of this solution is presented in the first part of this research [28], including the control design and the motion performance comparison against the valve-controlled cylinder (VCC) discussed in [29]. Concerning the paper structure, Section 2 presents the two considered actuation systems while Section 3 the theoretical background. In Section 4, the experimental results are introduced and discussed. The comparison study will show that the novel self-contained system is a valid alternative to conventional hydraulics also for applications where passive load-holding is required because huge energy savings are enabled.

2. The Considered Actuation Systems

　　　Two actuation systems are investigated in this research, namely a new self-contained electro-hydraulic cylinder and state of the art valve-controlled architecture that is typically used on load-carrying applications.

2.1. The Self-Contained Electro-Hydraulic Cylinder

　　　The combination of an electric drive and a fixed-displacement axial piston machine drives the hydraulic cylinder arranged in a closed-circuit configuration, as illustrated in Figure 1.
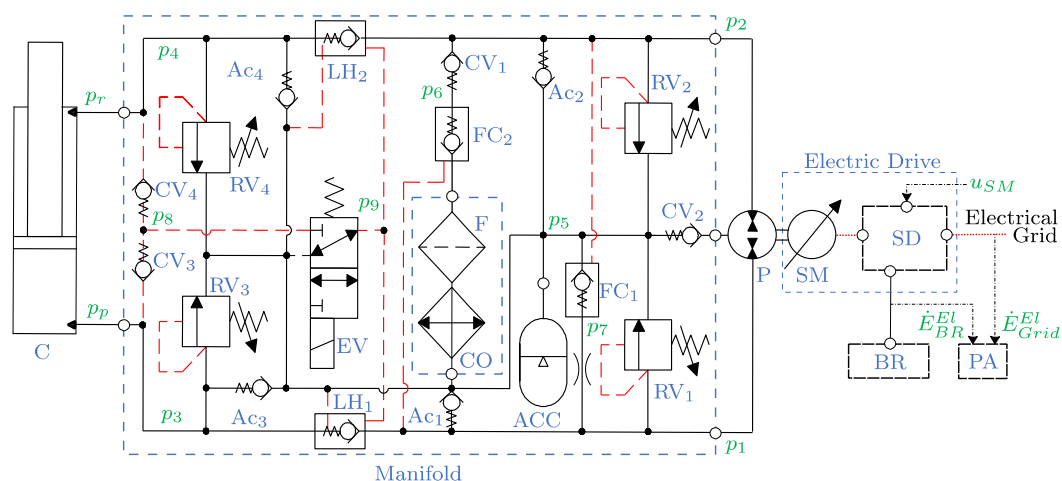
Figure 1. Schematic of the self-contained system addressed in this research.

　　　The auxiliary hydraulic components are implemented in a manifold and the bladder-type accumulator represents the sealed reservoir. The differential flow dictated by the cylinder's unequal areas is balanced by the two pilot-operated check valves FC_1 and FC_2, the check valves Ac_1 and Ac_2, and the check valve CV_1. The pilot-operated check valves LH_1 and LH_2 are used for passive load-holding purposes by isolating the cylinder when the 3/2 electro-valve is not actuated. The electro-valve must be activated to enable the actuator motion, resulting in transferring the highest cylinder pressure, selected through CV_3 and CV_4, into the opening pilot line of the load-holding valves. Anti-cavitation valves are installed on both actuator sides, whereas pressure-relief valves are present on the pump ports and

on the cylinder ports to protect from over-pressurizations. Finally, a cooler and a low-pressure filter complete the hydraulic system.

The electric drive consists of the servo-motor and the servo-drive. The frequency converter is controlling the speed of the permanent magnet synchronous motor with field-oriented control whereas an outer closed-loop position controller is implemented on an embedded programmable logic controller (PLC) to supervise the motion of the hydraulic cylinder, sending the desired rotational speed (u_{SM}) to the servo-drive. In addition, an external brake resistor is connected to the servo-drive to dissipate the regenerated power into heat. According to Ristic et al. [30], there exist solutions where this regenerated power is used profitably (e.g., power-sharing via common DC bus between multiple electric drives, return the electrical power to the grid, and energy storage on a battery or in a capacitor). Lastly, a power analyzer measures both the electric power consumed from the electrical grid ($\dot{E}_{Grid}^{El}$) and the electric power dissipated in the brake resistor ($\dot{E}_{BR}^{El}$). For more details about the self-contained system, Padovani et al. [12] describes its functionality, while the components used to implement this solution are presented in Table 1.

Table 1. Components used to implement the self-contained system.

Symbol	Component	Manufacturer	Model
C	Hydraulic cylinder	PMC Cylinders [1]	25CAL
SM	Servo-motor	Bosch Rexroth [2]	MSK071E-0300
P	Axial piston machine	Bosch Rexroth	A10FZG
SD	Servo-drive	Bosch Rexroth	HCS02.1E-W0054
ACC	Hydro-pneumatic accumulator	Bosch Rexroth	HAB10
CO	Oil cooler	Bosch Rexroth	KOL3N
F	Hydraulic return line filter	Bosch Rexroth	50LEN0100
LHV$_{1,2}$	Pilot-operated check valves	Sun Hydraulics [3]	CVEVXFN
FC$_{1,2}$	Pilot-operated check valves	Sun Hydraulics	CKEBXCN
RV$_{1-4}$	Pressure-relief valves	Sun Hydraulics	RDDA
CV$_{1,3,4}$	Check valves	Hawe Hydraulik [4]	RB2
CV$_2$, **Ac**$_{1,2}$	Check valves	Hawe Hydraulik	RK4
Ac$_{3,4}$	Check valves	Hawe Hydraulik	RK2
EV	3/2 Directional valve	Argo Hytos [5]	SD1E-A3
p_{1-9}	Pressure transducers	Bosch Rexroth	HM20
$p_{p,r}$	Pressure transducers	Parker [6]	SCP-400
x_C	Cylinder position sensor	Regal [7]	PS6300
PLC	Embedded controller	Bosch Rexroth	XM22
BR	Brake resistor	Bosch Rexroth	HLR01.1N-03K8
PA	Power analyzer	Hioki [8]	PW6001

[1] Sävsjö, Sweden; [2] Lohr, Germany; [3] Sarasota, USA; [4] München, Germany; [5] Zug, Switzerland; [6] Cleveland, USA; [7] Uppsala, Sweden; [8] Nagano, Japan.

A hydraulic cylinder with piston diameter of 65 mm, rod diameter of 35 mm, stroke length of 500 mm, and an integrated position sensor is common to both actuation systems (i.e., also to the valve-controlled layout recalled in the sequel). The piston's velocity ($\dot{x}_C$) is estimated by differentiating and lowpass filtering the measured position (x_C). Pressure transducers are installed directly on the piston-side (p_p) and rod-side (p_r) ports of the cylinder.

2.2. The Valve-Controlled System

The valve-controlled system taken as a benchmark consists of a centralized hydraulic power unit (HPU) providing a constant supply pressure (p_S) and a fixed return pressure (p_R) to the valve-controlled cylinder according to the schematic depicted in Figure 2.
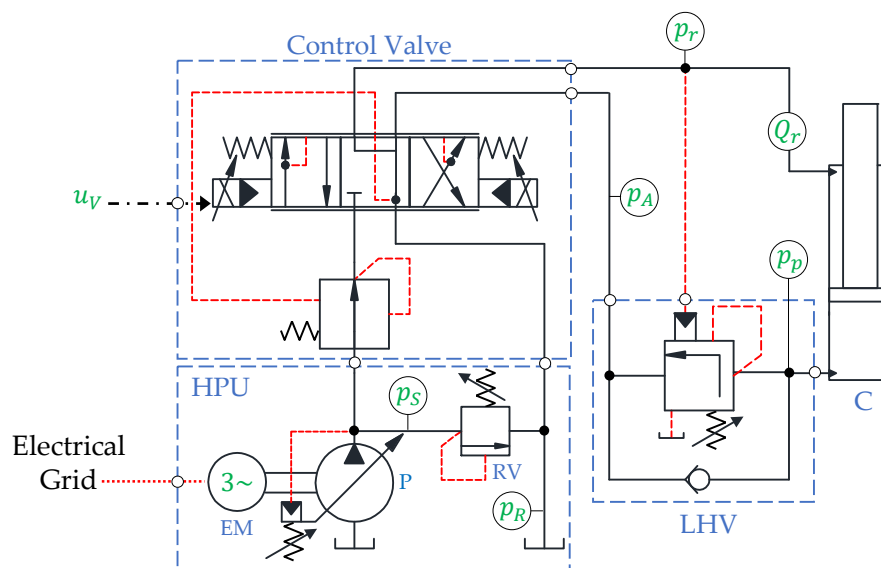
Figure 2. Schematics of the valve-controlled system under investigation.

The components of the HPU are an electric motor running at the constant speed of 1500 rpm and a variable-displacement axial piston pump with a maximum displacement of 75 cm^3/rev. The supply pressure is controlled by the absolute pressure limiter as $p_S = 180$ bar, while a pressure-relief valve is installed for safety. The motion of the hydraulic cylinder is controlled by a state of the art, pressure-compensated flow control valve (i.e., a proportional directional control valve (PDCV)) that receives the control input (u_V) from the PLC. The load-holding valve is installed to control overrunning loads and for safety purposes during standstill, according to regulations. Finally, the system is instrumented with sensors for measuring the pressures labeled in Figure 2 as well as the rod-side flow rate (Q_R) and the piston position. For a more detailed description of the functionality of the valve-controlled cylinder, see for instance [29]. Details about the components implemented in the valve-controlled system are presented in Table 2.

Table 2. Components used to implement the valve-controlled system.

Symbol	Component	Manufacturer	Model
EM	Electric motor	ASEA [1]	M225S60-4
P	Axial piston variable pump	Brueninghaus Hydraulik [2]	A4V-S0-71
RV	Pressure-relief valve	Bosch Rexroth	DBDH6
V	Flow control valve	Sauer Danfoss [3]	PVG32-9781
LHV	Counterbalance valve	Sun Hydraulics	CWCA
$p_{S,R,A}$	Pressure transducers	Parker	SCP-400
Q_r	Flow rate meter	Parker	SCQ-150

[1] Västerås, Sweden; [2] Horb, Germany; [3] Nordborg, Denmark.

3. Theoretical Background

This section describes the analysis performed to process the experimental data collected from the two drive systems. The objective is highlighting the power levels, the energy consumption, and the efficiency of the architectures.

3.1. Power and Energy Distribution

The different power terms characteristic of both systems and highlighted in Figure 3 are evaluated using the equations presented below. For the sake of clarity, the input, the transferred, and the output powers are addressed in separate subsections.
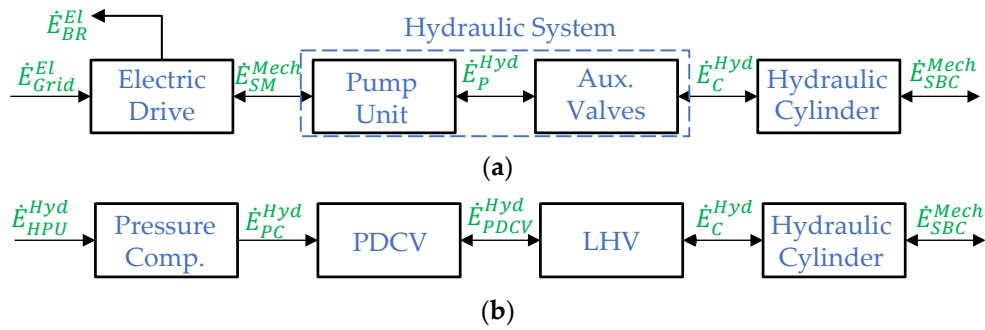
Figure 3. The different power terms: (**a**) Self-contained system; (**b**) valve-controlled system.

3.1.1. Input Power

The input power of the SCC corresponds to the electric power supplied by the electrical grid:

$$\dot{E}_{Grid}^{El} = v_a \cdot i_a + v_b \cdot i_b + v_c \cdot i_c, \tag{1}$$

where v_i and i_i are the voltage and current of the *i*-th phase, respectively. Furthermore, when the external load is overrunning (i.e., when the cylinder is retracting), the SCC has the potential to regenerate power, while the VCC still consumes energy. For the test setup investigated in this study, the electric power regenerated by the SCC is dissipated in the brake resistor and is estimated according to:

$$\dot{E}_{BR}^{El} = v_{BR} \cdot i_{BR}, \tag{2}$$

where v_{BR} is the pulse width modulated voltage, and i_{BR} is the direct current, transferred from the servo-drive to the brake resistor. Hence, the combined input and output powers of the electric drive define the SCC's total electric power related to the power supply:

$$\dot{E}_{PS}^{El} = \dot{E}_{Grid}^{El} + \dot{E}_{BR}^{El}. \tag{3}$$

The VCC's input power is the hydraulic term calculated by involving the actuator's flow demand (Q_P) and the supply pressure of the HPU:

$$\dot{E}_{HPU}^{Hyd} = p_S \cdot |Q_P|, \tag{4}$$

where the demand depends on the valve command (u_V), the measured flow rate (Q_r), and the areas of the actuator according to the following logic:

$$Q_P = \begin{cases} Q_r \cdot \dfrac{A_p}{A_r}, & u_V < 0 \\ 0, & u_V = 0 \\ Q_r, & u_V > 0 \end{cases} \tag{5}$$

3.1.2. Transferred Power Losses

The mechanical power transferred between the SCC's servo-motor and the axial piston machine:

$$\dot{E}_{SM}^{Mech} = i_q \cdot k_t \cdot \omega_{SM}, \tag{6}$$

is described by the torque-producing current component (i_q), the torque constant ($k_t = 2.05\,\text{Nm/A}$), and the measured rotational speed (ω_{SM}) of the prime mover. The hydraulic power shared between

the hydraulic machine and the manifold is defined by involving the effective flow supplied to the actuator and the pressure drop across the unit:

$$\dot{E}_P^{Hyd} = \dot{x}_C \cdot A_p \cdot (p_1 - p_2). \tag{7}$$

Then, the hydraulic power distributed between the manifold and the cylinder results as:

$$\dot{E}_C^{Hyd} = \dot{x}_C \cdot \left(A_p \cdot p_p - A_r \cdot p_r\right). \tag{8}$$

The power losses of the SCC take place in the electric drive (i.e., electric and mechanical losses), in the axial piston machine (i.e., mechanical-hydraulic and volumetric losses), in the auxiliary components (i.e., reduced throttling losses in the check valves), and in the hydraulic cylinder (i.e., friction losses and internal leakage).

Concerning the VCC's, the hydraulic power available downstream the pressure compensator is calculated based on the valve command as:

$$\dot{E}_{PC}^{Hyd} = \begin{cases} \left(p_p + p_0\right) \cdot |Q_P|, & u_V < 0 \\ 0, & u_V = 0, \\ (p_r + p_0) \cdot |Q_P|, & u_V > 0 \end{cases} \tag{9}$$

including the fixed pressure-drop across the control valve's metering edge (p_0). Further on, the hydraulic power delivered by the control valve is again function of u_V:

$$\dot{E}_{PDCV}^{Hyd} = \begin{cases} p_p \cdot Q_P, & u_V < 0 \\ 0, & u_V = 0. \\ p_r \cdot Q_P, & u_V > 0 \end{cases} \tag{10}$$

Then, the hydraulic power related to the hydraulic cylinder results as described in Equation (8). The power losses taking place in the VCC are the throttling losses of the pressure compensator, the throttling losses of the control valve's spools, the throttling losses in the counterbalance valve, and the friction losses and internal leakages of the hydraulic cylinder. Finally, the losses of the HPU are neglected in this experimental study to be conservative, since it is sized for delivering constant pressure to several applications available in the lab.

3.1.3. Output Power

When actuating the considered single-boom crane depicted in Figure 4a, the mechanical output power that is applicable to both systems, is defined as:

$$\dot{E}_{SBC}^{Mech} = \frac{d}{dt} \cdot (E_K + E_P), \tag{11}$$

where E_K and E_P are the kinetic and potential energy, obtained according to Equations (12) and (13).

The diagram shown in Figure 4b identifies the parameters used in the calculation of the total mechanical energy. Relevant numerical values describing the kinematics are listed in Table 3.
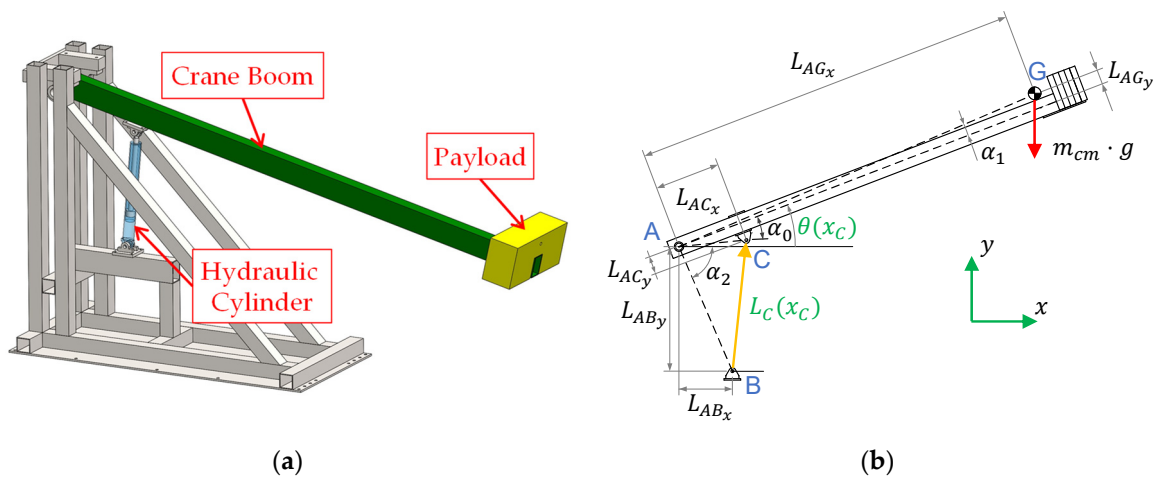
(**a**)   (**b**)

Figure 4. The considered application: (**a**) The hydraulic actuator connected to the crane-boom; (**b**) simplified schematic diagram of the crane's kinematics.

Table 3. Kinematic parameters of the single-boom crane with full payload.

Parameter	Value	Parameter	Value
m_{cm}	415.08 (kg)	L_{AB}	1136 (mm)
J_{cm}	159.63 (kg·m^2)	α_0	0.232 (rad)
L_{AGx}	3139 (mm)	α_1	0.020 (rad)
L_{AGy}	64 (mm)	α_2	1.192 (rad)
L_{AC}	565 (mm)	g	9.81 (m/s^2)

The kinetic energy and the potential energy, as a function of the angular speed ($\dot{\theta}$) and angular position (θ) of the boom, are defined according to the following equations:

$$E_K(\dot{\theta}) = \frac{1}{2} \cdot \left(m_{cm} \cdot L_{AGx}^2 + m_{cm} \cdot L_{AGy}^2 + J_{cm} \right) \cdot \dot{\theta}^2, \tag{12}$$

$$E_P(\theta) = m_{cm} \cdot g \cdot \left(L_{AGy} \cdot \cos(\theta + \alpha_1) + L_{AGx} \cdot \sin(\theta + \alpha_1) \right), \tag{13}$$

where the angular position of the boom and the effective length of the hydraulic cylinder (L_C), including the initial length ($L_{C,0} = 772$ mm), are given below as a function of the piston position:

$$\theta(x_C) = \cos^{-1}\left(\frac{L_{AC}^2 + L_{AB}^2 - L_C^2(x_C)}{2 \cdot L_{AC} \cdot L_{AB}} \right) - \alpha_2 + \alpha_0, \tag{14}$$

$$L_C(x_C) = x_C + L_{C,0}. \tag{15}$$

3.2. Efficiency of the Systems

Starting from the SCC, the overall efficiency ($\eta_{Overall}$), the efficiency of the electric drive (η_{ED}), and the efficiency of the hydraulic sub-system (η_{HS}) are given in Equations (16)–(18). Due to the dual behavior of the system being regenerative while retracting the cylinder (i.e., the load is overrunning when the crane boom is lowered), and consuming when extending the cylinder (i.e., the load is resistant when the crane boom is lifted), two alternatives are introduced in the following definitions:

$$\eta_{Overall}^{SCC} = \begin{cases} \frac{\dot{E}_{PS}^{El}}{\dot{E}_{SBC}^{Mech}}, & \dot{E}_{PS}^{El} > 0 \text{ (resistant load)} \\ \frac{\dot{E}_{SBC}^{Mech}}{\dot{E}_{PS}^{El}}, & \dot{E}_{PS}^{El} \leq 0 \text{ (overrunning load)} \end{cases}, \tag{16}$$

$$\eta_{ED}^{SCC} = \begin{cases} \dfrac{\dot{E}_{PS}^{El}}{\dot{E}_{SM}^{Mech}}, & \dot{E}_{PS}^{El} > 0 \text{ (resistant load)} \\[2ex] \dfrac{\dot{E}_{SM}^{Mech}}{\dot{E}_{PS}^{El}}, & \dot{E}_{PS}^{El} \leq 0 \text{ (overrunning load)} \end{cases}, \tag{17}$$

$$\eta_{HS}^{SCC} = \begin{cases} \dfrac{\dot{E}_{SM}^{Mech}}{\dot{E}_{C}^{Hyd}}, & \dot{E}_{SM}^{Mech} > 0 \text{ (resistant load)} \\[2ex] \dfrac{\dot{E}_{C}^{Hyd}}{\dot{E}_{SM}^{Mech}}, & \dot{E}_{SM}^{Mech} \leq 0 \text{ (overrunning load)} \end{cases}. \tag{18}$$

Similar terms are also proposed for the VCC, where the efficiency of the control valve (η_V) and of the remaining hydraulic system, namely the load-holding valve (η_{LHV}), are given as follows:

$$\eta_{Overall}^{VCC} = \begin{cases} \dfrac{\dot{E}_{HPU}^{Hyd}}{\dot{E}_{SBC}^{Mech}}, & \dot{E}_{HPU}^{Hyd} > 0 \text{ (resistant load)} \\[2ex] 0, & \dot{E}_{HPU}^{Hyd} \leq 0 \text{ (overrunning load)} \end{cases}, \tag{19}$$

$$\eta_{V}^{VCC} = \begin{cases} \dfrac{\dot{E}_{HPU}^{Hyd}}{\dot{E}_{PDCV}^{Hyd}}, & \dot{E}_{HPU}^{Hyd} > 0 \text{ (resistant load)} \\[2ex] 0, & \dot{E}_{HPU}^{Hyd} \leq 0 \text{ (overrunning load)} \end{cases}, \tag{20}$$

$$\eta_{LHV}^{VCC} = \begin{cases} \dfrac{\dot{E}_{PDCV}^{Hyd}}{\dot{E}_{C}^{Hyd}}, & \dot{E}_{PDCV}^{Hyd} > 0 \text{ (resistant load)} \\[2ex] \dfrac{\dot{E}_{C}^{Hyd}}{\dot{E}_{PDCV}^{Hyd}}, & \dot{E}_{PDCV}^{Hyd} \leq 0 \text{ (overrunning load)} \end{cases}. \tag{21}$$

4. Experimental Results and Discussion

After mentioning the experimental test-beds, the considered working cycle is addressed. Then, the power levels and efficiencies of the different sub-systems are separately evaluated while lifting and lowering the single-boom crane. Finally, the overall energy consumption and efficiency are assessed. The experimental data were collected by using the test setups illustrated in Figure 5.
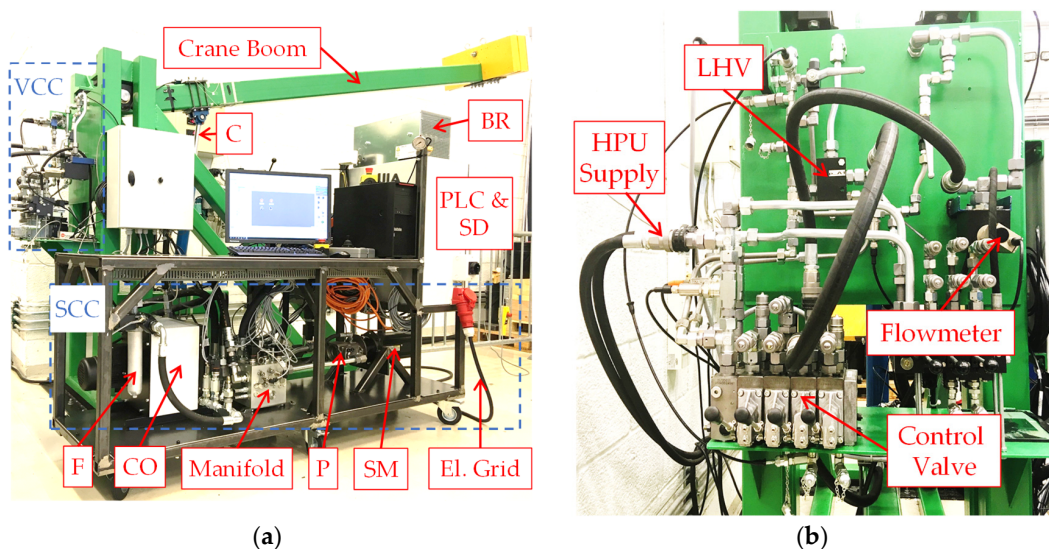

Figure 5. The experimental setups: (**a**) The self-contained electro-hydraulic system; (**b**) a portion of the valve-controlled system.

All data, besides the electric power, is processed through a real-time interface (i.e., 1 ms sample rate) between the PLC and MATLAB-Simulink®. The measured electric power is collected with a 50 ms sample rate and further processed in the MATLAB-Simulink® environment. Mineral oil ISO VG 46 is used as the hydraulic fluid in both actuation systems. All tests were carried out for a working cycle with maximum payload (i.e., with a load mass equal to 304 kg). The motion profile generator, presented in [27], provides reference signals for the desired piston position and velocity, as illustrated in Figure 6. The cylinder's piston extends and retracts between the start position $x_{C,0} = 50$ mm and the desired position $x_{C,ref} = 450$ mm, at a desired maximum velocity $v_{C,max} = 120$ mm/s.
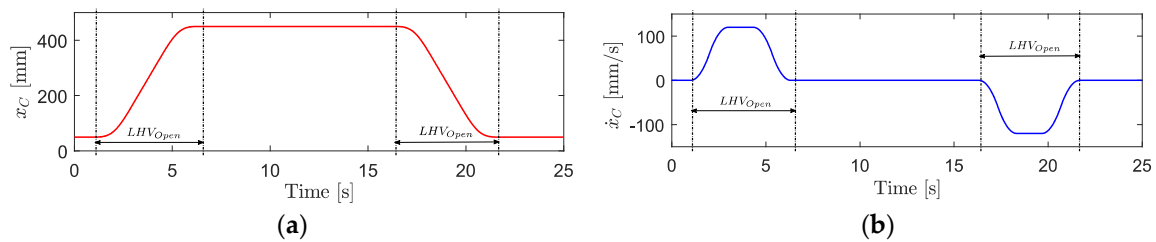

Figure 6. Generated motion profile: (**a**) Desired piston position; (**b**) desired piston velocity.

The SCC is operated in closed-loop, including position feedback control, velocity feedforward, pressure feedback, and passive load-holding, according to the control strategy and the control algorithm presented in the first part of this comparison study [28]. In passive load-holding mode, the load-holding valves are closed by deactivating the electro-valve and switching off the signal enabling power to the prime mover when motion is not desired.

4.1. Power Levels

The power levels of the different terms mentioned in Section 3.1 are shown in Figure 7.
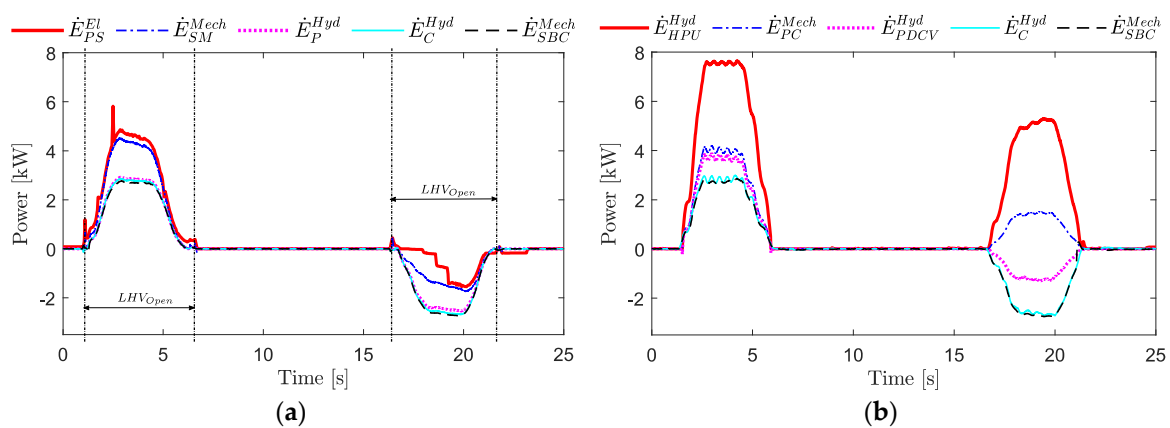
Figure 7. Power measurements: (**a**) Self-contained system; (**b**) valve-controlled system.

When the values in Figure 7 are positive, then the power is transferred to the actuator. Vice versa (i.e., when the trends are negative), there is potential to recover energy. During the crane's lowering phase, the SCC outputs electrical power, while the VCC dissipates hydraulic energy in the valves. It is worth mentioning that, during steady-state operations, the VCC requires a maximum power of about 7.6 kW while the SCC demands only 4.8 kW (37% less).

4.2. Systems Efficiency

The overall efficiency of both systems is plotted in Figure 8 together with the terms related to the different sub-systems.
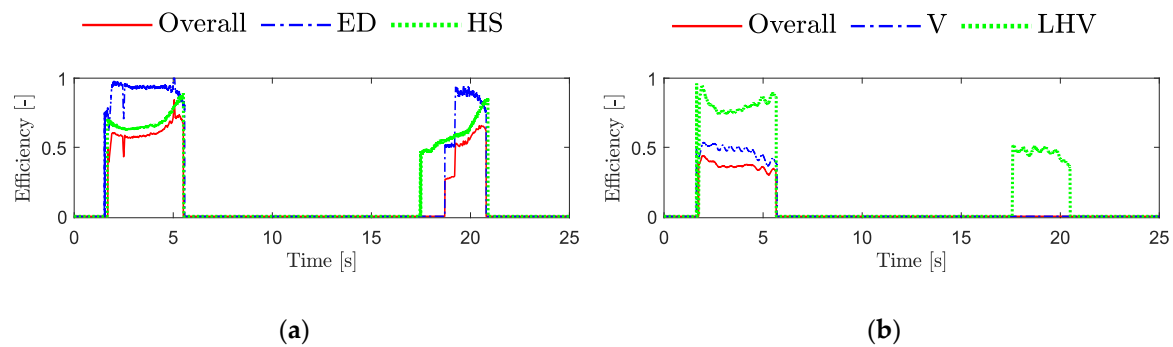
Figure 8. Efficiency of the systems: (**a**) Self-contained system; (**b**) valve-controlled system.

The results in Figure 8a show that the SCC's efficiency, when the cylinder is lifting the crane at steady-state (i.e., at 4 s) is about 60% for the overall system, 93% for the electric drive, and 65% for the hydraulics. The overall efficiency when lowering the crane boom, assuming full recovery of the regenerated power, varies at 51–65%. It can be observed in Figure 8a that there is a 1.2 s delay between when the SCC starts to lower the crane boom, and the electric drive starts to regenerate power. For the benchmark system (Figure 8b), the overall efficiency is 36% when the cylinder is lifting the crane boom at steady-state (i.e., at 4 s). Furthermore, almost 50% of the VCC's input power is dissipated in the control valve (the most in the pressure-compensator). The efficiency of the counterbalance valve, during lifting (i.e., the flow is bypassed through the LHV's check valve), is 74% at the lowest, and at the maximum 51% through the lowering phase (i.e., the LHV's poppet introduces a desired pressure-drop).

4.3. Energy Consumption

As described in the first part of this study [28], the SCC can be operated with two different load-holding strategies, namely passive load-holding (PLH) and active load-holding (ALH). The electric power and energy consumption when utilizing these two strategies are compared in Figure 9.
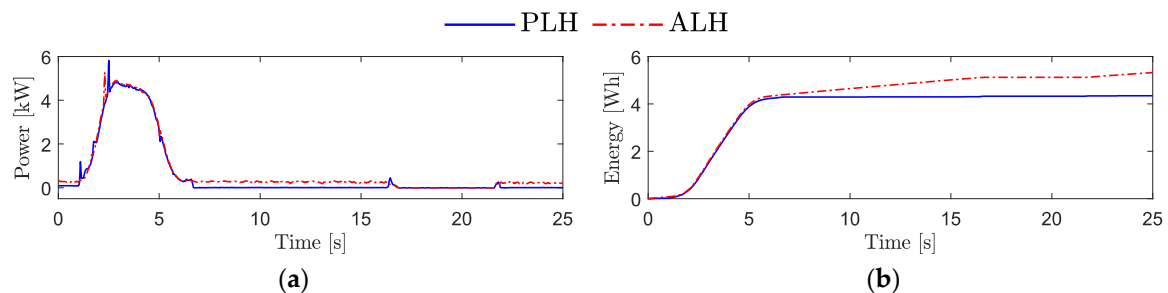

Figure 9. Comparison between passive and active load-holding for the self-contained cylinder: (**a**) Input power; (**b**) energy consumption.

When the SCC maintains the desired piston position between 6.5 and 16 s (Figure 9a), the measured electric input power varies at 5–7 W with passive load-holding, and at 187–312 W with active load-holding. Active load-holding results in an energy consumption of 5.32 Wh for the entire working cycle considered here (Figure 9b), compared to 4.34 Wh with passive load-holding (i.e., 18.4% less). However, performing active load-holding for a reduced amount of time is still acceptable since the power consumption remains relatively low.

Moving to the valve-controlled layout, load-sensing pumps are used instead of constant-pressure supplies to increase the overall efficiency in many applications. Two scenarios are therefore addressed; the first one (Figure 10a) focuses on measurements from the test setup. The scenario #2 (Figure 10b) considers an HPU equipped with a load-sensing pump and driven by an induction motor running at 1500 rpm (the losses of the HPU are simulated based on the model presented in [27]). Full energy

recovery is then assumed for the SCC in this second situation (i.e., the energy dissipated in the brake resistor when the SCC is lowering the crane boom is now reused).
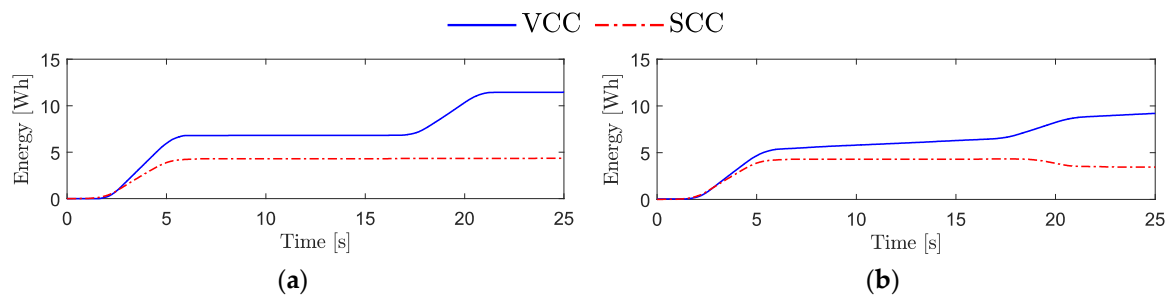

Figure 10. Energy consumption comparison: (**a**) The scenario #1; (**b**) the scenario #2.

The results in Figure 10a show that the SCC does not consume any energy when lowering the load, resulting in 62.1% less consumption compared to the 11.44 Wh of the VCC. This improvement is expected since the VCC needs to build up pressure to enable flow through the counterbalance valve that introduces functional losses, while the SCC uses the highest actuator pressure to fully open the two load-holding valves. For scenario #2 (Figure 10b), the VCC consumes energy also when the cylinder is not moving because the electric-motor is continuously running; due to the load-sensing unit, then 19.6% less energy is taken compared to the VCC in scenario #1. When comparing the two systems in scenario #2, the SCC still consumes less energy than the VCC (62.4% less); this behavior favorable to the SCC is also the case when there is no useful usage of the recovered energy.

4.4. Energy Distribution

The energy distribution between the main components of the two systems, initially monitored when the cylinder is lifting the crane boom, is illustrated in Figure 11.
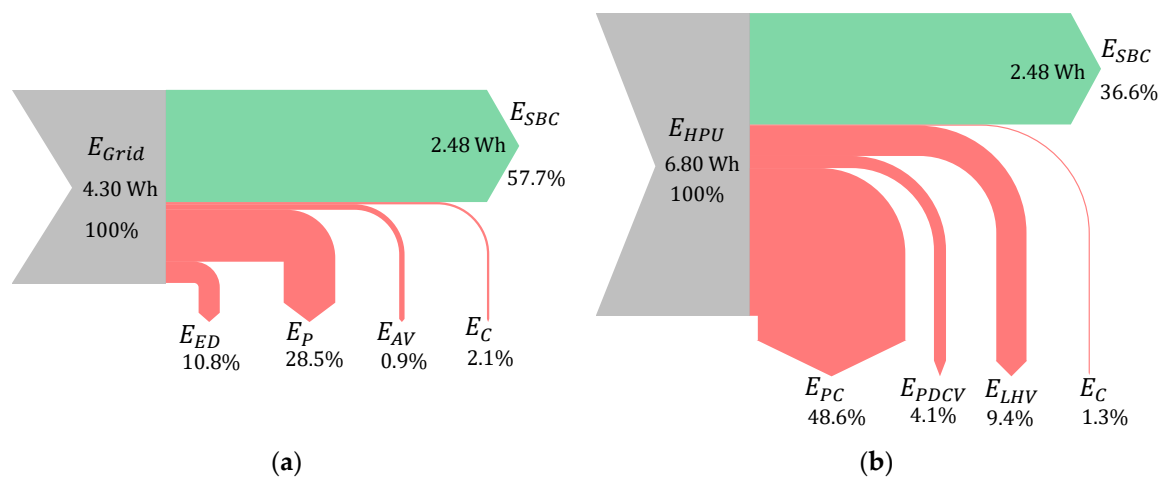
Figure 11. The energy distribution when lifting the crane boom: (**a**) Self-contained system; (**b**) valve-controlled system.

The complete energy conversion from the source (i.e., the electric grid for the SCC and the hydraulic power supply for the VCC) to the end user (i.e., the payload of the crane) is handled. The total amount of energy being lost in the SCC is 42.3%, while it increases up to 63.4% in the VCC (this is a conservative estimation because the losses of the HPU are neglected). It should be noted that all losses in the SCC are parasitic, with the pump being the predominant source followed by the electric motor. This aspect does not hold true for the VCC since the compensator introduces a relevant dissipation that is functional (this term could be reduced for higher loads, or when using a

load-sensing power supply). Moreover, only the SCC has the potential to recover energy; Figure 12 illustrates the energy distribution in the SCC when the crane boom is lowered.

Figure 12. The energy distribution of the self-contained system when lowering the crane boom.

A significant portion (35.9%) of the energy delivered by the load that is lowered can be outputted by the electric drive; it is worth noticing that this quantity is completely lost in the valve-controlled architecture. In particular, the total energy being dissipated in the SCC during piston retraction (64.1% of the input) is mainly due to the losses in the axial piston machine and in the electric drive.

Finally, the energy distribution during a complete working cycle is depicted in Figure 13 for both the SCC and the VCC, where the energy taken from the grid is now considered also for the VCC (i.e., scenario #2 with the power supply equipped with a load-sensing pump).
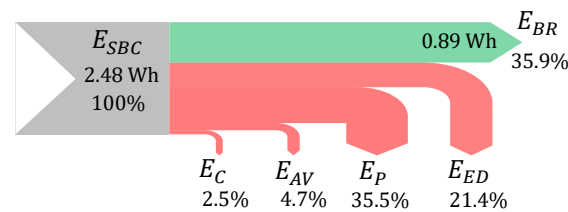

(**a**)   (**b**)
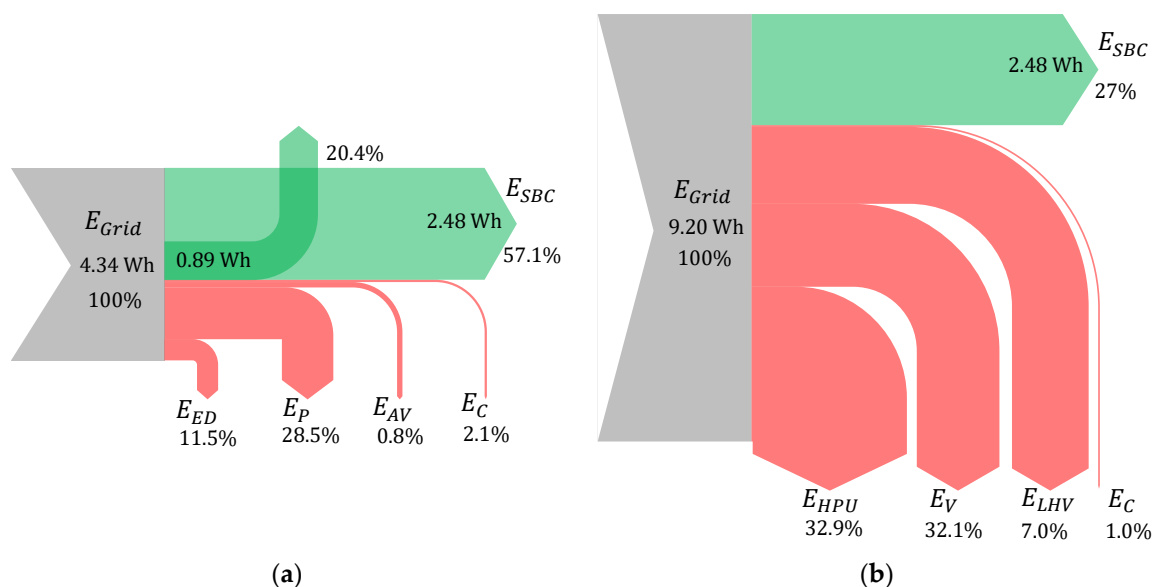
Figure 13. The energy distribution during a complete working cycle: (**a**) Novel self-contained system; (**b**) valve-controlled system when simulating a load-sensing pump and hydraulic power unit losses.

The results show that 57.1% of the input energy is transferred to the load for the SCC and 27% for the VCC. Figure 13a reveals that the SCC may recover 20.4% of the electrical energy taken from the grid during a complete working cycle. Assuming a realistic 94% conversion efficiency to return the recovered energy to the grid, then 76.5% of the total energy taken from the source can be used effectively. Further on, when considering a VCC supplied by a load-sensing pump (Figure 13b), the efficiency increases due to the major reduction of the functional losses in the control valve (E_V). However, including also the inefficiencies of the HPU (i.e., the losses of the electric motor and of the pump), the overall efficiency is only increased by 5.3% compared to the VCC supplied with constant pressure supply (scenario #1) that is characterized by an overall energy efficiency of 21.7%.

5. Conclusions

This research paper experimentally compares a novel self-contained electro-hydraulic cylinder and a hydraulic, valve-controlled, linear actuator representative of the state of the art in many fields of

industry. A single-boom crane requiring passive load-holding is taken as the reference application, while the emphasis of the study is placed on the energy efficiency of the drives. The results show that the electro-hydraulic layout reduces the energy consumption significantly (up to 62% less) due to its throttleless nature and power-on-demand functioning. More specifically, the following aspects emerge from the study:

- The power demand to the prime mover during steady-state operations reduces to 4.8 kW against the 7.6 kW in the valve-controlled system (37% less) throughout the investigated working cycle;
- Utilizing passive load-holding results in an energy saving of 18.4% compared to actively controlling the SCC's desired position using the prime mover during load holding phases;
- The system's overall efficiency of the self-contained drive, being approximately 57% during actuation, turns out to be highly satisfactory compared to the 22% efficiency of the valve-controlled system with a constant-pressure supply;
- A significant amount of energy (i.e., 20% of the consumed energy) is recovered by the self-contained solution during the proposed working cycle. Hence, when assuming a realistic 94% conversion efficiency to return the recovered energy to the grid, then 77% of the total energy taken from the source can be used effectively. In contrast, this efficient operation is not possible in the valve-controlled system where, rather than being recovered, the available energy is dissipated when the load acting on the actuator is overrunning;
- An alternative scenario based on the load-sensing concept is also considered for the valve-controlled system; its energy consumption reduces from 11.44 Wh to 9.20 Wh but remains inefficient with respect to the electro-hydraulic actuator (i.e., total consumption 4.34 Wh).

Recalling the positive outcomes about motion control obtained in the first part of the research and disseminated in a different article, it is therefore concluded that the novel energy-efficient, self-contained drive represents a valid alternative to conventional hydraulic systems for load-carrying applications. Introducing a self-sufficient and completely sealed device also reduces the risk of oil spill pollution, helping fluid power to become a cleaner technology. Concerning future developments about the self-contained system, effort will be placed on both optimizing the sizing procedure to maximize energy efficiency as well as on designing and testing advanced solutions that reuse the recovered energy.

Author Contributions: Conceptualization, D.H. and D.P.; methodology, D.H.; software, D.H.; validation, D.H.; formal analysis, D.H.; investigation, D.H.; data curation, D.H.; writing—original draft preparation, D.H.; writing—review and editing, D.H., D.P., and M.C.; visualization, D.H.; supervision, D.P. and M.C.

Conflicts of Interest: The authors declare no conflict of interest.

Nomenclature

Abbreviations

AC	Alternating current
ACC	Accumulator
Ac	Anti-cavitation valve
ALH	Active load-holding
AV	Auxiliary valves
BR	Brake resistor
C	Hydraulic cylinder
CO	Oil cooler
CV	Check valve
DC	Direct current
ED	Electric drive
EM	Electric motor
EV	Electro-valve

F	Low pressure oil filter
FC	Flow compensation valve
HPU	Hydraulic power unit
HS	Hydraulic system
LHV	Load-holding valve
P	Axial piston machine (pump)
PDCV	Proportional directional control valve
PLC	Programmable logic controller
RV	Pressure-relief valve
SBC	Single-boom crane
SCC	Self-contained electro-hydraulic cylinder
SD	Servo-drive
SM	Servo-motor
V	Control valve
VCC	Valve-controlled cylinder

Symbols

A_p	Cylinder area on the piston-side
A_r	Cylinder area on the rod-side
E_K	Kinetic energy
E_P	Potential energy
E	Energy
$\dot{E}$	Power
i_a, i_b, i_c	Three-phase current of the electric power supply
i_{BR}	Direct current of the brake resistor
i_q	Torque-producing current component
J_{cm}	Inertia at center of mass
k_t	Torque constant
L_{AB}	Length between joint A and B
L_{AC}	Length between joint A and C
L_{AGx}	Length between joint A and G in x-direction
L_{AGy}	Length between joint A and G in y-direction
$L_{C,0}$	Length of the hydraulic cylinder when fully retracted
L_C	Effective total length of the hydraulic cylinder
m_{cm}	Mass at center of mass
ω_{SM}	Rotational speed of the servo-motor in radians per seconds
Q_P	Actuator's flow demand
Q_r	Rod-side flow rate
p_0	Fixed pressure-drop across the proportional directional control valve
p_1	Pressure at the pump/motor port on the piston-side of the actuator
p_2	Pressure at the pump/motor port on the rod-side of the actuator
p_p	Actuator's piston chamber pressure
p_r	Actuator's rod chamber pressure
p_R	Return pressure
p_S	Supply pressure
u_{SM}	Commanded servo-motor speed
u_V	Commanded opening of the control valve's spool position
v_a, v_b, v_c	Three-phase voltage of the electric power supply
v_{BR}	Direct current voltage of the brake resistor
x_C	Actuator's piston position
$\dot{x}_C$	Actuator's piston velocity

Greek Symbols

α_i	Arctangent of the xy-length between the *i*-th joints
η_i	Efficiency of the *i*-th system
θ	Angular position of the boom

References

1. Pawlus, W.; Choux, M.; Hansen, M.R. Hydraulic vs. electric: A review of actuation systems in offshore drilling equipment. *Model. Identif. Control* **2016**, *37*, 1–17. [CrossRef]
2. Hagen, D.; Pawlus, W.; Ebbesen, M.K.; Andersen, T.O. Feasibility Study of Electromechanical Cylinder Drivetrain for Offshore Mechatronic Systems. *Model. Identif. Control* **2017**, *38*, 59–77. [CrossRef]
3. Michel, S.; Weber, J. Electrohydraulic Compact-Drives for Low Power Applications Considering Energy-efficiency and High Inertial Loads. In Proceedings of the 7th FPNI PhD Symposium on Fluid Power, Reggio Emilia, Italy, 27–30 June 2012; pp. 27–30.
4. Minav, T.A.; Sainio, P.; Pietola, M. Direct Driven Hydraulic Drive without Conventional Oil Tank. In Proceedings of the ASME/BATH 2014 Symposium on Fluid Power and Motion Control, Bath, UK, 10–12 September 2014.
5. Altare, G.; Vacca, A.; Richter, C. A Novel Pump Design for an Efficient and Compact Electro-Hydraulic Actuator. In Proceedings of the IEEE Aerospace Conference, Big Sky, MT, USA, 1–8 March 2014.
6. Altare, G.; Vacca, A. A design solution for efficient and compact electro-hydraulic actuators. *Procedia Eng.* **2015**, *106*, 8–16. [CrossRef]
7. Rexroth, B. Electrification and Digitalization: The Fitness Program for Hydraulics. 2015. Available online: https://www.boschrexroth.com/en/xc/products/product-groups/industrial-hydraulics/the-fitness-program-for-hydraulics (accessed on 21 September 2019).
8. Helbig, A.; Boes, C. Electric Hydrostatic Actuation-Modular Building Blocks for Industrial Applications. In Proceedings of the 10th International Fluid Power Conference, Dresden, Germany, 8–10 March 2016; pp. 93–102.
9. Pedersen, H.C.; Schmidt, L.; Andersen, T.O.; Brask, M.H. Investigation of New Servo Drive Concept Utilizing Two Fixed Displacement Units. *Int. J. Fluid Power Syst.* **2014**, *8*, 1–9. [CrossRef]
10. Hagen, D.; Padovani, D.; Ebbesen, M.K. Study of a Self-Contained Electro-Hydraulic Cylinder Drive. In Proceedings of the 2018 Global Fluid Power Society Ph.D. Symposium (GFPS), Samara, Russia, 18–20 July 2018.
11. Michel, S.; Weber, J. Energy-Efficient Electrohydraulic Compact Drives for Low Power Applications. In Proceedings of the ASME/BATH 2012 Symposium on Fluid Power and Motion Control, Bath, UK, 12–14 September 2012; pp. 93–107.
12. Padovani, D.; Ketelsen, S.; Hagen, D.; Schmidt, L. A Self-Contained Electro-Hydraulic Cylinder with Passive Load-Holding Capability. *Energies* **2019**, *12*, 292. [CrossRef]
13. Jalayeri, E.; Imam, A.; Tomas, Z.; Sepehri, N. A throttle-less single-rod hydraulic cylinder positioning system: Design and experimental evaluation. *Adv. Mech. Eng.* **2015**, *7*, 1687814015583249. [CrossRef]
14. Weber, I.J.; Schneider, D.I.; Shabi, M.S.; Sitte, D.I.; Weber, D.I.; Willkomm, D.I.; Beck, D.I.; Fischer, D.I.; Ivantysyn, M.S.; Kolks, D.I.; et al. Novel System Architectures by Individual Drives. In Proceedings of the 10th International Fluid Power Conference, Dresden, Germany, 8–10 March 2016; pp. 29–62.
15. Ketelsen, S.; Padovani, D.; Andersen, T.; Ebbesen, M.; Schmidt, L. Classification and Review of Pump-Controlled Differential Cylinder Drives. *Energies* **2019**, *12*, 1293. [CrossRef]
16. Schmidt, L.; Ketelsen, S.; Brask, M.H.; Mortensen, K.A. A class of energy efficient self-contained electro-hydraulic drives with self-locking capability. *Energies* **2019**, *12*, 1866. [CrossRef]
17. Minav, T.A.; Laurila, L.I.E.; Pyrhönen, J.J. Analysis of electro-hydraulic lifting system's energy efficiency with direct electric drive pump control. *Autom. Constr.* **2013**, *30*, 144–150. [CrossRef]
18. Minav, T.A.; Sainio, P.; Pietola, M. Efficiency of Direct Driven Hydraulic Setup in Arctic Conditions. In Proceedings of the Fourteenth Scandinavian International Conference on Fluid Power, Tampere, Finland, 20–22 May 2015.
19. Schmidt, L.; Roemer, D.B.; Pedersen, H.C.; Andersen, T.O. Speed-Variable Switched Differential Pump System for Direct Operation of Hydraulic Cylinders. In Proceedings of the ASME/BATH Symposium on Fluid Power and Motion Control, Chicago, IL, USA, 12–14 October 2015.
20. Schneider, M.; Koch, O.; Weber, J. Green Wheel Loader—Improving Fuel Economy through Energy Efficient Drive and Control Concepts. In Proceedings of the 10th International Fluid Power Conference, Dresden, Germany, 8–10 March 2016; pp. 63–78.

21. Schmidt, L.; Ketelsen, S.; Padovani, D.; Mortensen, K.A. Improving the Efficiency and Dynamic Properties of a Flow Control Unit in a Self-Locking Compact Electro-Hydraulic Cylinder Drive. In Proceedings of the ASME/Bath Symposium on Fluid Power and Motion Control, Longboat Key, FL, USA, 7–9 October 2019.

22. Michel, S.; Weber, J. Prediction of the Thermo-Energetic Behaviour of an Electrohydraulic Compact Drive. In Proceedings of the 10th International Fluid Power Conference, Dresden, Germany, 8–10 March 2016; pp. 219–234.

23. Minav, T.; Papini, L.; Pietola, M. A Thermal Analysis of Direct Driven Hydraulics. In Proceedings of the 10th International Fluid Power Conference, Dresden, Germany, 8–10 March 2016; pp. 235–248.

24. Karlén, N.; Minav, T.A.; Pietola, M. Investigation of Thermal Effects in Direct Driven Hydraulic System for Off-Road Machinery. In Proceedings of the 9th FPNI Ph.D. Symposium on Fluid Power, Florianópolis, Brazil, 26–28 October 2016.

25. Schmidt, L.; Groenkjaer, M.; Pedersen, H.C.; Andersen, T.O. Position Control of an Over-Actuated Direct Hydraulic Cylinder Drive. *Control Eng. Pract.* **2017**, *64*, 1–14. [CrossRef]

26. Ketelsen, S.; Schmidt, L.; Donkov, V.H.; Andersen, T.O. Energy saving potential in knuckle boom cranes using a novel pump controlled cylinder drive. *Model. Identif. Control* **2018**, *39*, 73–89. [CrossRef]

27. Hagen, D.; Padovani, D.; Choux, M. Enabling Energy Savings in Offshore Mechatronic Systems by using Self-Contained Cylinders. *Model. Identif. Control* **2019**, *40*, 89–108. [CrossRef]

28. Hagen, D.; Padovani, D.; Choux, M. A Comparison Study of a Novel Self-Contained Electro-Hydraulic Cylinder versus a Conventional Valve-Controlled Actuator—Part 1: Motion Control. *Actuators* **2019**, in press.

29. Hagen, D.; Padovani, D.; Choux, M. Design and Implementation of Pressure Feedback for Load-Carrying Applications with Position Control. In Proceedings of the Sixteenth Scandinavian International Conference on Fluid Power, Tampere, Finland, 22–24 May 2019.

30. Ristic, M.; Wahler, M. Electrification of Hydraulics Opens New Ways for Intelligent Energy-Optimized Systems. In Proceedings of the 11th International Fluid Power Conference, Aachen, Germany, 19–21 March 2018.

Paper H

Guidelines to Choose Between Self-Contained Electro-Hydraulic and Electro-Mechanical Cylinders

Daniel Hagen, Damianio Padovani, and Martin Choux

Guidelines to Select Between Self-Contained Electro-Hydraulic and Electro-Mechanical Cylinders

1st Daniel Hagen
Department of Engineering Sciences
Univeristy of Agder
Grimstad, Norway
daniel.hagen@uia.no

2nd Damiano Padovani
Department of Engineering Sciences
Univeristy of Agder
Grimstad, Norway
damiano.padovani@uia.no

3rd Martin Choux
Department of Engineering Sciences
Univeristy of Agder
Grimstad, Norway
martin.choux@uia.no

Abstract—This research paper presents guidelines on how to select between self-contained electro-hydraulic and electro-mechanical cylinders. An example based on the motion control of a single-boom crane is studied. The sizing process of the different off-the-shelf components is analyzed in terms of design impact when replacing a traditional valve-controlled hydraulic cylinder. The self-contained electro-hydraulic solution is the best choice when a risk for high impact forces is present, when the required output power level lies continuously above 2 kW, or when installation space, weight, and cost are critical design objectives. However, the electro-mechanical solution is expected to show more controllability due to the fact that it has higher levels of drive stiffness, and energy efficiency as well as lower system complexity. This solution also requires less effort to control the actuator's linear motion accurately. All of these factors result in a more straightforward design approach.

Index Terms—hydraulic systems, electric drives, self-contained acutators, linear actuators, actuation system design, component selection, electro-mechanical cylinders, electro-hydraulic cylinders, valve-controlled cylinders, load-carrying applications

I. INTRODUCTION

Traditional valve-controlled linear hydraulic actuators can be implemented in many architectures [1]. They are characterized not only by reliability, high force and power capability, and excellent overload protection (e.g., shock absorption) but also relevant power losses due to flow throttling in the valves, demanding efforts needed for installation and maintenance, and costly piping due to centralized hydraulic power supplies. Yet in spite of their disadvantages, these actuators are still commonplace in industry.

Over the course of several years, efforts have been made to replace these conventional hydraulic systems with electro-mechanical cylinders (EMCs). This has been a popular research topic and engineering task, especially in aerospace systems. To date, a great deal of work has been done to reduce the system's weight, installation time, and maintenance requirements [2]–[6]. However, predicting this system's service life is challenging, and there is a considerable risk of failure (e.g., jamming, which can result in dangerous consequences) since the actuator cannot absorb shocks in standby mode. Consequently, these actuators are still not accepted in commercial airplanes as primary actuators for flight control. Alternatively, electro-hydraulic cylinders (EHCs) that are self-sufficient and

completely sealed have been introduced. These cylinders typically contain a dedicated variable-speed pump that controls the cylinder's motion. This technology, as explained by [7], was first introduced in aerospace systems, demonstrating the idea that the disadvantages of traditional hydraulics can be significantly reduced. Indeed, EHC are now used for flaps control in commercial airplanes [8].

In other fields of industry, especially in low-power applications (below 5 kW) where disadvantages such as increased wear, difficult overload protection, and lower load forces are accepted [9], hydraulic systems have been replaced by EMCs in order to increase energy efficiency and eliminate oil spills. Subsequently, the idea of combining EMC's advantages and hydraulics has been further developed in recent years to compete against EMCs themselves [9]–[15]. For instance, Michel and Weber created a prototype and compared it with a commercial EMC containing a ball screw drive [9]. The overall efficiency of the EMC was 74.6%, including 13% losses in the electric drive and 12.4% losses in the screw transmission. Comparatively, the EHC had about 25% losses in the hydraulic transmission, proving it to be a valid alternative to the EMC. One unusual aspect of the EHCs, namely their thermal behavior, remains an ongoing research topic [16]–[18], as does their durability [19]. An EHC concept comprised of passive load-holding devices, a sealed reservoir, four quadrants operations, capable of recovering energy, and suitability for power levels above 5 kW was proposed in [14], and implemented on a load-carrying application in [15]. Hagen et al. present further investigations of this concept with a focus on motion performance [20] and energy efficiency [21], showing that EHCs significantly improve conventional hydraulics.

The two actuator technologies mentioned above can be used in several applications as an alternative to conventional valve-controlled actuators. However, more specific comparative analyses regarding their design impact in terms of installation space, design complexity, speed and force (power) capability, reliability, service life (durability), and cost – when implemented on load-carrying applications – are still lacking in the technical literature. Hence, this paper aims to present general guidelines on how to size and select the best self-contained linear actuation system for a given working cycle. The two actuators being considered (Fig. 1) are the off-the-

(a) Electro-mechanical cylinder.
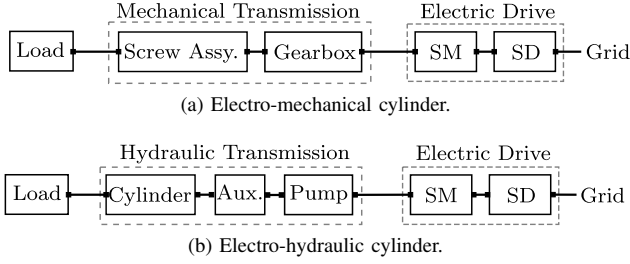

(b) Electro-hydraulic cylinder.

Fig. 1: The two considered self-contained cylinders.

shelf heavy-duty electro-mechanical cylinder from Rexroth [22] and the self-contained electro-hydraulic concept presented in [15] using off-the-shelf components. An example based on a single-boom crane's motion control is studied, and the sizing process of the different off-the-shelf components is also considered.

II. SIZING PRINCIPLES

Both actuation systems consist of an electric drive and a transmission system that converts rotary motion to linear motion (Fig. 1).

The electric drive includes the servo-drive (SD) that is connected to the electrical three-phase grid controlling the rotational speed of the servo-motor (SM) and a number of accessory components which have not been considered in detail in this study. The electric drive can be chosen based on the following steps [23]:

1) determine the drive requirements, including the torque, speed, power, control performance, and interfaces;
2) select the power unit/motor combination;
3) identify the control unit performance and interface (i.e., communication standards, input/outputs, and safety features);
4) define the firmware function (e.g., open-loop or closed-loop controller architecture);
5) select the accessories (e.g., mains filters and chokes, brake resistors/units, capacity modules, cables, and software).

The following section shows the sizing of the servo-motor for both the EMC and EHC. The servo-drive has been selected to deliver a continuous output current i_{cont} so that:

$$i_{cont} \geq \frac{\tau_{cont}}{\tau_0} i_0, \tag{1}$$

where τ_{cont} is the required continuous torque, and τ_0 and i_0 are the motor's continuous torque and current at standstill, respectively. The continuous operating characteristic S1 (60K) according to EN 60034-1 has been used when sizing the electric drive.

A. Electro-Mechanical Cylinder

The mechanical transmission system includes the screw assembly (i.e., ball screw or roller screw), the gearbox (optional), and the motor attachment (i.e., direct via either flange and coupling or timing belt side drive). The main components of the EMC are illustrated in Fig. 1a. According to common industrial practice [22], the EMC has been designed based on the following steps:

1) select the type of screw assembly and its dimensions (i.e., diameter and lead) based on the required cylinder stroke length, average power and dynamic load requirements of the considered working cycle in addition to the desired service life;
2) select the motor and gearbox combination based on the desired control performance, maximum speed, and continuous torque requirements.

These aspects are addressed in detail in the following paragraphs.

1) The screw assembly: The type of screw assembly (SA), diameter (d_0), lead (l), gear reductions (i_g), and the size of the electric motor must be selected to meet the minimum requirements without being overly conservative. They should state the desired working cycle (i.e., desired motion and resulting load profile) as accurately as possible. First, to avoid overheating the mechanical transmission system, the application's average output power must not exceed the screw assembly's permissible transmitted power

$$\dot{E}_{emc,p} \geq \dot{E}_{c,avg}. \tag{2}$$

Secondly, the screw assembly is selected in order that its given dynamic load capacity (C) will be at least five times greater than the resulting average equivalent dynamic load ($F_{c,avg}$), which will satisfy the nominal life calculation:

$$L_{10,emc} = \frac{\left(\frac{C}{F_{c,avg}}\right)^3 l \cdot 10^3}{\dot{x}_{c,avg} \cdot 3.6}, \tag{3}$$

where $\dot{x}_{c,avg}$ is the average absolute linear velocity of the actuator.

2) The motor and gearbox: The motor and gearbox combination is selected in order that the conditions addressed in (4)-(8) will be satisfied.

The maximum speed of the electric machine is constrained by

$$n_{emc,max} \geq \dot{x}_{c,max} \frac{i_g \cdot 60}{l}, \tag{4}$$

where $\dot{x}_{c,max}$ is the maximum required linear velocity.

The ratio of the load moments of inertia (J_R) serves as an indicator for the control performance of a motor/controller combination according to:

$$J_R = \frac{J_{mech}}{J_m} \leq \begin{cases} 6.0, & \text{handling} \\ 1.5, & \text{processing} \end{cases}, \tag{5}$$

where J_{mech} is the moment of inertia of the mechanical transmission system and the external load referred to the motor side, and J_m of the electric motor and brake unit (i.e., the passive load-holding device if needed). Industrial experience has shown that an appropriate moment of inertia ratio will result in high control performance for different applications (e.g., handling or processing applications) [22].

The permissible force of the transmission system is constrained by

$$F_{emc,p} \geq F_{c,max}, \tag{6}$$

where $F_{c,max}$ is the the maximum resulting load force acting on the cylinder.

The permissible torque of the transmission system is constrained by

$$\tau_{emc,p} \geq \frac{F_{c,max}}{\mu_{emc}} \frac{l}{2\pi \cdot i_g}, \tag{7}$$

where μ_{emc} is the efficiency level of the mechanical transmission.

The torque ratio must verify

$$\tau_R = \frac{\tau_{emc,r}}{\tau_{emc,cont}} \leq 1.0, \tag{8}$$

where $\tau_{emc,r}$ is the rated torque (i.e., the maximum continuous torque available at the continuous speed) of the servo-motor identified from the motor's characteristics curve provided by the manufacturer and $\tau_{emc,cont}$ is the continuous driving torque

$$\tau_{emc,cont} = \frac{F_{c,RMS}}{\mu_{emc}} \frac{l}{2\pi \cdot i_g}, \tag{9}$$

where $F_{c,RMS}$ is the root mean square (RMS) value of the cylinder's force profile. If an accurate load profile is not available, the manufacturer [22] proposes using an empirical value $\tau_R \leq 0.6$ instead of $\tau_R \leq 1.0$. Lastly, the rated torque is considered at the continuous speed

$$n_{emc,cont} = \dot{x}_{c,RMS} \frac{i_g \cdot 60}{l}, \tag{10}$$

where $\dot{x}_{c,RMS}$ is the RMS of the cylinder's velocity profile.

B. Electro-Hydraulic Cylinder

In place of the mechanical transmission in the EMC, the EHC includes a hydraulic (hydrostatic) transmission with a fixed-displacement hydraulic pump/motor unit (P) driving the hydraulic cylinder and being arranged in a closed-circuit configuration (Fig. 2). The hydraulic unit operates as a pump when the cylinder's piston is extending and as a motor when the piston is retracting — allowing the electric drive to regenerate power. The hydraulic auxiliary components, which include load-holding valves, pilot-operated check valves used for balancing the differential flow of the single-rod cylinder due to uneven areas, anti-cavitation valves, and pressure relief valves used to counteract over-pressurization, are placed in a manifold and installed directly on the hydraulic cylinder. A bladder-type accumulator (AC) represents the sealed reservoir, and a low-pressure return filter is connected to the circuit. Lastly, the electric motor is mounted directly to the manifold by a bell housing and servo coupling. For more details about the considered hydraulic circuit, Padovani et al. [15] have described its functioning and experimental testing.

The self-contained electro-hydraulic cylinder is designed based on the following steps:
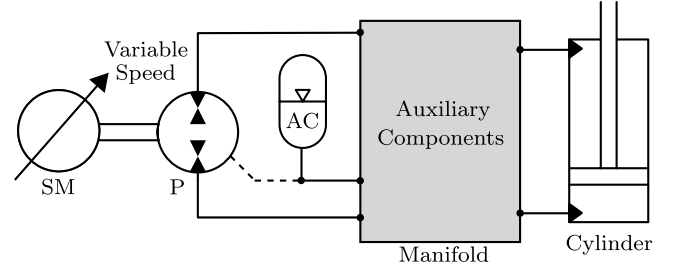

Fig. 2: A possible system architecture for self-contained electro-hydraulic cylinders (simplified schematic) [14].

1) size the cylinder's stroke capability according to the requirements of the application and size the piston and rod diameter based on the maximum load force and buckling criteria;
2) size the hydraulic pump/motor unit based on the displacement and speed required to deliver the required flow dictated by the actuator's desired motion profile;
3) size the electric drive in terms of maximum and continuous speed, torque, and current requirements;
4) size the hydro-pneumatic accumulator based on the exchange volume and the desired maximum and minimum pressure levels in the reservoir;
5) size the load-holding valves so that the pressure drop will be kept minimal to maintain an efficient throttle-less system (i.e., increased throttling may result in the need for an oil cooler) and select a proper pilot ratio and cracking pressure to ensure functionality;
6) size the flow balancing valves and oil filter so that the reservoir pressure will be kept below the pressure limits of the hydraulic components to ensure proper functionality;
7) size the pressure-relief valves based on the maximum allowed pressure levels of the hydraulic components and on the force limitations of the cylinder in order to satisfy the buckling criteria.

Details about the above-mentioned procedure are given in the following paragraphs.

1) Hydraulic cylinder: The buckling factor is an essential design parameter when sizing the hydraulic cylinder. According to existing regulations (DNVGL-CG-0128), the accepted criterion to avoid buckling is to use a safety factor $f_s = 4$. The cylinder dimensions can be chosen according to standards (e.g., ISO 6022) based on the minimum rod diameter

$$d_r \geq \sqrt[4]{\frac{64 f_s h_{max}^2 F_{c,max}}{\pi^3 E}}, \tag{11}$$

and minimum piston diameter

$$d_p \geq \sqrt{\frac{4}{\pi} \frac{F_{c,max}}{p_{p,ref} - p_{ac,max}\varphi}}, \tag{12}$$

where h_{max} is the maximum length of the cylinder in the extended position, E is the elasticity modulus (206 GPa for steel), $p_{p,ref}$ is the desired piston-side pressure (i.e., the

desired operating pressure of the hydraulic pump), $p_{ac,max}$ is the highest accumulator pressure, and φ the ratio between rod and piston areas.

2) Hydraulic pump/motor unit: When the size of the cylinder's piston area (A_p) is known and the maximum required velocity of the actuator ($\dot{x}_{c,max}$) is given, then the maximum flow demand

$$Q_{max} = A_p \dot{x}_{c,max}, \tag{13}$$

is used to calculated the required displacement (D_P) of the hydraulic unit. This step, based on the nominal operating speed (n_{nom}) and the estimated volumetric efficiency (η_{vol}) of the selected pump/motor unit, is determined according to:

$$D_P \geq \frac{Q_{max}}{n_{nom}} \frac{60}{\eta_{vol}}. \tag{14}$$

The lifetime of the axial piston machine (i.e., the roller bearings are the limiting factor) is estimated based on data provided by the manufacturer as:

$$L_{10,ehc} = L_{10N} a_{23} C_0, \tag{15}$$

where L_{10N} is the nominal bearing life at nominal operating data and a_{23} and C_0 are the correcting factors for the viscosity influence and the flow influence (swivel angle), respectively.

3) Servo-motor: The conditions addressed in (16) and (17) must be satisfied when sizing the electric machine.

They are the maximum speed

$$n_{ehc,max} \geq \frac{Q_{max}}{D_P} \frac{60}{\eta_{vol}}, \tag{16}$$

and the motor's continuous rated torque

$$\tau_{ehc,r} \geq \tau_{ehc,cont} = \frac{D_P}{2\pi} \frac{F_{c,RMS}}{A_p} \frac{1}{\eta_{mh}\eta_c}, \tag{17}$$

where $\tau_{ehc,cont}$ is the continuous driving torque. It is assumed that the rod-side pressure is insignificantly low, but the mechanical-hydraulic efficiency of the hydraulic pump/motor unit (η_{mh}), and the efficiency of the hydraulic cylinder (η_c) should be included for a conservative sizing. Lastly, the rated torque is considered at the continuous speed

$$n_{ehc,cont} = \frac{A_p \dot{x}_{c,RMS}}{D_P} \frac{60}{\eta_{vol}}. \tag{18}$$

4) Accumulator: The size of the bladder accumulator is derived according to the required effective gas volume

$$V_{ac,0} \geq C_a \frac{\Delta V}{\left(\frac{p_{0,(T_{min})}}{p_{ac,min}}\right)^{\frac{1}{\kappa}} - \left(\frac{p_{0,(T_{min})}}{p_{ac,max}}\right)^{\frac{1}{\kappa}}}, \tag{19}$$

where $C_a = p_{ac,max} / p_{ac,min}$ is the adiabatic correction factor, $\kappa = 1.4$ is the adiabatic exponent, ΔV is the total exchanged volume (i.e., the cylinder's differential volume $(A_p - A_r)x_{c,max}$ + 20% overhead), $p_{ac,max}$ and $p_{ac,min}$ are the desired maximum and minimum pressure levels. Lastly, based on the maximum and minimum ambient temperature

(T_{max} and T_{min}), the gas precharge pressure at the minimum ambient temperature ($p_{0,(T_{min})}$) is calculated as:

$$p_{0,(T_{min})} = 0.9 p_{ac,min} \left(\frac{T_{min}}{T_{max}}\right). \tag{20}$$

5) Auxiliary valves: The flow capacity of the load-holding valves must be greater than Q_{max}, while the flow balancing valves are sized based on the highest differential flow

$$\Delta Q_{max} = Q_{max} \left(1 - \frac{A_r}{A_p}\right). \tag{21}$$

The cracking pressure (p_{cr}) and pilot ratio (α_p) of the load-holding valves must be selected in order that the highest reservoir pressure (i.e., the pressure connected to the pilot line when motion is not desired) cannot open the pilot-operated check valves, according to:

$$p_{cr} > \alpha_p p_{ac,max}. \tag{22}$$

Furthermore, a vented pilot-operated check valve is preferable for ensuring a complete opening of the load-holding valves [15]. For a detailed description of the auxiliary valves and their function as well as selected components thereof, see [15].

III. DESIGN ANALYSIS

This section describes the design analysis carried out for the purpose of selecting suitable components for the EMC and EHC; the single-boom crane depicted in Fig. 3 is used as the case study. The heavy-duty version (EMC-HD) from Rexroth (Fig. 5a) [22] has been chosen as an exemplary drive due to its specific characteristics in terms of accuracy, dynamics, controllability, and heavy load capability. According to the survey carried out in [24], this type of electro-mechanical linear actuators was considered to be one of the most relevant commercial EMCs for load-carrying applications (see, for instance, [24] for a more detailed description of the EMC-HD). Consequently, the same manufacturer has also been chosen for the main components of the EHC (i.e., the servo-drive [25], the servo-motor [26], the axial piston machine [27], and the accumulator [28]), as illustrated in Fig. 5b.
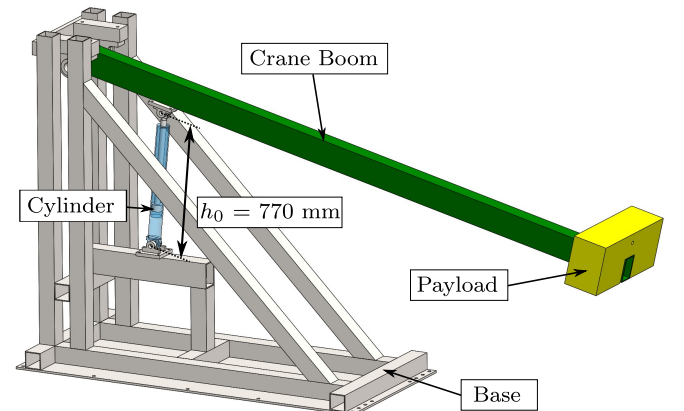

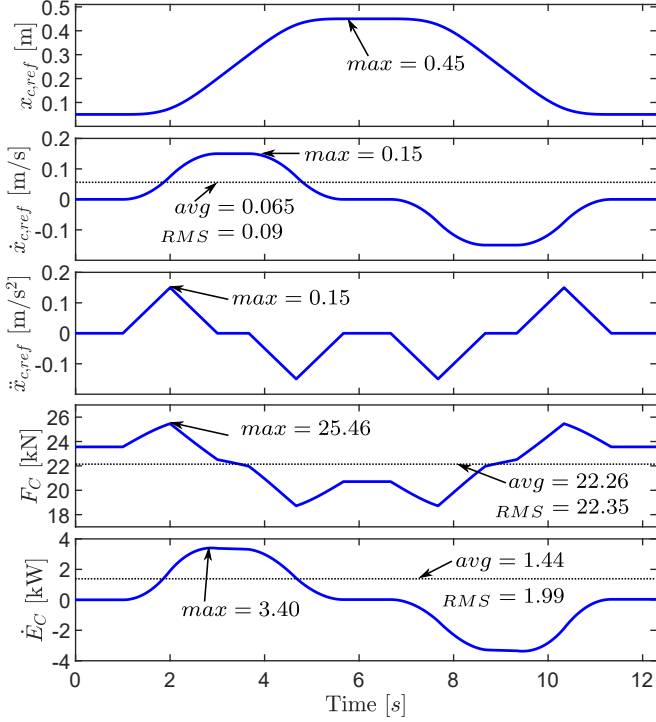Fig. 3: The single-boom crane and the original hydraulic cylinder.

Fig. 4: Key magnitudes of the considered working cycle.

(a) Electro-mechanical cylinder.

(b) Electro-hydraulic cylinder.

Fig. 5: Installation size of the two self-contained cylinders.

A. Actuator Requirements

The nonlinear model of the single-boom crane is described using the Newton's Second Law of Motion for the actuator dynamics:

$$M_{eq}(x_c)\ddot{x}_c = F_c - F_{eq}(x_c), \qquad (23)$$

where $\ddot{x}_c$ is the acceleration of the equivalent mass (M_{eq}), F_c is the mechanical force delivered by the linear actuator, and F_{eq} is the equivalent gravitational force as a function of the piston position (x_c).

The motion profile generator presented in [29] is used to generate motion reference signals (i.e., desired position ($x_{c,ref}$), velocity ($\dot{x}_{c,ref}$), and acceleration ($\ddot{x}_{c,ref}$) of the linear actuator). Further on, the required cylinder force and output power are defined by the following equations:

$$F_c = M_{eq}(x_{c,ref})\ddot{x}_{c,ref} + F_{eq}(x_{c,ref}), \qquad (24)$$

$$\dot{E}_c = F_c\dot{x}_{c,ref}. \qquad (25)$$

The identified maximum motion and load requirements that the two linear actuation systems must satisfy for the considered working cycle are highlighted in Fig. 4 along with the average and RMS values.

B. Selection of Electro-Mechanical Components

The screw assemblies that satisfy the permissible average power (2) and have a dynamic load capability $C > 5 \cdot F_{c,avg}$ for the considered working cycle are listed in Tab. I.
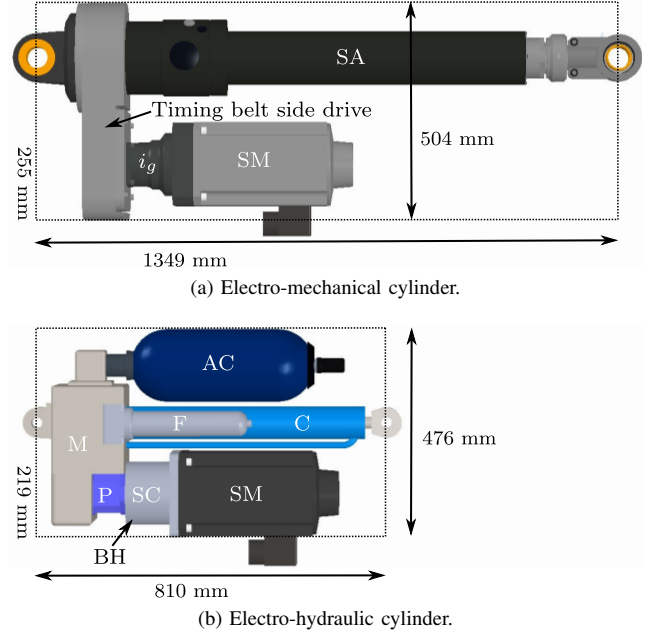
The diameter of the screw, dynamic load capacity, maximum permissible force (F_p), calculated nominal life (L_{10}) derived in (3), and the initial length (h_0) of the fully retracted cylinder are also listed. All the suitable assemblies are ball screws with a lead of $l = 20$ mm, and a limited permissible continuous transmitted power of $\dot{E}_{emc,p} = 2$ kW to ensure that the mechanical transmission will not overheat during continuous operation.

The initial length of the EMC-HD 150 is too long to fit inside the base of the single-boom crane (Fig. 3). Further, only the timing belt side drive has been considered since the direct mounting adds additional installation length. Hence, the suitability, when considering the conditions mentioned earlier in (4)-(8) for the available motor and gear combinations from the catalog [22], has been considered for the ball screw assembly with a diameter of 50 mm (HD 105) and 63 mm (HD 125), and further analyzed in Tab. II. Three suitable configurations have resulted from the analysis mentioned above. Subsequently, the configuration, including the smallest (i.e., the cheapest) servo-motor requiring the smallest servo-drive, has been chosen. The selected EMC includes the HD 125 ball screw assembly [22], the MSK100B-0300 servo-motor with integrated load-holding brake [26] mounted on a timing belt side drive along with the gearbox and resulting in an overall gear ratio $i_g = 4.5$. The chosen combination requires a

TABLE I: Suitable screw assemblies.

SA	d_0 [mm]	C [kN]	F_P [kN]	L_{10} [h]	h_0 [mm]
105	50	117	56	11,873	1274
125	63	131	62	16,804	1349
150	80	307	115	217,267	1586

TABLE II: Analysis of the available electro-mechanical cylinder configurations with timing belt side drive.

SA HD	SM MSK	i_g [22] [-]	μ [22] [-]	τ_P [22] [Nm]	$\dot{x}_{max}$ [22] [m/s]	$n_{cont}(10)$ [rpm]	$\tau_{cont}(9)$ [Nm]	τ_r [26] [Nm]	$i_{cont}(1)$ [A]	m [22] [kg]	$J_R(5)$ [-]	$\tau_R(8)$ [-]	OK?
105	071D	1.5	0.87	136.1	1.00	405	54.5	16	28.4	103	30.9	3.41	No
105	071D	4.5	0.83	47.7	0.33	1215	19.1	13	9.9	111	**3.85**	1.47	No
105	071D	7.5	0.83	28.6	0.20	2025	11.4	10	5.9	111	**1.61**	1.14	No
105	100B	1.5	0.87	136.1	1.00	405	54.5	25	33.9	120	**3.92**	2.18	No
105	101D	1.5	0.87	136.1	1.00	405	54.5	41	33.4	127	6.50	1.33	No
105	101E	1.5	0.87	136.1	1.00	405	54.5	53	32.4	141	**4.77**	1.03	No
125	071D	7.5	0.83	43.5	0.20	2025	11.4	10	5.9	158	**1.75**	1.14	No
125	100B	1.5	0.87	164.9	0.80	405	54.5	22	33.9	168	**4.40**	2.18	No
125	100B	4.5	0.83	72.5	0.33	1215	19.1	21	11.8	175	**0.54**	**0.91**	Yes
125	101D	1.5	0.87	164.9	0.80	405	54.5	41	33.4	175	7.29	1.33	No
125	101D	4.5	0.83	72.5	0.33	1215	19.1	28	11.7	183	**0.90**	**0.68**	Yes
125	101E	1.5	0.87	164.9	0.80	405	54.5	53	32.4	188	**5.35**	1.03	No
125	101E	4.5	0.83	72.5	0.33	1215	19.1	24	11.3	196	**0.66**	**0.79**	Yes

continuous current $i_{cont} \geq 11.8$ A. Hence, the IndraDrive C HCS02.1E-W0054 [25] with $i_{cont} = 22$ A has been selected, resulting in a nominal power (i.e., installed power) of $\dot{E}_{in,nom} = 7.5$ kW.

C. Selection of Electro-Hydraulic Components

The dimensions of the hydraulic cylinder have already been given by the real application (Fig. 3) used as a case study. The hydraulic cylinder has a piston diameter $d_p = 65$ mm, rod diameter $d_r = 35$ mm, initial length when the cylinder is fully retracted $h_0 = 770$ mm, and stroke length $x_{c,max} = 500$ mm.

Based on the identified minimum requirements in accordance with the sizing principles presented in Section II, the components' sizes have been selected from the catalogs and presented in Tab. III. The following values have been used when sizing the accumulator: $p_{max} = 1.0$ bar, $p_{min} = 0.5$ bar, $T_{max} = 50$ °C, and $T_{min} = -20$ °C. The mass of the mineral oil, filter (F), manifold (M), bell housing (BH), and servo coupling (SC) are also included.

According to the diagram provided by the manufacturer, the nominal bearing life of the axial piston machine is equal to 30,000 h for nominal operating pressures below 200 bar. The viscosity correcting factor is $a_{23} = 2.5$ for the considered hydraulic fluid (i.e., ISO VG 46), and the flow correcting factor is $C_0 = 1$ for a fixed displacement unit. Derived in (15), the estimated life of the hydraulic unit is 75,000 h. According to the manufacturer, values above 30,000 h are not accurate because other factors influence the lifetime of the axial piston machine.

IV. COMPARATIVE ANALYSIS AND DISCUSSION

Both the considered EMC and EHC can continuously perform the required motion in the considered case study. However, the final selection depends on additional design objectives, including installation space, weight, service life, ingress protection classification, energy efficiency, power density, control performance, and cost. Environmental factors such as temperatures, ingress protection, and potentially explosive atmospheres (ATEX), have been omitted in the considered design requirements.

TABLE III: The selected components for the EHC.

	Characteristics	Requirements	Size	Model
C	A_p [m^2]	–	0.0033	PMC
	A_r [m^2]	–	0.0024	25CAL
	η_{vol}	–	0.9	
	m_c [kg]	–	20.1	
SM	n_{max} [rpm]	2968	4500	MSK
	τ_r [Nm]	15	18	100B-0300
	m_{sm} [kg]	–	34	[26]
SD	$\dot{E}_{in,nom}$ [kW]	3.82	4	HCS02.1E
	i_{cont} [A]	9.3	11	W0028 [25]
P	D_P [$\frac{cm^3}{rev}$]	8.74	10.6	A10FZG
	n_{nom} [rpm]	2968	3600	[27]
	η_{vol}	–	0.95	
	η_{mh}	–	0.84	
	m_p [kg]	–	9	
AC	V_0 [L]	5.32	5.9	HAB6 [28]
	m_{ac} [kg]	–	20	
	m_{oil} [kg]	–	10	ISO VG 46
F	m_f [kg]	–	2	50LEN0100 [30]
M	m_m [kg]	–	29.6	Custom
BH	m_{bh} [kg]	–	3.5	PSG-200
SC	m_{sc} [kg]	–	1.5	Rotex-GS28

Regarding controllability, this study does not evaluate motion tracking performance (accuracy) since that would require completing an experimental investigation in order to make a fair comparison between the two factors. However, it is generally known that the driving stiffness of EMC is significantly high compared to that of the EHC [9]. To accurately control the linear speed and position of the EMC, it is sufficient to have the standard control architecture, including a position controller in cascade with the speed controller (FOC), implemented in the servo-drive using the angular encoder initially included on the servo-motor as feedback. In the case of the EHC, instead of using the angular encoder as position feedback, an additional linear transducer (position sensor) must be implemented on the hydraulic cylinder for feedback to supervise the cylinder's piston position. The EHC's position controller can be implemented on an embedded controller, pro-

viding a reference speed signal to the servo-drive [20]; alternately, a more complex control firmware [31] can be installed on the servo-drive. Furthermore, previous research related to a similar EHC [20] shows that the uncompensated hydraulic system suffers from very low damping. Consequently, extra sensors are needed to implement active damping (e.g., pressure sensors for pressure feedback), which is necessary to achieve satisfactory motion performance.

Based on the selected components and maximum values (force and power) of the working cycle (Fig. 4), Tab. IV compares relevant characteristics of the two designed self-contained drive systems relative to the valve-controlled cylinder (VCC) presented in [20], [21], [32]. It is assumed that the valve-controlled system can deal with the motion profile's required piston velocity. The energy efficiencies experimentally identified in [21] for a similar EHC, along with the considered VCC driving the same application with a similar motion cycle, are used for comparison. As regards the EMC, the efficiency of the electric drive identified in [9] is used in combination with the efficiency of the selected mechanical transmission system according to [22]. As a side note, the energy efficiency of the two self-contained cylinders can be significantly increased if the energy regenerated when lowering the crane boom is recovered [21].

The quantities in Tab. IV and the illustration in Fig. 5 clearly show that not only does the EHC take less space, but it also weighs less, making it more suitable for applications where conventional hydraulic cylinders are used, including the considered single-boom crane. Hence, the EHC performs better in terms of force per mass (35% better) and power density (106% better). The EMC can move 0.15 m/s faster than the EHC and permits faster acceleration (114%), where the hydraulic unit is the limiting component. Morover, the EMC has 5% better energy efficiency than the EHC.

The estimated service life of the EHC is almost twice that of the EMC. In general the EMC has low overload protection compared to hydraulic alternatives. This is the case for the mechanical system since it is very stiff and cannot absorb any additional external impact force. Consequently, the screw transmission may fail (jamming); if this occurs, the EMC must be replaced to resume operations. The EMC has a higher price on the electric drive that has more installed power than the EHC. Based on experience, the cost of the EMC's screw assembly is believed to be about twice as expensive as the hydraulic transmission system due to the high price resulting from low production numbers.

Finally, in order to evaluate the impact of moving from conventional hydraulic cylinders to self-contained cylinders, a comparison between EMC and EHC concerning conventional valve-controlled systems (without considering the space occupation, cost, and energy losses of the centralized hydraulic power unit) [32] is presented in Tab. V. Additional general knowledge from the technical literature is also included here. This comparison is intended to act as a general guideline for choosing between EMC or EHC.

TABLE IV: Performance characteristics of the self-contained cylinders compared to the valve-controlled cylinder.

Characteristics	VCC	EMC	EHC
Length [mm]:	770	1349 (+75.2%)	810 (+5.2%)
Volume [L]:	4.8	173.4 (+3513%)	84.4 (+1658%)
Installed mass: [kg]:	30	175 (+483%)	130 (+333%)
Installed power [kW]:	10.5	7.5 (-29%)	4 (-62%)
Force pr mass [N/kg]:	852	146 (-83%)	197 (-77%)
Power density [W/L]:	708	19.6 (-97%)	40.3 (-94%)
Energy efficiency [%]:	22	60 (+173%)	57 (+159%)
Max force [kN]:	82.5	62 (-25%)	82.5 (0%)
Max power [kW]:	5.1	2 (-61%)	2.4 (-53%)
Max service life [h]:	30,000	16,804 (-44%)	30,000 (0%)
Enclosure rating:	IP65	IP65	IP65

TABLE V: Advantages and disadvantages of replacing valve-controlled cylinders with self-contained solutions. Five different grades are used ranging from (– –) to (+ +), with (– –) being the worst, and 0 representing similar performance to the conventional VCC. Results that are based on general knowledge from the technical literature are denoted by *, while results that are related to ongoing research are denoted by ?.

Category:	Criterion:	EMC	EHC
Design	Compactness	– –	–
	Force per mass	– –	–
	Power density	– –	–
	Design complexity	+	–
	Enclosure protection	0	0
	Control effort*	+	0
	Scalabillity*	– –	–
	Cost	– –	–
Operation	Impact absorption*	– –	0
	Reliability*	– –	0?
	Energy efficiency	++	++
	Thermal absorption	– –	–?
	Accuracy*	++	+
	Drive stiffness*	++	–
	Max force	–	0
	Max velocity	++	+
	Max acceleration	++	–
	Max continuous output power	– –	–
Safety	Passive load-holding	-?	0
	Fail-safe*	–	0
	Overload protection*	–	+
Application	Installed power	+	++
	Oil spill risk*	++	+
	Maintenance effort*	++	+?
	Durability*	– –	0?
	Commissioning effort	++	+

V. CONCLUSIONS

Two self-contained linear actuator technologies, namely an electro-mechanical and electro-hydraulic cylinder, have been investigated in this paper; whose focus is on their design when replacing a traditional valve-controlled hydraulic cylinder. After explaining why they are potential alternatives for many state-of-the-art applications, a single-boom crane has been chosen as the baseline for applying these drives. The sizing process to select available off-the-shelf components has been illustrated, and relevant characteristics of the systems

have been discussed. The following main aspects are, therefore highlighted:

- The electro-hydraulic drive shows several benefits over the electro-mechanical counterpart, for example 20% higher continuous power capability, 47% less installed electric power, 79% longer expected service life, 33% higher maximum force capability, 25% less overall mass, and 40% less installation length.

- The electro-hydraulic cylinder is more robust against impact forces, and is expected to have around a 50% lower initial cost. In the case of working cycles requiring a continuous transmitted power above 2 kW, there are no available configurations of the considered electro-mechanical actuator due to the limitations on the permissible continuous power being transmitted by the screw assembly. Regarding the electro-hydraulic solution, the rated torque of the servo-motor is a limiting factor. However, asynchronous induction machines are available when higher torque is needed, i.e., above 180 Nm, as pointed out in [33].

- The electro-mechanical solution is expected to show a higher level of controllability due to higher drive stiffness and energy efficiency as well as lower system complexity. All of these factors result, in a more straightforward design approach.

This analysis also shows that the electro-hydraulic solution is the best choice when a risk for high impact forces exists, the required output power is continuously above 2 kW, and when minimal installation space, weight, and cost are key design objectives. Future work in this field will include efforts to make the sizing procedure automated in terms of component selection.

ACKNOWLEDGMENTS

REFERENCES

[1] D. Padovani, M. Rundo, and G. Altare, "The Working Hydraulics of Valve-Controlled Mobile Machines: Classification and Review," *ASME Journal of Dynamic Systems, Measurement, and Control*, vol. 142, no. 7, 2020.

[2] C. Helsley, "Power by Wire for Aircraft - The All-Electric Airplane," *SAE Technical Paper*, 1977.

[3] W. Swingle and J. Edge, "The Electric Orbiter," in *National Aerospace*, 1981.

[4] A. Garcia, J. Cusido, J. Rosero, J. Ortega, and L. Romeral, "Reliable electro-mechanical actuators in aircraft," *IEEE Aerospace and Electronic Systems Magazine*, vol. 23, no. 8, pp. 19–25, aug 2008.

[5] A. Boglietti, A. Cavagnino, A. Tenconi, S. Vaschetto, and P. di Torino, "The safety critical electric machines and drives in the more electric aircraft: A survey," in *35th Annual Conference of IEEE Industrial Electronics*, 2009, pp. 2587–2594.

[6] F. Jian, J.-C. Maré, and F. Yongling, "Modelling and simulation of flight control electromechanical actuators with special focus on model architecting, multidisciplinary effects and power flows," *Chinese Journal of Aeronautics*, vol. 30, pp. 47–65, 2016.

[7] S. Frischemeier, "Electrohydrostatic actuators for aircraft primary flight control-types, modelling and evaluation," in *5th Scandinavian International Conference on Fluid Power*, 1997.

[8] D. van den Bossche, "The A380 Flight Control Electrohydrostatic Actuators, Achievements and Lessons Learnt," in *25th International Congress of the Aeronautical Sciences*, 2006, pp. 1–8.

[9] S. Michel and J. Weber, "Energy-efficient electrohydraulic compact drives for low power applications," in *ASME/BATH 2012 Symposium on Fluid Power and Motion Control*, 2012, pp. 93–107.

[10] C. Boes and A. Helbig, "Electro Hydrostatic Actuators for Industrial Applications," in *9th International Fluid Power Conference*, 2014.

[11] A. Helbig, "Electrohydrostatic Actuation: An Energy-Efficient Option for Machine Builders," in *Hydraulics & Pneumatics*, 2015.

[12] A. Helbig and C. Boes, "Electric Hydrostatic Actuation-modular building blocks for industrial applications," in *10th International Fluid Power Conference*, 2016, pp. 93–102.

[13] Rexroth, "Electrification and digitalization: The fitness program for hydraulics," https://bit.ly/2U5zyXI, Accessed: 2020-03-12.

[14] D. Hagen, D. Padovani, and M. K. Ebbesen, "Study of a Self-Contained Electro-Hydraulic Cylinder Drive," in *2018 Global Fluid Power Society PhD Symposium (GFPS)*. IEEE, 2018.

[15] D. Padovani, S. Ketelsen, D. Hagen, and L. Schmidt, "A Self-Contained Electro-Hydraulic Cylinder with Passive Load-Holding Capability," *Energies*, vol. 12, no. 2, 2019.

[16] S. Michel and J. Weber, "Prediction of the thermo-energetic behaviour of an electrohydraulic compact drive," in *10th International Fluid Power Conference*, 2016, pp. 219–234.

[17] T. Minav, L. Papini, and M. Pietola, "A Thermal Analysis of Direct Driven Hydraulics," in *10th International Fluid Power Conference*, 2016, pp. 235–248.

[18] N. Karlén, T. A. Minav, and M. Pietola, "Investigation of Thermal Effects in Direct Driven Hydraulic System for Off-Road Machinery," in *The 9th FPNI Ph.D. Symposium on Fluid Power*, 2016.

[19] S. Michel and J. Weber, "Investigation of Self-Contamination of Electrohydraulic Compact Drives," *10th JFPS International Symposium on Fluid Power*, no. June 2018, pp. 1–7, 2017.

[20] D. Hagen, D. Padovani, and M. Choux, "A Comparison Study of a Novel Self-Contained Electro-Hydraulic Cylinder versus a Conventional Valve-Controlled Actuator—Part 1: Motion Control," *Actuators*, vol. 8, no. 4, p. 79, 2019.

[21] D. Hagen, D. Padovani, and M. Choux, "A Comparison Study of a Novel Self-Contained Electro-Hydraulic Cylinder versus a Conventional Valve-Controlled Actuator—Part 2: Energy Efficiency," *Actuators*, vol. 8, no. 4, p. 78, 2019.

[22] Rexroth, *Electromechanical Cylinder EMC – HD: Catalog R999000326*. Bosch Rexroth AG, 2019.

[23] Rexroth, *Rexroth drive system IndraDrive: Catalog 71511EN*. Bosch Rexroth AG, 2012.

[24] D. Hagen, W. Pawlus, M. K. Ebbesen, and T. O. Andersen, "Feasibility Study of Electromechanical Cylinder Drivetrain for Offshore Mechatronic Systems," *Journal of Modeling, Identification and Control*, vol. 38, no. 2, pp. 59–77, 2017.

[25] Rexroth, *Rexroth IndraDrive C Drive Controllers HCS: Catalog R911314905*. Bosch Rexroth AG, 2006.

[26] Rexroth, *Synchronous Servomotors MSK: Catalog R911296289*. Bosch Rexroth AG, 2018.

[27] Rexroth, *Axial piston units for variable-speed drives: Catalog RE91485*. Bosch Rexroth AG, 2016.

[28] Rexroth, *Bladder-type accumulator, type HAB: Catalog RE50171*. Bosch Rexroth AG, 2016.

[29] D. Hagen, D. Padovani, and M. Choux, "Enabling Energy Savings in Offshore Mechatronic Systems by using Self-Contained Cylinders," *Journal of Modeling, Identification and Control*, vol. 40, no. 2, pp. 89–108, 2019.

[30] Rexroth, *Inline filter with filter element: Catalog RE51447*. Bosch Rexroth AG, 2014.

[31] Rexroth, *Rexroth Sytronix SvP 7020 PFC Variable-Speed Positioning of Hydraulic Axes: Catalog R911379550*. Bosch Rexroth AG, 2017.

[32] D. Hagen, D. Padovani, and M. Choux, "Design and Implementation of Pressure Feedback for Load-Carrying Applications with Position Control," in *Sixteenth Scandinavian International Conference on Fluid Power*, 2019.

[33] S. Ketelsen, T. O. Andersen, M. K. Ebbesen, and L. Schmidt, "Mass Estimation of Self-Contained Linear Electro-Hydraulic Actuators and Evaluation of the Influence on Payload Capacity of a Knuckle Boom Crane," in *BATH/ASME 2019 Symposium on Fluid Power & Motion Control*, 2019.